CESDN 29a

DNA 2782F

FINAL REPORT

Covering the Period 15 March 1969 through 30 March 1970

LOW IMPEDANCE SIMULATOR STUDIES

Contract No. DASA 01-69-C-0091

Submitted to:

Defense Nuclear Agency
Washington, D.C.

Program Manager: R. N. Cheever

R. N. Cheever
Manager
Technology Division

"Approved for Public Release; Distribution Unlimited"

ION PHYSICS CORPORATION IPC

A Subsidiary of High Voltage Engineering Corporation

BURLINGTON, MASSACHUSETTS

"Approved for Public Release;
Distribution Unlimited"

DNA 2782F

FINAL REPORT

Covering the Period 15 March 1969 through 30 March 1970

THIS WORK SPONSORED BY THE DEFENSE NUCLEAR
AGENCY UNDER NWER SUBTASK LB065.

LOW IMPEDANCE SIMULATOR STUDIES

Contract No. DASA 01-69-C-0091

Submitted to:

Defense Nuclear Agency
Washington, D.C.

Program Manager: R. N. Cheever
Manager, Technology Division

ION PHYSICS CORPORATION
BURLINGTON, MASSACHUSETTS

TABLE OF CONTENTS

TABLE OF CONTENTS (Continued)

TABLE OF CONTENTS (Continued)

TABLE OF CONTENTS (Continued)

TABLE OF CONTENTS (Concluded)

LIST OF ILLUSTRATIONS

LIST OF ILLUSTRATIONS (Continued)

LIST OF ILLUSTRATIONS (Continued)

LIST OF ILLUSTRATIONS (Continued)

LIST OF ILLUSTRATIONS (Continued)

LIST OF ILLUSTRATIONS (Continued)

LIST OF ILLUSTRATIONS (Continued)

LIST OF ILLUSTRATIONS (Continued)

LIST OF ILLUSTRATIONS (Continued)

LIST OF TABLES

FOREWORD

The activities of this program were under the overall direction of R. D. Cheever who acted as Program Manager and also made important technical contributions to the design of the solid line, vacuum flashover and electron beam diode experiments and particularly to the energy flow analyses (section 2.1).

J. R. Uglum was responsible for the task of Energy Flow/Diode Studies in which he was assisted by H. Wilhelmsen, who made most of the laboratory modelling experiments (section 2.2) and R. Crocker, who did the computer modelling work (section 2.3). Valuable assistance was provided by S. Graybill during the electron beam diode experiments.

The Solid Dielectric Studies were supervised by W. Bell, who did the bulk of the work with some assistance from F. Tse.

H. Milde was responsible for the Water Line Studies in which he was ably assisted by N. Harris who supervised the realization of the Neptune B modifications. G. Simcox was consulted during the design of the modifications. J. Hipple did much of the trigger generator development work and G. Cooperstein performed the beam diagnostics on the completed Neptune B system in consultation with S. Graybill.

Needless to say, the accomplishment of the experimental work depended heavily on the efforts of a number of engineering aides and technicians, including R. Lutz, C. Litchfield, R. Parsons and G. Aliengena, D. Bryant, G. Guse, D. Rumson and A. Selin.

ABSTRACT

This report describes work done in support of the low impedance pulsed electron beam generator development goals of the Defense Atomic Support Agency. The purpose of the work was the development of new technology upon which the design of future low impedance simulators can be based. Of particular interest are the results obtained using gas trigatron switches with a coaxial water-insulated pulse forming network (PFN) to drive an electron beam diode. The low prepulse and repeatable switch characteristics resulted in very reproducible and predictable electron beams. Transitions connecting beam diodes to PFN's were studied experimentally and analytically in an attempt to obtain improved energy flow. Computer modelling work is described and laboratory measurements on scale models are reported. The time development of the beam diode impedance has also been measured for a few combinations of cathode/anode materials and geometry. Some work with several solid dielectric materials, candidates for use as PFN and transition (tube) insulation, is reported including results of dielectric strengthened flashover (in high pressure gas) tests and vacuum flashover experiments in a low impedance (5 Ω) transition/diode design driven from a water-insulated, tapered-line transformer.

SECTION 1
INTRODUCTION AND SUMMARY

The purpose of these simulator studies has been the development of new technology upon which the design of future low impedance simulators can be based. The program was divided into three parts.

Energy Flow/Diode Studies were concerned with analytical and experimental approaches to the determination of the effects of output geometry on accelerator performance and of the factors influencing the behavior of very high current vacuum diodes. In particular, answers were sought to the questions of how great an impedance discontinuity can be allowed near the tube insulator to obtain better vacuum flashover performance (high output current) without serious loss of risetime, and of what role diode closure mechanisms play in determining or limiting beam fluence. The overall aim of these studies was the development of techniques for the prediction of simulator performance, to be used as design tools.

Solid Dielectric Studies have been aimed to provide design data and develop fabrication technology for solid dielectric materials for use both as transition/tube insulators and as the energy storage medium in a dc-charged, low-impedance coaxial line store. All present day types of simulators require solid insulation in the output section to separate the prime energy storage medium from the vacuum necessary in the electron beam diode. The reason for the solid line is the prospect that it may provide output power comparable to a water line with the predictability of the gas line. The predictability results from the absence of prepulse and the use of a single (gas) switch rather than a sequence of switches.

Water Line Studies were intended to improve the predictability of the output pulses from water lines, through the use of triggered rather than overvolted switching, and the suppression of prepulse. The IPC Neptune facility was modified and renamed Neptune B. This is described in section 4.1. The Neptune B system will itself serve as an experimental tool in further energy flow and diode investigations and provide high ν/γ beams for continuing studies of energy transport by electron beams.

The studies have been generally successful. In particular, the performance of Neptune B using trigatron gas switches has been gratifying. The original intention of using a mid-plane water switch was abandoned in view of the severe dificulties others have experienced in the use of this type of switch. The gas trigatron, although mechanically more complicated, has worked well both as a switch and as a prepulse isolator. The resultant output pulses from the Neptune B system are very reproducible. Near the end of the program some effort was spent in characterizing the beam from Neptune B to confirm the reproducibility under operational conditions.

The dielectric work has had mixed success. The results encourage the view that a coaxial, gas-insulated, solid line could be built up out of sections of manageable size. Tests have shown that surface flashover can be discouraged by flaring the ends of the tubular sections, which are then butted together one after another to form a storage line of the desired length. Unfortunately, extensive testing showed the dielectric orginally intended for use in such a line, a castable filled epoxy, to have inferior dielectric strength and so the fabrication of a prototype line was abandoned. However, later tests on other dielectrics showed very good results with a high quality polystyrene material which can be molded to shape by the supplier or purchased as thick-wall tube and machined to shape. The coaxial line conductors should probably be formed by metallizing the plastic surfaces since the results with cast-in electrodes using epoxy were not encouraging. The polystyrene material is relatively expensive so that the cost of a solid line made with it would be greater than had been originally envisioned with the cheaper epoxy.

Toward the end of the program, some vacuum flashover experiments were performed using polystyrene and lucite tube insulators in a front end especially designed for smooth energy flow and even field distribution along the solid/vacuum interface. The driving impulse was provided by an FX-25 machine connected via a tapered water line transformer having a 5 Ω output impedance. Thus, flashover was studied in a low impedance configuration wherein energy flowed from water through a solid into vacuum - an arche typical situation. The results were encouraging in that very high peak stresses were supportable in

the interface region, but disappointing in that beam voltages achieved were not as high as expected. This apparent contradiction arose from the fact that the driving pulse rose much more quickly (< 5 ns) than the cathode could turn on (~ 10 ns) so that it was reflected as if from an open circuit with the attendant voltage doubling. Thus, the peak stresses were a factor of two higher than expected. It would be interesting to redo these experiments with a slower driving pulse to see if higher beam voltages are then achievable, but time did not allow this during the present program.

Effort spent in considering the problems of energy flow at the front end of low impedance simulators shows up primarily in the design of the flashover experiment described above and, to a lesser degree, in the design of Neptune B. Since the constraints of time and the existing hardware left little room for maneuver in Neptune B, it was not feasible to do anything startlingly original but rather only to confirm in advance that the rather straightforward front end design would be adequate. This was done through experiments performed on a half-scale model. An attempt to devise a combination transmission line-lumped circuit element model to enable calculation of front end performance by computer was only partly successful, useful results having been obtained for some cases.

Of particular interest to future simulation work were the measurements of the time development of beam diode impedance for various cathode/anode materials and geometries. This work, which was greatly facilitated by the ability of IPC gas line FX machines to reproduce experimental conditions, is only a beginning since only a few possibilities were investigated. Many more materials and geometries should be studied in order to determine optimum configurations for low impedance simulator applications.

SECTION 2
ENERGY FLOW/DIODE STUDIES

2.1 Summary

The objective of this program was to study the problems of energy flow in the front end section of pulsed electron accelerators. By front end is meant both the tube/diode structure used to produce the electron beam and also any transmission line structure which is used to focus the energy into the tube/diode region. Since the performance of any system can be limited by a poor design of the output section, it was felt that a thorough study of it was required.

The program was broken down into three sub-tasks, each of which examined a specific aspect of front end performance. They were:

(1) System Modelling
(2) Energy Flow
(3) Diode Studies

Each is described below and the main results summarized. A detailed discussion of each task is then presented.

System Modelling

Two modelling experiments were carried out in this task. One experimental program consisted of studying a one-half scale model of the front end design of Neptune B. Parametric studies of risetime versus number of switch channels and switch channel length were performed. The effect of varying the water/vacuum interface was also investigated, and pre-pulse amplitude measurements were made. The 28 ns risetime predicted from the modelling data agreed very well with the results obtained on the final system. The measured pre-pulse amplitude of 3% indicated that the design did in fact minimize the capacitive coupling between the coaxial pulse forming network (PFN) and the output section.

A complete description of the modelling work can be found in section 4.9 of this report describing the Neptune B program.

Another experimental modelling program consisted of a parametric study of the transit time and risetime degradation in capacitively graded segmented tubes. These results were intended for use in developing a physical model for the tube which would be convenient for numerical calculations. Although it was originally thought that a tube's insulating dielectric would make it look like a slow wave structure, the experimental results showed otherwise. In fact, the wave velocity through the tube models was close to the speed of light in vacuum. The risetime degradation appears to be a combination of the RC time constant associated with the stray capacitance to ground and the L/R time constant associated with the coaxial shank feeding the load. Efforts to develop a satisfactory model to explain the results were unsuccessful. Details of the experiment and the results can be found in section 2.2.

Finally, a computer code was written which models a pulsed accelerator as a coaxial line feeding a front end which is represented by lumped circuit elements. The code was checked out against experimental results obtained during the diode studies, and it was found that for the higher impedance flash x-ray machines feeding a load which is matched or undermatched, the model works quite well. For over-matched loads it is necessary to deal with many reflections, and the model seems to break down after two reflections. The reason is apparently that the cumulative effects of many small system discontinuities, which are not included in the model, show up in later reflections. Details of the code can be found in section 2.3.

Energy Flow

Analyses have been made of several problems of energy flow in coaxial systems. The results were useful in the design of Neptune B and some are of sufficiently general interest to warrant their being summarized here.

For a fixed load voltage, V_L, it can be shown that the energy flow (power) from a coaxial store of outer radius b is maximized when the inner radius, a, satisfies the transcendental relation

$$\ell n \frac{b}{a} = \sqrt{\frac{V_L}{Ea}} \quad ,$$

where E is the maximum electric stress which may be safely sustained on the inner conductor. The store voltage is

$$V_o = E a \ell n \frac{b}{a} = \sqrt{EaV_L} \quad ,$$

whence it follows that

$$\ell n \frac{b}{a} = \frac{V_L}{V_o} \leq 1 \; .$$

Thus, the optimum store impedance is always less than that for maximum store voltage (at which $\ell n \frac{b}{a} = 1$) and is given by the relation

$$Z_o = \frac{60}{\sqrt{\epsilon}} \sqrt{\frac{V_L}{Ea}} \quad ,$$

where ϵ is the relative permittivity of the storage dielectric (the relative permeability is assumed to be unity). The corresponding value of the load impedance is

$$Z_L = \frac{60}{\sqrt{\epsilon}} \frac{V_L}{Ea} \frac{1}{\left(1 - \sqrt{\frac{V_L}{Ea}}\right)}$$

Note that for fixed V_L, the greatest load power is achieved with the smallest load impedance which in turn results from choosing the store dielectric having the largest value of $\sqrt{\epsilon}\ E$. This expression can therefore be taken as a figure of merit for storage dielectrics. Among the materials of interest in pulse-power applications, it is interesting that oil and gas have figures of merit near 40 MV/m, while water is far superior at 180 MV/m and the polystyrene examined in the dielectric studies reported in section 3 is far better yet at 540 MV/m (for 1000 shot lifetime; perhaps 360 MV/m for greater than 10,000 shots duty). These figures of merit are generally valid independent of store geometry, whether coaxial, strip, or whatever.

When efficiency is maximized in coaxial systems, the store and load impedances turn out equal (matched) in case

$$\sqrt{\frac{V_L}{Ea}} = \frac{1}{2} \left(= \ell n \frac{b}{a}\right)$$

which is also the condition for maximum energy storage. Thus, for a given load voltage, V_L, and dielectric strength, E, there is a particular store radius, b_o, for which the energy storage and transfer efficiency to the load are simultaneously maximized. This optimum store size is characterized by

$$b_o = 6.6 \frac{V_L}{E} \quad .$$

Larger stores must be overmatched to the load ($Z_o > Z_L$), and smaller ones undermatched, in order to maintain the load voltage at V_L, and in either case

the load power is greatest for a store impedance different from that giving maximum energy storage, as noted previously.

Of course, the use of tapered line transformers, which is not uncommon with water dielectric, theoretically enables the optimum matching of any size store to the load. However, it is well to note that even large mismatches between store and load result in only modest losses of energy transfer efficiency (4:1 corresponds to 65% efficiency), and that the stored energy varies but weakly as the store impedance is varied from that of optimum energy storage. Thus, in many cases it may be cheaper to operate mismatched with somewhat increased stored energy than to build a transformer.

It has been widely appreciated for some time that mismatches are even desirable when using electron beam loads. In order to confine the electron flow to desired regions of the vacuum tube, it is necessary that the impedance of the tube outside of the beam region be higher than the beam impedance. When this is so, the magnetic field of the beam current inhibits electron flow in the rest of the tube, cutting it off entirely when the mismatch exceeds a critical level depending on the tube geometry and beam voltage. For example, in the case of a coaxial tube at 1 MV, a mismatch of about 1.3:1 is required according to crude calculations. At lower beam voltages, even greater mismatches are necessary.

Another reason for mismatching arises out of consideration of vacuum flashover along the insulator separating the vacuum of the electron beam tube from the dielectric of the transition connecting the tube to the store. Breakdown of this interface is, no doubt, one of the factors limiting the power levels attainable in simulators which depend on generation of electron beams. In general, it is desirable to make the interface as long as possible to discourage flashover, and clearly this end is promoted by making the impedance of the transition as high as possible since higher impedance corresponds to larger radial separation of the coaxial conductor pair. The arguments of this and the last paragraph suggest that a front end design satisfying

$$Z_{transition} > Z_{tube} > Z_{beam}$$

with, perhaps, a 2:1 overall mismatch from transition to beam (more at lower beam voltages) is desirable. Recalling the derivation of conditions for maximum load power, note that a sudden transition from source impedance to load impedance was assumed. If the two are separated by an intervening transmission line, the result is unchanged if the line has either the load or the source impedance and varies but little for intermediate values, showing, in fact, a weak optimum for the geometric mean impedance $\sqrt{Z_o Z_L}$. Thus, the steadily rising impedance level from beam back to store proposed above actually enhances energy transfer to the load and provides the additional advantage that the store output switch operates into the higher input impedance of the transition (generally equal to the store impedance) rather than the lower load impedance and thus achieves a better L/Z risetime.

Continuing the discussion of vacuum flashover and its role in limiting energy flow, it is worth noting that improved performance is also obtained by placing the solid/vacuum interface at the greatest possible radial distance, since the increased conductor separation allows longer flashover length. Flashover length also increases as the dielectric constant of the transition insulation increases (for fixed transition impedance) so that water is particularly good in this respect. This raises the question of what happens in the flow of energy from water through a solid insulator into vacuum, with substantial disparities in dielectric constant among the three media. Fundamental considerations lead to the conclusion that, as long as the thickness of the solid corresponds to a propagation time short compared to the risetime of the incident pulse, the discontinuity has no noticeable effect on the energy flow. It is obvious that this is the usual case. In addition, further consideration leads to the conclusion that, if all dimensions of a dielectric interface correspond to propagation times short compared to the risetime of an incident pulse, the pulse proceeds through the discontinuity quasi-statically so that the local electric field at any instant in the region of the interface is a solution of Laplace's equation. Thus, the "refraction" of the wave at the discontinuity obeys the electrostatic relation

$$\epsilon_1 \tan\theta = \epsilon_2 \tan\phi$$

rather than the familiar Snell's law of optics

$$\sqrt{\epsilon_1}\ \text{Sin}\ \theta\ =\ \sqrt{\epsilon_2}\ \text{Sin}\ \phi\quad ,$$

where θ and ϕ are, respectively, the directions of the incident and transmitted waves relative to the normal at the surface of discontinuity and the ϵ_i are the respective relative permittivities.

Since the transmission line conductors are parallel to the direction of propagation of a TEM wave, it follows that the first of the above relations also describes the discontinuity of the transmission line which is appropriate to the dielectric interface. The importance of this is that, if the conductors are bent accordingly, the electric field in the interface is uniform (in a stripline; it is, of course, slightly greater at the inner conductor in coaxial geometry). This in turn, is desirable for achieving good vacuum flashover performance. If the conductors are not bent accordingly, the electric field is intensified at one or the other end of the dielectric interface, promoting breakdown. Since the field distribution obeys Laplace's equation, it is clear that electrolytic tanks may be used to aid in the design of solid/vacuum interfaces in real cases where practical constraints prevent the realization of the simple, ideal configurations.

Furthermore, as is well known, vacuum flashover performance is enhanced if the electric field at the solid/vacuum interface is directed away from the surface into vacuum. This draws electrons out, thus preventing their skipping down the surface generating an avalanche of secondaries which can lead to flashover. This condition is met if the angle between the negative polarity conductor and the interface is acute ($< 90°$). In all cases of interest here, $\epsilon_1 > \epsilon_2$ so that $\phi \geq \theta$. For $\theta = 0°$, $\phi = 0°$ and the interface is normal to the transmission line conductors. The impedance on the vacuum side of the interface is greater than that in the solid insulation. As the angle of incidence is increased by angling the interface relative to the conductors (tilting toward the negative conductor), the interface length increases, the impedance of the

vacuum line decreases and it becomes inclined to the solid line by the angle $\phi - \theta$. At the so-called Brewster angle of incidence, θ_B, given by

$$\tan \theta_B = \sqrt{\frac{\epsilon_2}{\epsilon_1}} \quad ,$$

the line impedances on both sides of the discontinuity are equal so that there is no reflection. At the Brewster angle, the electrostatic and optical relations given above are both satisified by the same angle ϕ of the transmitted wave. For angles of incidence greater than the Brewster angle, the flashover length of the vacuum/solid interface increases and the impedance of the vacuum line becomes lower than that of the solid line. As discussed previously, this kind of mismatch is desirable from a vacuum flashover standpoint.

The optical relation predicts a transmitted wave angle of 90 ° (total reflection) at the so-called critical angle which is just beyond, and quite close to, the Brewster angle. If Snell's law actually governed the energy flow across the interface, it would be extremely difficult to design it so as to avoid total reflection over portions of it. This could only be achieved by deliberately making the vacuum line higher in impedance than the solid by keeping to incidence angles well below the Brewster and critical angles. The electrostatic relation which governs the energy flow across the interface in the quasi-static approximation exhibits no such catastrophe as a critical angle close to the Brewster angle, yielding a 90 ° transmission angle only for a 90 ° incidence angle. It is thus feasible to design the interface so that the vacuum line is undermatched to the solid line. Note, however, that a very fast-rising incident wave may violate the quasi-static condition (risetime >> propagation time along the interface) and in this case, the highest frequency components of the wave may be governed by the optical relation. These components would, in general, be

totally reflected from the interface, which thus acts as a low pass filter. The transmitted wave would show a degraded risetime as a result. Another way of stating this is to say that a solid/vacuum interface designed near or beyond the Brewster angle limits the risetime of the transmitted pulse to values large compared to the propagation time along the interface. This is not a serious limitation in systems of immediate interest.

It seems appropriate to close out this discussion of energy flow with some further observations on the effects of discontinuities. One which is easily overlooked is due to the turn-on delay of the cathode. As reported later, this can be as much as 10 ns, during which time the beam load impedance is much higher than the generator impedance, resulting in an in-phase reflection. If the pulse risetime is short compared to this turn-on time, the reflection may lead to voltage doubling at the front end of the system which could overstress the tube insulator and induce vacuum flashover. This phenomenon was in fact observed during the vacuum flashover tests reported in section 3 which used a very fast rising (<5 ns) incident pulse.

This leads naturally to the general observation that the time length of any discontinuity should be short compared to pulse risetime to avoid transient voltage doubling (or reversal in case of low impedance discontinuities). In high dielectric constant (HDC) media, such as water, physically small and seemingly inconsequential discontinuities can have relatively long time lengths because of the low propagation velocity. On the other hand, risetimes in such media tend to be longer anyway because discontinuities have large associated stray capacitances which degrade rapidly an initially fast-rising pulse. These discontinuities steal energy from the pulse both dynamically through transient reflections and statically through the energy required to charge the stray capacitances to the pulse voltage. The latter is recovered as a tail at the end of the main pulse. However, since many HDC systems have overall time

length much greater than pulse length, reflections from discontinuities are effectively lost because their eventual arrival at the load, after re-reflection, occurs long after the main pulse is over. This can be a serious source of energy loss, particularly in view of the large stray capacitance discontinuities inevitable in HDC systems.

Simple calculations show that, in addition to the usual TEM reflections, large diameter coaxial HDC systems can also support higher order modes which are excited at discontinuities. For example, Neptune B will propagate $TE_{1,1}$ and $TE_{2,1}$ modes at the frequency of the second harmonic in its output pulse (the second peak in the Fourier spectrum) so that substantial amounts of excitation power are available. In addition, the four-channel version of the output switch (Switch III) has exactly the electric field symmetry of the $TE_{2,1}$ mode, which must therefore be strongly excited. The wave impedance for this mode is about ten times the impedance for the TEM mode so that it can conceivably constitute a small but significant power drain. It is a drain because the mode will not propagate through the smaller diameter transition into the tube and so cannot carry energy into the beam load, but rather saps it away into trapped oscillations.

The chief conclusions to be drawn from the last paragraphs on the influence of discontinuities on energy flow in HDC media is that systems using such media will tend to exhibit poor energy transfer efficiency and poor rise-time unless great care is taken in their design. The significant thing is that such results are probably inherent in the use of HDC media.

Diode Studies

Time-resolved voltage and current measurements were used to parametrically study diode impedance as a function of diode geometry and cathode/anode material. Optimization of diode design is important in obtaining the maximum energy transfer efficiency in a pulsed accelerator. Ideally, the diode should turn on as quickly as possible and hold a constant impedance without closing (shorting) during the pulse.

The results of the experiments can be summarized as follows:

(1) Cathode turn-on time for flat metal cathodes is approximately 10 ns. Flat carbon cathodes exhibited a turn-on time of about 5 ns.

(2) Time to gap closure is dependent on the anode material. Specifically, carbon anodes show a much longer time period of constant impedance before gap closure.

(3) For the diodes studied, Child's law did not apply. Not only was the current larger than predicted theoretically, the impedance scaling with aspect ratio (gap spacing/cathode radius) was linear and not quadratic.

The results of the diode program are detailed in section 2.4.

2.2 Experimental Investigation of the Pulse Transmission Properties of Field-Emission Tubes

2.2.1 Introduction

The purpose of this study was to gather experimental data pertaining to the pulse transmission characteristics of hollow dielectric tubes for electromagnetic pulses with risetimes in the sub-nanosecond region, travelling in the general direction of the tube axis, but penetrating the tube wall from the region external to the tube to the region inside the tube. The experimental data will be used later in an effort to find a simple and practically useful model consisting of lumped circuit elements and/or transmission line pieces which can adequately describe the tube and its immediate surroundings as they may appear in a typical flash x-ray machine, electromagnetic pulser, electron-beam machine or similar equipment.

The tubes studied are of roughly 12-inch OD and 8-inch ID and ranging in length from approximately 4-inches to about 2 feet. They are either constructed entirely of dielectric material or of a succession of dielectric and metal rings. The metal rings are flat and spaced at constant intervals along the tube, these being approximately 1-inch, 2-inches or 3-inches. The dielectrics investigated are styrofoam, lucite and Corning glass No. 7740 with relative dielectric constants of 1, 2.6, and 4.5, respectively. Two aspects of the pulse transmission characteristics are investigated here, namely, the risetime degradation of an incident step voltage pulse and the pulse propagation velocity along the tube axis.

The test bed which serves to launch a TEM wave into the region occupied by the tube and to re-establish a TEM wave beyond the tube, is designed with a view to minimizing its transmission-line discontinuities, except in the region of the tube where its geometry is kept as simple as possible. This ensures that the incident pulses are approximately step pulses with sufficiently fast risetimes. The wave impedance of the test bed input and output lines is chosen to be 40 ohms for the following reason. Since this study is ultimately aimed at finding a physically meaningful model for the tube and tube region, i.e.,

in particular, one that is independent of the parameters of the structures surrounding the tube and tube region and therefore of the most general applicability, it is important to choose a test bed that is not a priori expected to obscure significant characteristics of the tube under study. Assuming that an adequate tube model can be constructed with capacitances and inductances, a test bed of very low wave impedance would have this fault as would one of very high impedance. The former would cause electric stray fields (capacitances) to charge up very quickly and inductive fields to develop very slowly, with the result that the capacitive character of the structure tested would be obscured by its inductive character, the latter would cause the opposite situation to prevail, making the structure appear capacitive and yielding no information about any inductive behavior which may turn out to be significant under somewhat different conditions. A test bed which is to give information about both the inductive and the capacitive nature of the tube should therefore be of intermediate impedance. What constitutes "intermediate" in this case depends, of course, on the values of the capacitances and inductances to be expected in the model. These can only be estimated very roughly since they are complicated functions of the geometry of the tube and tube region, but they may be expected to be of the order of 20 to 40 pF and 15 to 30 nH, respectively, for a tube approximately 4-inches long and perhaps 40 to 60 pF and 90 to 180 nH for a tube approximately 2 feet long. In order to have equal inductive and capacitive time constants one must satisfy the condition $Z = (L/C)^{1/2}$, where Z is the line wave impedance. This in turn results in desired line impedances of 40 to 70 ohms for a long tube and 20 to 40 ohms for a short tube. A line wave impedance of about 40 ohms thus appears to be the choice that will result in the greatest yield of experimental information.

2.2.2 Experimental Apparatus

The test bed is shown schematically in Figure 2-1 and in photographs in Figures 2-2 and 2-3. It consists of a coaxial, cylindrical transmission line with a straight, tapered input section and a section in which the diameter of the line is reduced sufficiently to permit insertion of the tube under test, with its axis on the test bed axis and its end surfaces resting against the flat portions of

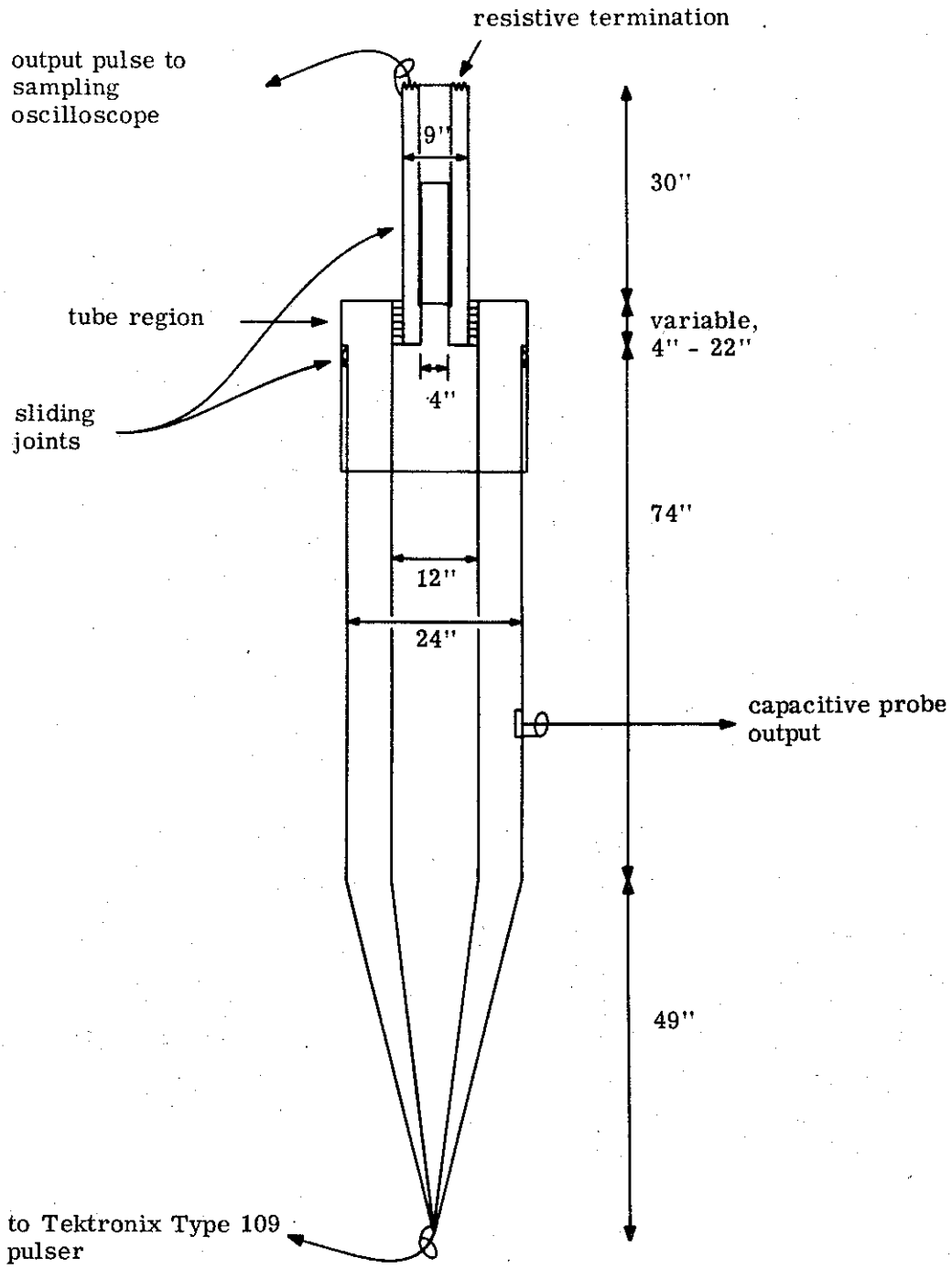

Figure 2-1. Schematic representation of tube studies test bed.

1-4384

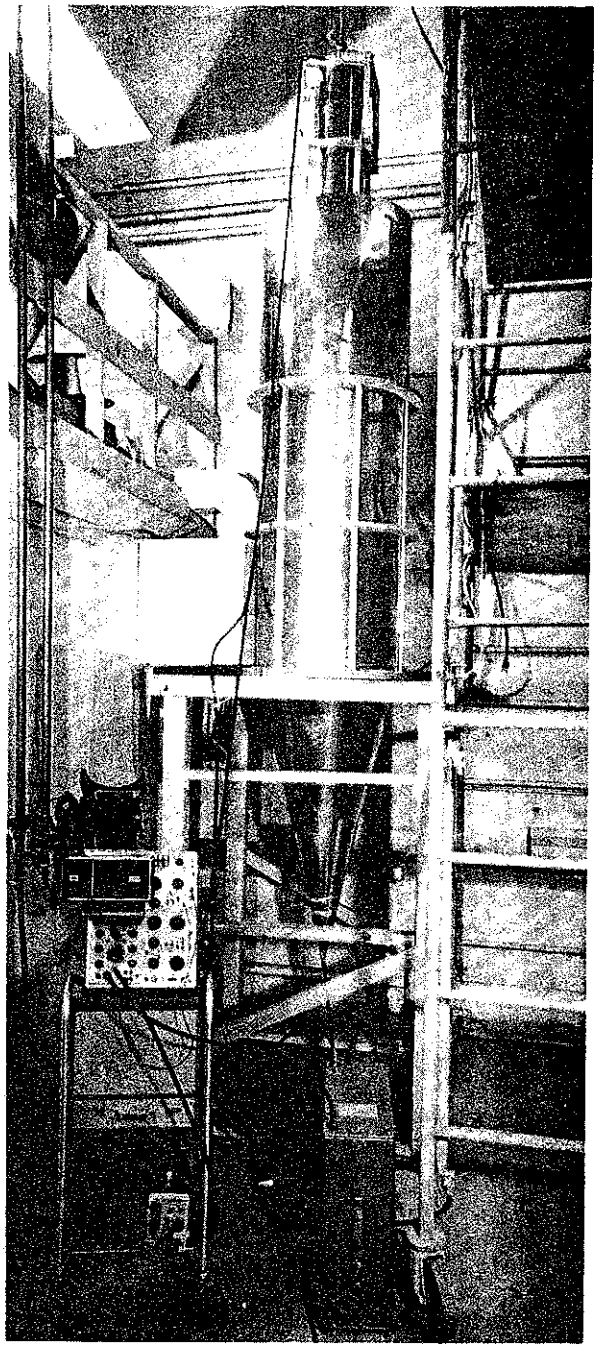

Figure 2-2. Tube Test Bed

2-1470

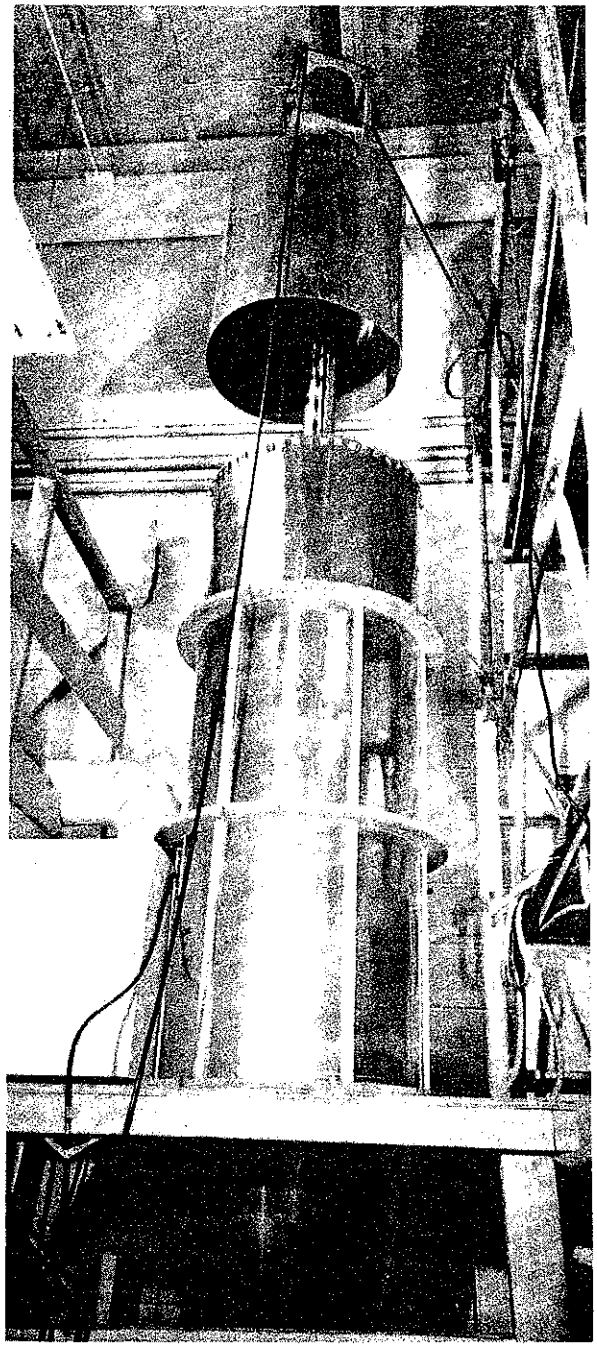

Figure 2-3. Tube Test Bed Open for Tube Modification

2-1471

the inner and outer conductors of the line, respectively. The small-diameter part of the test bed ends in a matched resistive termination. The wave impedance of the test bed is approximately 40 ohms both before and after the tube region. The tube region is shown in detail in Figures 2-4 and 2-5 and the various tube building blocks can be seen in Figure 2-6. Both the inner and outer conductors of the test bed consist of two parts, with sliding joints to permit easy removal of the test bed front end for tube modification. The outer conductor joint is located ahead of the tube and can be seen in Figures 2-3, 2-4 and 2-5, which also show the flexible sheet-metal tabs used to ensure good sliding contact. The inner conductor joint (see Figure 2-5) is located just beyond the tube region. Here the first half of the inner conductor fits snugly inside the second half; a conducting lubricant is used to reduce friction.

The test bed is positioned vertically as shown in Figure 2-2, since horizontal positioning would require quite an elaborate structure to support the heavy tube (up to more than 100 lbs.) in cantilever and still permit easy assembly, disassembly and alignment of the tube. The upper part of the test bed can be hoisted up to give access to the tube region for tube modification (see Figure 2-3).

A Tektronix Type 109 fast pulser is used as pulse source. A 5-foot length of RG-8 low-loss cable leads to a carefully constructed transition section and tapered input cone. A capacitive probe is located on the inside of the outer conductor of the test bed between the tapered input section and the tube region. This probe permits driving-pulse monitoring and can also supply either oscilloscope triggering signals or reference pulses for propagation-velocity measurements. The resistive termination consists of approximately 240 resistors (almost one per square centimeter of area) mounted between five one-half-inch long flat copper rings, located concentrically and spaced so as to coincide with the proper equipotential surfaces of a transmission-line wave on the test bed. About 10% of the line voltage is sampled by a resistive divider built into the termination and fed via RG-8 cable to the Tektronix sampling oscilloscope used to monitor the output pulses. A close-up photograph of the termination is shown in Figure 2-7, and Figure 2-8 shows the termination in place on top of the test bed. This termination alone has a risetime between 10% and 90% amplitude

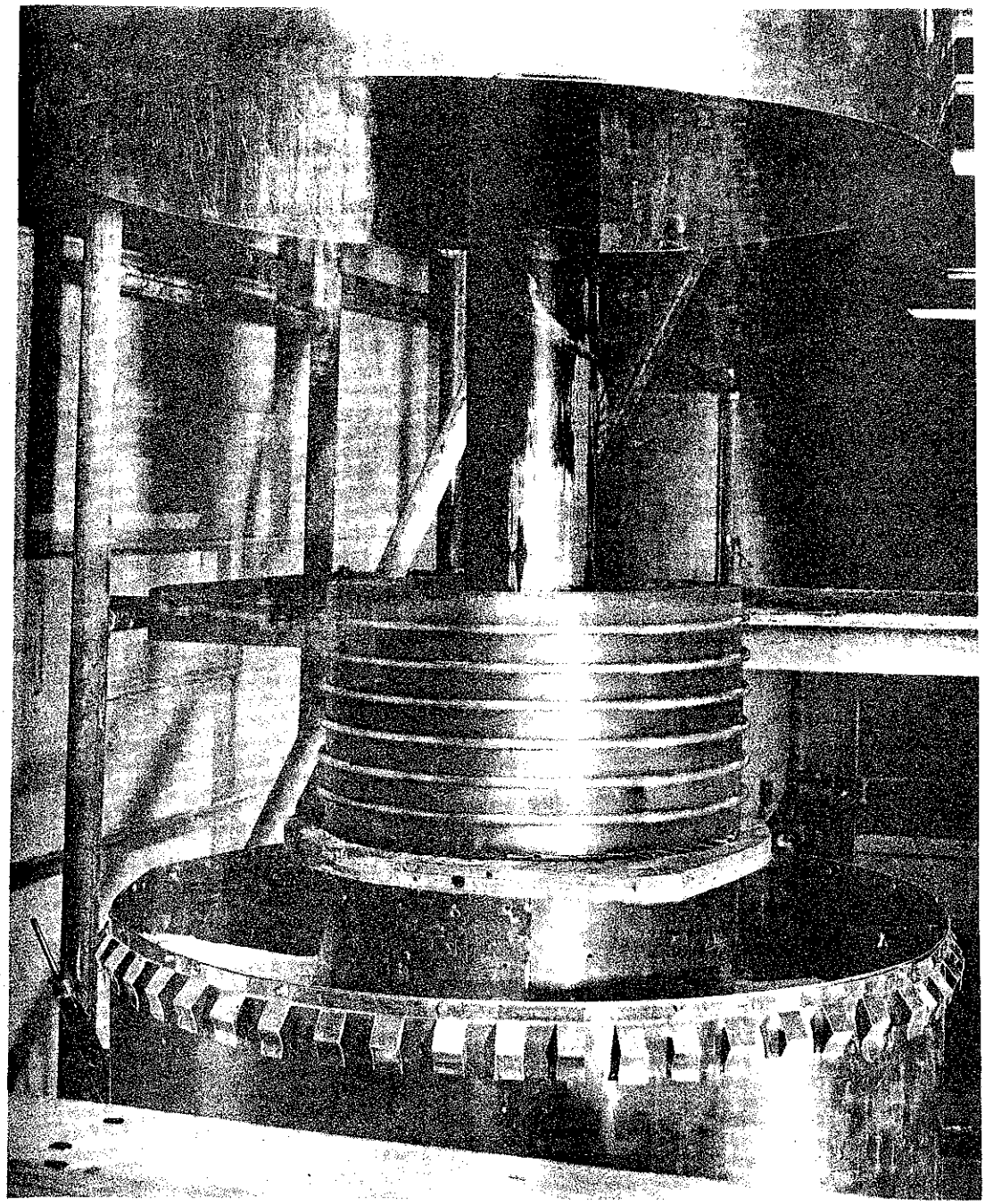

Figure 2-4. Tube Installed in Test Bed
Note: Ring stack is approximately 12" diameter.

2-1472

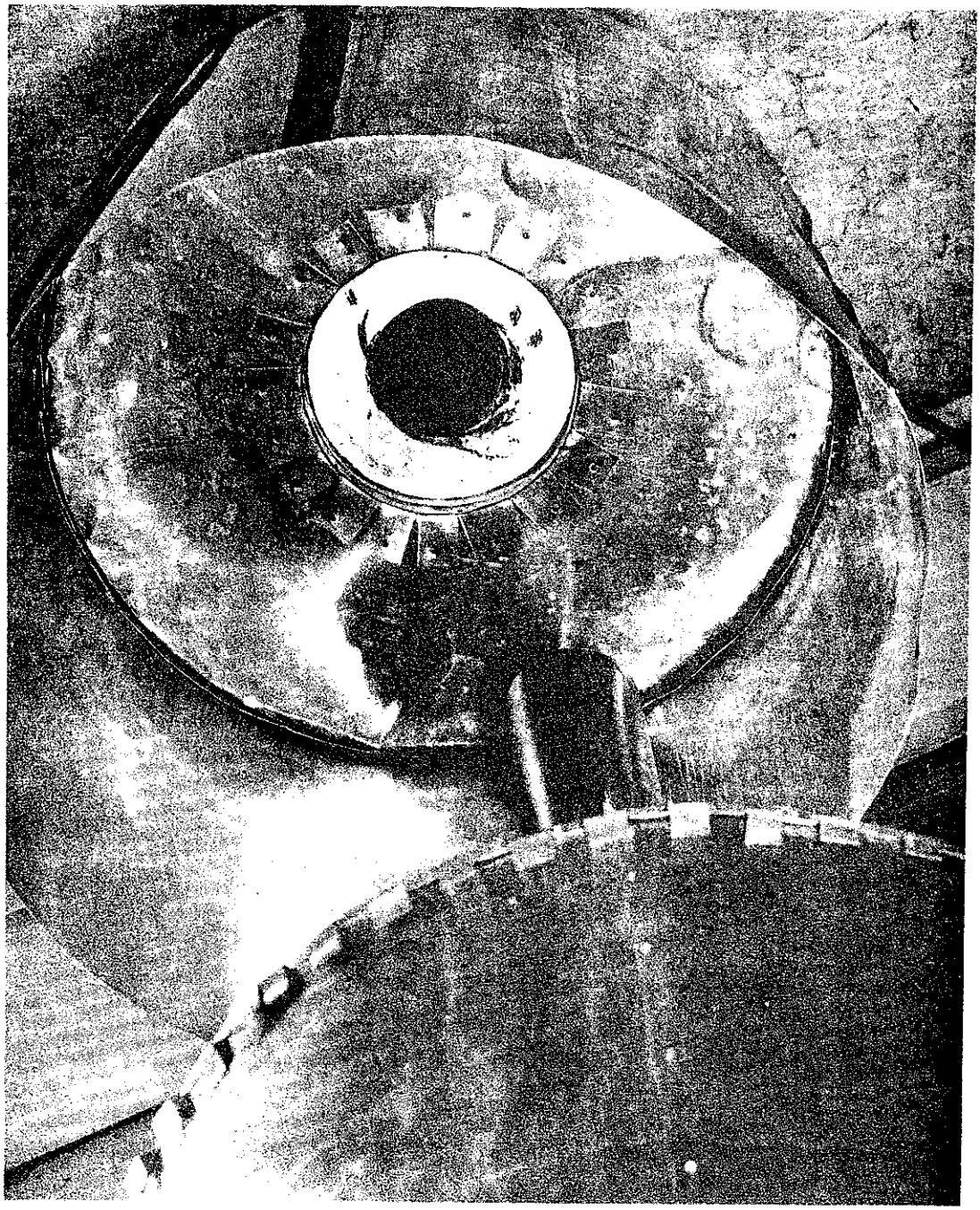

Figure 2-5. Detail of the Test Bed Tube Region, Looking Up Inside the Top Part of the Test Bed

2-1473

Figure 2-6. The Various Tube Building Blocks

2-1474

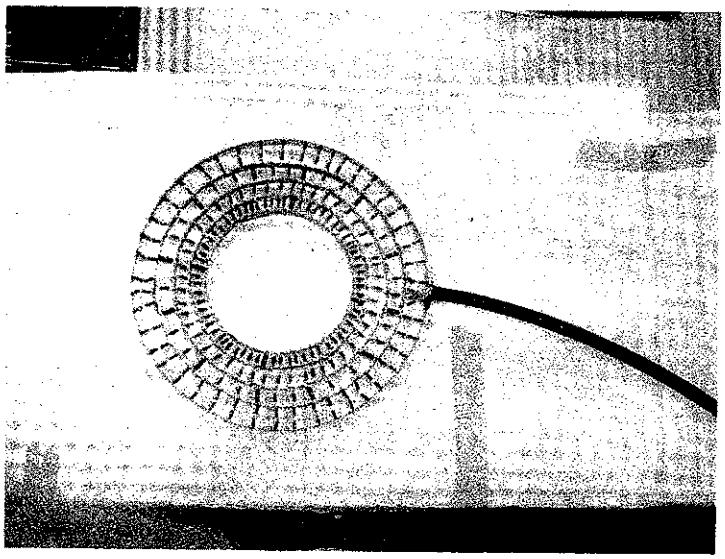

Figure 2-7. The Resistive Termination and Resistive-Divider Output Probe

2-1475

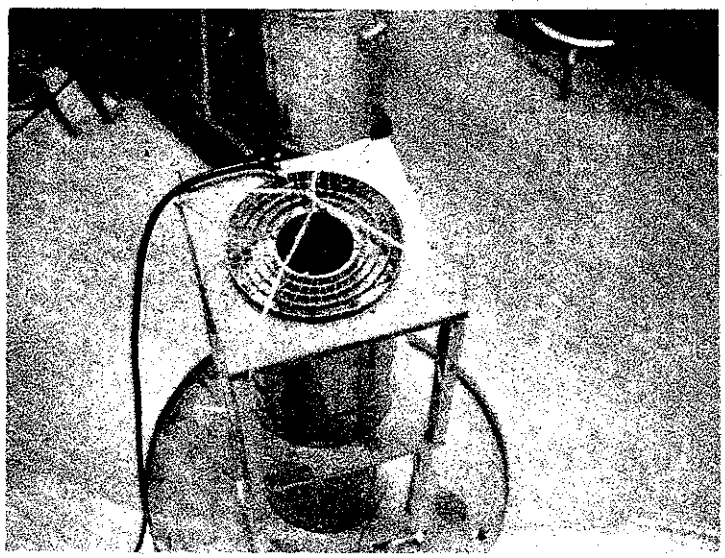

Figure 2-8. The Resistive Termination in Place on Top of The Test Bed

points of about 400 ps and exhibits almost no overshoot. The performance of the termination and the diagnostic equipment in general is discussed more fully in section 2.2.3.

A time-domain reflectometry (TDR) trace of the test bed with matched termination is shown in Figure 2-9. The extreme left-hand portion of the trace corresponds to the 52 ohm RG-8 input cable. This is followed by a fairly smooth transition to an indicated 33 ohms at the beginning of the input taper, the impedance increasing to about 39 ohms in the cylindrical section of the test bed ahead of the tube region. Then there is a peak indicating the existence of the high-impedance tube region, which is approximately 4-inches long and has a calculated impedance of about 100 ohms. Following this, one can see the small-diameter cylindrical portion of the test bed, with an indicated impedance of about 44 ohms. Finally, the resistive termination appears as an infinite transmission line of impedance 38 ohms. It is obvious from the TDR picture that the high-impedance tube region registers a much too low impedance in this picture and that the small-diameter section of the test bed shows up as a higher impedance than it should according to calculations. This is because the TDR pulse has a risetime of about 1 ns and cannot quite resolve impedances separated by less than about one-half foot, which is more than the length of the tube region in this picture. (The fast-pulse mode of the TDR unit which would give better spatial resolution, cannot be used for a line of as large a diameter as the test bed, since the fast pulse will cause excitation of waveguide modes rather than the desired transmission-line mode.)

The test bed as described above is capable of propagating a sufficiently fast pulse towards the tube region. Figure 2-10 shows this input pulse as monitored by the capacitive probe. The pulse risetime between 10% and 90% amplitude points is seen to be about 400 ps. The test bed is also convenient for the present experiment involving study of a large number of different tube configurations, as it can be opened up, the tube modified and the test bed reassembled, all in a matter of minutes.

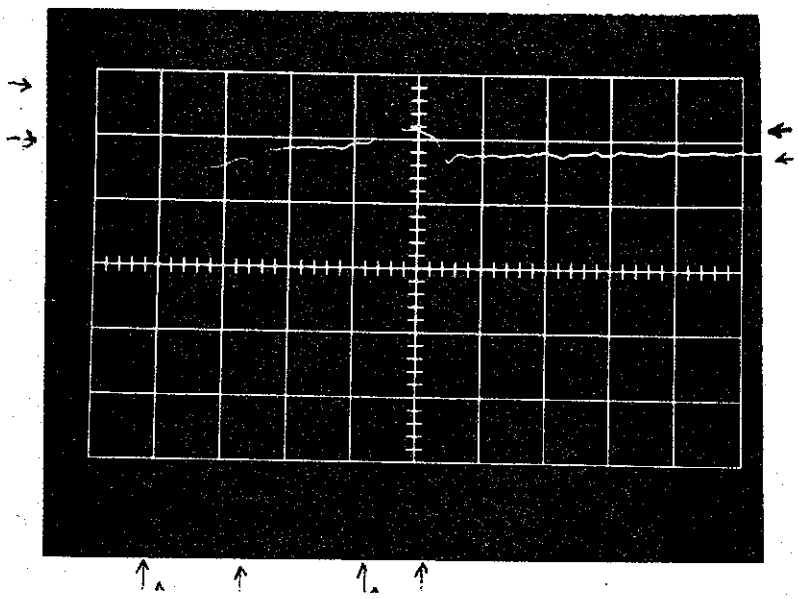

Figure 2-9. Time-Domain Reflectometry Trace of The Test Bed with Matched Resistive Termination and 52 Ohm Input Cable

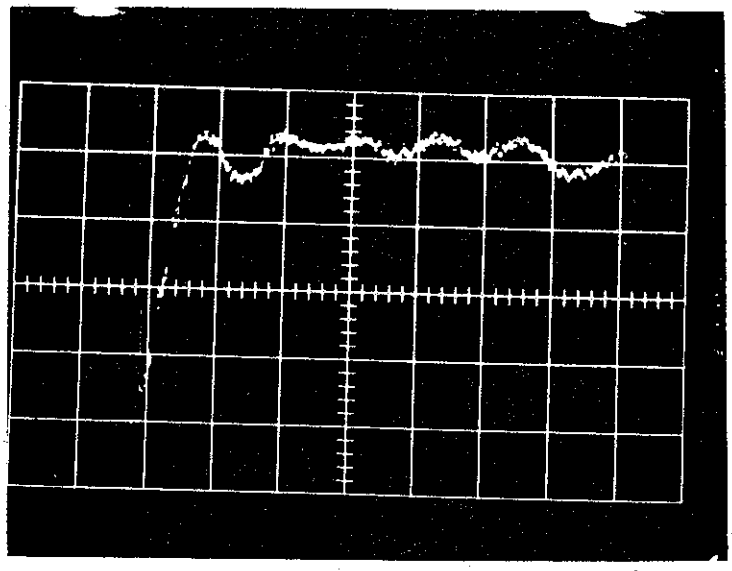

Figure 2-10. Capacitive Probe Output
Showing The Front of The Pulse
Incident on The Tube Region
Vertical Sensitivity: 5 mV/div
Horizontal Sensitivity: .5 ns/div

2-1478

2.2.3 Performance of the Resistive Termination and General Electronic Equipment

Originally, a ten-point resistive star was built to serve as matched termination for the test bed and to sample its output voltage by means of a 100 : 1 resistive divider. The step response of this device is shown in Figure 2-11. A large overshoot followed by damped oscillations mask the risetime information completely. This is probably due to the small fraction of the line voltage sampled as well as to the small number of resistors used in the termination, which cause significant amounts of stray capacitance and inductance.

The 240-element resistive termination that was built to replace the ten-point star (see Figure 2-7) performs very well. This is probably due in part to the greater number of resistors and in part to the increased amount of voltage sampled (about 10% of total line voltage, rather than the previous 1%). The test bed built to check out the termination and the general electronic equipment is shown in Figure 2-12. It differs from the tube test bed in that it does not include a large-diameter coaxial line and a discontinuous tube region.

Figure 2-13 shows the step response of a system consisting of the Tektronix 109 pulser, an eight-foot length of RG-8 cable, and the Tektronix sampling oscilloscope. Figure 2-14 shows the output from the capacitive probe of the termination test bed when the latter is driven by the Tektronix pulser. It appears from a comparison between Figures 2-13 and 2-14, that the test bed input taper does not cause noticeable risetime degradation. Figure 2-15 shows the step response of a system consisting of the pulser, input cable, termination test bed, resistive termination, short (2.5 feet) output cable and oscilloscope. The risetimes are about 340 ps between 20% and 80% amplitude points and about 550 ps between 10% and 90% amplitude points. Finally, Figure 2-16 shows the step response of a system which differs from the one of Figure 2-15 only by having a longer output cable (20 feet instead of 2.5 feet). The risetime between 20% and 80% amplitude points has increased by about 25% to 420 ps, while the 10% to 90% risetime has doubled to 1.12 ns.

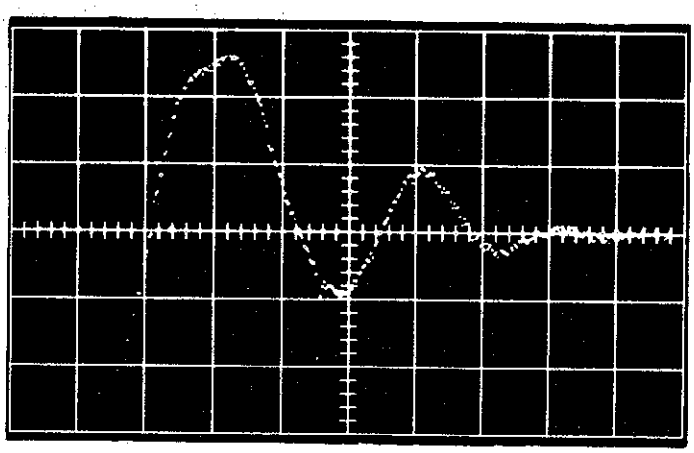

Figure 2-11. Step Response of a
10-Point Resistive Star
Vertical Sensitivity: 200 mV/div
Horizontal Sensitivity: .5 ns/div

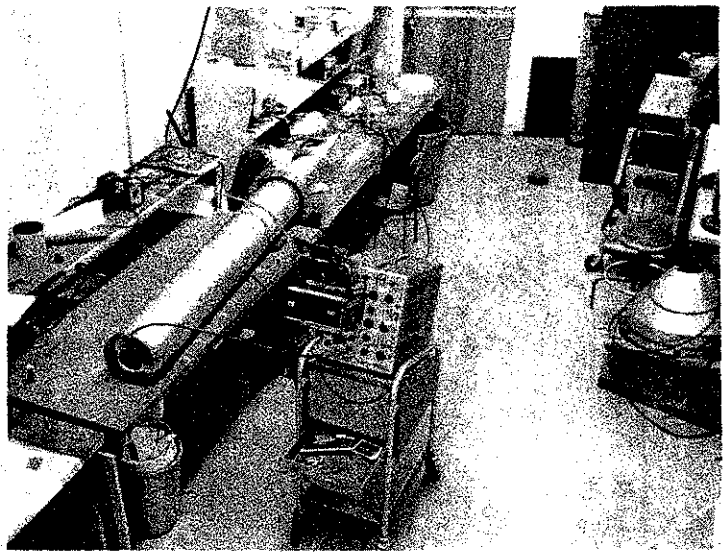

Figure 2-12. Test Bed for the Matched Resistive Termination

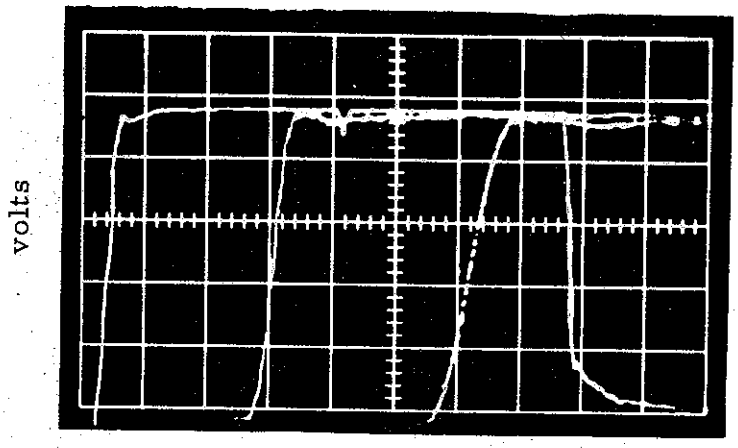

Figure 2-13. Step Response of Pulser, Cable and Oscilloscope
Vertical Sensitivity: 200 mV/div
Horizontal Sensitivity: 5, 1 and 0.5 ns/div (left to right).

2-1488

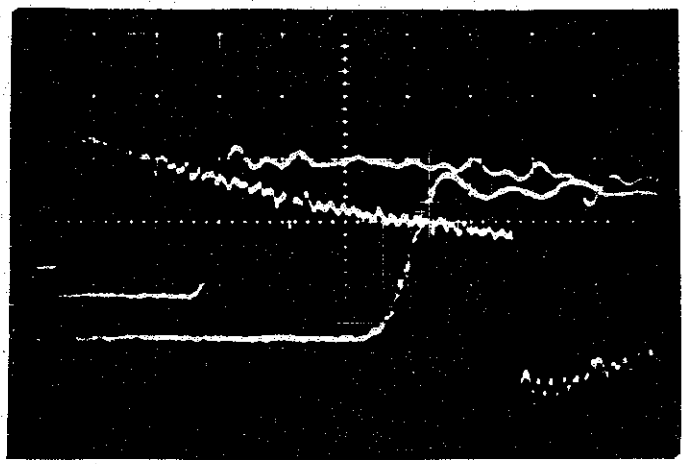

Figure 2-14. Output from the
Capacitive Probe of the
Termination Test Bed
Vertical Sensitivity: 10 mV/div
Horizontal Sensitivity: 5, 1
and 0.5 ns/div (left to right).

2-1489

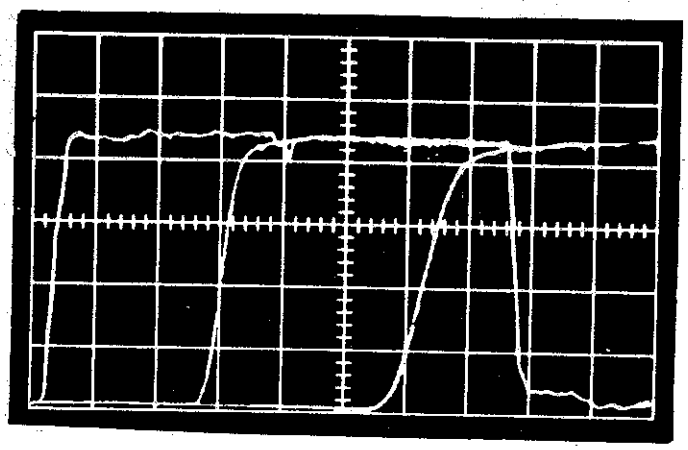

Figure 2-15. Step Response of Pulser, Cable, Test Bed, Resistive Termination, Short Cable and Oscilloscope
Vertical Sensitivity: 200 mV/div
Horizontal Sensitivity: 5, 1 and 0.5 ns/div (left to right)

2-1490

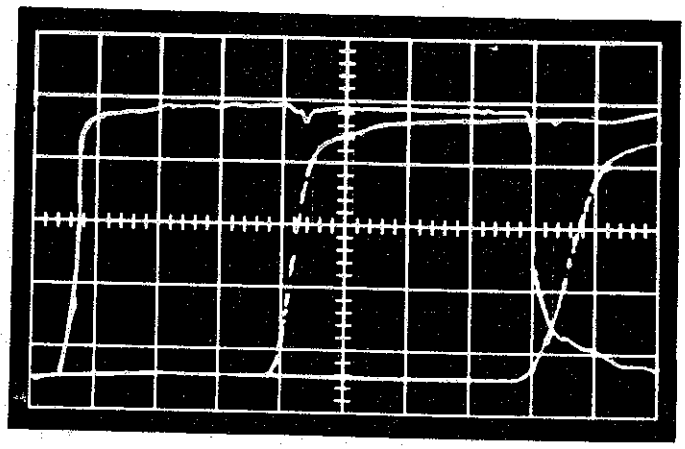

Figure 2-16. Step Response of
Pulser, Cable, Test Bed, Resistive
Termination, Long Cable and
Oscilloscope
Vertical Sensitivity: 200 mV/div
Horizontal Sensitivity: 5, 1
and 0.5 ns/div
(left to right)

2-1491

These pictures show that the resistive termination itself is very fast, with a 10% to 90% risetime of about 400 ps, but that the 20-foot long output cable reaching from the top of the tube test bed down to the laboratory floor, although fast for measurements of 20% to 80% risetimes, is relatively slow to reach 90% amplitude. In order to achieve maximum accuracy of the experimental results it is therefore necessary to correct for the response of the diagnostic equipment. This is especially important when a long output cable is used (Figure 2-16) but is also necessary even when a much shorter output cable is employed, due to the slow rise of the step response (see Figure 2-15) between about 95% and 100% amplitude, which will noticeably affect a step pulse for at least the first two nanoseconds. Fortunately, it is a relatively simple matter to arrive at a first-order correction for the diagnostics response in the case of smooth output pulses, as shown in Section 2.2.5.

2.2.4 Experimental Procedures and Results

The tubes tested are constructed of rings of styrofoam, lucite or Corning glass No. 7740, the number of rings being increased gradually through a test sequence so that tubes of increasing lengths are produced, the shortest being just over 4-inches long, the longest almost 2 feet. This is done first using dielectric rings only, then the sequence is repeated using flat metal rings as well as dielectric rings in making up the tube. First, one metal ring is inserted for roughly every three inches of dielectric, then the sequence is repeated with one metal ring for every two inches of dielectric, and finally with one metal ring for every inch of dielectric. In all about 50 different tube configurations are tested, varying with respect to length, dielectric material and spacing of the metal rings. The various components making up these tubes can be seen in Figure 2-6.

The tube step responses for transmission are detected at the resistive termination of the test bed. Using the storage capability of the Tektronix oscilloscope, three exposures of the output pulses are made, with horizontal sensitivities of 0.5 ns/div, 1 ns/div and 5 ns/div. The same type of pictures are taken throughout the test sequences with no tube in the tube region; these

give the response of the 4-inch long discontinuity region of the test bed and serve as a rough check on the working condition of the experimental apparatus.

Originally, it was intended to use these triple exposures to gain information about pulse propagation velocity along the tube as well as about pulse risetimes, by observing the gradual displacement of the pulses towards the right on the oscilloscope screen as the tubes were lengthened, using the picture corresponding to the 4-inch long, airfilled test bed discontinuity as reference. This could not be done, however, due to what appeared to be a random drift in the horizontal positioning of the pulses on the oscilloscope screen, a drift which amounted to as much as 600 ps. Instead, the velocity-of-propagation measurements were repeated with a slightly different experimental arrangement in which the signal from the capacitive probe in the test bed is fed through a small, variable series capacitor and an adder at which point it is superposed on the output signal from the resistive termination. With the capacitive probe cable length and the variable series capacitor properly adjusted a small reference pulse is produced on the oscillosoope screen, two nanoseconds or so before the arrival of the output pulse for the shortest tubes tested. These test sequences make possible accurate relative transit-time measurements, again using the no-tube configuration of the test bed as reference.

Figures 2-17 through 2-22 show six picture sequences, each sequence corresponding to one tube type but with increasing tube length through the sequence. Because of the general similarity of the picture sequences only these six are shown here; the graphs which follow, however, are produced using the entire body of experimental data (10 picture sequences).

The first two sequences (Figures 2-17 and 2-18) use styrofoam dielectric ($\epsilon_r \approx 1$). The first of these corresponds to a tube consisting of foam only, the second to a tube with foam and metal rings, the metal rings being of the type shown in Figure 2-6 and spaced 1.16-inches apart.

The next two sequences (Figures 2-19 and 2-20) show data for lucite tubes ($\epsilon_r = 2.6$ at 10 MHz), the first sequence again corresponding to a pure lucite tube, the second one corresponding to alternate lucite and metal rings, with the metal rings spaced 2.88-inches apart. The lucite rings are as shown

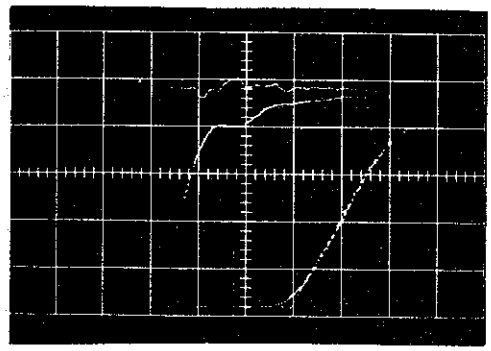

(a) No Tube. Length of Discontinuity Region: 4 Inches

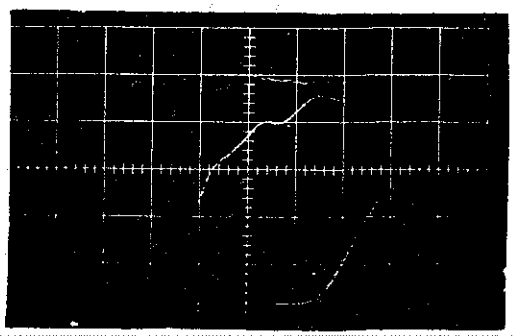

(b) Tube Length: 8.2 Inches

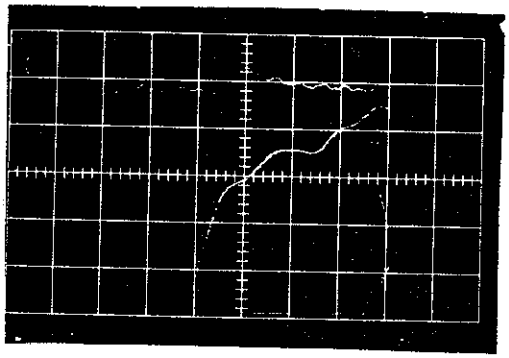

(c) Tube Length: 16.4 Inches

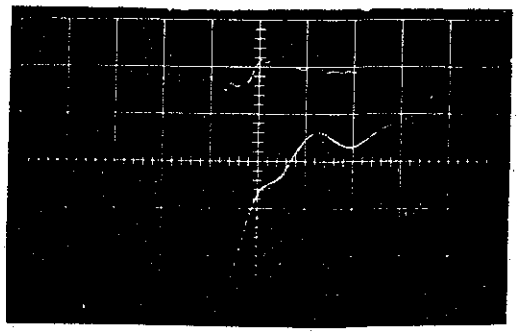

(d) Tube Length: 22.5 Inches

Figure 2-17. Step Response of Styrofoam Tubes
Vertical Sensitivity: 200 mV/div
Horizontal Sensitivity: 5 ns/div, 1 ns/div and .5 ns/div (left to right in all photographs).

2-1479

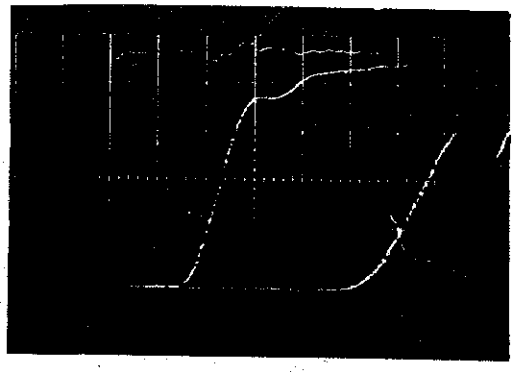

(a) No Tube. Length of Discontinuity Region: 4 Inches

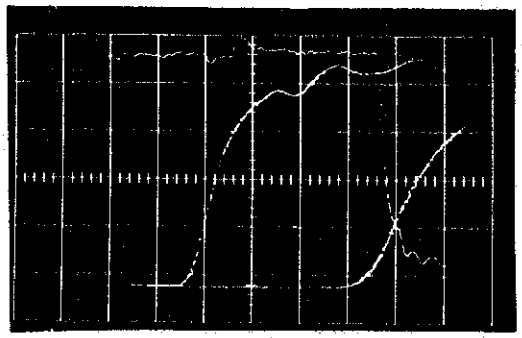

(b) Tube Length: 6.8 Inches

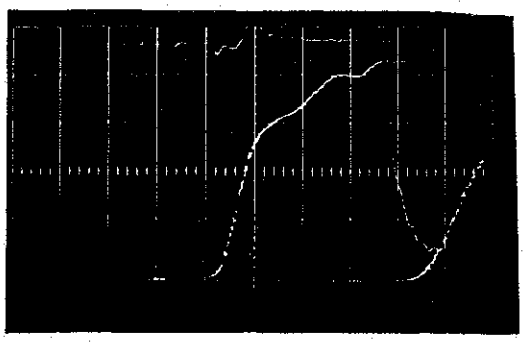

(c) Tube Length: 10.3 Inches

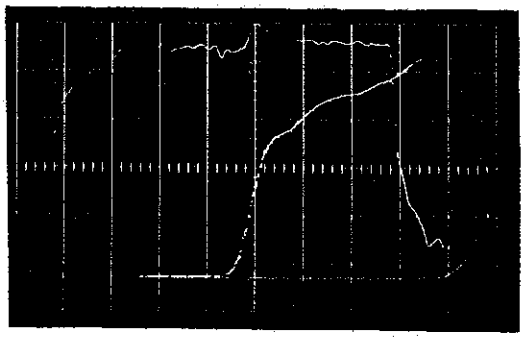

(d) Tube Length: 13.8 Inches

Figure 2-18. Step Response of Metal-and-Styrofoam Tubes
Metal Ring Separation: 1.16 Inches
Vertical Sensitivity: 200 mV/div
Horizontal Sensitivity: 5 ns/div, 1 ns/div and .5 ns/div (left to right in all photographs).

2-1480

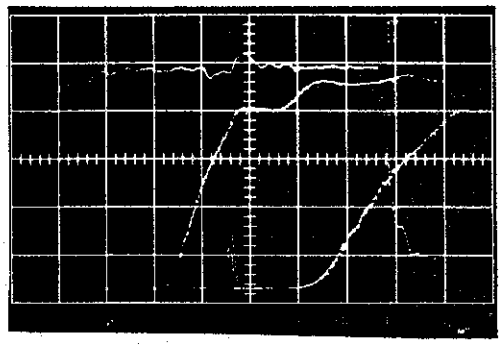

(a) Tube Length: 6.4 Inches

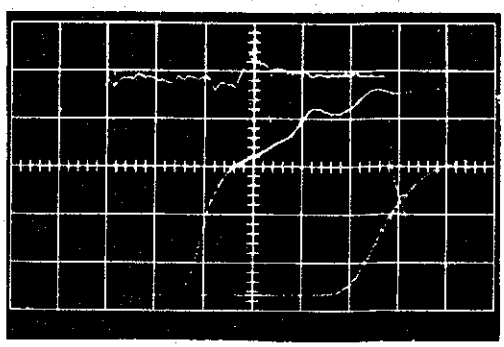

(b) Tube Length: 12.7 Inches

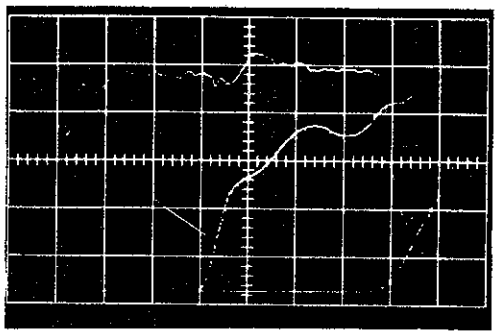

(c) Tube Length: 19 Inches

Figure 2-19. Step Response of Lucite Tubes
Vertical Sensitivity: 200 mV/div
Horizontal Sensitivity: 5 ns/div, 1 ns/div and .5 ns/div (left to right in all photographs).

2-1481

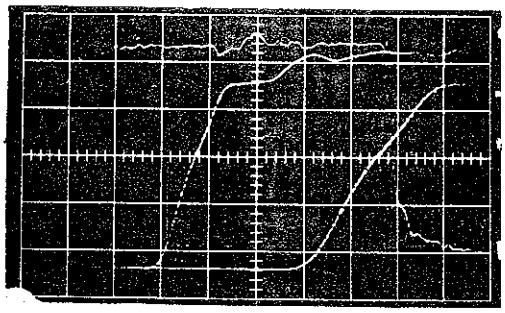

(a) Tube Length: 5.6 Inches

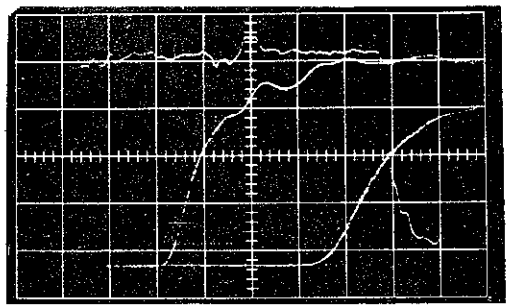

(b) Tube Length: 8.5 Inches

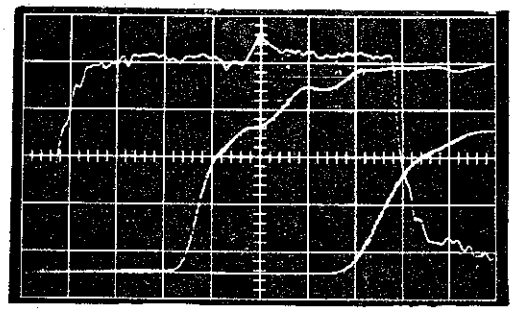

(c) Tube Length: 11.3 Inches

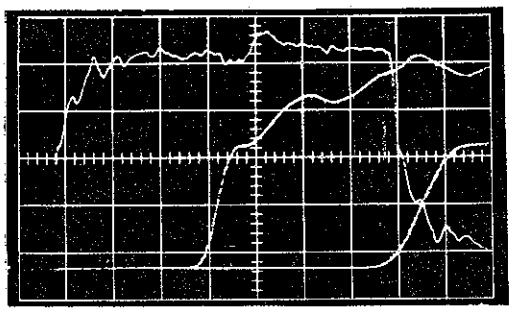

(d) Tube Length: 17.2 Inches

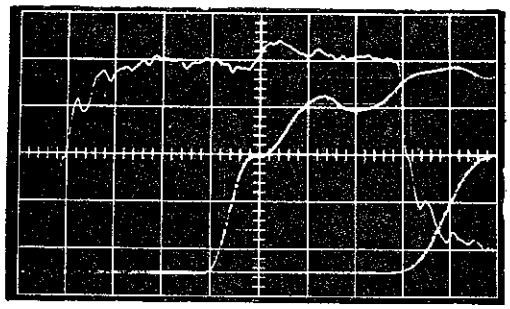

(e) Tube Length: 20 Inches

Figure 2-20. Step Response of Metal-and-Lucite Tubes
Metal Ring Separation: 2.88 Inches
Vertical Sensitivity: 200 mV/div
Horizontal Sensitivity: 5 ns/div,
1 ns/div and .5 ns/div
(left to right in all
photographs).

2-1482

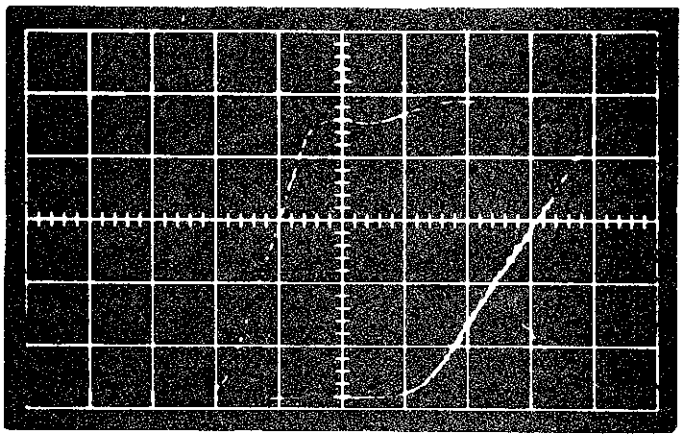

(a) Tube Length: 5.6 Inches

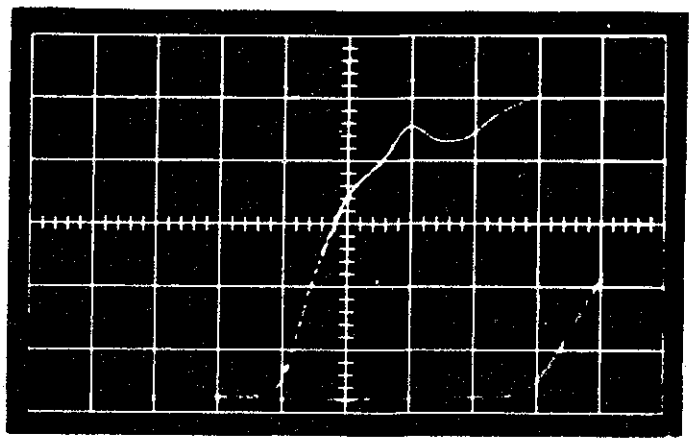

(b) Tube Length: 9.3 Inches

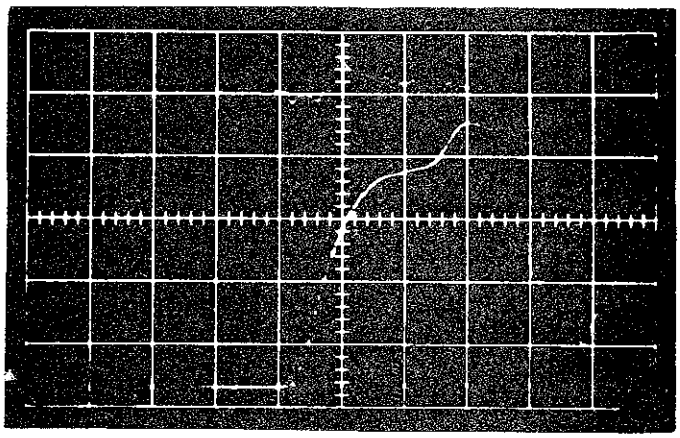

(c) Tube Length: 12.9 Inches

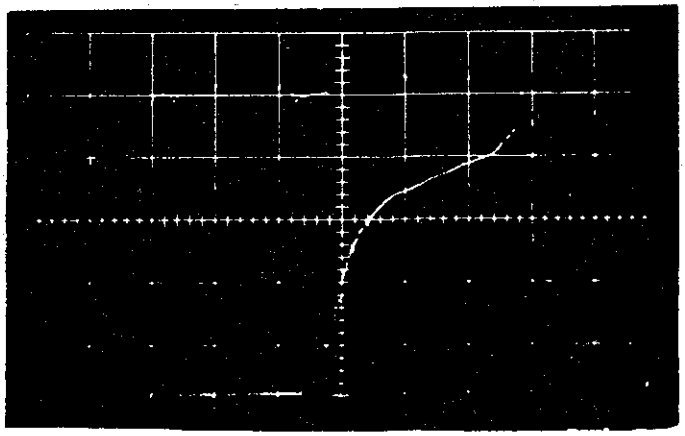

(d) Tube Length: 16.7 Inches

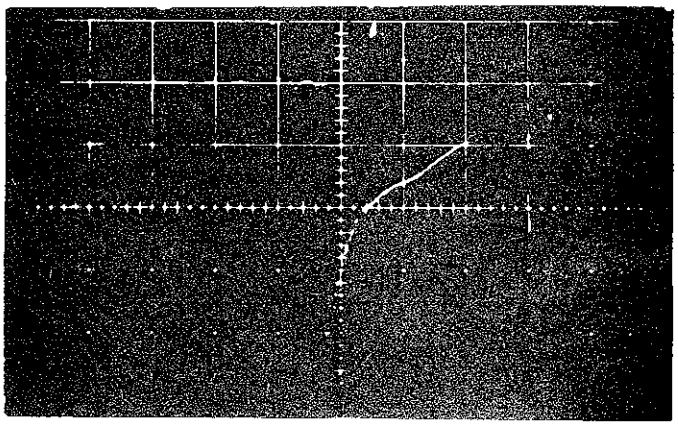

(e) Tube Length: 19.5 Inches

Figure 2-21. Step Response of Glass Tubes
Vertical Sensitivity: 200 mV/div
Horizontal Sensitivity: 5 ns/div, 1 ns/div and .5 ns/div (left to right in all photographs).

2-1483

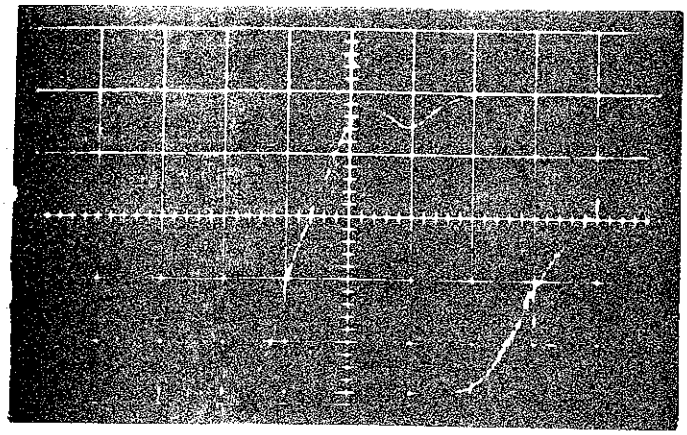

(a) Tube Length: 6.2 Inches

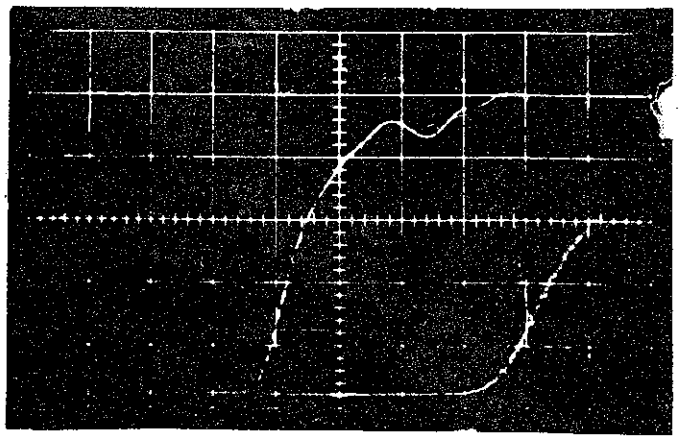

(b) Tube Length: 8.3 Inches

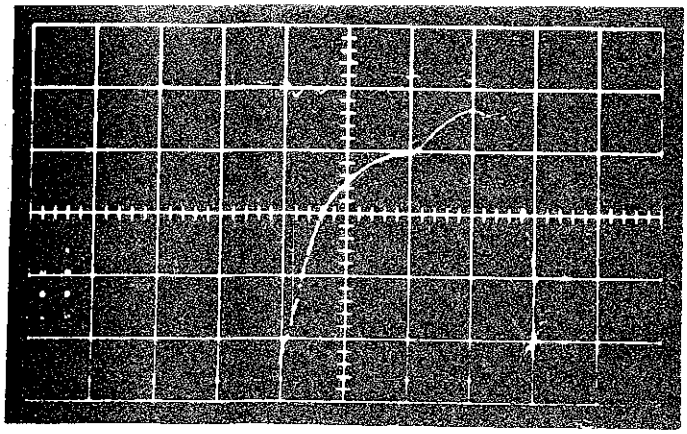

(c) Tube Length: 12.7 Inches

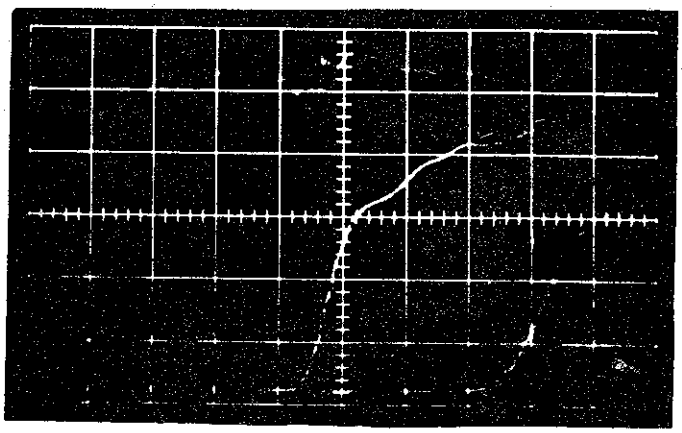

(d) Tube Length: 16.9 Inches

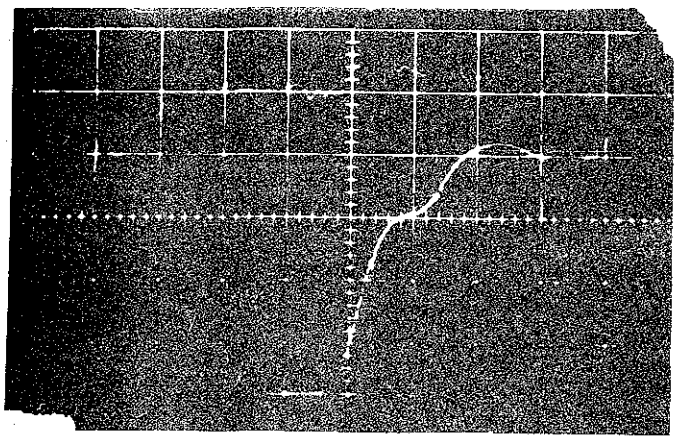

(e) Tube Length: 21.4 Inches

Figure 2-22. Step Response of Metal-and-Glass Tubes
Metal Ring Separation: 2.17 Inches
Vertical Sensitivity: 200 mV/div
Horizontal Sensitivity: 5 ns/div,
1 ns/div and .5 ns/div
(left to right in all photographs).

2-1484

in Figure 2-6, with an outer diameter of 12.5-inches and inner diameters of 8.5-inches and 10.25-inches at the small end and large end, respectively, of the tapered inside wall.

The final two sequences (Figures 2-21 and 2-22) correspond to Corning glass No. 7740 which has a relative dielectric constant of $\epsilon_r \approx 4.5$ at 10 MHz. Already existing glass rings were used; these are larger than the lucite rings and also of somewhat different shape, see Figure 2-6. Their outer diameter is 13.875-inches, the inner diameter is 11-inches. The glass pictures thus refer to a somewhat wider tube than do the lucite pictures. However, in the graphs below, the glass curves have been scaled down in both space and time by a factor of 0.9 to yield data corresponding to glass tubes of a diameter roughly equal to that of the lucite tubes. The validity of this scaling was verified experimentally using a few small glass tubes that were available of lucite size and shape (Figure 2-6). Results obtained with the resulting short, small-diameter glass tubes were scaled in space and time by a factor of 1.1 and found to be equal to those obtained with the large-diameter tubes of corresponding lengths, within the accuracy of the experiment; not a surprising result.

The first of the glass tube sequences again refers to a tube made without metal, the second sequence corresponds to a glass and metal tube with the metal rings 2.17-inches apart. (For the graphs this becomes 1.95-inches because of the scaling.)

As can be seen from the photographs, a tube of a certain length has roughly the same response regardless of its dielectric constant and whether or not it has metal rings in it. The oscillatory component of the response causes some difficulties in the interpretation of the data for risetime determination, as explained in section 2.2.5. Therefore, two sets of risetime curves are plotted. First, curves giving the risetimes between 20% and 80% amplitude points are shown in Figures 2-23 through 2-25. These are not corrected for the response of the diagnostic equipment and are intended mainly to exhibit the similarity of the pulses with regard to these risetimes. Next, risetimes between the 10% and 90% amplitude points are plotted in Figures 2-26 through 2-28. These are the result of a rough averaging of the oscillations present on the pulse fronts so as

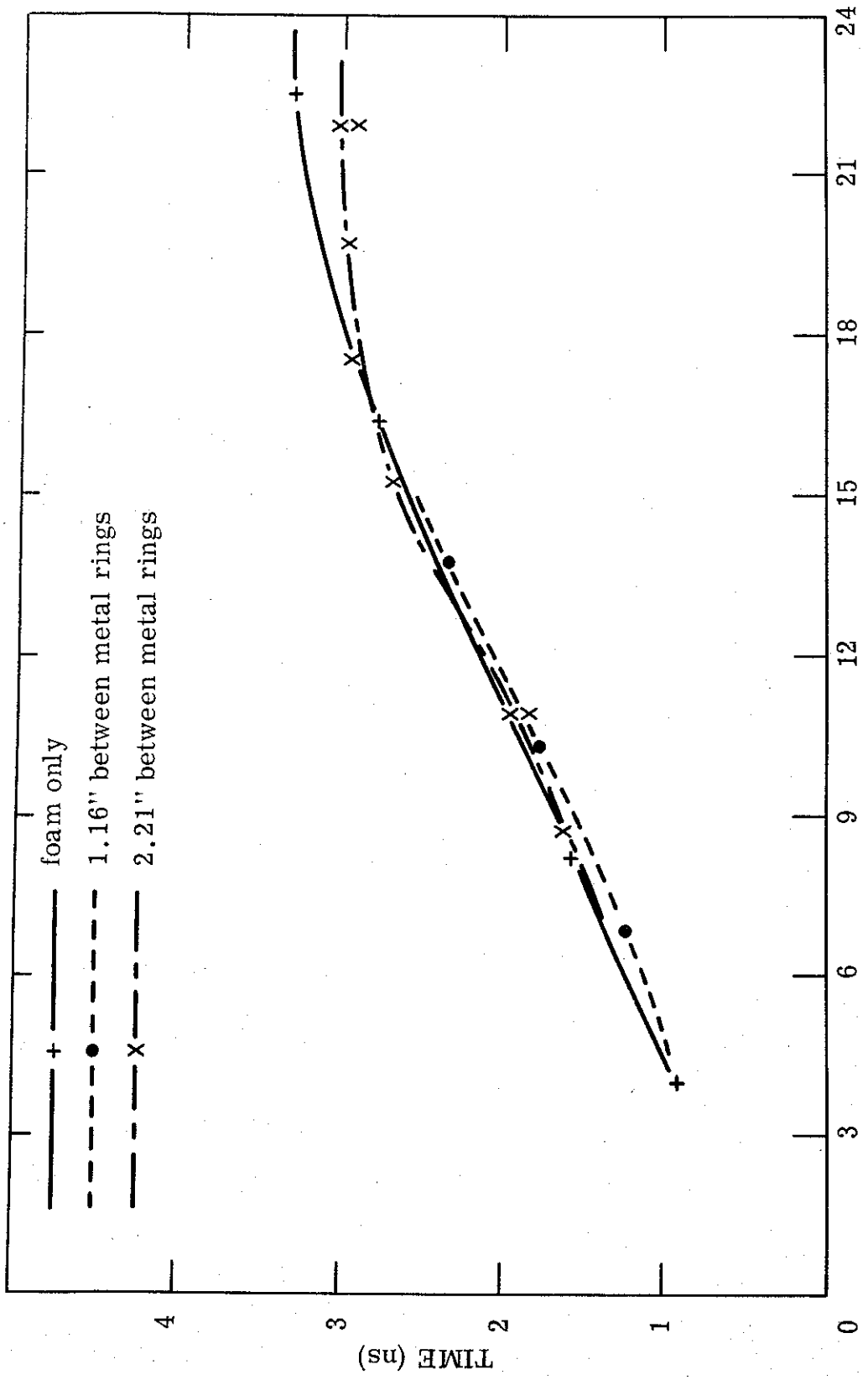

Figure 2-23. Uncorrected 20% - 80% Risetimes for Styrofoam Tubes.

1-4385

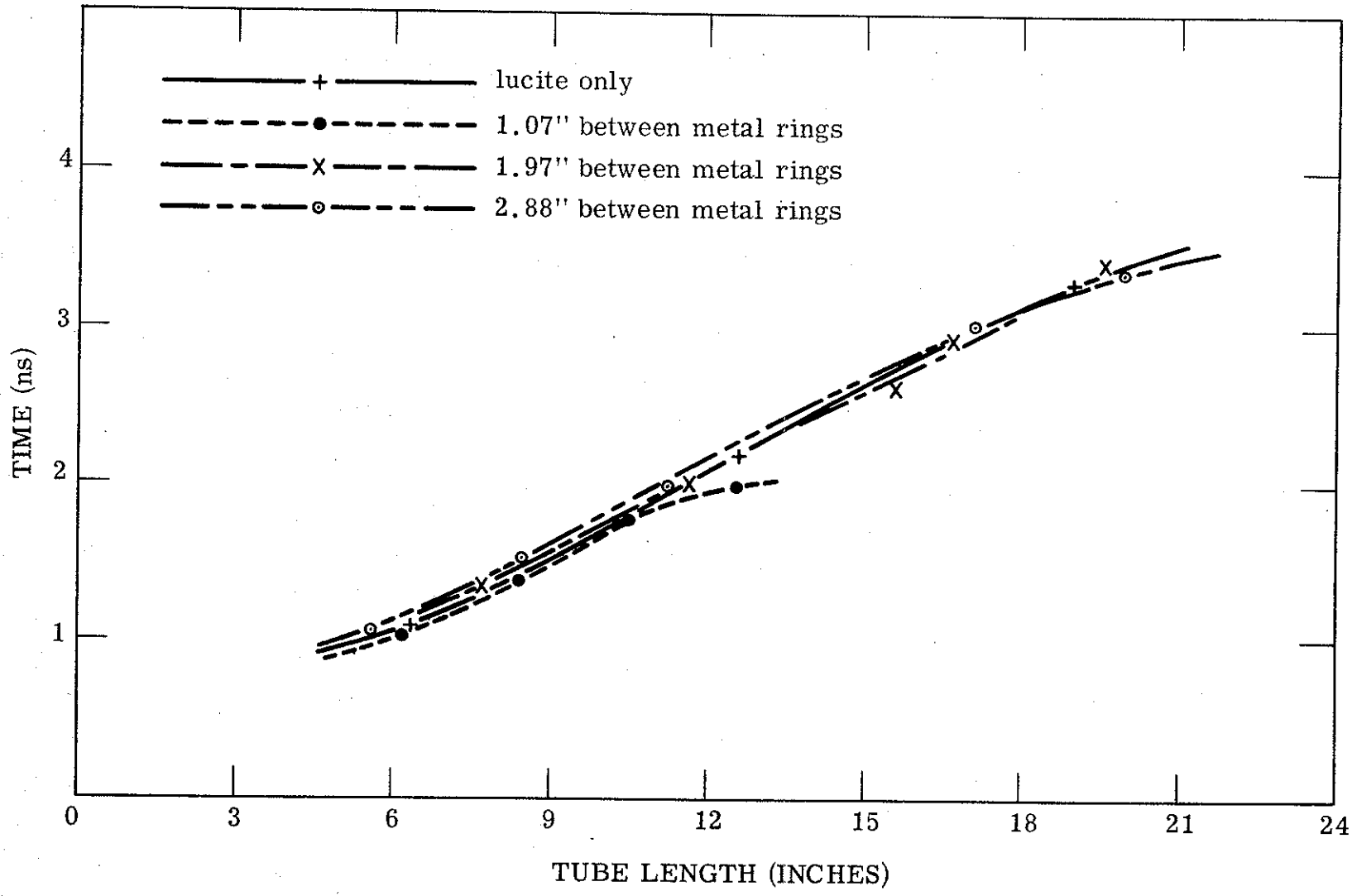

Figure 2-24. Uncorrected 20% - 80% risetimes for lucite tubes.

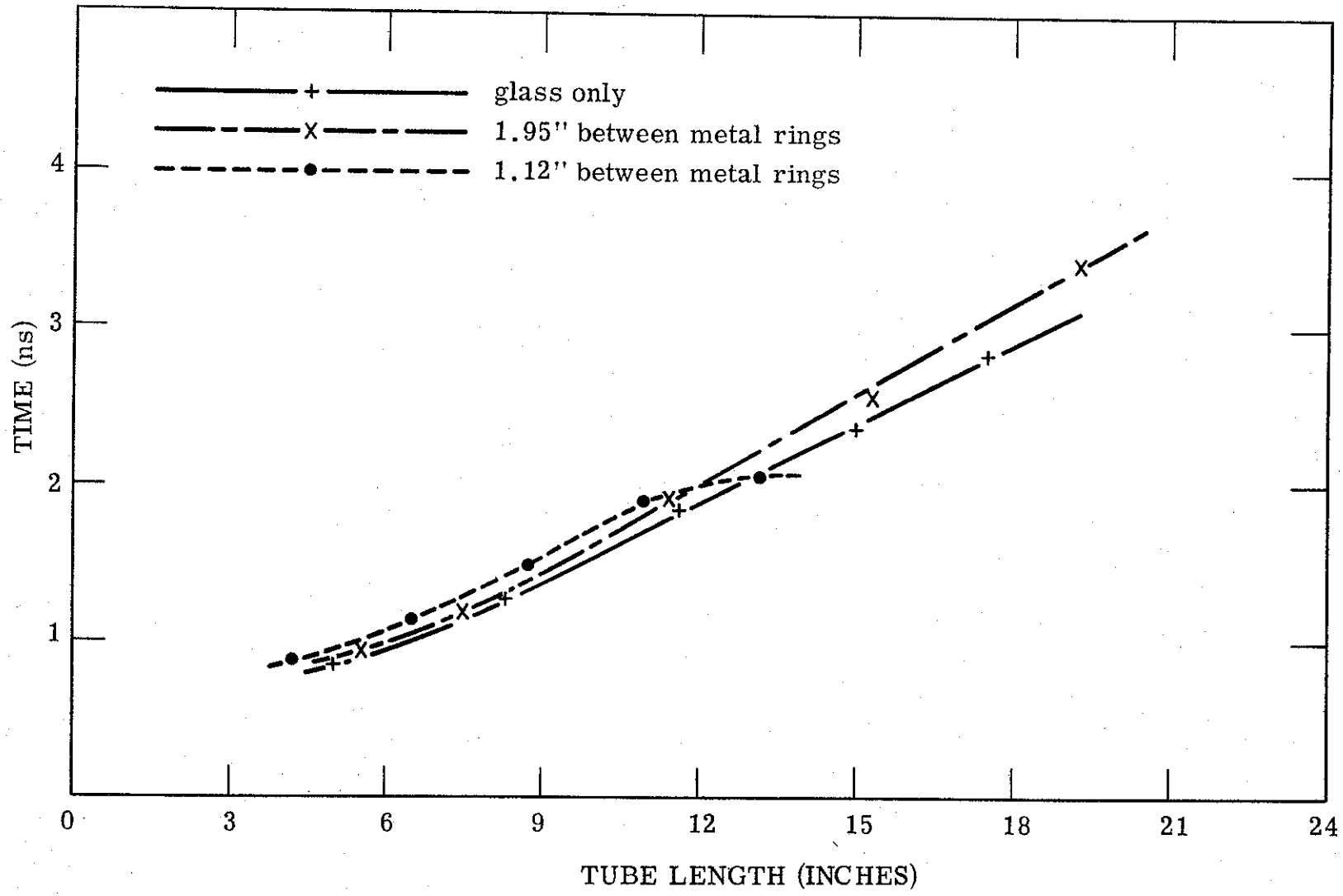

Figure 2-25. Uncorrected 20% - 80% risetimes for glass tubes, scaled by a factor of 0.9 relative to Figures 2-21 and 2-22.

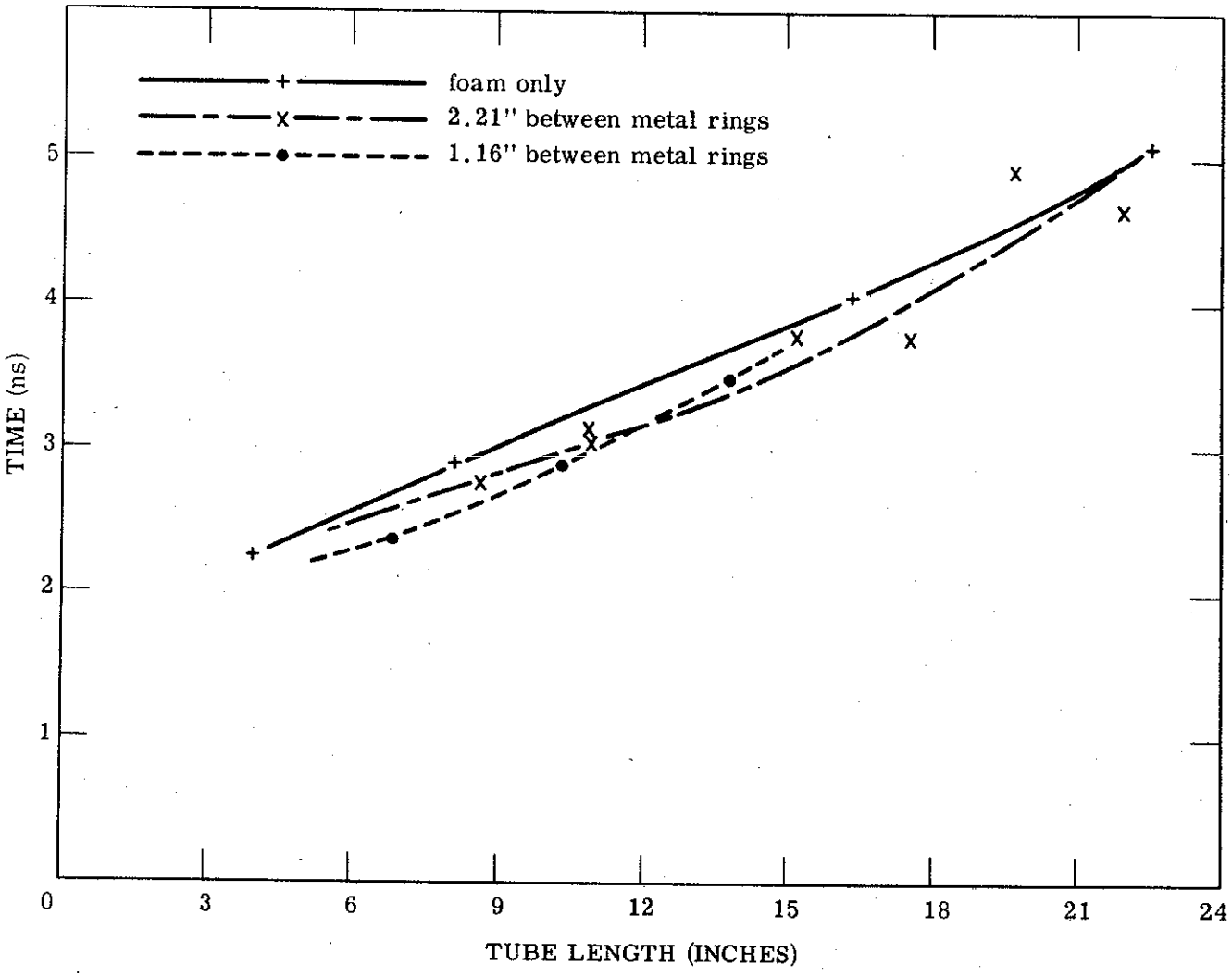

Figure 2-26. Uncorrected 10% - 90% Risetimes for Styrofoam Tubes.

1-4388

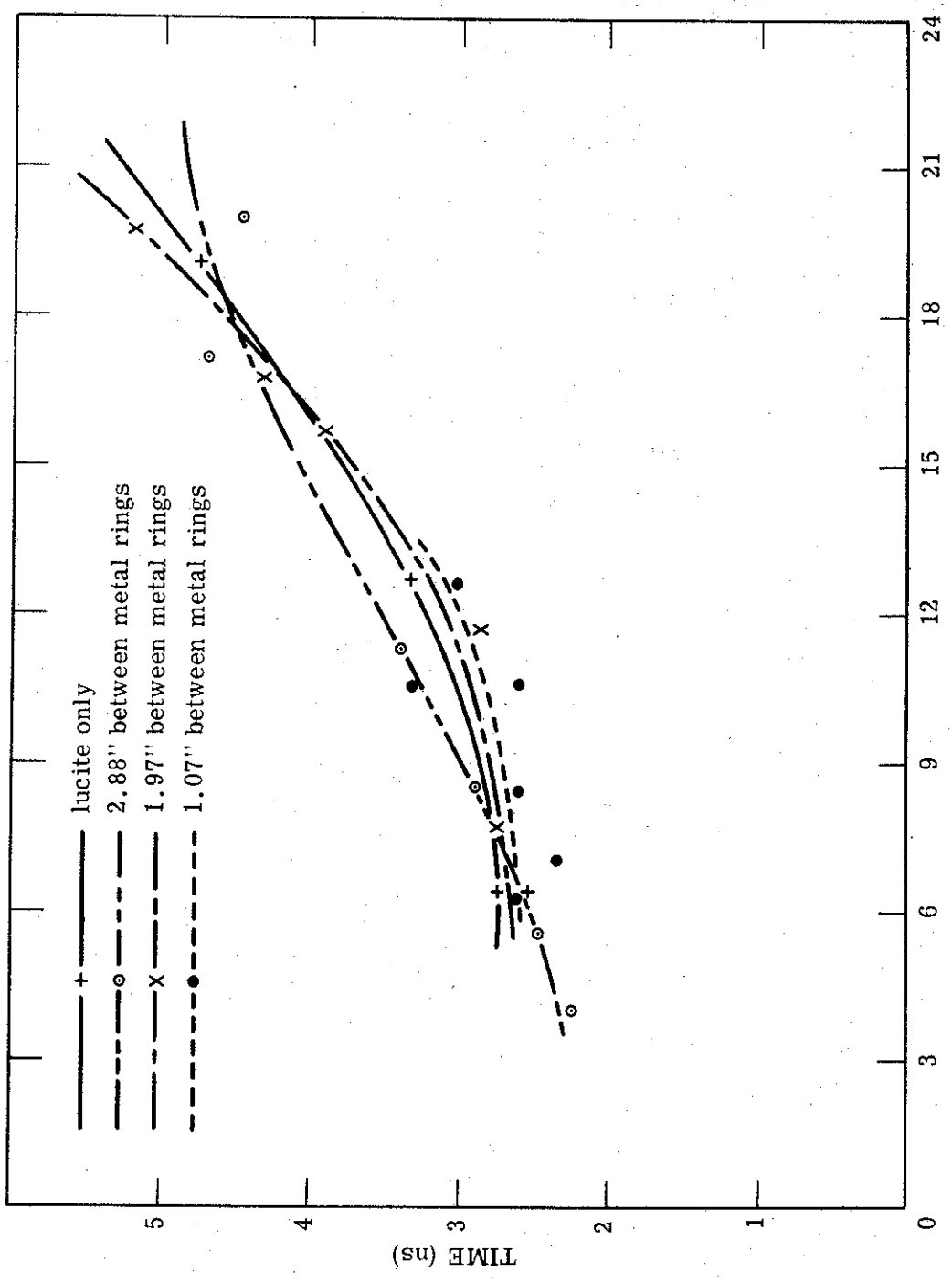

Figure 2-27. Uncorrected 10% - 90% Risetimes for Lucite Tubes.

1-4389

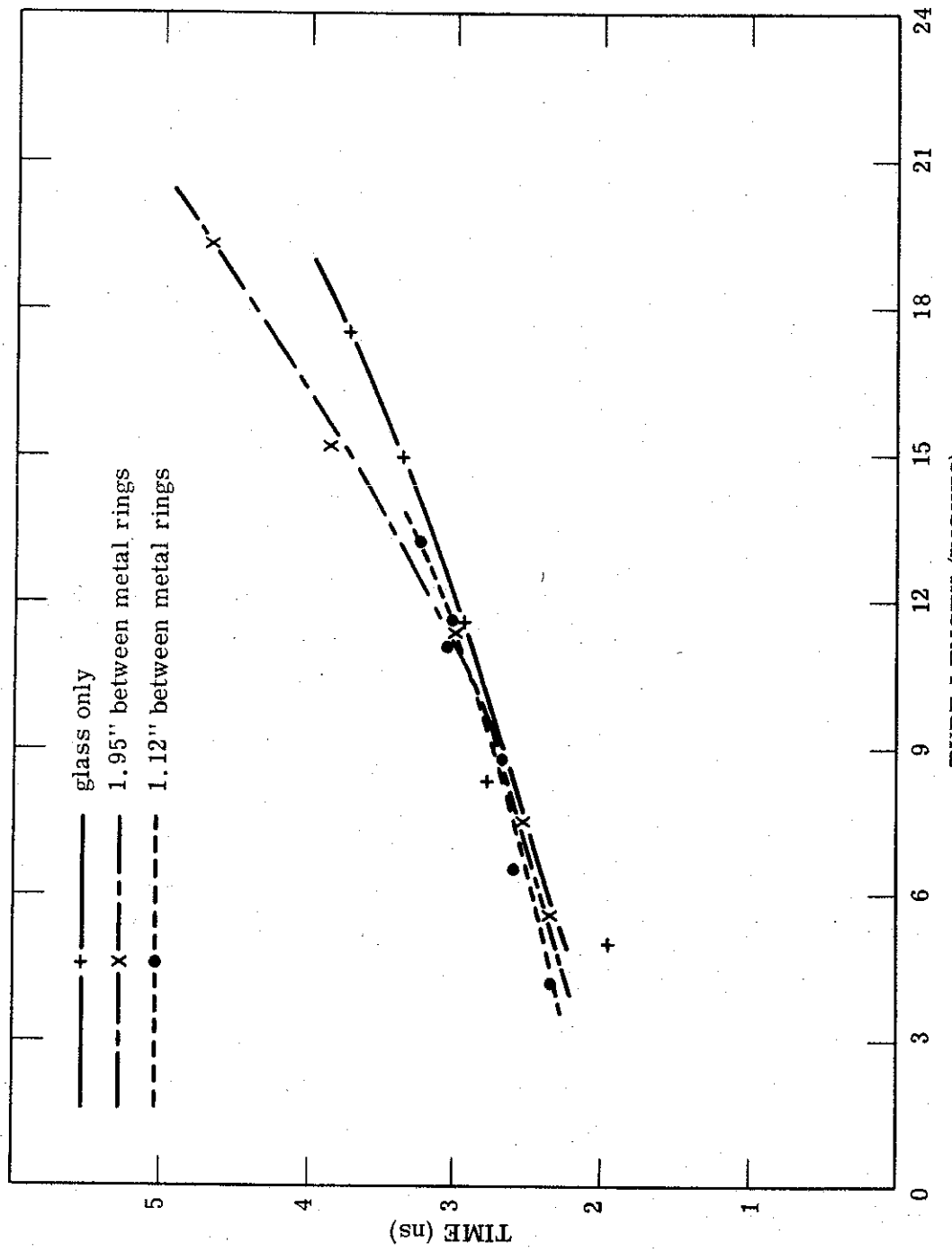

Figure 2-28. Uncorrected 10% - 90% risetimes for glass tubes, scaled by a factor of 0.9 relative to Figures 2-21 and 2-22.

1-4390

to produce a near-exponential pulse. The reasons for this procedure are explained in section 2.2.5. The agreement between the curves of Figures 2-26 through 2-28 is not as good as that exhibited in the preceding three graphs. But as in the case of the 20% to 80% risetimes, no systematic trend can be found to indicate any clear-cut dependence of risetime on either dielectric constant or spacing of the metal rings. Figures 2-26 through 2-28, like Figures 2-23 through 2-25, are not corrected for the diagnostics response.

Figure 2-29 shows 10% to 90% risetimes for all the tubes tested, with the pulse fronts smoothed as described above to give a near-exponential pulse, and the data for glass tubes scaled by a factor of 0.9 as explained earlier. A single curve is drawn as a rough best fit for all the data points, all of which fall within about 600 ps or 15% of this curve. Finally, the curve is lowered by 600 ps as a first-order correction for the response of the diagnostic equipment (see section 2.2.5).

An example of the velocity-of-propagation pictures is shown in Figure 2-30, which corresponds to a tube made up of lucite rings only. The time-reference pulse can be seen to the left of the main pulse. The other seven picture sequences (three more for lucite, two for foam and two for glass) are essentially similar and are not shown here. It should be pointed out that the identical, fast-rise pulse fronts indicated in these pictures are the result of a malfunctioning vertical deflection circuit in the oscilloscope which caused the display to limit on screen while the pulse is actually of much greater amplitude. The horizontal calibration of the oscilloscope is of course the only thing of interest here and was found to be accurate.

The velocity-of-propagation data are plotted in Figures 2-31 and 2-32. These graphs also show a straight line through the origin with slope 1/c as well as a hyperbola which gives the earliest possible arrival time of the pulse at the output line center conductor just beyond the tube region, measured from the time of arrival of the pulse at the beginning of the tube region. This earliest possible arrival time was found simply by using the shortest possible distance across the tube region, between two points on the test bed center conductor, and the greatest possible pulse propagation velocity, namely c. The data point

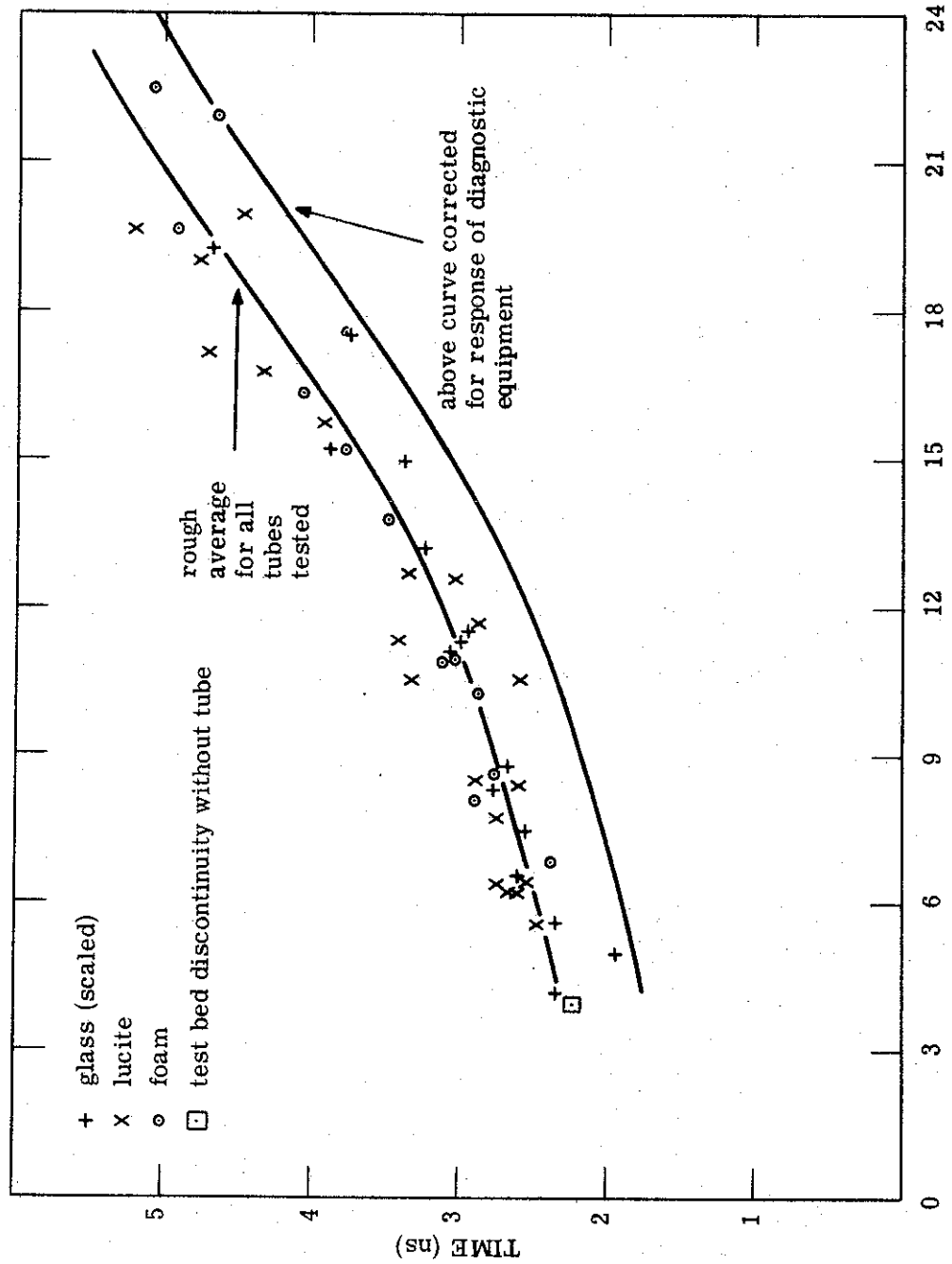

Figure 2-29. 10% - 90% Risetimes for all Tubes Tested.

1-4391

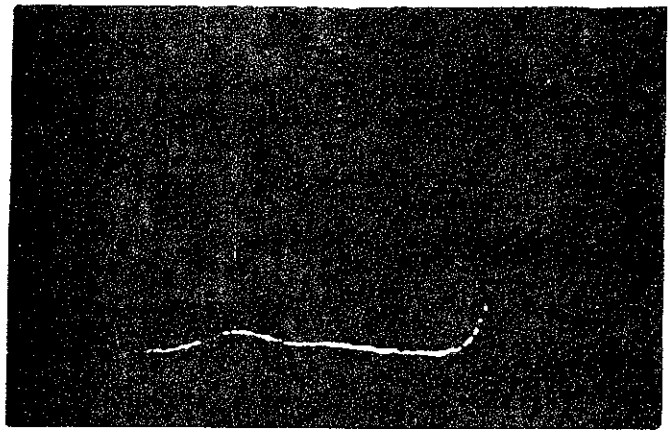

(a) No Tube. Length of Discontinuity Region: 4 Inches

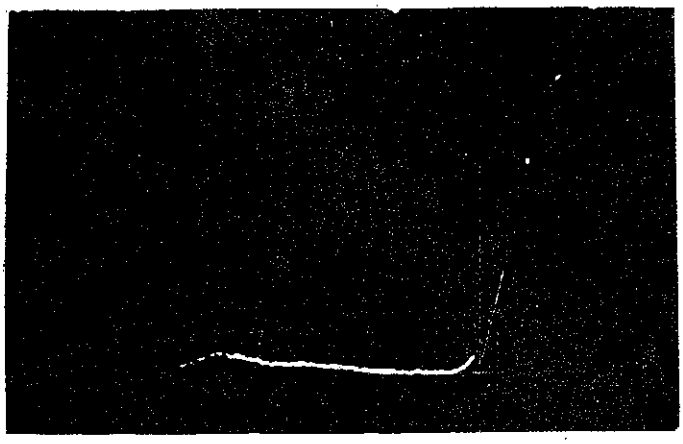

(b) Tube Length: 4.5 Inches

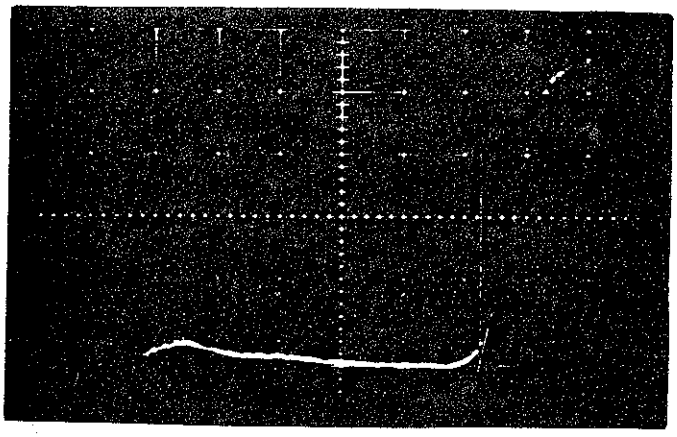

(c) Tube Length: 9.05 Inches

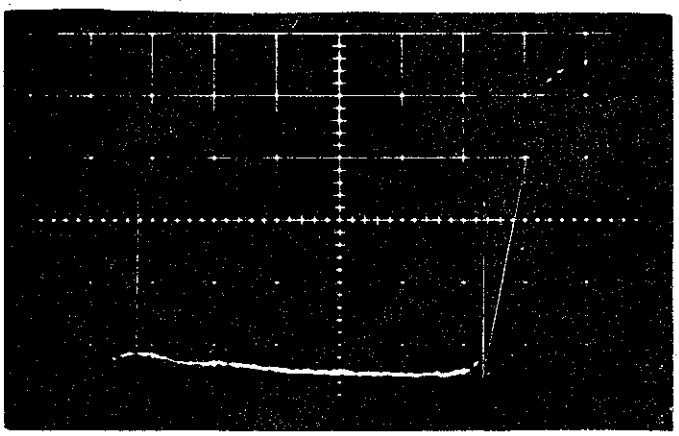

(d) Tube Length: 13.6 Inches

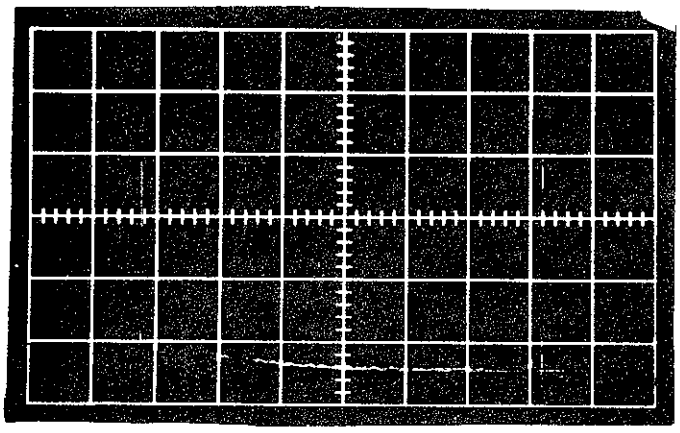

(e) Tube Length: 19 Inches

Figure 2-30. Velocity-of-Propagation Measurements for Lucite Tubes
Vertical Sensitivity: 20 mV/div
Horizontal Sensitivity: 0.5 ns/div

2-1485

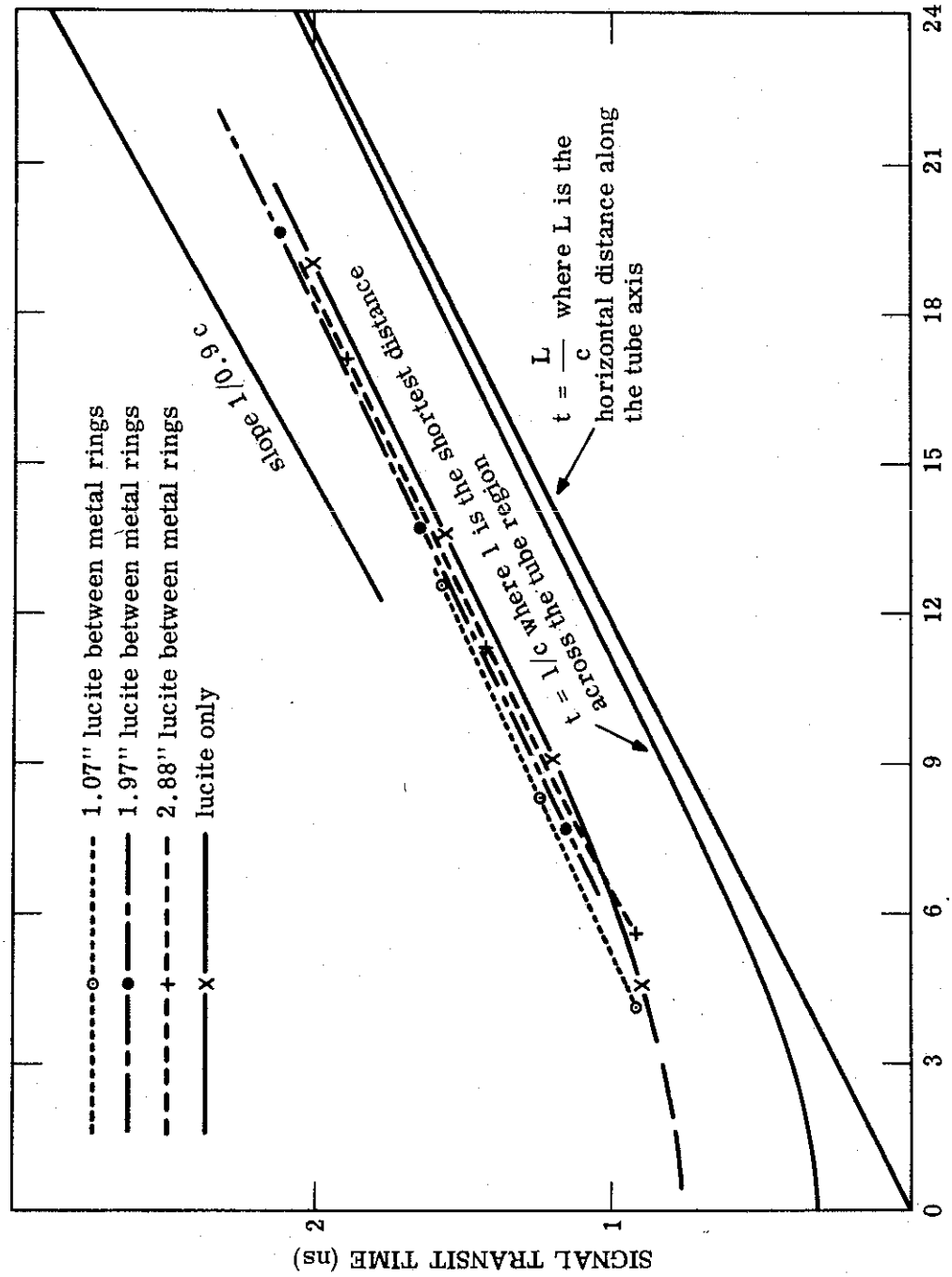

Figure 2-31. Signal transit time versus tube length for lucite tubes.

1-4392

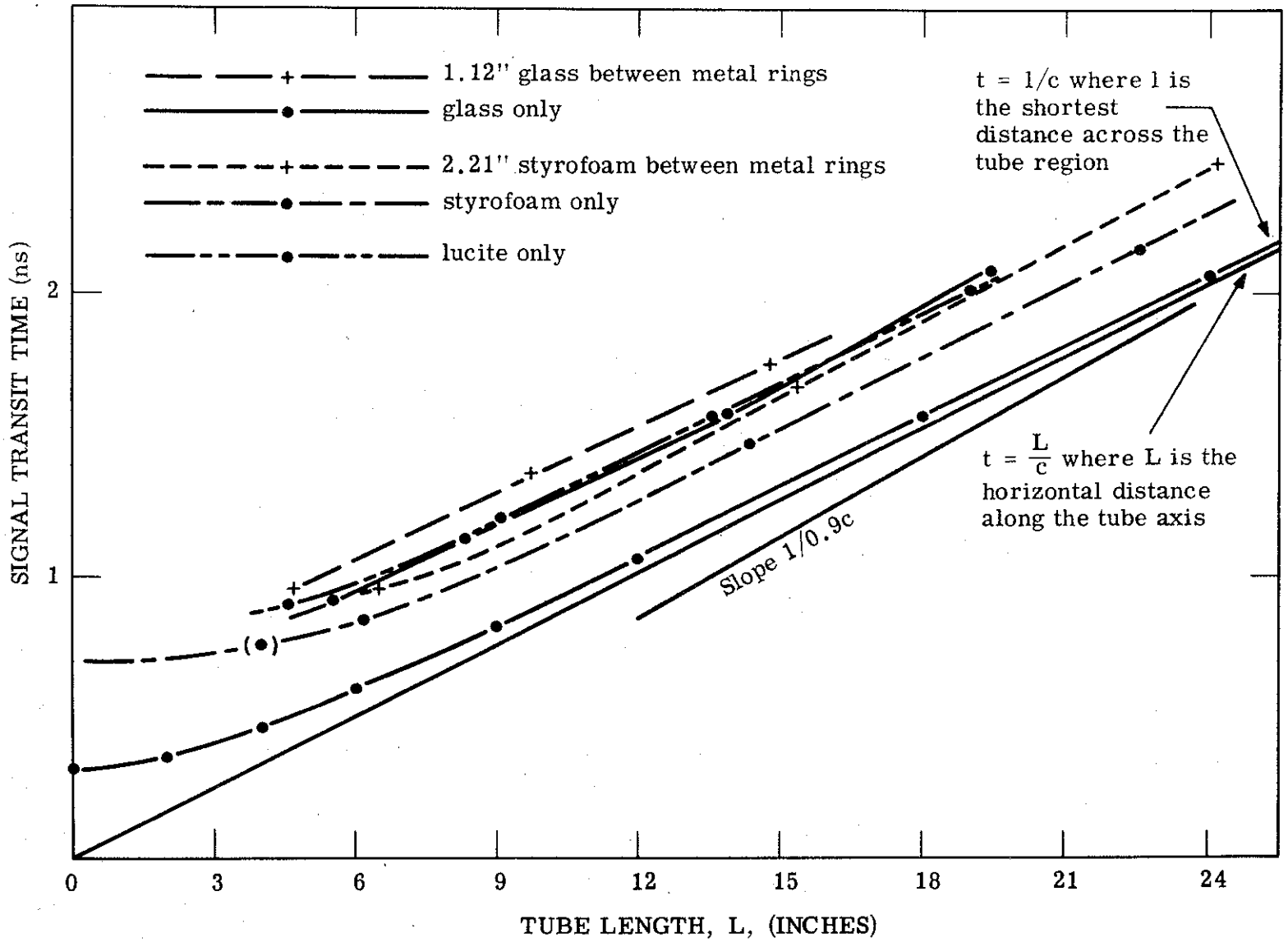

Figure 2-32. Signal transit time versus tube length for tubes of styrofoam, lucite and Corning glass #7740.

corresponding to the no-tube condition, i.e., a 4-inch long, airfilled discontinuity region, would lie on this hyperbola were it not for the criterion used to define the "beginning" of the pulse. All other times were determined relative to the time for the no-tube configuration; the curves are therefore in the correct relative positions and exhibit the correct slopes. They may, however, be too low by a fixed time, t, as a result of the above-mentioned assumptions, as explained more fully in section 2.2.5.

Figure 2-31 gives times of arrival for the four kinds of lucite tubes tested. It can be seen that the wave experiences what may be viewed as an initial delay as it reaches the discontinuity of the tube region (i.e., stray fields have to be charged) but then proceeds with very nearly the speed of light in air. There is no detectable slowing of the wave when metal rings are inserted, but the initial delay increases slightly as the spacing of the metal rings is decreased. The vertical distance between curves is only about 35 ps.

Figure 2-32 shows that the same increase in delay is also observed for foam and glass dielectrics, in addition it can be seen that the delay increases with increasing dielectric constant, at least for small ϵ_r up to about $\epsilon_r = 2.6$.

2.2.5 Data Reduction

2.2.5.1 Risetime Measurements

Risetime determination from the pictures of Figures 2-17 through 2-22 is not as straight-forward as it may seem at first glance, because of the oscillations superposed on many of the pulse fronts. These oscillations are probably a manifestation of reflections between the line discontinuities of the test bed in the tube region. The harsh geometry of this region, chosen for reasons of simplicity, may therefore not have been the best choice. A tapered outer conductor surrounding the tube as well as a tapered inner conductor inside the tube may have reduced or eliminated these oscillations and made the data interpretation easier.

The oscillations cause difficulties for several reasons. First, slight changes in tube parameters which cause only slight changes in the

qualitative aspects of the output pulse, may result in drastic changes in the pulse risetime, regardless of how one may choose to define the latter. This happens, for instance, when an oscillation peak on the pulse front increases in amplitude from just below to just above the 90% amplitude level. Secondly, it is also difficult to accurately correct for the step response of the diagnostic equipment since the effect of the latter is much more pronounced on fast, oscillatory pulses than on smooth, quasi-exponential pulses. Thirdly, and most importantly, even if accurate risetime curves (reflecting the presence of these oscillations) could be produced, it would not at all be clear how to use this information to predict risetimes for a larger system such as an EMP machine, of which the tube is merely a sub-system, since simple rules for adding risetimes of series-connected systems would not apply.

For these reasons two sets of risetime curves are produced. First, risetimes between 20% and 80% amplitude points are plotted in Figures 2-23 through 2-25, based on the pulses as they appear in Figures 2-17 through 2-22. The 80% point is taken to be that at which the pulse crosses the 80% level for the last time. Second, risetimes between the 10% and 90% amplitude points are plotted in Figures 2-26 through 2-28, based on manually smoothed pulses of quasi-exponential shape. Neither of the two sets of curves are corrected for the step response of the diagnostic equipment. The 20% to 80% risetimes are intended mainly to exhibit the similarity between all the tubes tested, the 10% to 90% curves show that no clear-cut trend is discernible in the data, with the exception of the dependence of risetime on tube length. Figure 2-29 shows one risetime curve based on all the data points, it also shows the same curve corrected for the response of the diagnostic equipment. This correction is arrived at as follows.

Figure 2-33 is an approximate representation of the diagnostics step response shown in Figure 2-16. Since this pulse when differentiated twice yields a series of delayed, scaled impulses, it is a simple matter to find input-output pairs for a system corresponding to this step response. Doing this for several exponential pulses with different time constants in the range of interest for present purposes, one gets the input-output pairs shown in Figure 2-34. Output

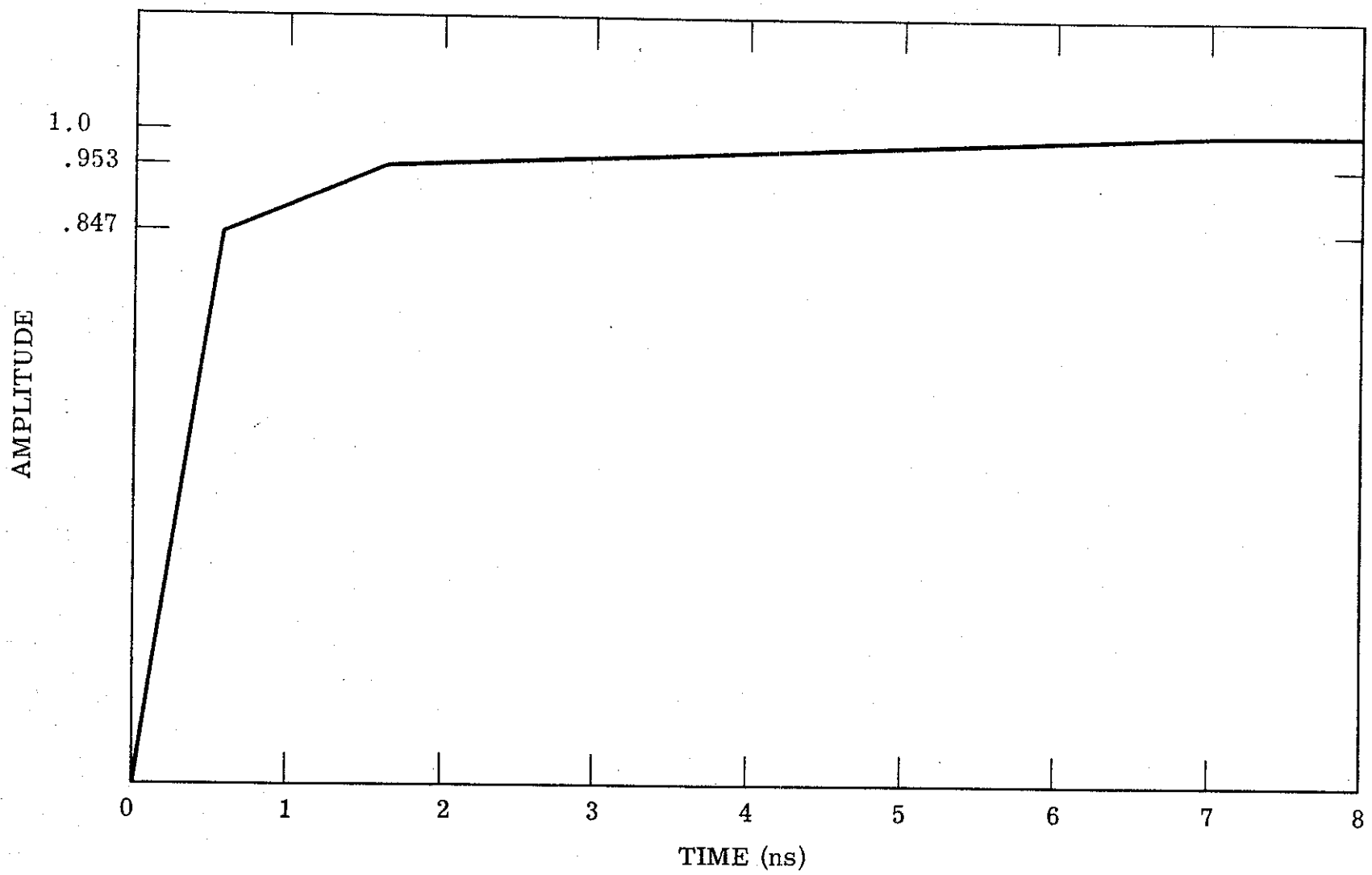

Figure 2-33. Approximate Step Response of the Diagnostic Equipment.

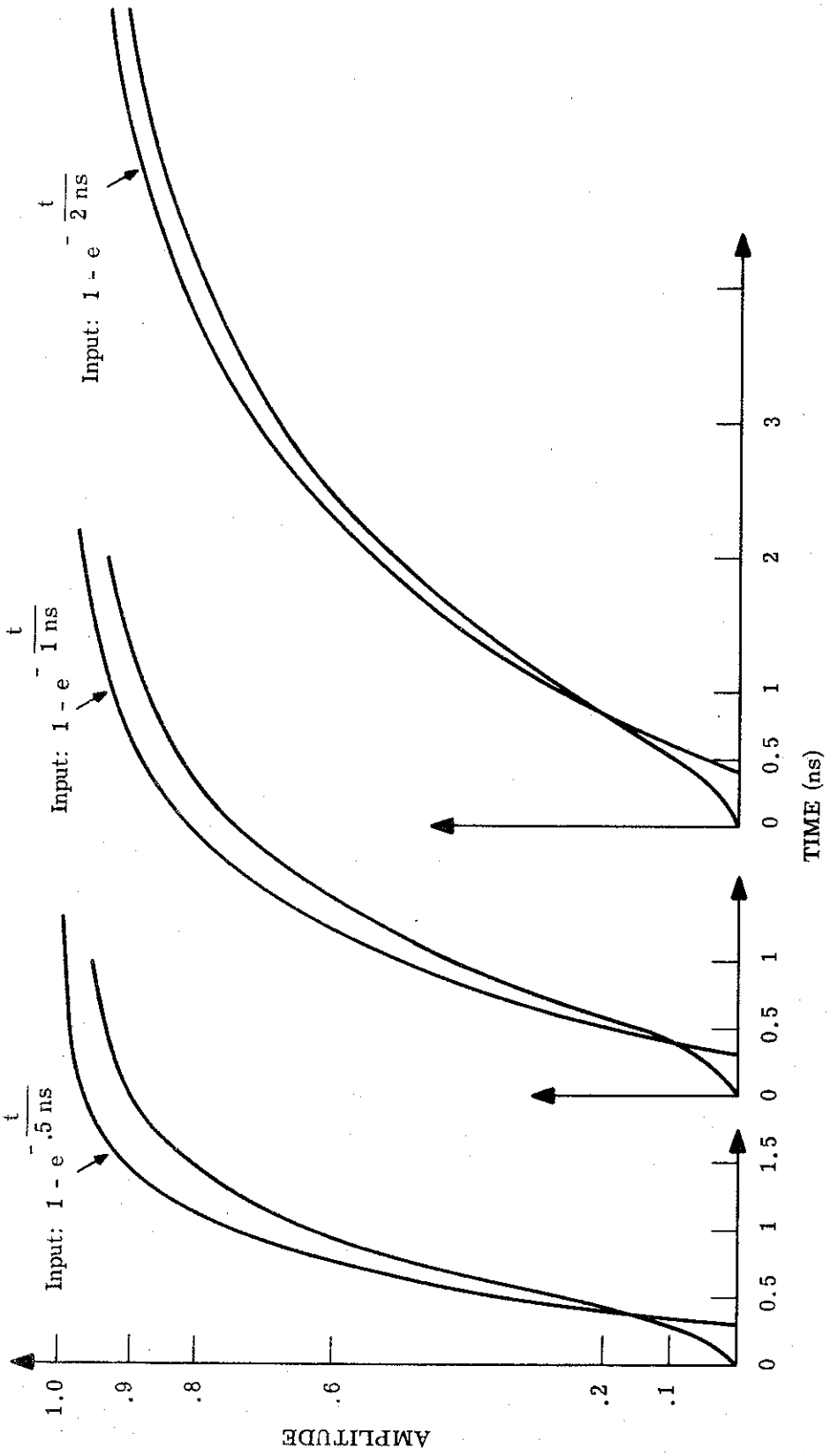

Figure 2-34. Input-output pairs for a system with step response as shown in Figure 2-33. The input curves are delayed for purposes of comparison.

1-4395

risetimes are plotted versus input risetimes in Figure 2-35. It can be seen that the limited response rate of the diagnostic equipment results in an increase in risetime of very nearly 600 ps for all the pulses of interest. One cannot, of course, be sure that the pulses of Figures 2-17 through 2-22 do indeed have an underlying exponential main body, but because of the quasi-exponential character of the pulses the above process should be sufficiently accurate for purposes of a first-order correction.

2.2.5.2 Velocity-of-Propagation Measurements

The velocity-of-propagation measurements are intended mainly to determine the slopes of the time-versus-distance curves as shown in Figures 2-31 and 2-32. No provision was made for determining the absolute values of signal transit times across the tube region and the picture corresponding to a 4-inch long, airfilled discontinuity region was used as reference, with an assumed transit time for this configuration, all other transit times being measured relative to this.

The time of arrival of the pulses was taken to be the time of arrival of the "pulse starting point", defined as the beginning of a linear ramp drawn so as to coincide with the steepest part of the pulse front. The transit time for the pulse corresponding to the no-tube configuration was arrived at assuming the pulse to follow a straight line diagonally across the discontinuity region between a point on the test bed inner conductor just ahead of the tube region and a point on the inner conductor just beyond the tube region, and to propagate with velocity c. These assumptions put the origin of the time scale 468 ps before the earliest detectable pulse portion. The "pulse starting point" as defined above is another 290 ps after the earliest detectable pulse portion.

It is of course possible that the pulse does not follow a straight line across the tube region and/or travels with a velocity less than c, and that a pulse precursor of small amplitude arrives before the earliest point on the picture at which the pulse front can be detected. This would have the effect of making the curves of Figures 2-31 and 2-32 too low by some fixed time, t. The

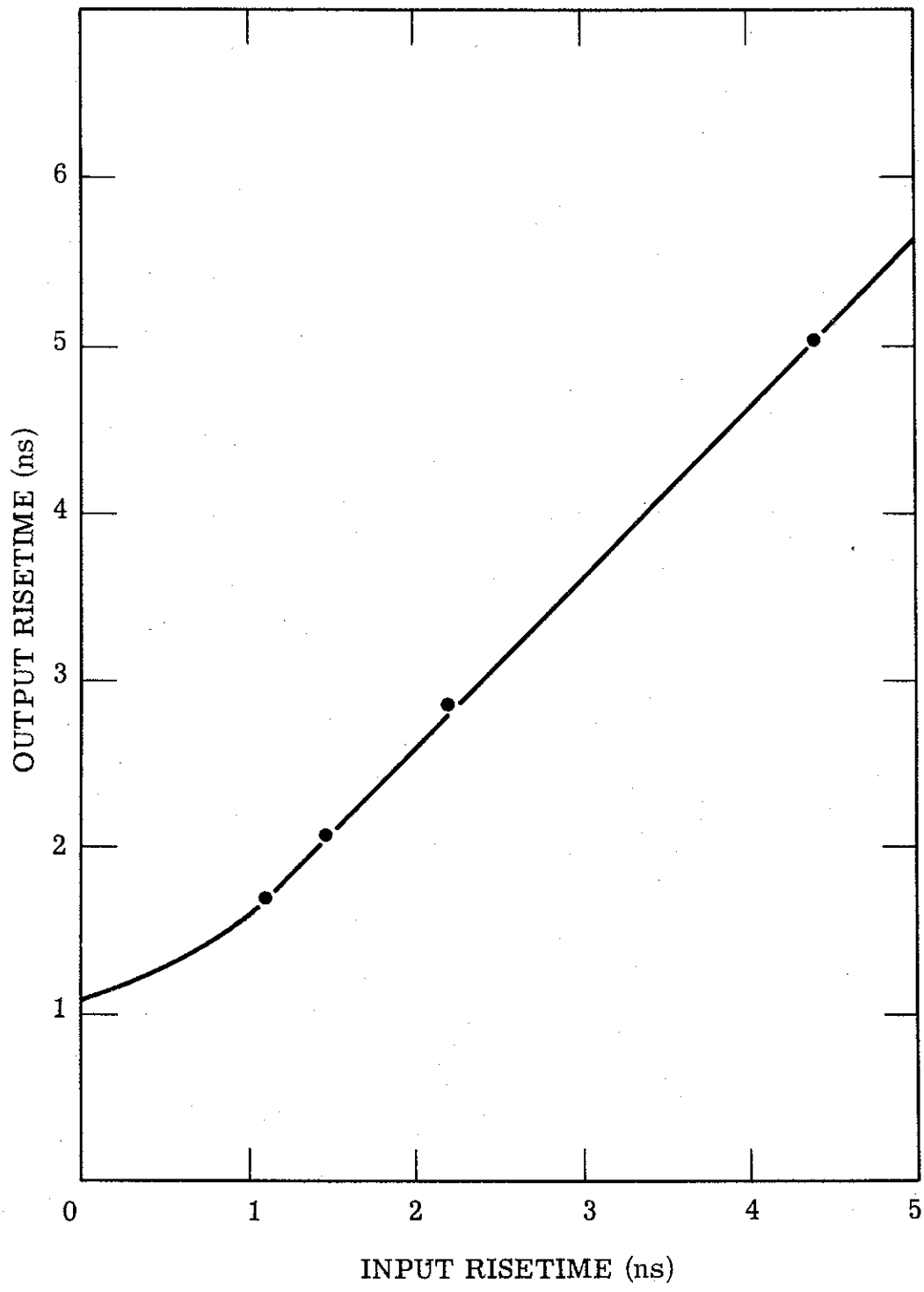

Figure 2-35. Output risetimes (10% - 90%) versus input risetimes for a system with step response as shown in Figure 2-33, for exponential input pulses.

1-4396

curves cannot be too high, however, unless there is a significant deviation from TEM conditions throughout the small-diameter test bed section.

In any case, since all transit times were measured relative to the one corresponding to the no-tube configuration, the curve slopes as well as the relative positioning of the curves are correct.

2.2.6 Summary

The main results of the present investigation are as follows. No clear-cut differences can be seen in the pulse characteristics in general and risetimes in particular for tubes of different dielectric materials with relative dielectric constants of from 1 to 4.5. Insertion of thin metal rings at intervals along the tube ranging from approximately 3-inches to approximately 1-inch likewise does not seem to have much of an effect. The tube step response does vary significantly with tube length, however.

Bearing in mind that the tubes studied here are of approximately 1 foot OD and are located in a 40 ohm environment with the geometry shown in Figure 2-1, one may summarize the risetime information obtained in the following simple way:

$$t_r \approx \ell + 1.5 \qquad 0.3 < \ell \leq 1$$

$$t_r \approx 2.5\,\ell \qquad 1 \leq \ell < 2,$$

where t_r is the pulse risetime between 10% and 90% amplitude points, in nanoseconds; ℓ is the tube length, in feet. For tubes of different transverse dimensions, scaling in both space and time appears to be valid.

The pulse propagation velocity appears to be very nearly c for all tubes tested. There is, however, what appears to be an initial delay of the pulse; this delay is found to increase as the dielectric constant of the tube material increases, at least for low ϵ_r up to about 3. It also increases as the separation of the metal rings in the tube is decreased. The amount of increase of the delay is only slight, however; about 100 ps where the tube configuration is changed from one in which metal rings are not used to one in which the metal ring separation is only about 1-inch, and about 150 ps when the relative dielectric constant of the tube material is increased from 1 to 2.6 - 4.5. A simple and quite plausible explanation for this pulse delay is that the stray fields in the tube region must be charged up by the incoming pulse before the latter can proceed, and that these fields store more energy when metal tube rings are inserted or when the dielectric constant of the tube material is increased, thus increasing the time needed for the stray fields to store a given fraction of this maximum energy.

It would be of interest in future studies to try to eliminate the oscillations present on the pulse fronts as these make it somewhat difficult to interpret the experimental data and reduce the accuracy of the risetime information. This may perhaps be accomplished by tapering the inner and outer conductors of the test bed in the tube region. It may also be worthwhile to shorten the co-axial cable from the test bed termination to the oscilloscope since this cable is the slowest element of the diagnostic equipment. Shortening the cable would entail somehow elevating the oscilloscope to the 15-foot elevation of the top of the test bed. Even with a short output cable, however, it would be necessary to correct the observed pulses for the response of the resistive termination, pulser, oscilloscope, and short coaxial cables in order to achieve maximum accuracy of the data.

2.3 Computer Modelling Code

2.3.1 Introduction

This program is written in Fortran for use on the GE-420 time-sharing computer system. The program calculates the Laplace transformation of the response of a resistive load when a charged transmission line is switched into a lumped-element network, illustrated schematically in Figure 2-36. The inverse transformation is then numerically evaluated.

2.3.2 Analysis

The response of a lossless, initially charged transmission line switched into a load impedance having transform ZL(s) is discussed in Cheng.[1] The Laplace transform of the output current is

$$I(S) = \frac{E}{S\,(ZL\,(s) + ZO\,(s))} \qquad \frac{(1 - e^{-2s\tau})}{(1 - \Gamma\, e^{-2s\tau})}$$

where ZO(s) is the transform of the line impedance, E is the voltage to which the line is initially charged, τ is the signal one-way transit time, and $\Gamma = \frac{ZL - ZO}{ZL + ZO}$. By expanding the expression for I(s), the effect of multiple reflections on the response can be easily seen:

$$I(s) = \frac{E}{s\,(ZO\,(s) + ZL\,(s))}\ (1 + (\Gamma - 1)\,e^{-2s\tau} + \Gamma\,(\Gamma - 1)\,e^{-4s\tau} + \Gamma^2\,(\Gamma - 1)\,e^{-6s\tau} + \ldots)$$

The first term represents the transform of the initial current pulse. The second term is the first reflection from the open end of the line, delayed by a time 2τ, etc.

These results are easily extended to the case illustrated in Figure 2-36 by making the substitution

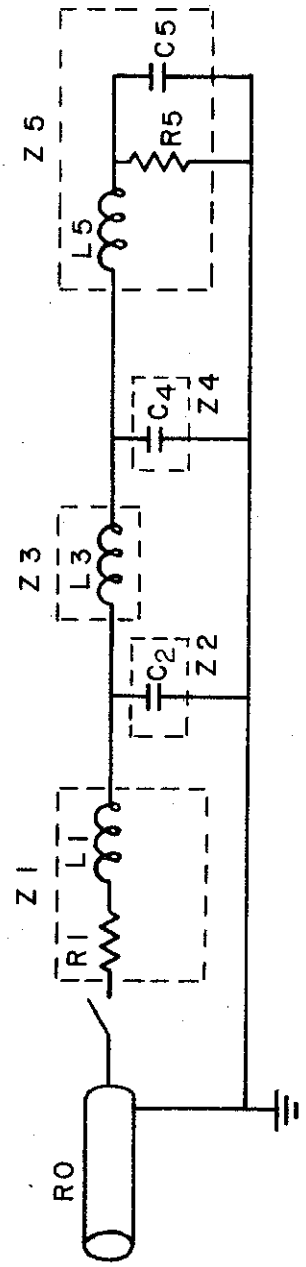

Figure 2-36. Network for Computer Modelling

1-4076

$$ZL = Z1 + \frac{Z2\,(Z3 + Z4\,Z5/(Z4 + Z5))}{Z2 + Z3 + Z4\,Z5/(Z4 + Z5)}$$

The program determined the voltage across the resistance R5. The current through this resistance is some fraction $\alpha(s)$ of the total output current from the line, I(s). The transform of the voltage across R5 is then

$$V(s) = R5 \quad \alpha(s)\ I(s)$$

where

$$\alpha(s) = \left(\frac{Z2\ Z4}{(Z2 + Z3)\ (Z4 + Z5) + Z4\ Z5}\right) \quad \frac{1}{(sC5\ R5 + 1)}$$

The charging voltage E is set to unity, here, and the Z's are the transforms of the corresponding impedances.

The incident voltage V1 and each of the first two reflections V2 and V3 respectively are considered separately.

$$V1(s) = \frac{R5\ \alpha(s)}{s\,(ZL + ZO)} \;;\; V2(s) = V1(s)\left(\frac{-2ZO}{ZL + ZO}\right) \;;\; V3(s) = V2(s)\left(\frac{ZL - ZO}{ZL + ZO}\right)$$

In more detail

$$V1(s) = \frac{R5\ (Z1D)\ (Z5D)}{s\,(Z1D)\,(Q1) + sQ3} \quad \left(\frac{1}{sC5\ R5 + 1}\right) ,$$

$$V2(s) = V1(s) \quad \frac{(-2ZO)\ (Z1D)\ (Q2)}{Q3 + Q1} ,$$

$$V3(s) = V2(s) \quad \frac{Q4 + Q1}{Q3 + Q1}$$

The Z1D, Z5D, Q1, Q2, Q3 and Q4 are polynomials in s defined below.

$$Q1 = Z3\,(Z5D + Z5N/Z4) + Z5N$$

$$Q2 = (1 + Z3/Z2)\,(Z5D + Z5N/Z4) + Z5N/Z2$$

$$Q3 = ((ZO)\,(Z1D) + Z1N)\,Q2$$

$$Q4 = ((-ZO)\,(Z1D) + Z1N)\,Q2$$

As before the various Z expressions are polynomials in s representing the transformed impedances (see Figure 2-36).

$ZO = RO$, the line impedance

$$Z1 \equiv \frac{Z1N}{Z1D} = \frac{R1 + sL1}{1}$$, represents 

$Z2 = 1/sC2$, represents 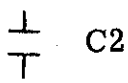

$Z3 = sL3$, represents 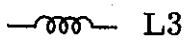

$Z4 = 1/sC4$, represents 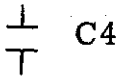

and

$$Z5 \equiv Z5N/Z5D = \frac{s^2L5C5R5 + sL5 + R5}{sC5R5 + 1}$$

represents 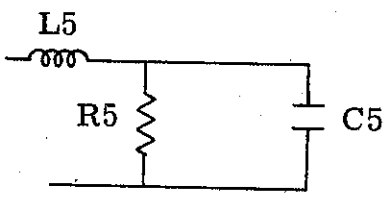

2.3.3 Program

The program calculates the incident voltage V1 and the first and second reflections, V2 and V3 respectively, across the resistance R5. As previously described, first several basic polynomials, $Z_m(s)$, are defined in terms of the input values. These are combined to form an intermediate set of polynomials, $Q_m(s)$, which are in turn used to calculate the transformed voltages in terms of the ratio of two polynomials:

$$V1(s) = V1N(s)/V1D(s),\ V2(s) = V2N(s)/V2D(s) \ ,$$

$$V3(s) = V3N(s)/V3D(s) \ .$$

Throughout the program polynomials are expressed according to the following convention: An nth degree polynomial in s, A(s), is written:

$$A(s) = A(n+1)\,s^n + \ldots + A(2)\,s + A(1) \ .$$

The inputs to the program (see line 230 of program listing) are the values of the network elements expressed in ohms and units of inductance and capacitance compatible with the desired output time scale. For example, if nano-second output pulses were expected, inductances would be entered in units of nano-henrys, capacitances in units of nano-farads, and resistances in ohms. The output would therefore be volts versus nano-seconds.

After the numerator and denominator polynomials, VN and VD, are calculated the program normalizes the highest order denominator coefficient to unity. This procedure, although not required, was included so that other Laplace inversion routines such as the GE Library program TRANS could be used instead of the numerical method ZTRAN, described below.

Subroutine MULTY

This subprogram multiplies a polynomial A of order MM by a polynomial B of order NN to obtain C, the product polynomial of order KK.

Subroutine ZTRAN

A numerical Laplace inversion method formulated by Zakian[2] is the basis of this subprogram. The inverse transform is approximated as a ten term polynomial expansion of the transform function with constant complex coefficients. The inputs to ZTRAN are N and D, the numerator and denominator polynomials, respectively, of the voltage transform; M, the order of D, and TMAX and DT, the maximum time and the time increment. The voltage calculation is made first for time t = DT and then for each time increment DT thereafter until the limit TMAX is reached. The output is presented in a two column format: time in the first and voltage in the second column.

2.3.4 Operation of the Program

Operator intervention is required several times in the running of this program. The first, on line 230, is in the listing of the input parameters, i.e. the network component values. The units chosen for the input values determine, of course, the time scale of the program output. In responding to the questions asked on lines 800 and 930, the operator can bypass sections of the program which calculate the incident voltage pulse or either of the two reflected voltage pulses. The remaining program inputs are the values of the maximum time and the time increment requested on lines 770, 900, and 1040. The units of these time values are determined by the units chosen for the input values of line 230.

The program output lists each of the three component voltages as functions of time. To construct the actual output voltage pulse, these three results must be superimposed. This is done by adding V2 (t) and V3 (t) to the incident pulse V1 (t) after having shifted the time base of each by 2τ and 4τ, respectively, where τ is the signal one-way transit time.

REFERENCES:

(1) Cheng, D. K., Analysis of Linear Systems. p. 375ff.

(2) Zakian, V. "Numerical Inversion of Laplace Transform", Electronics Letters, 1969, 6, pp 120-121.

2.3.5 Program Listing

```
99C          MANIPULATION AND INVERSION PROGRAM
100C
101 DIMENSION ZKN(10),Z5D(10),RZ5D(10),ZIN(10),AQ1(10),AQ2(10)
110 DIMENSION VINN(24),VIDN(24),ZQ(24),Z1E(24),RZ1D(24),VIN(24),
120+VID(24),AQ3(24),AQ4(24),Q1(24),Q2(24),Q3(24),Q4(24),ZQ1(24),
130+VQ2(24),Q31(24),Q41(24),V2N(24),V2D(24),V3N(24),V3D(24),
140+V2NN(24),V2DN(24),V3NN(24),V3DN(24)
150 REAL L1,LW,L3
160 DO 10 I=1,10
170 Z5N(I)=0.0;Z5D(I)=0.0,RZ5D(I)=0.0;Z1N(I)=0.0;VINN(I)=0.0
171 VIDN(I)=0.0;AQ1(I)=0.0;AQ2(I)=0.0
175 10 CONTINU
180 DO 11 I=1,24
181 Z1D(I)=0.0;RZ1D(I)=0.0;V1N(I)=0.0;V1D(I)=0.0;AQ3(I)=0.0;AQ4(I)=0.0
185 Q1(I)=0.0;Q2(I)=0.0;Q3(I)=0.0;Q4(I)=0.0;ZQ1(I)=0.0;ZQ2(I)=0.0
190 Q31(I)=0.0;Q41(I)=0.0;V2N(I)=0.0;V2D(I)=0.0;V3N(I)=0.0;V3D(I)=0.0
200 V2NN(I)=0.0;V2DN(I)=0.0;V3NN(I)=0.0;V3DN(I)=0.0
205 V1NN(I)=0.0;V1DN(I)=0.0;ZQ(I)=0.0
210 11 CONTINUE
211C
212C          ENTER ELEMENT VALUES  (RO IS R ALPHA 0 NOT R ZERO)
213C
220 PRINT,"TYPE VALUES: RO,R1,L1,C2,L3,C4,R5,L5,C5"
230 READ,(RO,R1,L1,C2,L3,C4,R5,L5,C5)
240 Z5N(1)=R5  ;Z5N(2)=L5  ;Z5N(3)=R5*C5*L5
250 Z5D(1)=1.0 ;Z5D(2)=C5*R5  ;RZ5D(1)=R5 ;RZ5D(2)=C5*R5*R5
260 Z1D(1)=1.0 ;Z1D(2)=0.0 ;Z1D(3)=0.0 ;Z1N(1)=R1 ;Z1N(2)=L1
261C
262C         CALCULATE V1N
263C
270 V1N(1)=R5 ; V1N(2)=RZ5D(2)+Z1D(2)*R5
280 V1N(3)=Z1D(2)*RZ5D)+Z1D(3)*R5 ; V1N(4)=Z1D(3)*RZ5D(2)
281C
282C        CALCULATE Z1,Q2,Q3,Q4
283C
290 AQ1(1)=Z5D(1)
300 DO 20 I=2,4
310J J=KI-1
320 AQ1(I)=Z5D(I)+C4*Z5N(J)
330 20 CONTINUE
340 Q1(1)=Z5N(1)
```

```
350 DO 30 I=2,5
360 J=I-1  ;Z1(I)=L3*AQ1(J)+Z5N(I)
370 30 CONTINUE
380 AQ2(1)=AQ1(I)  ;AQ2(2)=AQ1(2)
390 DO 40 I=3,6
400 J=I-2  ;AQ2(I)=AQ1(I)+C2*L3*AQ1(J)
410 40 CONTINUE
420 Q2(1)=AQ2(1)
430 DO 50 I=2,6
440 J=I-1;Q2(I)=AQ2(I)+C2*Z5N(J)
450 50 CONTINUE
460 DO 60 I=1,3
470 AQ3(I)=RO*Z1D(I)+ZIN(I)  ;AQ4(I)=-RO*Z1D(I)+ZIN(I)
480 60 CONTINUE
490 CALL MULTY(Q2,5,AQ3,2,Q3,7)
500 CALL MULTY(Q2,AQ4,2,Q4,7)
```

```
501C
502C       CALCYLATE V1D
503C
510 CALL MULTY(Q1,4,Z1D,2,ZQ1,6)
520 ZQ(1)=0.0
530 DO 70 I=2,9
540 J=I-1 ; ZQ(I)=ZQ1(J)+Q3(J)
541 70 CONTINUE
542 V1E(1)=0.0
543 DO 75 I=2,10
544 J=I-1 ; V1D(I)=ZQ(I)+C5*R5*ZQ(J)
550 75 CONTINUE
551C
552C        CALCULATE V2N,V2D,V3N,V3D
553C
560 DO 80 I=1,3
570 RZ1E(I)=-2*RO*Z1D(I)
580 80 CONTINUE
590 CALL MULTY(RZ1D,2,Q2,5,ZQ2,7)
600 CALL MULTY(ZQ2,7,V1N,3,V2N,10)
610 DO 90 I=1,8
620 Q31(I)=Q3(I)+Q1(I)  ;Q41(I)=Q4(I)+Q1(I)
630 90 CONTINUE
640 CALL MULTY(V1E,9,Q31,7,V2D,16)
650 CALL MULTY(V2N,10,Q41,7,V3N,17)
660 CALL MULTY(V2D,16,Q31,7,V3D,23)
665C
692C      NORMALIZE HIGHEST ORDER DENOMINATOR
693C      COEFFICIENT OF V1 TO ONE
694C
700 95 IF=-1
710 100IF=IJ+1
713 K=10-IJ
717 CV1=V1D(K)
720 IF(CV1)110,100,110
730 110 K1=K-1
740 DO 120 I=1,K
750 V1DN(I)=V1D(I)/V1D(K)  ; V1NN(I)=V1N(I)/V1D(K)
760 120 CONTINE
761C
762C      CALCULATE INVERSE TRANSFORMATION OF V1
763C
770 PRINT,"INCIDENT PULSE:TYPE VALUES:MAXTIME + TIME INCREMENT"
780 INPUT,ATM,ADT
790 CALL ZTRAN(K1,V1NN,V1DN,ATM,ADT)
800 122 PRINT,"DO YOU WANT 1ST REFLECTION? 1=YES 0=NO"
810 INPUT,REF1
820 IF(REF1)160,160,125
821C
822C      NORMALIZE HIGHEST ORDER DENOMINATOR
823C      COEFFICIENT OF V1 TO V↑E0N24C
830 125 IF=-1
840 130 IK=IK+1
843 JK=16-IK
847 CV2=V2D(JK)
850 IF(CV2)140,130,140
860 150 K2=JK-1
```

```
870 DO 150 I=1,JK
880 V2DN(I)=V2D(I)/V2D(JK)  ; VWNN(I)=V2N(I)/V2D(JK)
890 150 CONTINUE
891C
892C      CALCULATE INVERSE TRANSFORMATION OF V2
893C
900 PRINT,"1SR REFLECTION-TYPE VALUES:MAXTIME & TIME INCRECENT"
910 INPUT,ATM,ADT
920 CALL ZTRAN(K2,V2NN,V2DN,ATM,ADT)
925C
930 160 PRINT,"DO YOU WANT 2ND REFLECTION? 1=YES 0=NO"
940 INPUT,REF2
950 IF(REF2)250,250,170
951C
952C      NORMALIZE HIGHEST ORDER DENOMINATOR
953C      COEFFICIENT OF V3 TO ONR
954C
96960 170 IL=-1
970 180 IL=IL+1
980 JL=23-IL  ;CV3=V3D(JL)
990 IF(CV3)190,180,190
1000 190 K3=JL-1
1010 DO 200 I=1,JL
1020 V3DN(I)=V3D(I)/V3D(JL)  ; V3NN(I)=V3N(I)/V3D(JL)
1030 200 CONTINUE
1031C
1032C      CALCULATE INVERSE TRANSFORMATION OF V3
1033C
1040 PRINT,"2ND REFLECTION:TYPE VALUES MAXTIME & TIME INCREMENT"
1050 INPUT,ATM,ADT
1060 CALL ZTRAN(K3,V3NN,V3DN,ATM,ADT)
1070 250 CONTINUE
1080 END
```

```
1081C
1082C
1083C      POLYNOMIAL MULTIPLICATION SUBROUTINE
1084C
1090 SUBROUTINE MULTY(A,MM,B,NN,C,KK)
1100 DIMENSION A(24),B(24),C(24)
1110 MMAX=MM+1;NMAX=NN+1;KK=MM+NN
1120 KMAX=KK+1
1130 DO 2 K=1,24
1140 2 C(K)=0.0
1150 DO 10 K=1,KMAX
1160 DO 7 M=1,K
1170 IF(M-MMAX) 3,3,7
1180 3 N=K-M+1
1190 IF(N-NMAX)5,5,7
1200 5 C(K)=A(M)*B(N)+C(K)
1210 7 CONTINUE
1220 10 CONTINUE
1230 RETURN
1240 END
```

```
1241C
1242C
1243C      NUMERICAL LAPLACE INVERSION SUBROUTINE
1244C
1245 SUBROUTINE ZTRAN(M,N,D,TMAX,DT)
1250 DIMENSION AL(10),A(10),AK(10),N(24),D(24)
1260 COMPLEX AL,A,AK,FJ,FJN,FJD
1270 REAL N
1300 AL(1)=(5.2038,-15.7212)    ;A(1)=(-10.15471,-4.260437)
1310 AL(2)=(5.2038,15.7212)     ;A(2)=(-10.15471, 4.260437)
1320 AL(3)=(8.7980, -11.9391)   ;A(3)=(189.2250,250.7353)
1330 AL(4)=(8.7980,11.9391)     ;A(4)=(189.2250,-250.7353)
1340 AL(5)=(10.9343,-8.4096)    ;A(5)=(-866.2283,-2313.588)
1350 AL(6)=(10.9343,8.4096)     ;A(6)=(-866.2283, 2313.588)
1360 AL(7)=(12.2261,-5.0127)    ;A(7)=(1560.540,8422.502)
1370 AL(8)=(12.2261, 5.0127)    ; A(8)=(1560.540,-8422.502)
1380 AL(9)=(12.8376,-1.666)     ; A(9)=(-872.8822,-15431.37)
1390 AL(10)=(12.8376,1.666)     ; A(10=(-872.8822,15431.37)
1400 DO 1 I=1,10
1410 AK(I)=AL(I)*A(I)
1420 1 CONTINUE
1430 T=0.0
1440 NT=TMAX/DT
1450 PRINT,"NUMBER OF DATA POINTS:  ",NT,!
1460 PRINT," TIME              OUTPUT",!2
1470 DO 30 I=1,NT
1480 T=T+DT
1490 FJ=(0.0,0.0)
1500 DO 20 J=1,10
1510 FJN=(0.0,0.0)   ;FJD=(0.0,0.0)
1520 M1=M+1
1530 DO 10 K=1,N1
1540 FJN=N(K)*(AL(J)/T)**(K-1)+FJN
1550 FJN=D(K)*(AL(J)/T)**(K-1)+FJD
1560 10 CONTINUE
1570 FJ=AK(J)*(FJN/FJD)+FJ
1580 20 CONTINUE
1590 ANS=FJ/T
1600 PRINT 40,T,ANS
1610 30 CONTINUE
1620 40 FORMAT(1X,F5.1,8X,E12.5)
1625 RETURN
1630 END
```

2.4 Diode Studies

2.4.1 Apparatus and Measuring Techniques

In order to study the temporal history of diodes, time resolved current and voltage diagnostics were used. The current monitor (shown in Figure 2-37) consisted of a low impedance (15 milliohm) resistive return current shunt mounted between the anode plane and the pressure tank of an IPC FX machine. The FX-1 facility was used for these experiments since Neptune B was not available for use.

A capacitive voltage divider was fabricated to give the voltage-time signature associated with the diode. If C_1 is the capacitive coupling to the cathode and C_2 is the probe capacitance then the output voltage is:

$$V_{out} = \frac{C_1}{C_2} \quad \frac{Z_o}{(R_L + Z_o)} \quad V_c \text{ if } C_2 >> C_1$$

Z_o is the oscilloscope impedance and R_L the load resistance. Since C_2 $(R_L + Z_o) = \tau$ the decay time which must be much greater than the pulse width, and Z_o is in practice 50 or 125 ohms, then C_1 is fixed and there remains a free choice between R_L and C_2. Fixing C_1 means that the area of the probe is defined and the choice between R_L and C_2 amounts to the choice of dielectric thickness.

In order to link as little length of the cathode as possible, the monitor was made as a band encircling the cathode in the post-tube section. It is positioned five inches back from the anode. The signal is brought out through a 50 ohm vacuum line to a 50 ohm G. R. connector. The load resistor is as close to the monitor as possible. A guard ring of the same capacitance, and with a resistance of $(R_L + Z_o)$ to ground, is on each side of the active element. The rings reduce the fringe fields of the monitor. The device in position is shown in Figure 2-38.

The calibration of the current and voltage diagnostics is accomplished with tapered transmission lines of constant impedance.

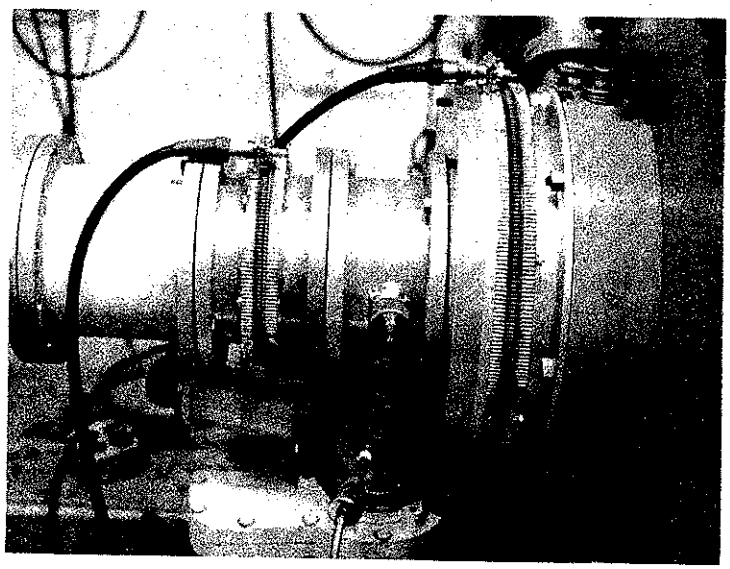

Figure 2-37. Drift Tube and Field Emission Tube Current Shunts

2-779

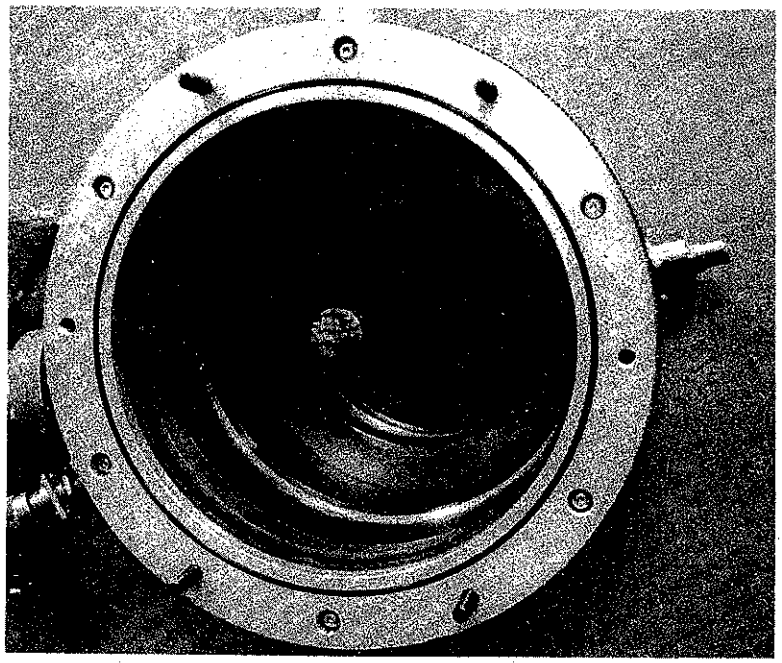

Figure 2-38. Capacitive Voltage Monitor and Return Current Shunt

2-1264

A modular set up was manufactured so that tapered lines are available to fit the drift tube size of the exit section of FX-1. The tapered section and diagnostic section have a nominal impedance of 50 ohms. The continuity of the impedance is checked with a Tektronix TDR. A pulse is launched from a transmission line (square wave) pulser, and is monitored at the end of the calibration line. The pulse from the current sensor is monitored on a sampling scope or on a Tektronix model 581. In this way the sensor is calibrated and its risetime measured. The arrangement is shown in Figure 2-39 where a pickup loop in a 6-inch pipe is under test. The conical sections seen in the background are for tapering up to the field emission tube diameter. The tapered line is also helpful in the design phase of diagnostic gear.

The response of the voltage monitor is shown in Figure 2-40 where it is seen that the risetime is subnanosecond. The slump was shown to be 0.5μs (e^{-1} time) in another test. The calibration of the voltage monitor has been done both with the 50 ohm transmission line test set up and by use of the Be (γ,n) threshold (1.67 MeV) determination. The calibration with the 1/8-inch shank did not agree with the others, and the measurements of the high impedance gap that is produced by this shank were erratic. This is probably due to the cloud of electrons emitted from the shank.

The traces must be corrected for the inductive contribution. The trace as displayed on the scope is $V_c + L\, di/dt$, where L is the inductance of the cathode from the point of the monitor to the gap. This effective inductance is measured by shorting the gap and simultaneously measuring the short circuit current and the resultant voltage which is L di/dt. One then differentiates the current pulse or integrates the voltage trace to ascertain L. This only needs to be done once for each cathode set-up. Once the value of L is obtained, the voltage pulses can be corrected by differentiating the current pulse and subtracting L di/dt.

2.4.2 The Effects of Diode Materials on Impedance

Experiments were carried out to determine the effects of cathode and anode material on the turn-on time of the diode and also the length of time

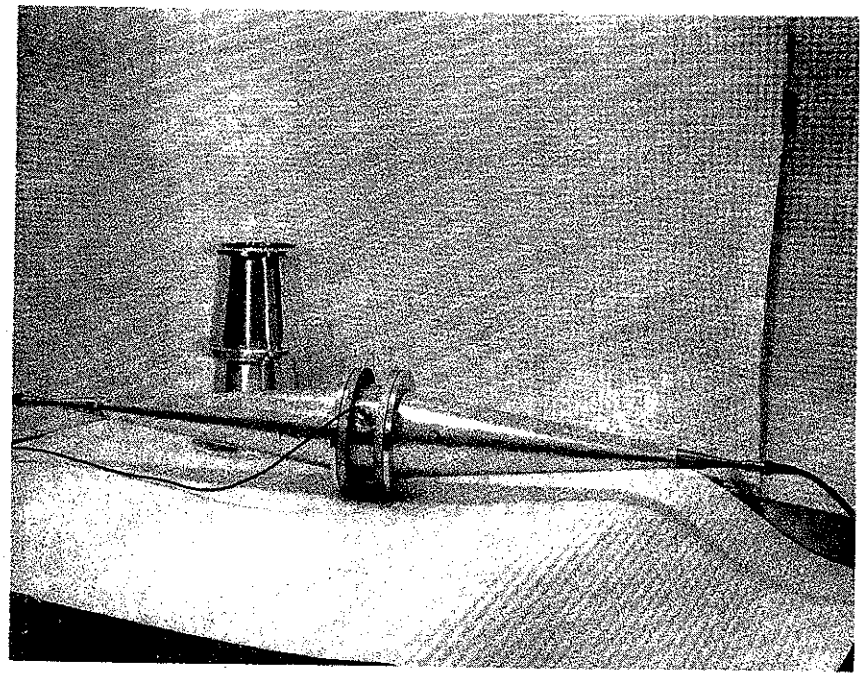

Figure 2-39. Calibration of Current Sensor with Tapered Transmission Line

2-1206

Sampling Oscilloscope Traces

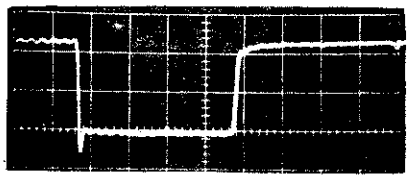

Test Pulse

5 ns/cm

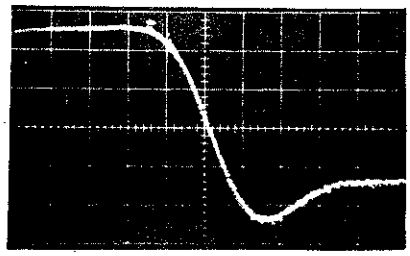

0.2 ns/cm

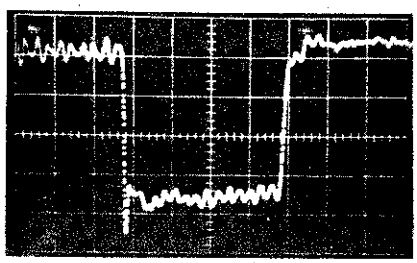

Voltage Monitor Output

5 ns/cm

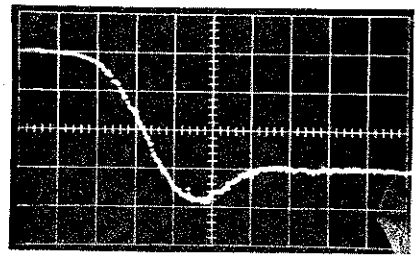

0.2 ns/cm

Figure 2-40. Biconical Transmission Line Calibration of Capacitive Voltage Monitor

2-1386

the diode remains on before closing (shorting). Figures 2-41 - 2-43 show the raw data obtained using three different cathode materials, namely carbon, brass, and aluminum. Each cathode was 2-inches in diameter, with the edge rounded off, and the gap spacing set at 1.5 centimeters. The main feature to note is the inductive over-shoot which occurs at the beginning of the voltage traces. It is clear that the over-shoot is less in Figure 2-41 than it is in Figures 2-42 and 2-43. Since the geometry of the experiment was kept fixed, this means that dI/dt was larger in the case of the metallic cathodes. Figure 2-44 shows the time resolved impedance data obtained from these traces. It is clear that the large dI/dt associated with the metallic cathodes is due to the fact that they do not start emitting as quickly as the carbon cathode. The difference is more clearly brought out in Figure 2-45, which shows the normalized impedance for carbon and aluminum cathodes. This plot, which normalizes the instantaneous actual impedance to what the Child's law impedance would be, is more meaningful since it removes any possible voltage dependence of the diode impedance. The faster turn-on of the carbon cathode is clearly evident.

A second feature worth noting on Figure 2-45 is that the steady-state impedance is only 1/3 of what Child's law would predict. Equivalently, about 3 times more current is flowing than would be expected from space charge limited considerations. Calculations showed that a counter-streaming ion current (of, say, singly ionized nitrogen) could double the electron current simply because the slower moving ions partially neutralize the space charge of the electron beam. Other calculations have shown that ionization of the residual gas in the diode gap could also double the electron current. It is believed that a combination of these two effects could account for the factor of 3.

Finally, Figure 2-46 shows data obtained on the influence of anode material on gap closure. The time to closure was defined as that time period over which the impedance remained within ±25% of its steady state value, the leveling off of the carbon anode data simply corresponds to the diode operating during the entire duration of the output pulse from the PFN. It should be noted that carbon seems to give at least twice as long a time period before closure than a titanium anode does. No theory has been developed to explain these

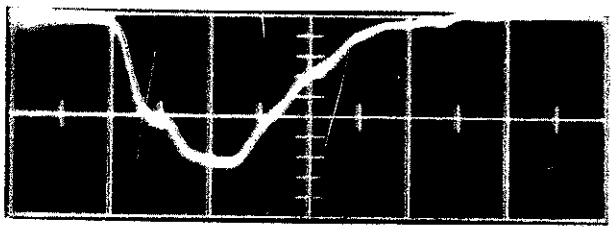

I (t)

29.4 kA/cm
20 ns/cm

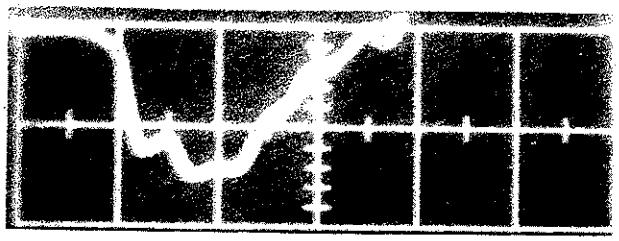

V (t)

657.5 kV/cm
20 ns/cm

Figure 2-41. Current and Voltage Data for Carbon Cathode (3 Shots Superimposed)

2-1361

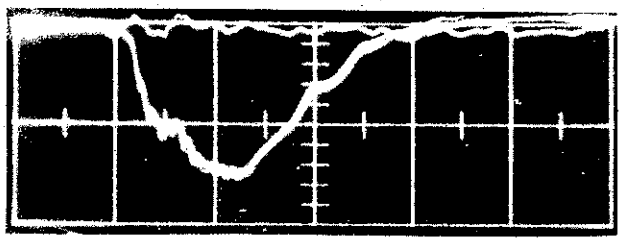

I (t)

29.4 kA/cm
20 ns/cm

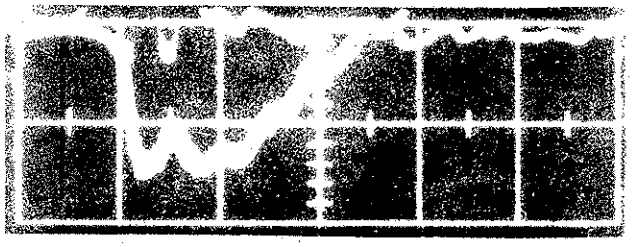

V (t)

657.5 kV/cm
20 ns/cm

Figure 2-42. Current and Voltage Data for Brass Cathode
(3 Shots Superimposed)

2-1362

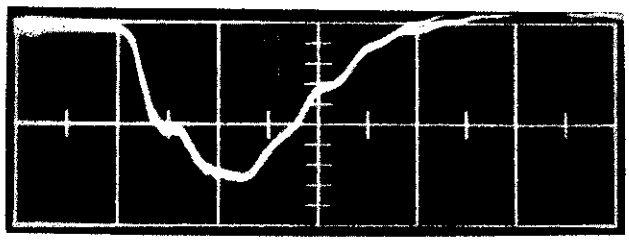

I (t)

29.4 kA/cm
20 ns/cm

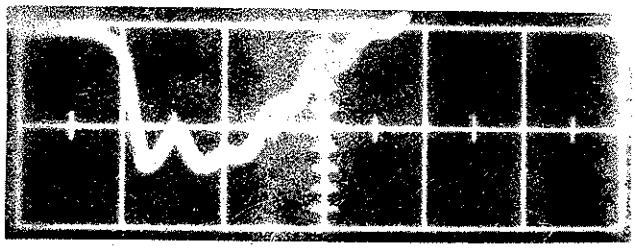

V (t)

657.5 kV/cm
20 ns/cm

Figure 2-43. Current and Voltage Data for Aluminum Cathode (3 Shots Superimposed)

2-1363

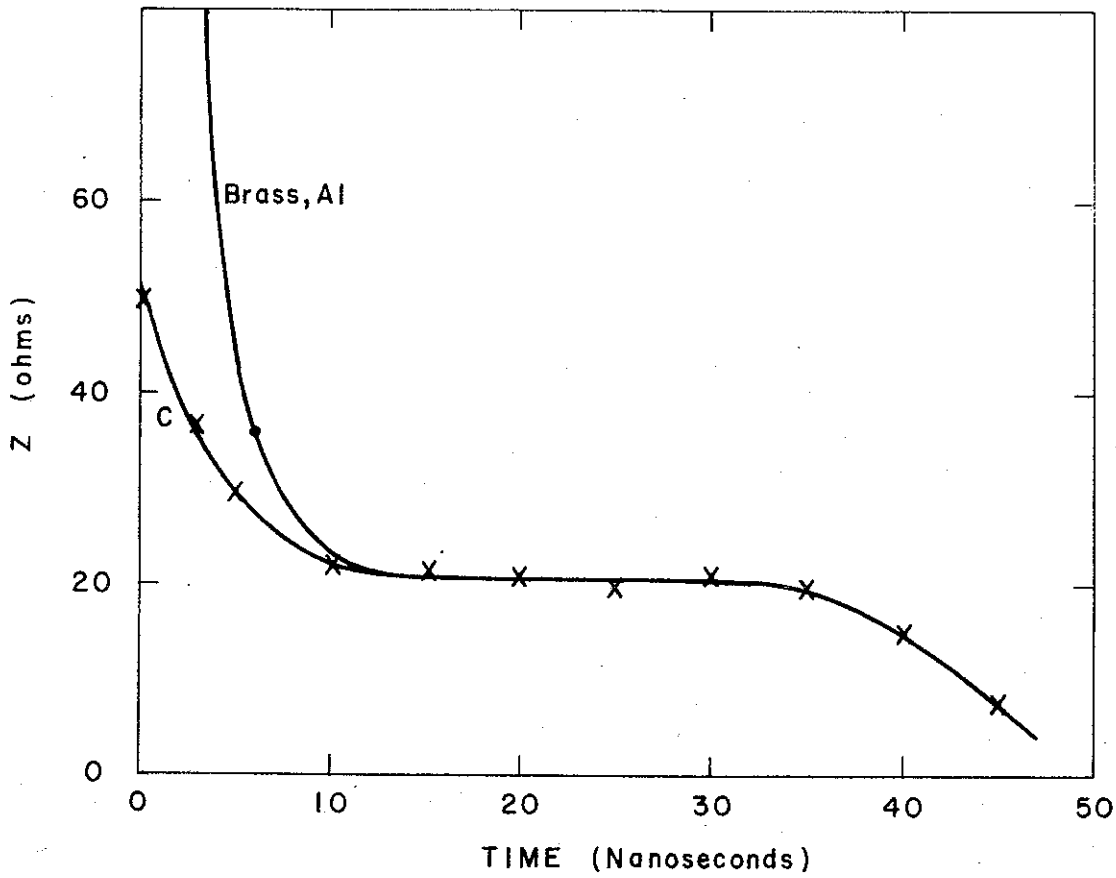

Figure 2-44. Time Dependent Cathode Impedance

1-4068

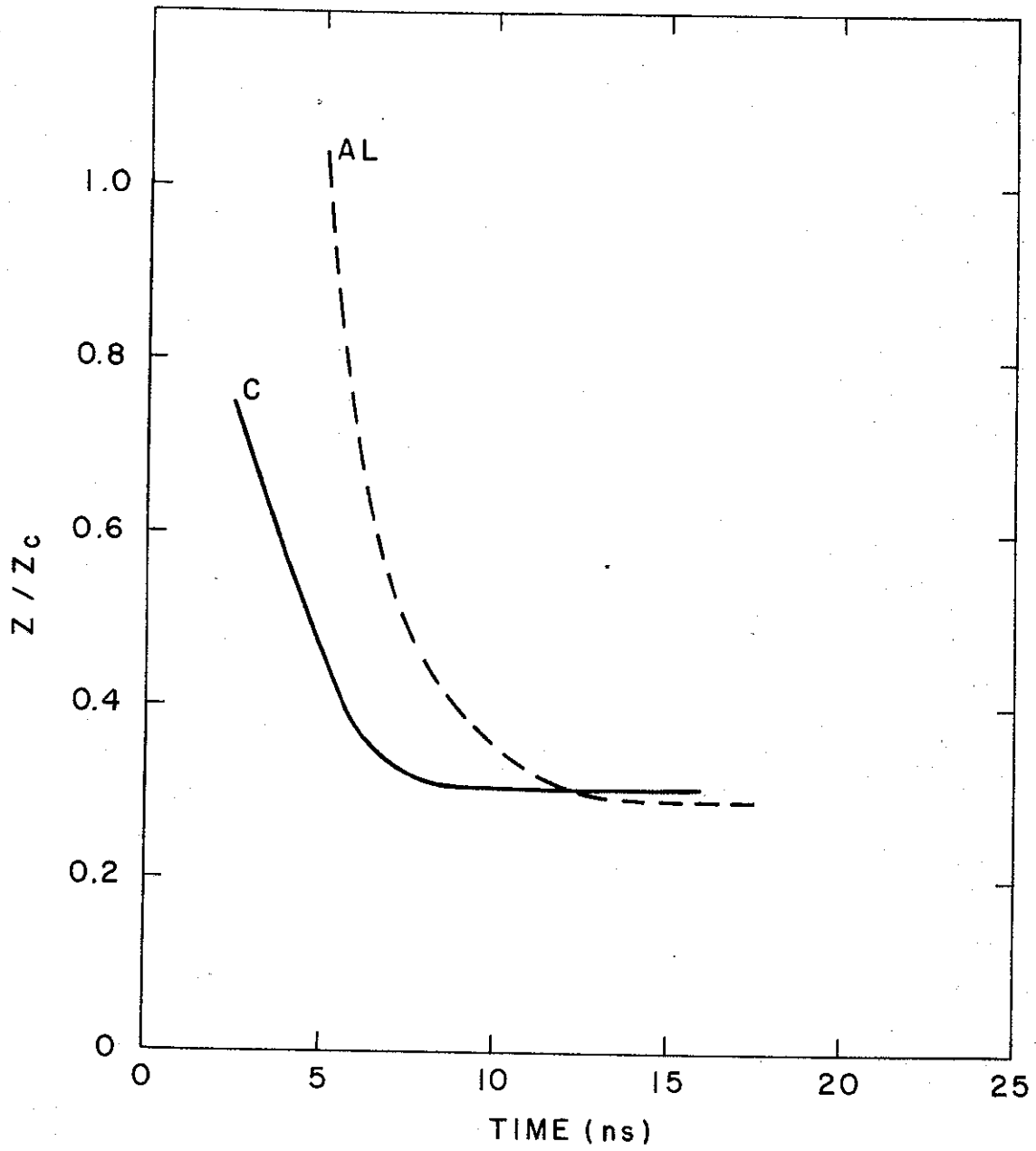

Figure 2-45. Normalized Diode Impedance as a Function of Time for Carbon and Aluminum Cathodes

1-4378

results, although the apparent constant velocity associated with gap closure could provide a clue to the closure mechanism.

2.4.3 The Effects of Diode Geometry on Impedance

Measurements were made on the effect of cathode radius and gap spacing on diode impedance. Carbon cathodes, of two different diameters, were used. The results, shown in Figure 2-47, indicate that the impedance scales linearly with gap spacing, not quadratically as would be required by Child's law. Also, the impedance did not seem to depend strongly on the cathode diameter. It should be noted that a linear scaling of impedance with gap spacing is predicted by the parapotential flow theory.[1]

---

[1] J.C. DePackh (NRL) DASA Simulator Review Meeting, Washington, 1968.

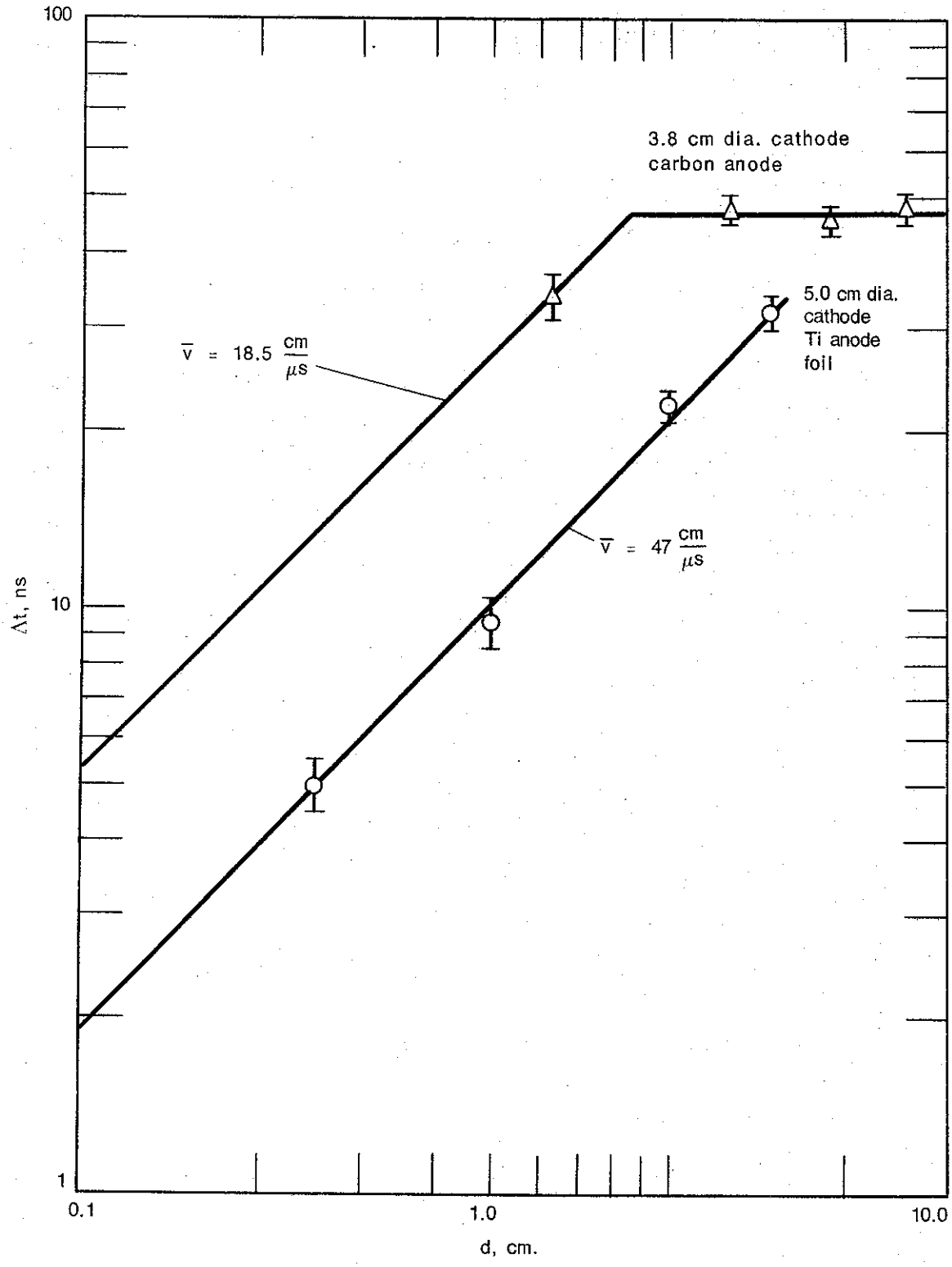

Figure 2-46. Time to Diode Closure versus Gap Spacing

1-4418

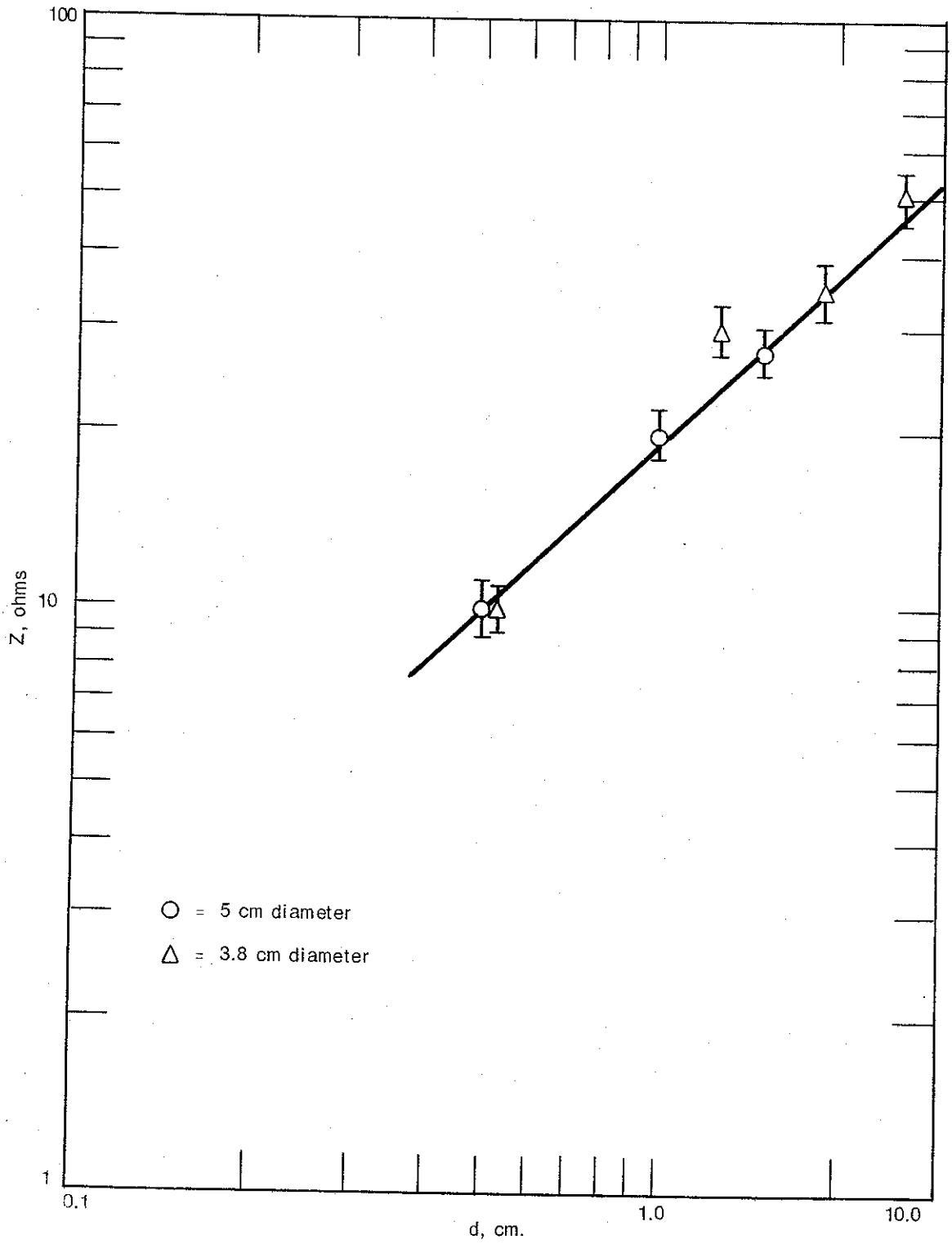

Figure 2-47. Diode Impedance versus Gap for Two Cathode Diameters

1-4417

SECTION 3
SOLID DIELECTRIC STUDIES

3.1 Introduction and Summary

3.1.1 General

The intrinsic dielectric strength of most insulating solids appears to be in excess of 10 MV/cm. Values in this region have been measured on thin, carefully prepared samples with pulsed voltages. In practical applications the design stress is well below this value. The electrical power industry operates insulation several orders of magnitude below the intrinsic stress, mainly because of cost and reliability requirements. Reliability usually dictates that the insulation be operated below or near the discharge inception stress. The design stress can be increased if greater quality control is used and/or a reduced life is acceptable.

Solid dielectrics fail due to one or more of the following processes:

(1) intrinsic
(2) erosion by discharges
(3) channel propagation
(4) thermal instability
(5) electromechanical
(6) chemical or thermal deterioration
(7) electrochemical

Insulation, subjected to low repetition rate pulses, is most likely to fail by partial discharge erosion or channel propagation. The discharges occur above a threshold field at imperfections (voids, impurities) and cause the insulation to have a finite life at this stress. Most solids appear to have a stress-life characteristic of the form E^nT = constant where 'n' lies between six and eight. Mylar for example, has $n \simeq 7.5$[1, 2] and polyethylene $n \simeq 7.0$.[3, 4] Alston[5] has reviewed the mechanism of partial discharges and factors affecting the life under pulse conditions. He concludes that both the void size and its location are important; voids adjacent to the cathode are more harmful than others. The peak-to-peak voltage, the peak voltage, rate of application and

removal of voltage, time at voltage and particularly voltage reversal affect the life of the insulation.

It is thus apparent that if solid insulation is to be used at maximum stress and have a reasonable life, then great care is needed to reduce the number of voids (none ideally). In addition, the material should have a good resistance to corona. Dakin[6] has studied several typical materials for their voltage endurance in the presence of corona. (The materials of interest had a spread in their endurance characteristics of only 2 to 1.)

Since the stress-life characteristic is probably most influenced by partial discharges in voids, it is important that the casting be made under closely controlled conditions. By suitable casting procedures, the probability of a void in a high field region can be greatly reduced. Such procedures include using a well degassed resin, an evacuated mold, optimum filling rate and a low curing temperature. The casting should then be checked for voids by normal discharge detection equipment. This gives an indication of quality and probable life.

It is relevant to note that industries involved in the manufacture of high voltage systems and components employing solid dielectrics in a stressed state with long life requirements, have developed procedures and facilities for mixing, pouring or extruding such solids almost completely free of voids or imperfections which lead to degradation and breakdown.[12] Good examples are the many instances the units have lifetimes up to 10's of years under continual ac or dc stressed conditions.

3.1.2 Significance of the Solid Dielectrics Data

(1) The use of cast insulation in single large volumes (> 5 liters) cannot be recommended for H.V. energy storage (pulse or d.c.). With present technology, an optimistic design stress is 1 MV/inch (at megavolt potentials) for large castings, yielding a figure of merit ($\epsilon_r^{1/2} E$) of only 1.0 ($E = 400$ kV/cm $\epsilon_r = 6.25$). For

pulse storage of energy, water and oil are clearly superior in the microsecond and less time scale. Solids show no improvement in breakdown strength until the pulse width is in the few nanoseconds region. For large pulses or where solid insulation is desirable, the use of thin sheet plastics (mylar, polyethylene for example) is recommended although lucite and cross linked styrene sheets and cylinders, suitably machined, offer certain advantages. Styrene for example, has a figure of merit greater than 2.0 and is much lighter than filled epoxy. Cast insulation suffers from a sizeable volume effect indicated by a large standard deviation in the breakdown strengths of small samples, although the standard deviation for the Castall 302 was reduced by improved material and procedures. Very low breakdown strengths were measured when the casting procedure was in error by a modest amount, e.g. 5 minutes degassing instead of 20 or too little curing agent. It thus becomes extremely difficult to cast a large volume and maintain strict control of material, electrodes and the procedure. Where it is necessary to cast in metal electrodes, consideration must be given to matching the thermal expansion coefficients and to the problem of shrinkage (fillers help in this respect). The development of an intermediate material with larger ϵ_r, lower resistivity and greater flexibility between the metal and the cast insulation should lead to significant improvements in this respect.

(2) Solid dielectrics are needed in all H.V. apparatus either as an interface or support structure. It is important to remember that the flashover strength is less than that of the surrounding medium. Breakdown along an interface can proceed extremely rapidly, especially

in vacuum and gas. To improve the voltage withstand, special attention must be paid to (i) the insulator end conditions (i.e., metal/solid/medium); (ii) the electric field distribution along the interface; (iii) the material tracking characteristics; (iv) the finish and contamination on the insulator surface (moisture is particularly bad in H.P. gas).

The present work has shown that styrene, a material with good puncture strength but poor tracking qualities can be greatly improved by corrugating the surface and applying a thin layer of material with good tracking characteristics (acrylic).

Interfaces in a gas or vacuum medium show significant conditioning effects (1.2 - 2.0 times the first flashover). This is very important in high energy devices where it is not always convenient to carry out low energy conditioning. When more is known about the processes involved in surface conditioning then higher reliable operating gradients can be employed. This is especially important for low impedance devices since discontinuities (switches, output ends, etc.) can then be reduced.

(3) The approach taken in this program developing a low impedance output end for F.E. tubes is believed to be sound and should be investigated further. Using short (2-inch axial length) machined pieces of styrene and acrylic with a 1-inch interface length, it was possible to operate a 5 ohm cathode at 120 kV (30 ns pulse width). With a cast dielectric piece in lieu of the machined piece (to reduce the triple joint problems) it is believed that design stresses approaching 500 kV/inch can be achieved.

(4) As a result of the experience gained during this program and from the published literature,[7-12] the following guidelines for casting insulation for high dielectric strength applications, will be found useful:

(a) Prevent bubble formation prior to cure by raising the temperature of the resin (> 60 °C) and lowering the pressure (2 - 20 Torr).

(b) Choose a resin with low viscosity, good wettability, low degassing pressure, low temperature cure and which is tough.

(c) Mold and Electrodes. System should have no flat horizontal regions in critical areas. Choose materials which can be easily cleaned. System vacuum tight to 10^{-5} Torr. Fill from the bottom of the mold at a rate slow enough to allow good wetting. Cleaning of surfaces is very important - mild abrasion, vapor degrease, solvent soak, wash in distilled water. Filled resins give a better match of thermal expansion coefficients with metals.

(d) Resin Preparation. Filter if possible. Preheat components separately to 140 °F or greater. De-aerate and stir at 1 - 2 Torr. Mix and continue stirring and de-aeration. Transfer to the mold with the mold pressure higher than the degassing pressure (15 - 30 Torr).

3.1.3 References

(1) Hayworth, B. R., "The High Voltage, High Frequency Characteristics of Polyester Film", Seventh Electrical Insulation Conference, p. 88 (1967).

(2) Martin, J. C., AWRE Report No. SSWA LCM/6611/106, Aldermaston, England.

(3) Alston, L. L., "Life of Polyethylene at Very High Stresses", Proceedings IEE, Volume 112, No. 4 Ap. (1965).

(4) Ware, P. H., "Polyethylene as High Voltage Cable Insulation", Seventh Electrical Insulation Conference, p. 255 (1967).

(5) Alston, L. L., "The Electrical Breakdown of Solid Insulation Subject to Voltage Pulses", Culham Laboratory Report, UKAEA, England, CLM-M9.

(6) Dakin, T. W., "Effect of Electrical Discharges on the Breakdown of Solid Insulation", Comm. and Electronics IEEE, p. 155 (May 1954).

(7) Currence, R., "Void Free Embedment of High Voltage Electronic Modules", IEEE, 68C6 FJ 53, p. 28.

(8) McGuiness, E. W., Giordano, J. J., "How Raytheon Packages a High Voltage Power Supply for Deep Space", Insulation, p. 14, (April, 1969).

(9) Bobo, S., Galligani, P., "High Vacuum Potting of High Voltage Assemblies", Research/Development, p. 48 (March, 1968).

(10) Olyphant, Jr., M., "Effect of Cure and Aging on Dielectric Properties", 6AE. Insulation Conference, p. 12, (1965).

(11) "Casting Resins and Application Technique for Embedment, Encapsulation and Impregnation", Electrotechnology, Vol. 2, (1961).

(12) Lee and Neville, "Handbook of Epoxy Resins", McGraw-Hill, (1967).

3.2 Impulse Puncture and Flashover Tests on Various Filled Epoxy Resins

3.2.1 Introduction

Different epoxy materials supplied by several manufacturers were evaluated for their volume puncture strength as well as flashover characteristics under impulse voltage application. The samples exhibited a range of volume electric strength and surface flashover characteristics. A good number of these provided very encouraging voltage withholding qualities which even allowing for pessimistic extrapolation for large volume and surface area effects still yield interesting coaxial store designs.

3.2.2 Apparatus

For both the puncture and flashover tests an impulse generator was used, which provided a 0.5/30 μs wave of positive polarity with energies up to about 10 kJ. Voltage and current waveforms were recorded on a 519 Tektronix Oscilloscope. These provided evidence and measure of breakdown voltage current and time and were backed up with visual and audio observation. In addition, the resistance of the breakdown paths for the puncture samples was subsequently measured using a dc supply. The impulse generator was calibrated to an accuracy of better than 5%.

3.2.3 Volume Puncture Test

A typical volume puncture test setup is shown in Figure 3-1 and three different shapes of samples were used initially. For two of these the metal electrodes were concentric cylinders so designed that the maximum electric stress was in the center rather than at the ends of the cylinders. For the third group the epoxy was cast around uniform field electrodes. Gap distances of 1/8 and 1/4-inch were used and the stressed electrode areas for the three samples ranged from about 6 to 70 square inches. The dimensions of the samples are given in Figures 3-2 , 3-3 and 3-4 .

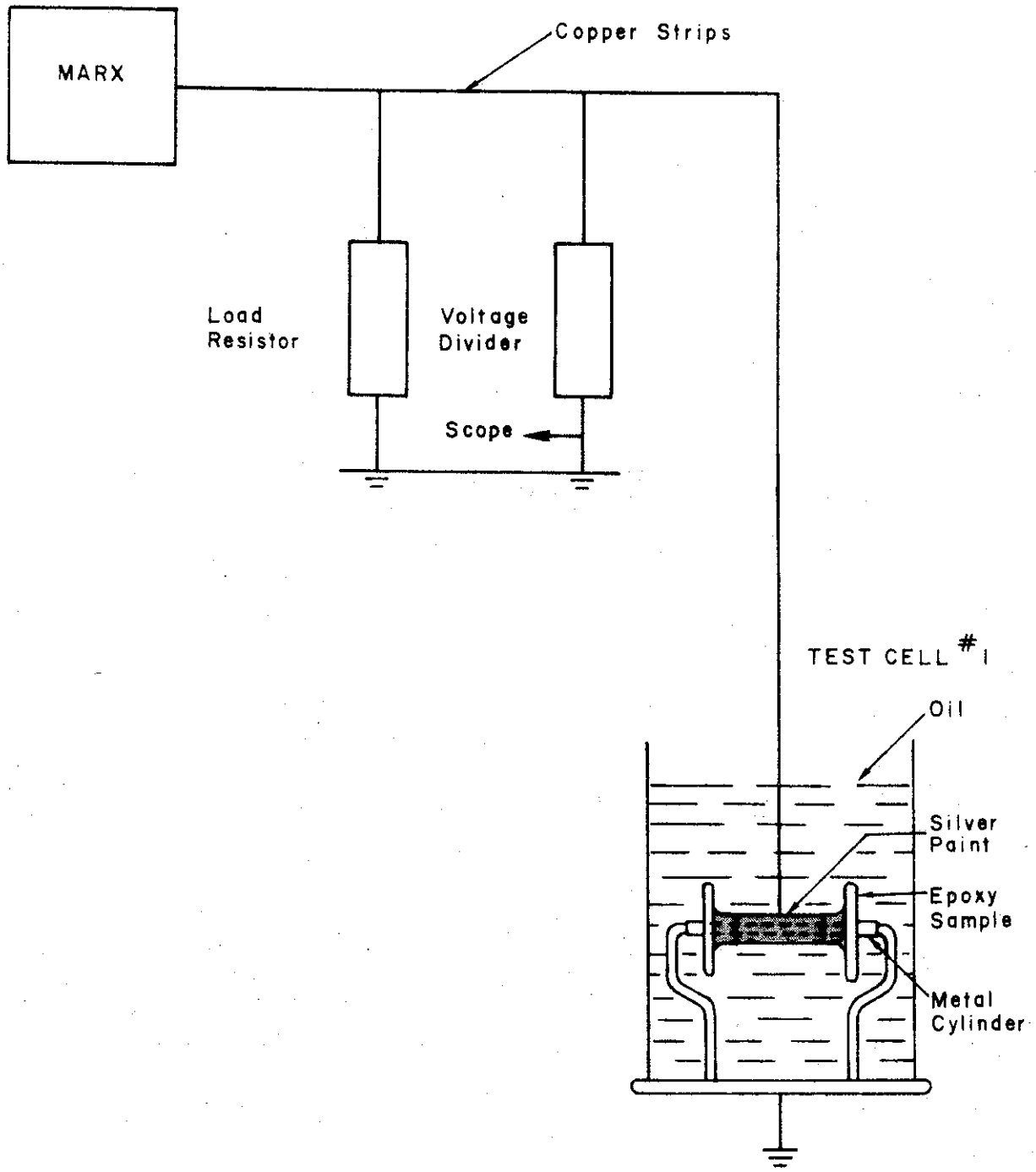

Figure 3-1. Experimental Set-Up for Puncture Test on Epoxy Samples Between Concentric Cylinders of Test Cell No. 1

1-3618

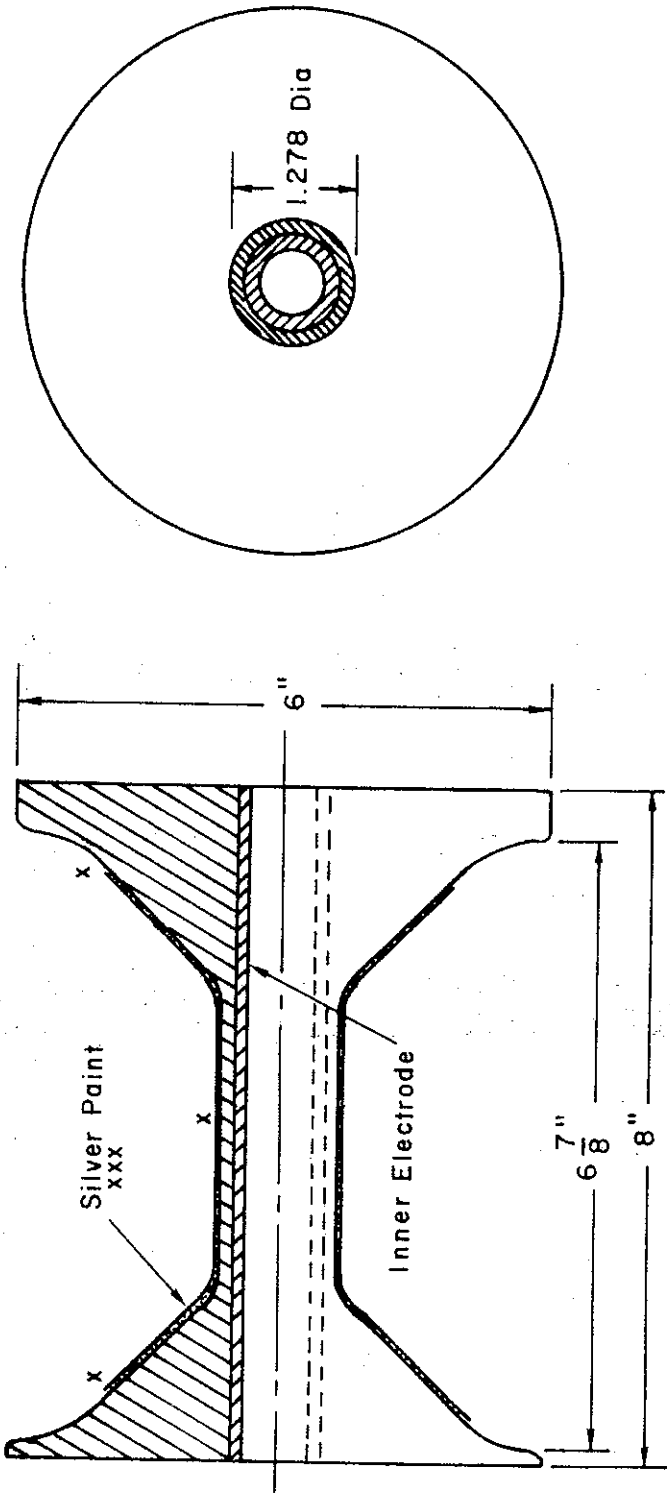

Figure 3-2. Concentric Cylinder Sample
(Small Diameter)

1-5057

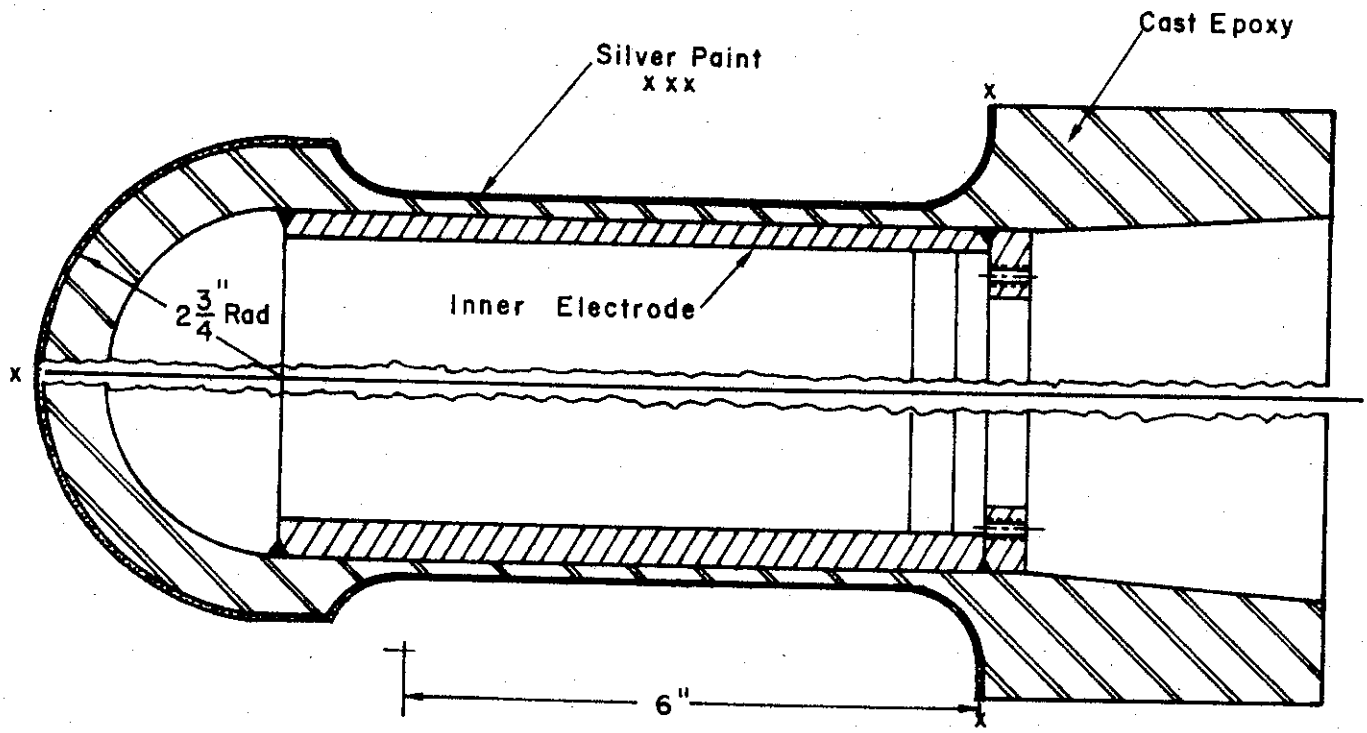

Figure 3-3. Concentric Cylinder Test Sample (Large Diameter)

1-5058

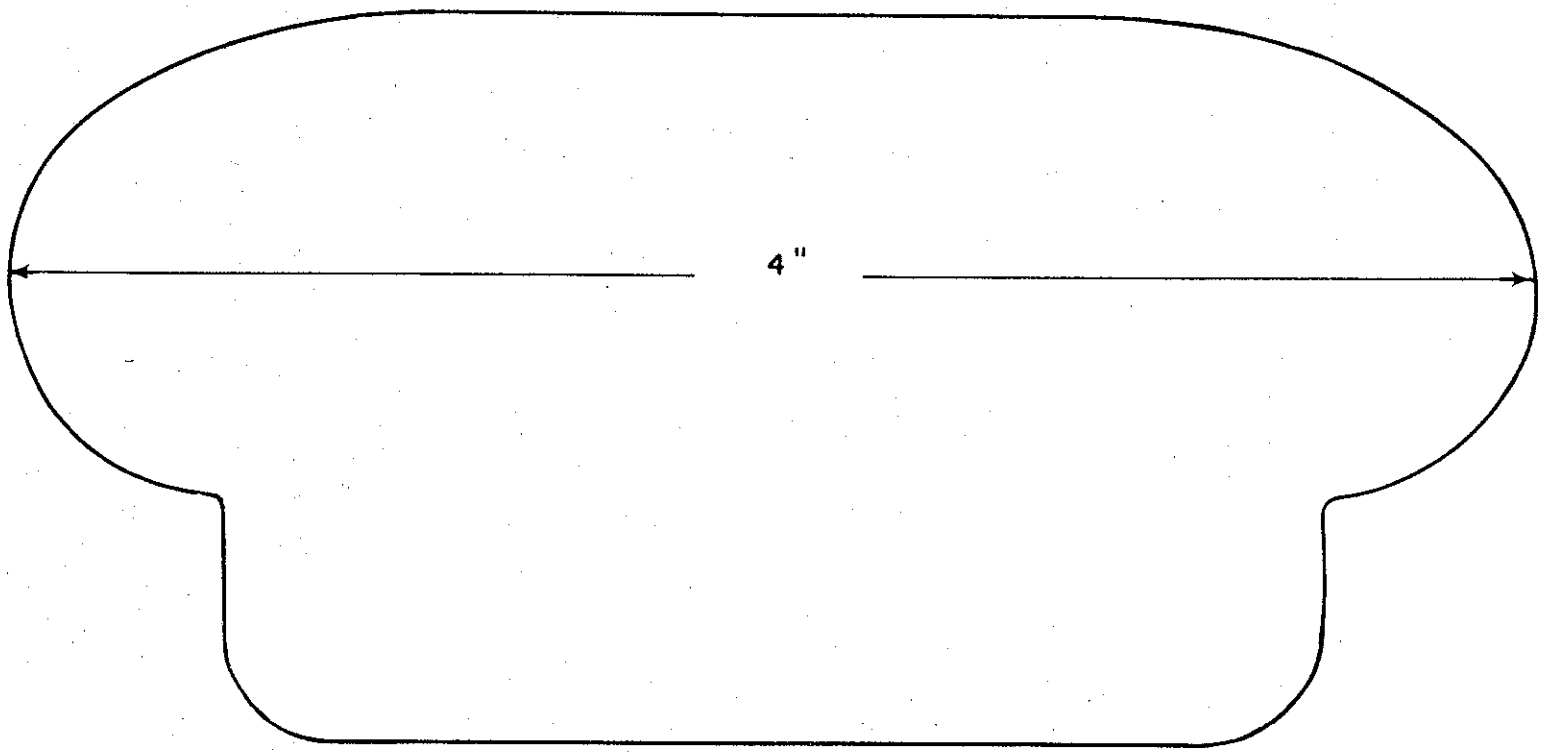

Figure 3-4. 4-Inch Diameter Bruce Profile Electrode and Support Base for Test Cell No. 3

To prevent external flashover the samples were immersed in transformer oil while subject to high voltage impulses. The voltage was raised in increments of approximately 14 kV until breakdown occurred. Breakdowns were monitored as discussed above and a typical breakdown trace is shown in Figure 3-5. After puncture, the samples were sectioned so that an accurate sample thickness could be measured. Up to four identical samples were evaluated at the same nominal thicknesses of 1/8- and 1/4-inch. Filled epoxies of various types were used for the tests with dielectric constants ranging up to at least six; higher values may, of course, be obtained by suitable choice and concentration of filler. The principal results are summarized in Figures 3-6 and 3-7. Figure 3-8 shows the cumulative probability of breakdown for samples tested.

Puncture voltage versus sample thickness is plotted. With the exception of one low value of 1.2 MV/in. for most cases, the puncture strengths were better than 1.5 MV/in. mean breakdown strength. Table 3-1 summarizes the above data for the mean breakdown electrical fields. Table 3-1 also contains the puncture data for the Stycast between the uniform field electrodes (Figure 3-4). Radiographs of all samples were taken to confirm that the electrodes were parallel and the gaps 1/8- and 1/4-inch respectively. From this it is clear that the mean breakdown field strength is about 1.9 MV/in. This figure can be corrected for the area or volume effect as follows. The stressed areas and volumes are 6 square inches and 1-1/2 cubic inches for the 1/4-inch samples. The generally accepted formula relating area and volume to breakdown voltage indicates a reduction by a factor of 2 in the latter for increases of a factor of 10^3 in either the area or volume. There are strong indications, however, that above 1,000 square inches of stressed electrode area or 1,000 cubic inches of stressed volume, a levelling off takes place with much slower subsequent decrease in the breakdown voltage level. When applied to the present samples, it is seen even with relatively pessimistic corrections for the area or volume effect, a reasonable breakdown field strength for 10 liter volumes would be 1-1.2 MV/in.

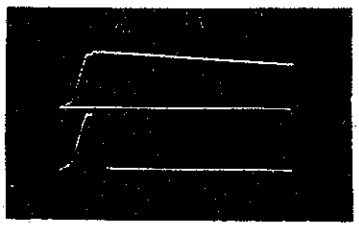

a) Volume Puncture of Epoxy
Test Cell I (1/4 inch thickness)

Trace 1: Marx Output

Trace 2: Volume Puncture

1 μs/cm

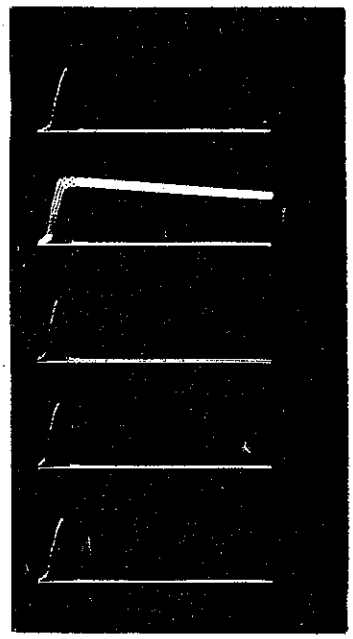

b) Flashover of Epoxy Cylinder
(2 inches Length in 25 psig)
Gas Mixture of: 10% SF_6
40% N_2
50% Ar

Traces 1, 3, 4, 5: Flashover

Trace 2: Marx Output
No Flashover (5 Shots)

Figure 3-5. Scope Traces of Volume Puncture and Flashover of Epoxy Samples

2-1266

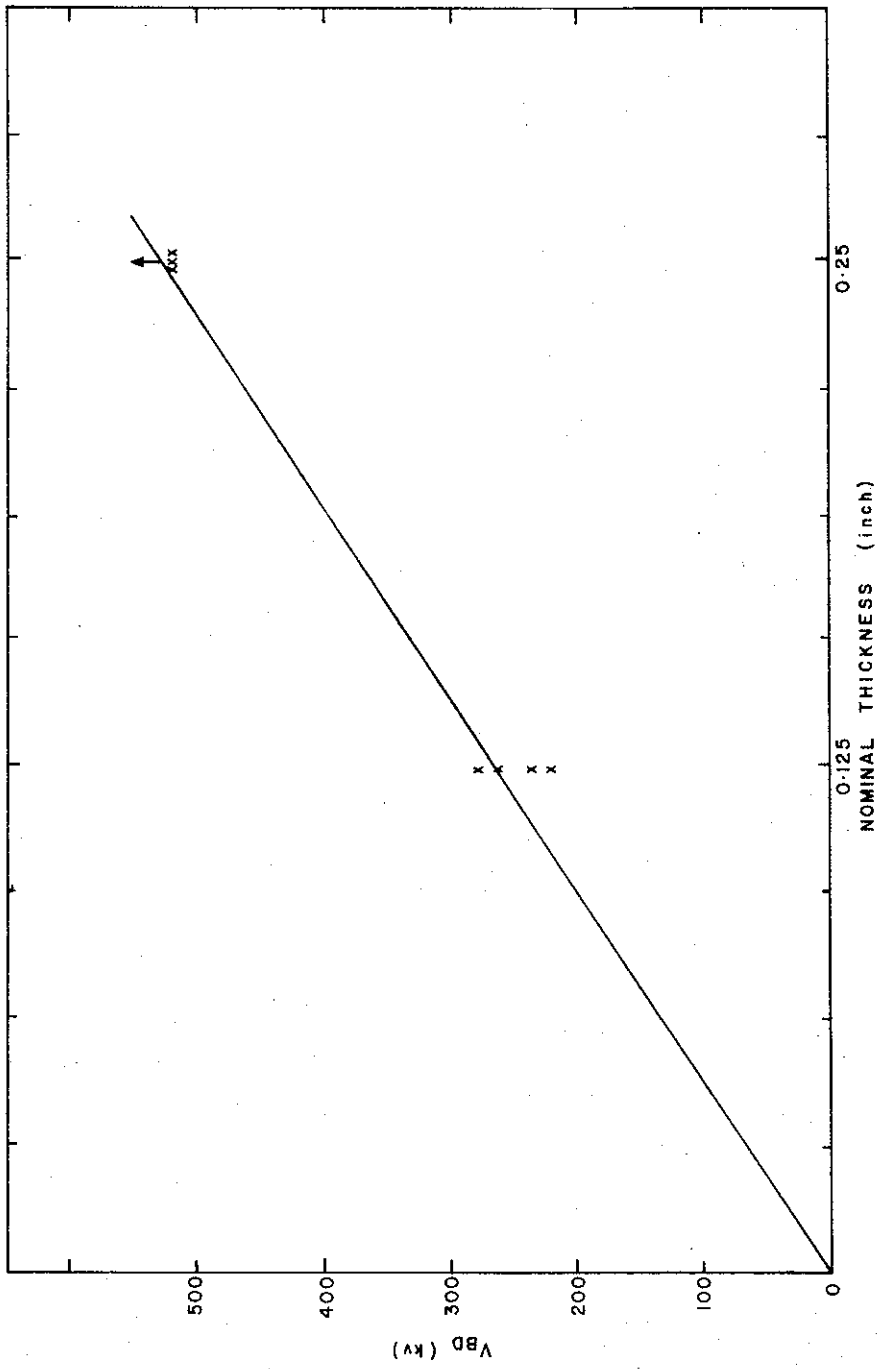

Figure 3-6. Volume Puncture for Blue Stycast Material

1-3681

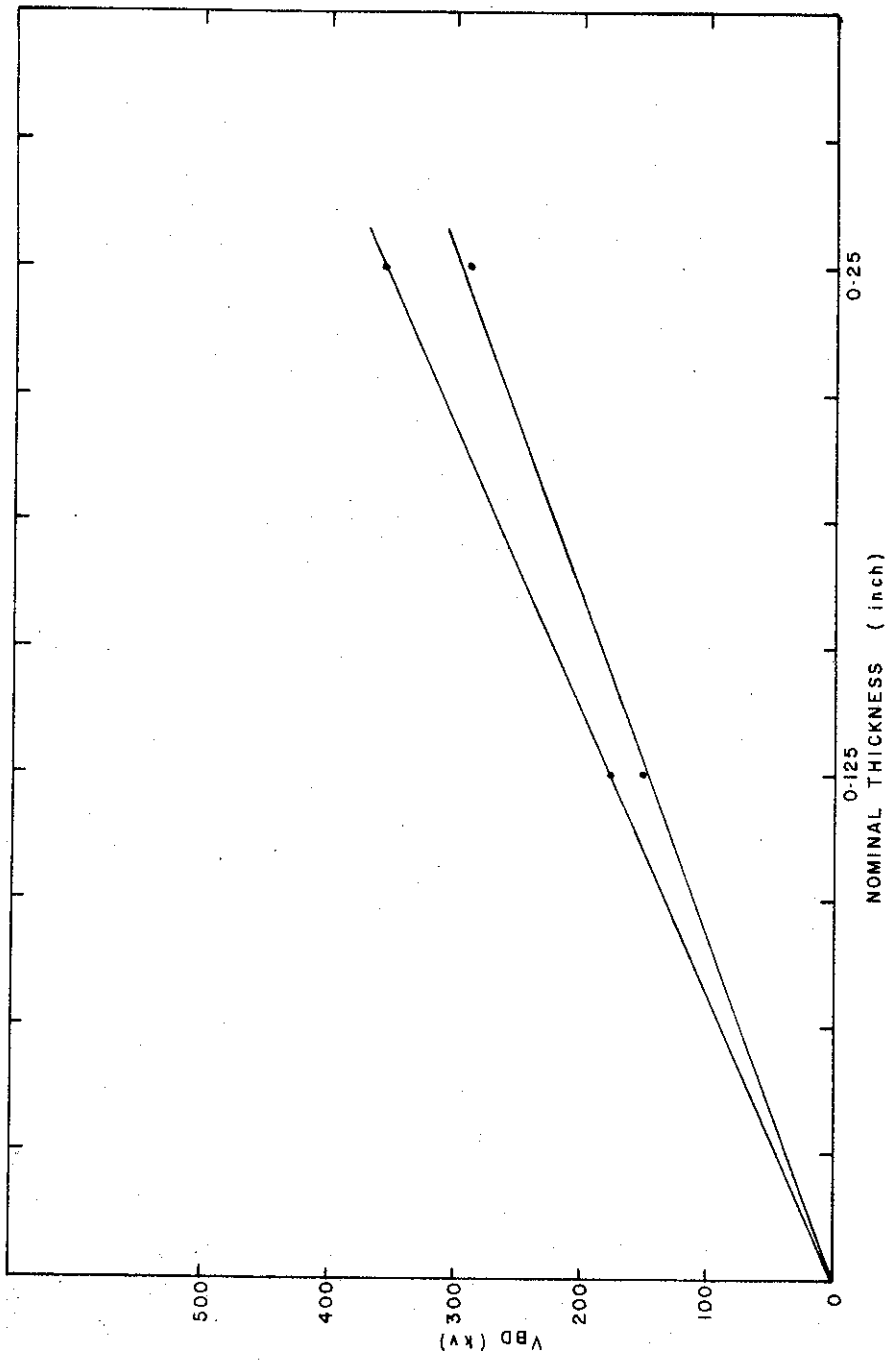

Figure 3-7. Volume Puncture for Permali Material

1-3682

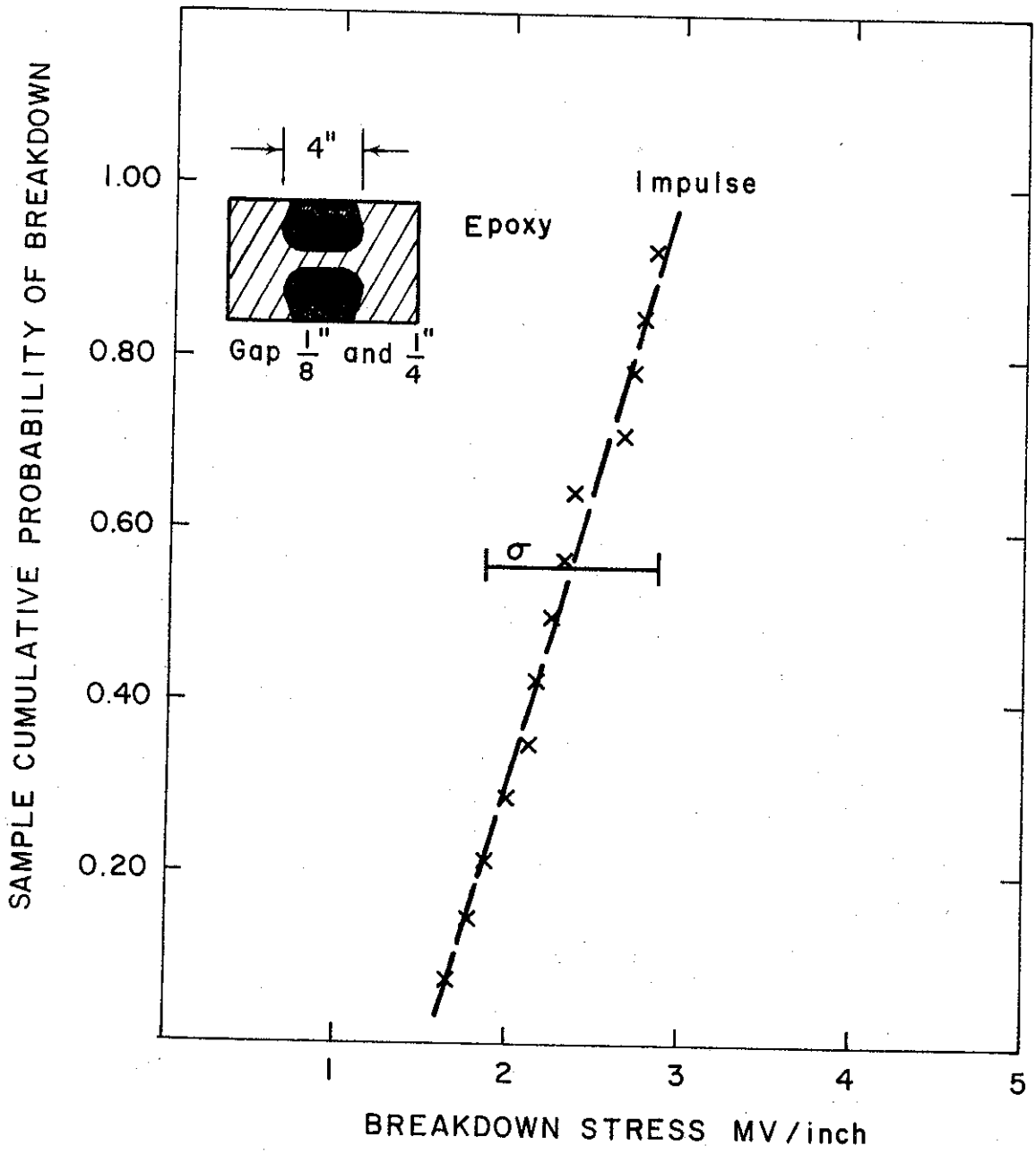

Figure 3-8. Cumulative Probability of Breakdown for Alumina Filled Epoxy Resin Tested Under Uniform Field Conditions - Impulse (0.3/30 μS) (2.36 MV/inch mean)

1-4025

Table 3-1. Volume Puncture Data for Filled Epoxy Materials Under Impulse

Sample	Nominal Thickness	Configuration	Puncture Voltage (kV)	Mean Field (MV/inch)
Permali	1/8-inch	Cylindrical	152	1.24
Permali	1/8-inch	Cylindrical	179	1.43
Permali	1/4-inch	Cylindrical	359	1.43
Permali	1/4-inch	Cylindrical	290	1.16
Stycast	1/8-inch	Cylindrical	193	1.54
Stycast	1/8-inch	Uniform Field	276	2.22
Stycast	1/8-inch	Uniform Field	235	1.87
Stycast	1/8-inch	Uniform Field	221	1.77
Stycast	1/8-inch	Uniform Field	262	2.09
Stycast	1/4-inch	Uniform Field	>469	>1.88
Stycast	1/4-inch	Uniform Field	>469	>1.88
Stycast	1/4-inch	Uniform Field	>469	>1.88
HVE	11/64-inch	Spherical Gap	400	2.33
HVE	11/64-inch	Spherical Gap	>469	>2.73
System's Resource	1/8-inch	Cylinder	110	0.88
System's Resource	1/4-inch	Cylinder	<83	<0.33
Stycast 2850 FT (I.P.C.)	1/8-inch	Uniform Field	234	1.9
Stycast 2850 FT (I.P.C.)	1/8-inch	Uniform Field	467	3.74
Stycast 2850 FT (I.P.C.)	1/8-inch	Uniform Field	344	2.75
Stycast 2850 FT (I.P.C.)	1/8-inch	Uniform Field	344	2.75

There is one further aspect of solid dielectric materials which is of interest, namely their lifetime under voltage stresses of various levels. Because of the importance of determining reasonable estimate of insulator lifetime and degradation effects, accelerated life tests using Stycast samples were carried out. These are reported below.

3.2.4 Accelerated Life Tests on Stycast Samples

The experimental setup for these tests was the same as that previously described. The impulse generator provided 1/50 μs pulses with a voltage capability up to 800 kV. One uniform field 1/4-inch gap Stycast sample was used for which material the breakdown field strength had previously been determined. The tests were carried out as indicated in Table 3-2. The voltage pulse was applied once per minute. Treating the results as an accelerated life test with n = 7.0 and allowing a stress reduction of 2 for a volume effect, a life of 1000 shots at 0.84 MV/in. is indicated. Since no failures were actually observed, the life calculation assumed the next application of voltage would produce failure and the results are therefore pessimistic.

3.2.5 Surface Flashover Test (Impulse Test)

The surface flashover test setup is given in Figure 3-9 . The samples were 1-inch diameter cylinders of 1/2, 1, 2, 3, 6 and 9-inch lengths. For cylinders of 2-inches and below, flashover test was carried out using 6-inch diameter stainless steel electrodes in a pressurized gas mixture of 10% SF_6, 40% N_2 and 50% Ar. For cylinders of 3-inches and above, flashover test was carried out in 1 atm of SF_6 with large plane electrode of 18-inches in diameter. Actual flashover was monitored by both visual observation and scope traces.

Standard impulse techniques were used for determining maximum, minimum and mean flashover voltages. The impulse voltage was raised in steps of 14 kV when no breakdown was observed and decreased in steps of 14 kV when breakdown was observed. This was continued until a stable level was attained. A typical sequence is shown in Figure 3-10. All flashovers were observed to

Table 3-2. Accelerated Life Tests on Stycast Samples

Voltage (kV)	Polarity	Waveshape (μs)	Field Strength (MV/in.)	No. of Shots	Breakdown
420	+ ve	1/50	1.68	230	No
475	+ ve	1/50	1.9	100	No
500	+ ve	1/50	2.0	10	No
525	+ ve	1/50	2.1	10	No
545	+ ve	1/50	2.18	10	No
560	+ ve	1/50	2.24	10	No
575	+ ve	1/50	2.30	10	No
590	+ ve	1/50	2.36	10	No
605	+ ve	1/50	2.42	10	No

Grouped and Averaged

Effective Voltage (kV)	Number of Shots
420	230
475	100
525	25
565	25
600	20

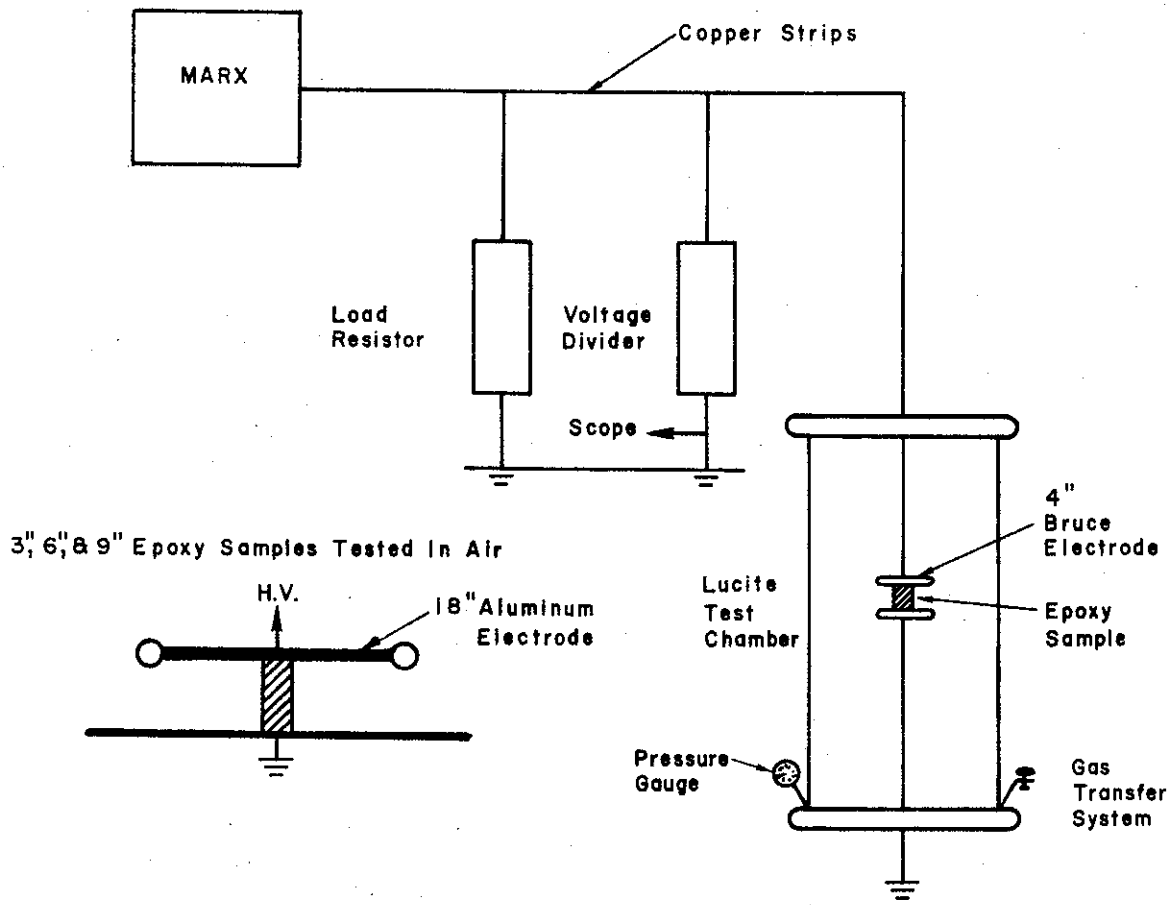

Figure 3-9. Experimental Set-Up for Flashover Test of Epoxy Cylinders in Compressed Gas Mixture and in Air

1-3621

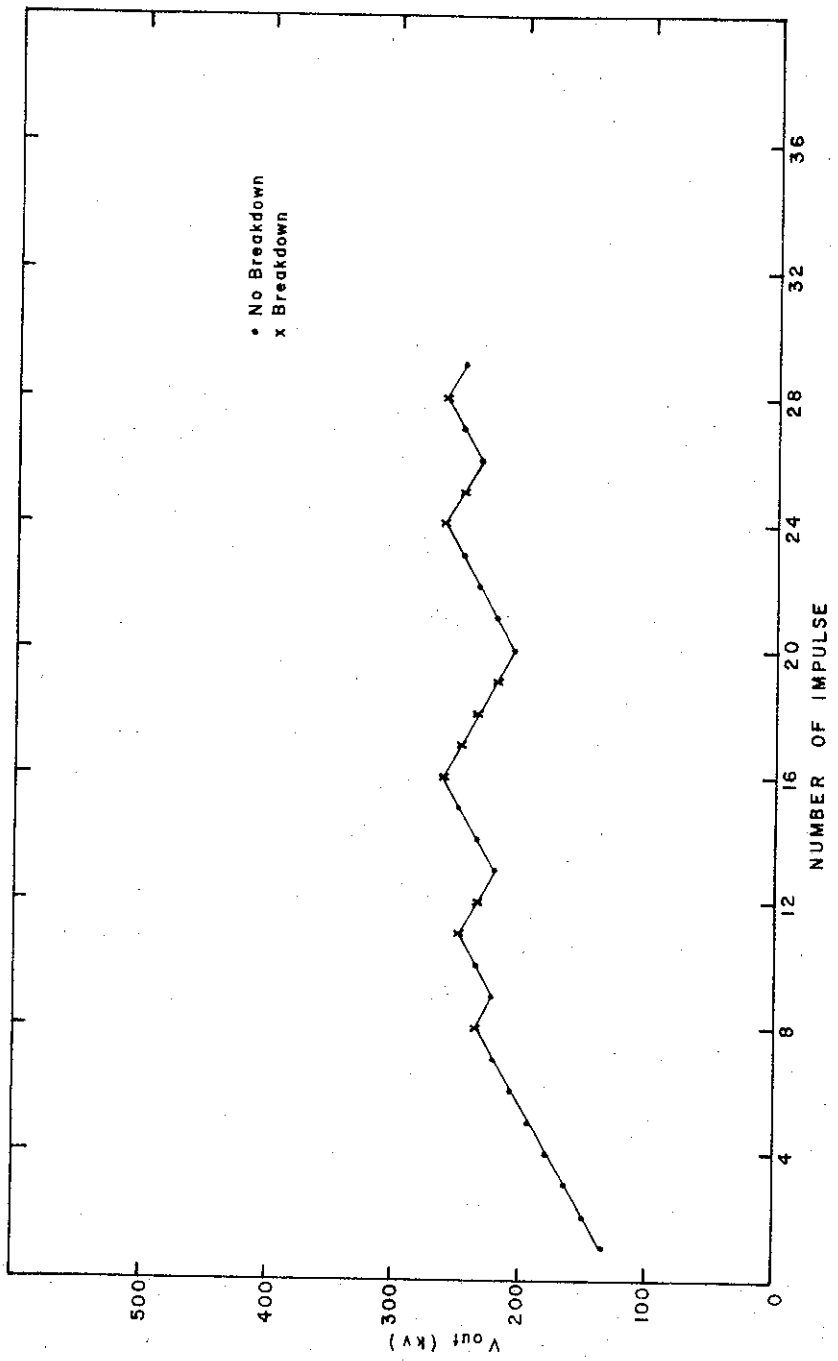

Figure 3-10. Typical Sequence for Flashover Test

1-3683

occur within 2 μs after the initiation of impulse. Table 3-3 summarizes the data for both maximum and mean flashover strength. Flashover voltage versus sample length is summarized in Figures 3-11, 3-12 and 3-13. These show that mean flashover field strength of up to 600 kV/in. are readily obtainable in a 300 psig, 10 SF_6/40 N_2/50 Ar mixture for ungraded albeit small samples. Even the poorer samples indicated that 300 kV/in. was reasonable for the same mixture and pressure and these were subsequently found to have inferior surface finish.

3.3 D.C. Puncture and Flashover Tests on Alumina Filled Epoxies and Two Plastics (Acrylic and Styrene)

3.3.1 Type I Tests Cast in Aluminum Electrodes, Filled Epoxy Resin

D.C. tests were carried out on two filled epoxy resins (Stycast 2850 FT and Castall 302 Tables 3-4 and 3-5). These are low temperature cure epoxies with a high percentage of tabular alumina as filler.

Shrinkage and exotherm are problems with any casting technique. Aluminum was chosen for mold and electrode material since its thermal coefficient of expansion (25×10^{-6} per °C) closely matches the filled epoxy resin. However, shrinkage ($\sim$ 1% volume) does take place in the liquid phase and is the reason for the reservoir (see Figure 3-14). Shrinkage in the "gelled" stage and during cure seems somewhat less. The result of an uncontrolled exotherm is shown in Figure 3-15.

3.3.2 Sample Preparation

The aluminum electrodes were 4-inches diameter with Bruce profile (Figure 3-14). After a smooth machine finish, the electrodes were polished to a 600 grit finish (wet), washed with green soap and water, rinsed in water then acetone and finally rinsed in distilled water. The aluminum mold was similarly cleaned before applying the release agent.

The filled resin and hardener were mixed by hand in a polyethylene container then degassed for 20 minutes in a glass vessel at about 1 Torr

Table 3-3. Flashover Data for Epoxy Materials

Sample	Length	Pressure (psig)	Average V_{BD} (kV)	Maximum V_{BD} (kV)
Permali	1/2-inch	150	220	230
Permali	1/2-inch	150	248	259
Permali	1/2-inch	150	235	235
Permali	1/2-inch	150	237	248
Permali	1-inch	150	400	428
Permali	1-inch	150	331	359
Permali	1-inch	150	372	414
Permali (Sand-Blasted)	1-inch	150	403	> 469
Permali	2-inches	25	436	> 469
Stycast	1/2-inch	150	103	110
Stycast	1/2-inch	150	110	124
Stycast	1/2-inch	150	120	124
Stycast	1/2-inch	150	115	132
Stycast	1-inch	25	152	166
Stycast	1-inch	25	155	166
Stycast	1-inch	150	257	290
Stycast	1-inch	150	340	359
Stycast (Sand-Blasted)	1-inch	150	345	345
Stycast	2-inches	25	363	414
Stycast	2-inches	25	375	414
Stycast	2-inches	25	314	345
Stycast	2-inches	25	362	414
EC-1339	1/2-inch	150	124	124
EC-1339	1-inch	150	309	331
E-170	3/4-inch	150	186	207
E-170	1-inch	150	317	345
System's Resource	2-inches	25	373	373

All tests carried out in a gas mixture of 10% SF_6, 40% N_2 and 50% Ar.

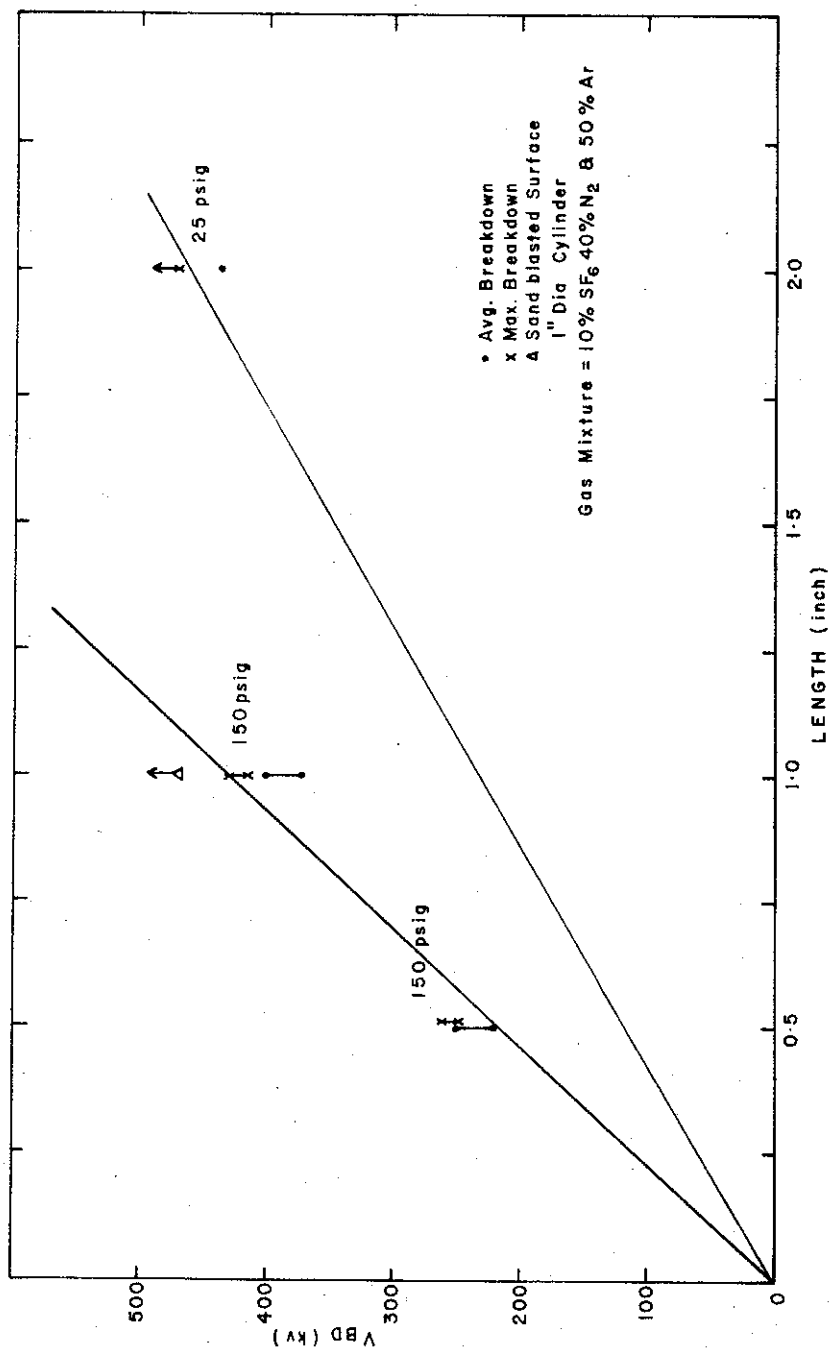

Figure 3-11. Surface Flashover Data for Permali Material

1-3684

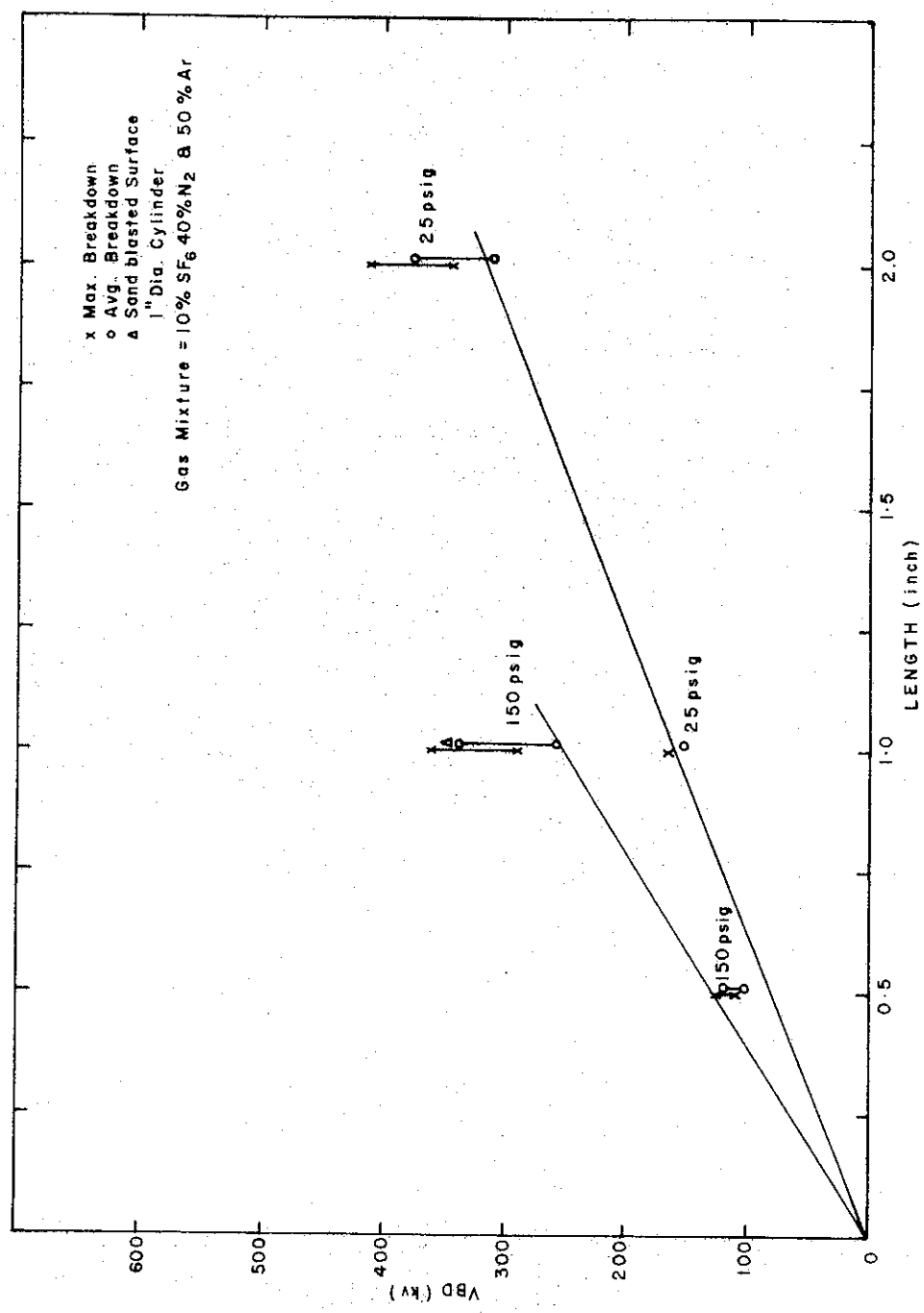

Figure 3-12. Surface Flashover Data for Blue Stycast

1-3685

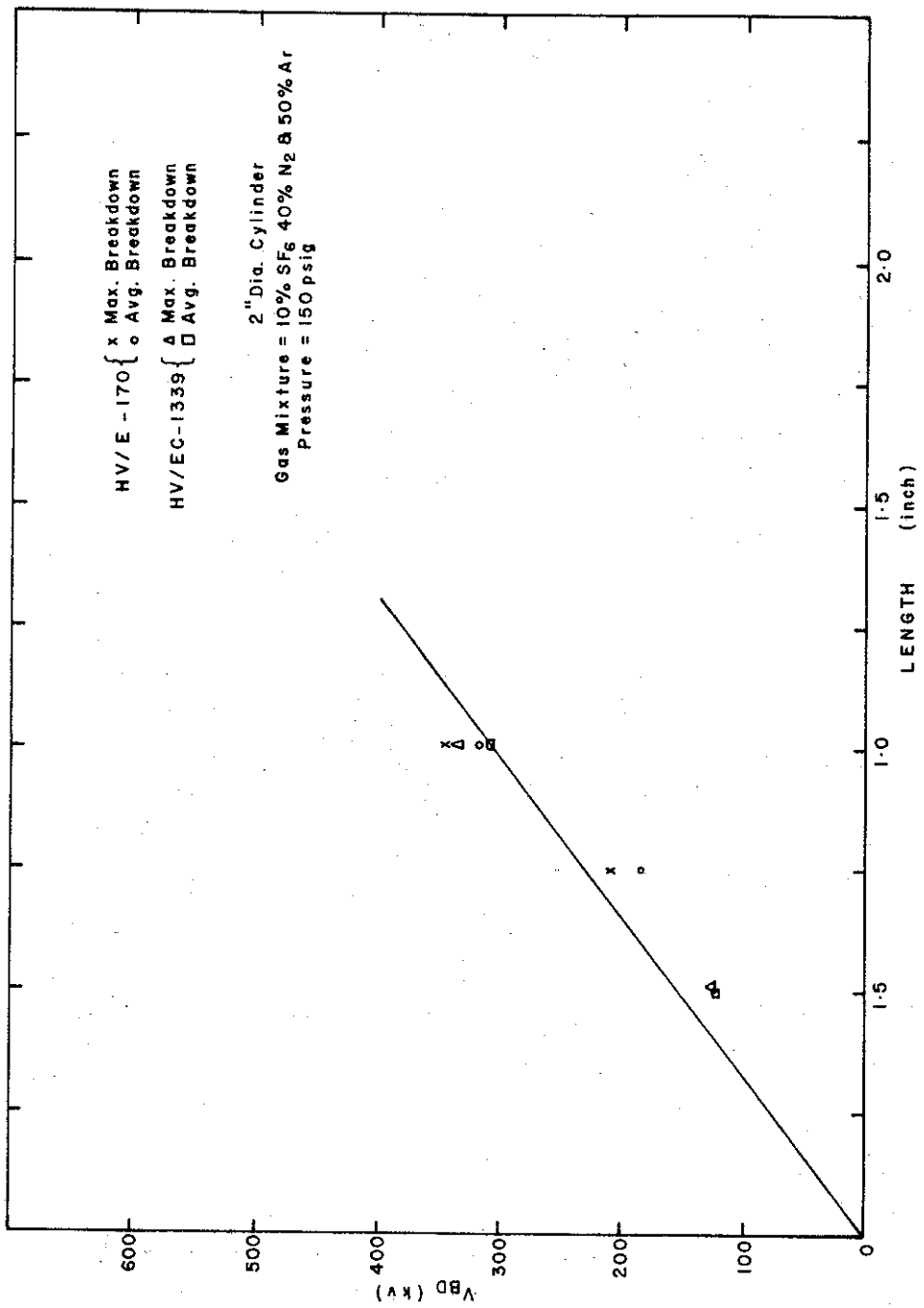

Figure 3-13. Surface Flashover Data for HVEC Epoxy Material

1-3686

Table 3-4. Stycast 2850FT (Emerson and Cuming, Inc.)

Stycast 2850FT is a highly filled epoxy formulation with remarkably good over-all general properties. In addition to having excellent electrical grade insulation properties Stycast 2850FT has unusually high thermal conductivity and low thermal expansion. This combination of properties has shown Stycast 2850FT to be invaluable in solving problems where electrical insulation and mechanical protection must be maintained while coping with heat transfer considerations.

Stycast 2850FT is a highly versatile epoxy resin system which may be cured with any one of three curing agents. The choice of Catalyst should be made after reviewing your requirements with regard to the following guidelines.

Typical Properties (Cured with Catalyst 11):

Cure Shrinkage, in/in	.001	Heat Distortion Point	347°F (175°C)
Viscosity at 25 °C (catalyzed), cps	70,000	Water Absorption (7 days)	less than 0.15%
Thermal Conductivity, BTU/ft^2/hr/°F/in.	10	Volume Resistivity (ohm-cm) 77 °F	5×10^{14}
		302 °F	1×10^{12}
Specific Gravity	2.3	Dielectric Constant, 60 Hz	6.5
Tensile Strength, psi	8400	1 kHz	6.3
Compressive Strength, psi	16,500	1 MHz	5.9
Flexural Strength, psi	13,300	Dissipation Factor, 60 Hz	0.02
Flexural Modulus, psi	2×10^8	1 kHz	0.008
Elastic Modulus, compressive, psi	1.1×10^6	1 MHz	0.02
Hardness (Shore D)	94	Dielectric Strength (volts/mil)	380
Izod Impact (ft. lb/in of notch)	0.3	Machinability	Poor (must be ground)
Thermal Expansion Coefficient per °C	29×10^{-6}		
per °F	14×10^{-6}		

Table 3-5. CASTALL® -- 302 - Aluminum Oxide Filled Casting Resin (Castall Research Lab., Inc.)

Castall 302 is a high viscosity, aluminum oxide filled casting resin which offers good thermal dissipation, excellent electrical insulation, high temperature properties, low thermal coefficient of expansion and extremely low shrinkage during cure. After cure, Castall 302 is a tough, opaque plastic with excellent adhesion to a variety of materials. Its expansion coefficient is closely matched to metals: therefore, it is one of the few epoxy resin ideally suited for use at cryogenic temperatures. To reduce viscosity, warm the resin to 150 °F. and use hardener E-34.

ELECTRICAL AND PHYSICAL PROPERTIES:

Specific Gravity	2.3
Viscosity (centipoise)	12000
Thermal Conductivity BTU/ft^2/hr/°F/in.	6.9
Tensile Strength P.S.I.	7000
Compressive Strength P.S.I.	14000
Izod Impact (ft. lbs./in. of notch)	0.32
Coefficient of thermal expansion/°C.	25 x 10^{-6}
Heat distortion °F.	350
Water Absorption (7 days) %	0.05
Volume resistivity (ohm cm)	8 x 10^{15}
Dielectric Constant (100 KC)	6.5
Dissipation Factor (100 KC)	0.02
Dielectric Strength (volts/mil.)	500
Shrinkage Linear -- %	.19
Service Temperature °F.	-400 to 400
Standard Color	BLACK

typical properties when cured with hardener E-34

For 4 hours at 250 °F

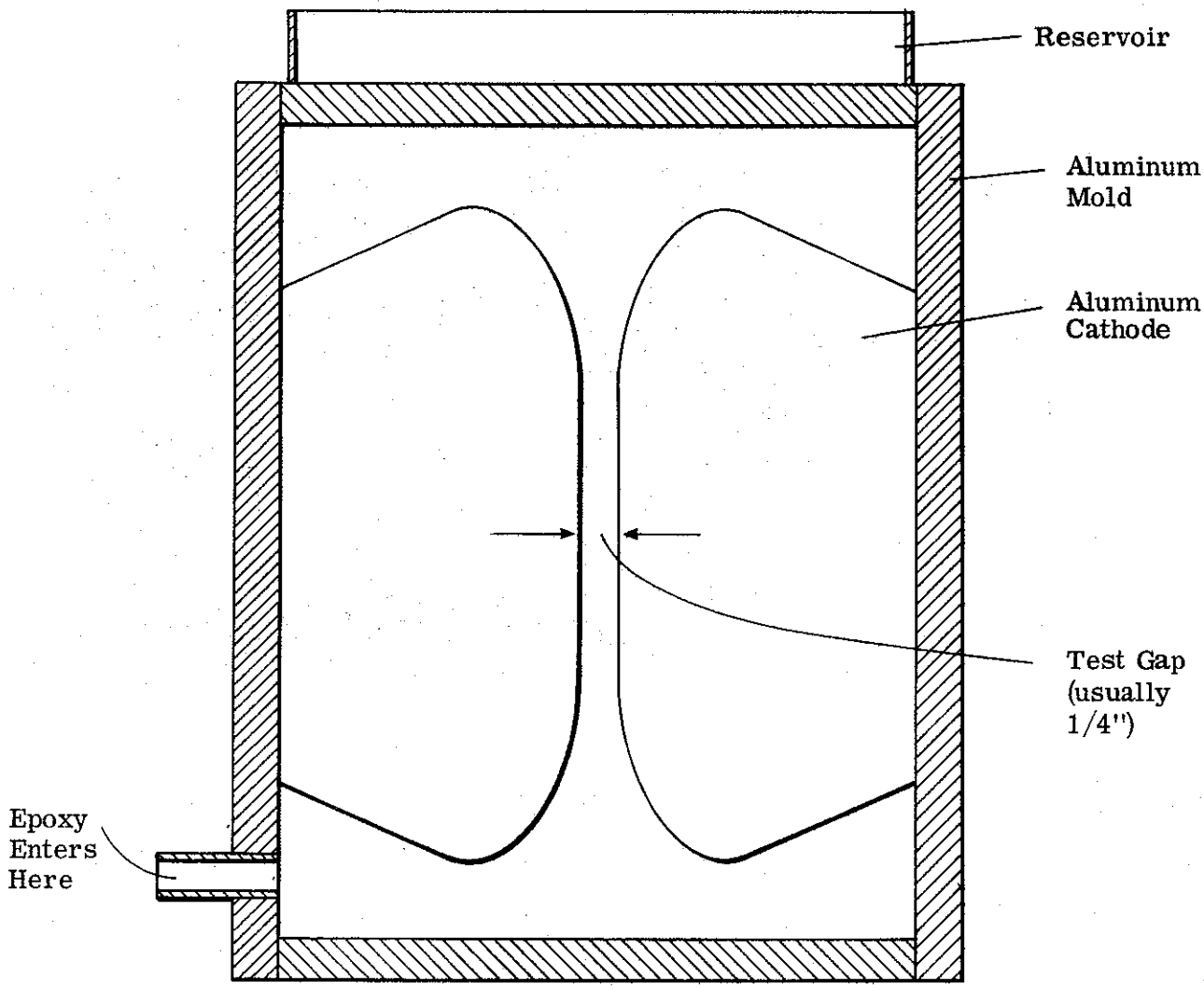

Figure 3-14. Electrodes and Mold for dc Tests (Approximately Full Size)

1-5059

Figure 3-15. Bubbles in Epoxy Caused by Run Away Exotherm

2-1321

(Figure 3-16). During degassing the volume of the mixture increased to about three times the original volume before settling down and bubbling gently. Transfer of the epoxy to the mold was achieved by keeping the mold under vacuum (30 to 50 mm Hg) and letting up the epoxy to atmosphere; the epoxy transferred in 40 to 60 minutes via a connecting 3/8-inch diameter plastic tube. Cure was carried out at 150 °F for 16 hours after the mold had been let up to atmosphere. Electrical tests were usually performed within three days of curing. Variations of the curing cycle were introduced later; e.g., the epoxy was allowed to stand at room temperature for 24 hours before curing for 2 hours at 120 °F and 14 hours at 150 °F.

3.3.3 Electrical Tests

The dc tests were carried out using a 1.5 MV Van de Graaff generator. The test samples were mounted inside the generator and had a high pressure gas environment which reduced the surface flashover problem (Figure 3-17). Surface flashover of the samples did occur and on some of the high strength samples it was necessary to add SF_6 to the gas mixture (Figure 3-18). Starting at half the estimated breakdown voltage, the test voltage was raised 20 kV per minute. After testing the samples were baked at 600 °F to separate the electrodes and epoxy and permit visual examination of the puncture (Figures 3-19 and 3-20). In all cases an erosion pit was found (usually at the anode) with a thin channel computing the breakdown.

The samples flashed over the surface many times before volume puncture. The discharge patterns were quite uniformly distributed suggesting that the surface was not degenerating rapidly, i.e., good discharge resistance. Sandblasting the surface gave no improvement. The main results are summarized in Table 3-6 and Figure 3-21.

3.3.4 Type 2 Tests - Filled Epoxy Resin - Recessed Metallised Electrodes

To investigate the possibility that the metal electrodes, cast into the epoxy in the previous tests, was a major factor in causing breakdown, recessed

Figure 3-16. Apparatus for Degassing and Vacuum Pouring Filled Epoxy Resin Samples

2-1317

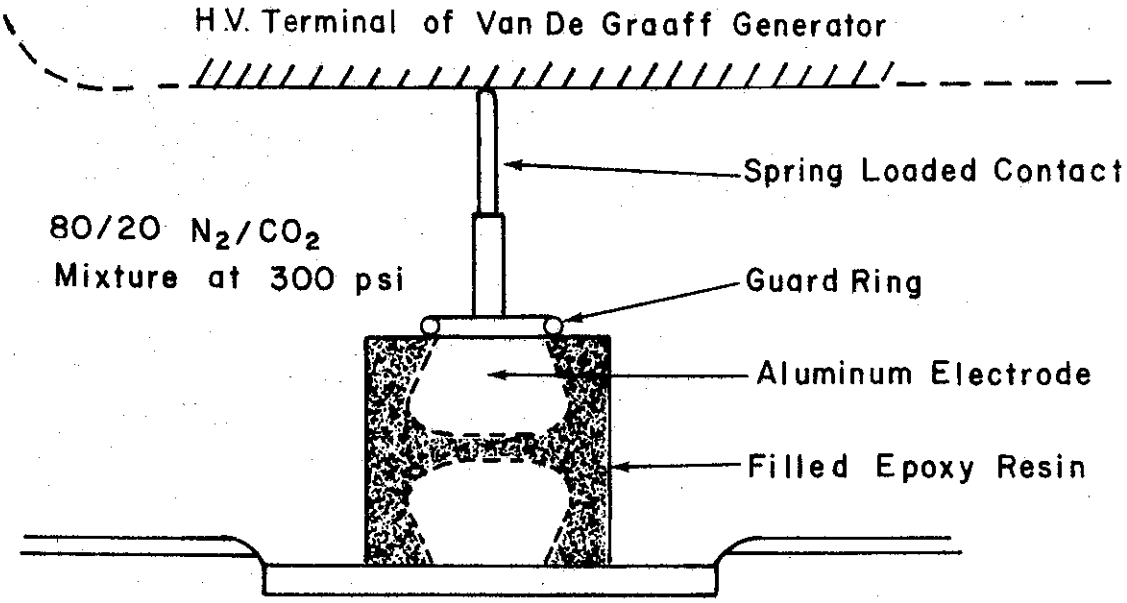

Figure 3-17. DC Test Arrangement

1-5056

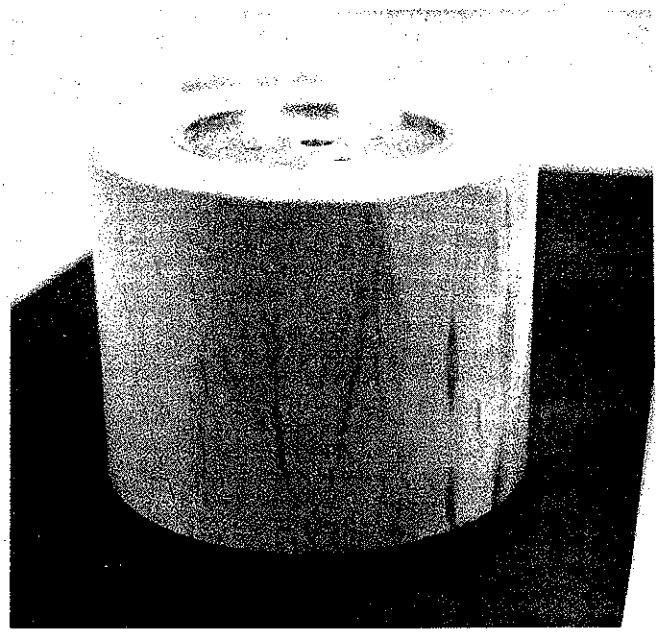

Figure 3-18. "Castall 302" Sample after dc Test Showing Surface Track Marks

2-1319

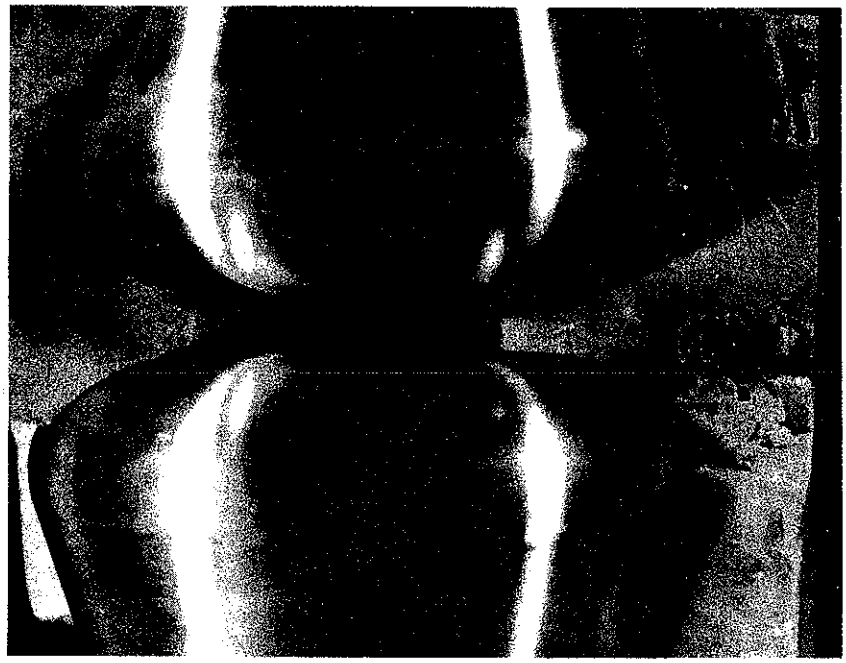

Figure 3-19. Cross Section of Test Sample Obtained by Baking at 600°F and Breaking Open

2-1318

$\frac{1}{4}$ Inch

Figure 3-20. Close Up of Puncture in "Castall 302" Sample

2-1320

Table 3-6. D.C. Volume Puncture Strength of Alumina Filled Epoxy Resin Tested in H.P. Gas Environment

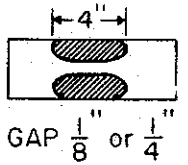

Material	Curing Procedure	Gap	Breakdown Voltage	B/D Stress MV/Inch.	Comments
High Voltage Eng. Corp. (Stycast)		1/8"	330* kV	2.64	
		1/4"	630*	2.52	
		1/4"	710*	2.84	
Stycast - prepared by Norm. Jones, Inc.		1/4"	720*	2.88	
Castall 302 + E34 Hardener	16 hrs. at 150 °F immediately after casting.	0.251	430*	1.71	resin degassed for 5 minutes only instead of usual 20
		0.254	525*	2.07	
		0.255	710*	2.78	
		0.248	700*	2.82	
	24 hrs. at room temp., then 2 hrs. at 120 °F, 6 hrs. at 150 °F, 3 hrs. at 200 °F, 6 hrs. at 250 °F	0.25	565*	2.26	
		0.271	480*	1.77	
	As above except room temp. done at 200 psi N_2	1/4"	576*	2.3	
	Copper electrodes, 16 hrs. at 150 °F	1/4"	670*	2.68	8 weeks before test
	16 hrs. at 150 °F immediately after casting	1/4"	630*	2.52	
		1/4"	560*	2.3	
	Mold baked 9 hrs. at 450 °F in vacuum	1/8"	360	2.88	room temperature cure
	Mold and Electrodes baked 12 hrs. at 325 °F in vacuum. Special vacuum dried alumina filler.	1/8"	320	2.56	
		1/8"	340	2.72	24 hrs. room temp. 2 hrs. at 120 °F, 14 hrs. at 150 °F.
		1/8"	320	2.56	
Stycast 2850 FT	16 hrs. at 150 °F immediately after pour	.252	446*	1.77	incorrect amount of curing agent
		.257	282*	1.1	
		.254	750*	2.95	
		.244	540*	2.23	
	Room temp. 24 hrs., 2 hrs. at 120 °F 14 hrs. at 150 °F	1/4"	220	0.88	May have been an inferior batch of resin.
		1/4"	255	1.02	
		1/4"	300	1.2	
		1/4"	580	2.32	
	Room temp. 24 hrs., 2 hrs. at 120 °F 14 hrs. at 150 °F	1/8"	320	2.56	graphite coated recessed samples
		1/8"	280	2.24	silver coated
		1/8"	304	2.43	silver coated
	Details in separate section	1/2"	400	0.80	Large volume flashover test piece
		1/2"	485	0.97	

*Corrected values

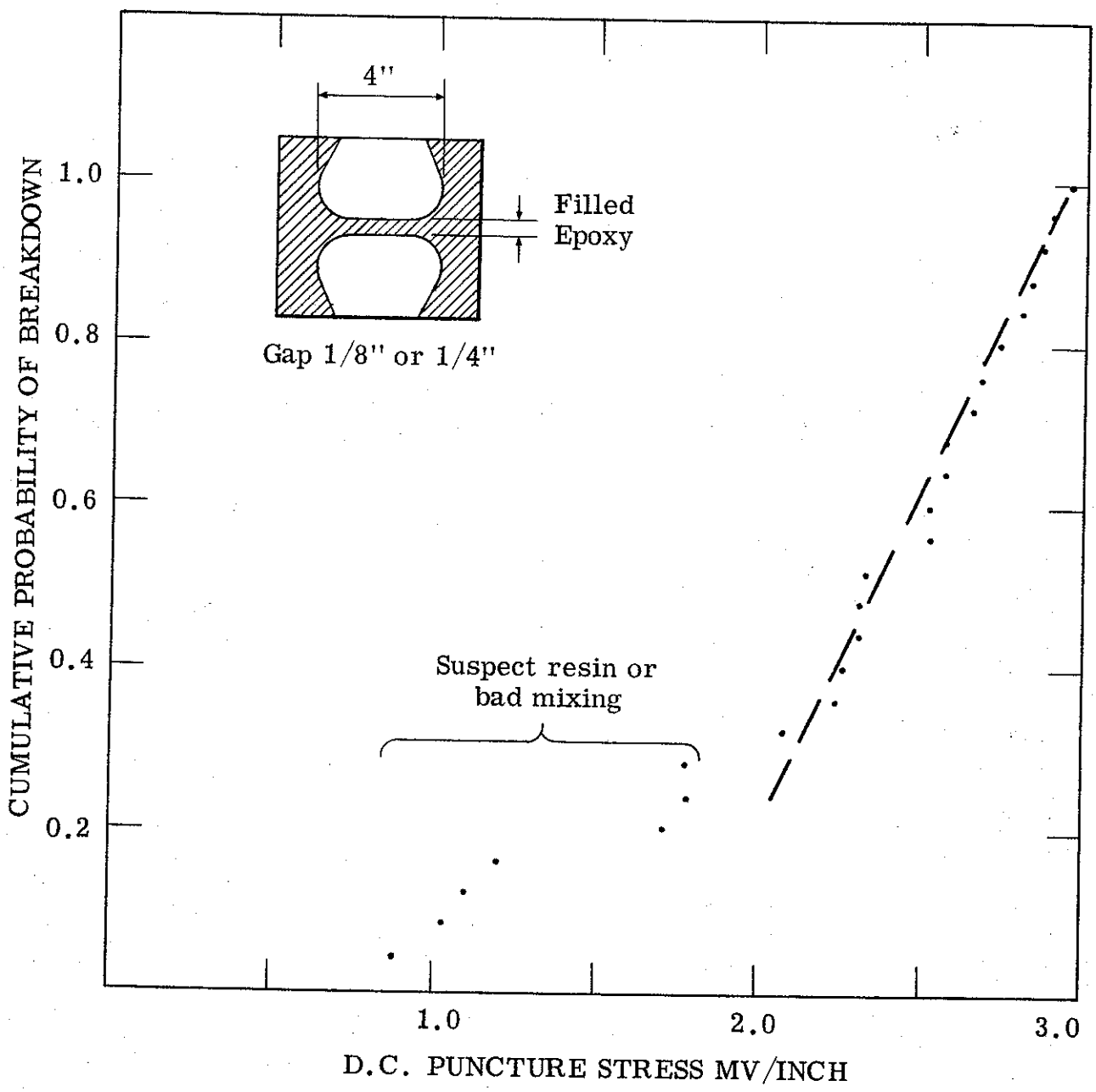

Figure 3-21. Filled epoxy resin tested under d.c. uniform field conditions.

1-5060

samples were made. The contour used was the same as the metal electrodes but this time the conducting surface was in the form of silver loaded epoxy. The limited results (included in Table 3-6) indicated that the mean breakdown strength was not raised but the scatter was greatly reduced. This is important where large volumes of highly stressed solid dielectrics are required.

The first sample tested in H.P. gas (75 psi SF_6 140 psi N_2) was prepared by brushing Aquedag (graphite dispersion) on the recessed regions only (XXX - Figure 3-22(a)). Surface flashover occurred at 260 kV. Improvement was effected by continuing the conducting layer to the edge of the sample (YXXXY) and mounting between flat metal planes. This put the solid/gas interface parallel to the uniform electric field. Surface flashover then first occurred at 280 kV even though the tracking distance was a factor 3 less. The interface flashover strength conditioned very rapidly until tests were stopped due to volume puncture.

3.3.5 Type 3 Tests - Machined Samples of Acrylic and Styrene (Table 3-7)

The early results with filled epoxies were disappointing in terms of energy density ($1/2\ \epsilon_o \epsilon_\gamma E^2$) in comparison with available test data on methyl methacrylate. Some tests were therefore done on acrylic and cross-linked styrene under similar conditions to the epoxy so that realistic comparison could be made.

Test pieces were machined from normal lucite 2-inch sheet, cast styrene and cast acrylic (last two from C-LEC, N.J.) in the same geometry as Figure 3-23. Results are given in Table 3-8 for test conditions shown in Figure 3-22(b).

Attempts at evaporating an aluminum layer on the acrylic were unsuccessful although a good bond could be made to the filled epoxy. Companies involved in the plating of plastics were approached to plate acrylics and styrene but did not suggest anything positive. All tests were done with conducting surfaces of silver loaded epoxy.

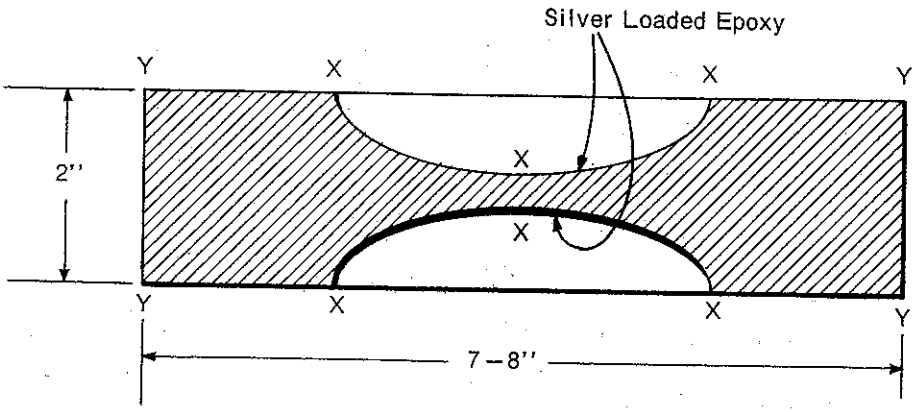

(a) Recessed Sample

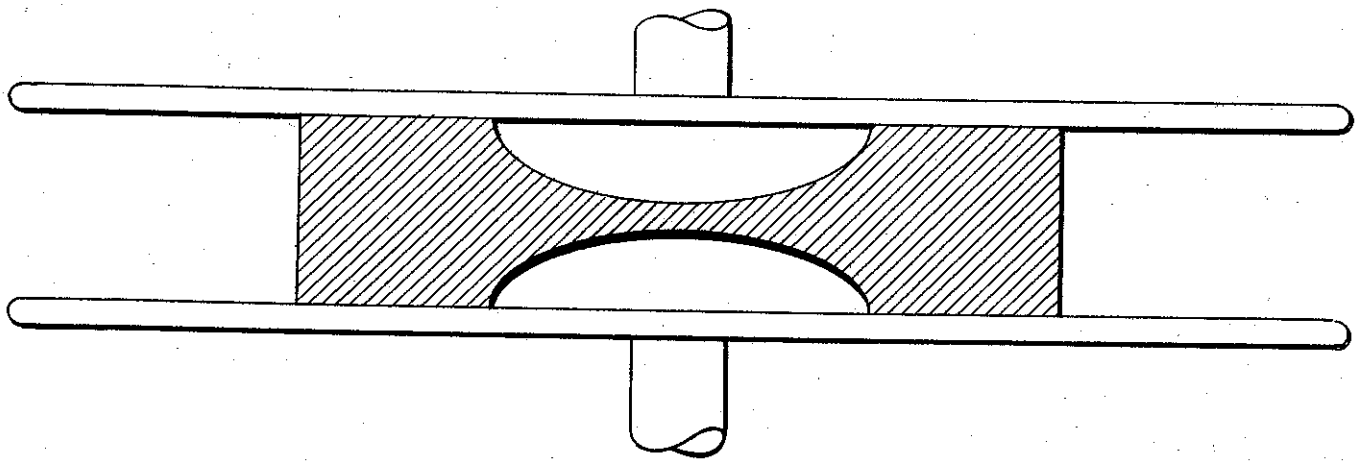

(b) Modified Test Condition

Figure 3-22. Dielectric Test Piece

1-4419

Table 3-7. Cross-Linked Styrene (Dielco 100 - CLEC, N.J.)

DIELCO 100 is a rigid, thermoset, general purpose plastic, mostly used in applications where a low electrical loss characteristic is important. The material is cementable and can be polished to optical clarity.

Electrical Properties	Test Method	Typical Value
Dielectric Const. 10 - 10,000 MC	M.I.T. Test	2.53
Dissipation Factor	M.I.T. Test	
1 MC		.00012
10 MC		.00025
10,000 MC		.00066
Dielectric Strength	L-P 406 Method 4031 ASTM D149	
Step by Step:		
1/32" thick		1100 Volts/Mil
1/8" thick		500 Volts/Mil
Short Time:		
1/32" thick		1200 Volts/Mil
1/8" thick		700 Volts/Mil
Volume Resistivity	ASTM D257	10^{16} ohm-cm
Surface Resistivity	ASTM D257	10^{14} ohms
Physical Properties	**Test Method**	**Typical Value**
Tensile Strength	L-P 406 - Method 1011 ASTM D-638	11,000 psi
Tensile Modulus	ASTM D-638	4.5×10^5 psi
Compressive Strength	ASTM 695	33,000 psi
Flexural Strength	L-P 406 - Method 1031 ASTM D790	16,000 psi
Flexural Modulus	ASTM D790	2×10^5 psi
Impact Strength	ASTM D256	.3 ft. #/inch of notch
Specific Gravity	ASTM D792	1.05
Coefficient of Linear Thermal Expansion	ASTM 696	7×10^{-5}/°C
Thermal Conductivity		3.5×10^{-4} cal/sec/cm^2/°C/cm
Water Absorption	L-P 406 - Method 7031	.05
Recommended Operating Temperature Range		-60 to +100 °C

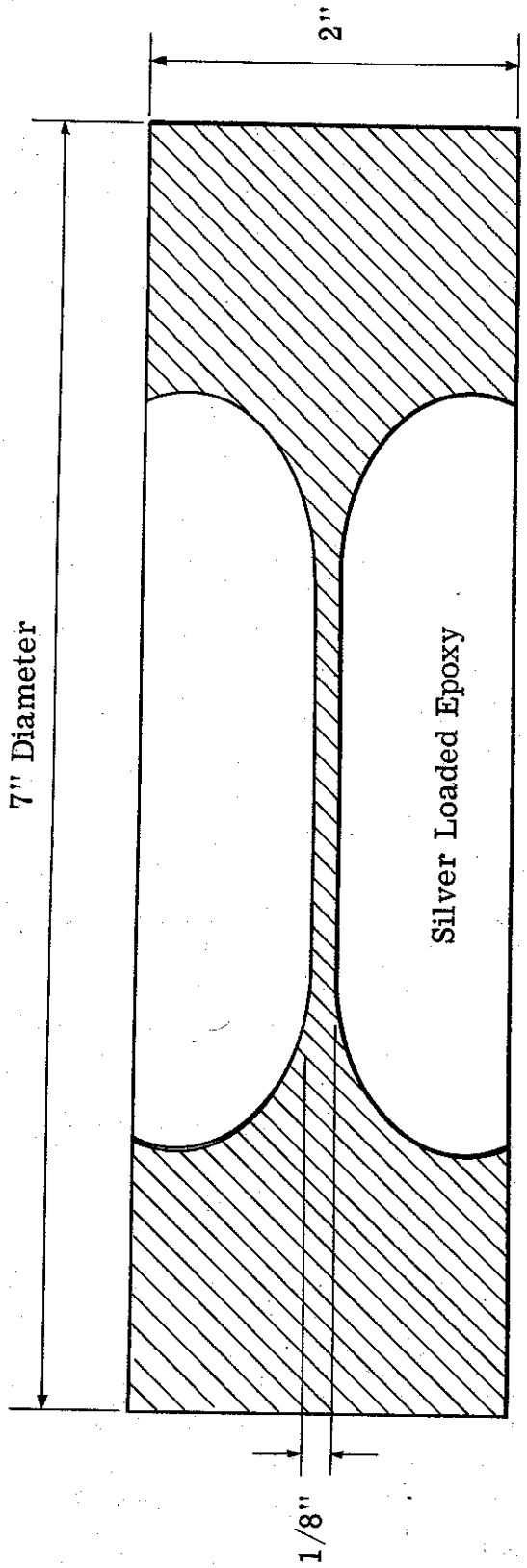

Figure 3-23. Section of Machined Sample

1-5061

Table 3-8. D.C. Puncture Strengths of Machined Plastics Tested in H.P. Gas

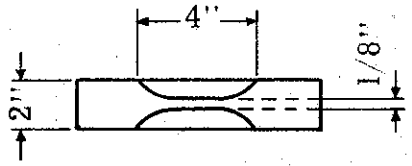

Material	Sample	Gas Conditions	First Surface Flashover	First Surface Flashover Strength	Puncture Voltage	Puncture Strength
Stycast 2850 Ft.	2-inch sides straight and parallel with electric field	75 psi SF_6 / 140 psi N_2 } 215 psi A	260 kV	130 kV/inch	320 kV 280 304	2.56 MV/inch 2.24 2.43
Lucite	Annealed once after machining 1) Straight 2) Straight 3) Straight Corrugated	75 psi SF_6 / 140 psi N_2 50:50 SF_6/N_2 215 psi A	860 410 620 780	420 205 310 390	1000 410 780	8.0 3.28 6.24
Lucite	Annealed three times during machining 1) Straight 2) Edge Radius 3) Straight	75 psi SF_6 140 psi N_2 50:50 SF_6/N_2 215 psi A	370 > 580 420 > 380	185 >290 210 >190	 580 860 380	 4.64 6.88 3.04
Styrene*	As machined 1) Straight Corrugated Corrugated and Acrylic Repeat - No Acrylic 2) Straight Corrugated Corrugated and Acrylic	75 psi SF_6 140 psi N_2	360 260 700 380 300 660 >1140	180 130 350 190 150 330 >570	 >820 1140	 >6.6 9.12
Cast* Acrylic	As machined 1) Type A (095") 2) Type A (095") 3) Type C (097") 4) Type C (095") Repeat	50:50 SF_6/N_2 215 psi A	620 > 740 660 540 860	310 >370 330 270 430	740 740 860 940	7.8 7.8 8.8 9.9

* C-LEC/N.J.

The limited number of samples makes it impossible to assign a high degree of confidence to the significance of the results. However, the following observations are worthy of note.

(1) Recessed samples cast with filled epoxy do not appear to be better than samples with cast-in metal electrodes. Mean dc breakdown strengths are about 2.5 MV/inch for thicknesses 1/8-inch to 1/4-inch over several square inches electrode area.

(2) Recessed lucite samples machined from standard 2-inch lucite sheet stock do not show significant improvement when annealed three times during machining compared with once only after final machining. There is a large scatter in the puncture strength (3 to 8 MV/inch).

(3) Cast Acrylic (obtained from C-Lec, N.J.) appears to be significantly better both in consistency and breakdown strength. No annealing was done. Breakdown strengths in excess of 7 MV/inch are achievable.

(4) Styrene appears to be a very useful material. The first sample was never punctured. The final test on it was F/O limited at 860 kV. Its poor flashover characteristic can be largely overcome by corrugating the interface and applying an acrylic coating. Although its dielectric constant is lower than that of lucite (2.5 compared with 3.2) its low loss at H.F. may be attractive for fast pulse work, especially in repetitive-pulse duty.

(5) The surface flashover strength of a solid/H.P. gas interface at fixed gas conditions depends on materials, geometry and conditioning history. The tests indicate that the materials, in order of increasing strength, are filled epoxy, styrene, lucite and cast acrylic. Corrugations are advantageous especially for the poorer

materials. A poor material, such as styrene, in terms of its ability to withstand surface flashover, can be upgraded by cleaning and coating with a superior dielectric (e.g. acrylic). (Figures 3-24 and 3-25 show track marks on styrene prior to corrugating and coating with acrylic.)

- Note: The first surface flashover voltage has been reported. In the literature, the final "conditioned" value is usually quoted whereas in a high energy apparatus the first breakdown is important unless low energy conditioning is permitted. The samples which were punctured obviously had conditioned to at least this voltage and could possibly have gone higher.

3.4 Sectioned Solid Dielectric Line

3.4.1 Introduction

In view of both the difficulty of casting a sound one piece solid line and the cost of replacing a failure, consideration was given to assembling a solid dielectric co-axial line from short cast sections. The length of the necessary high pressure gas interface would determine the impedance discontinuity and hence the acceptibility of this approach. Test pieces were made to determine the voltage withstand capability of a thin pressurized gas gap between epoxy castings (Figure 3-26). Figure 3-27 shows the test region in more detail. A straight profile was used for the interface for simplicity and flexibility in the interface length could be adjusted by machining.

3.4.2 Preparation and Testing of First Pair of Test Pieces

(1) Filled Epoxy - Preliminary test at one atmosphere SF_6 indicated that Stycast 2850 FT was slightly better than Castall 302. This filled epoxy resin was therefore chosen

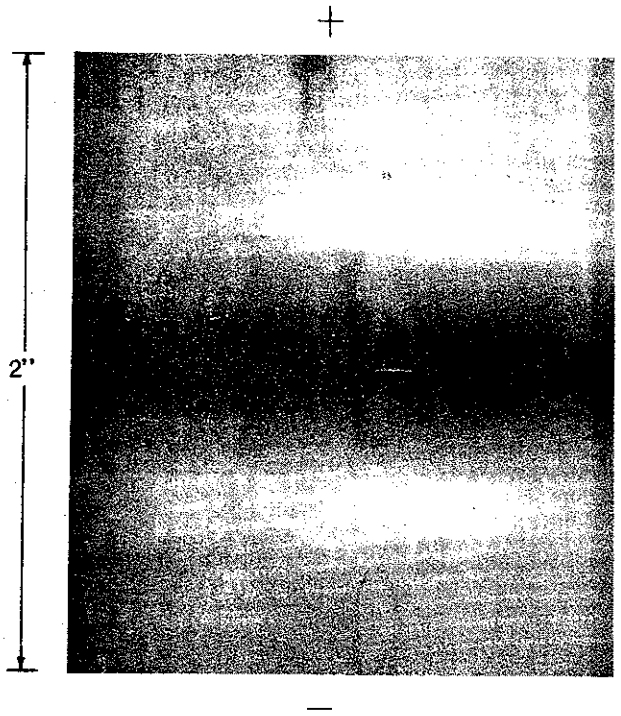

Figure 3-24. Flashover of Polystyrene Recessed Sample (Sample 1)

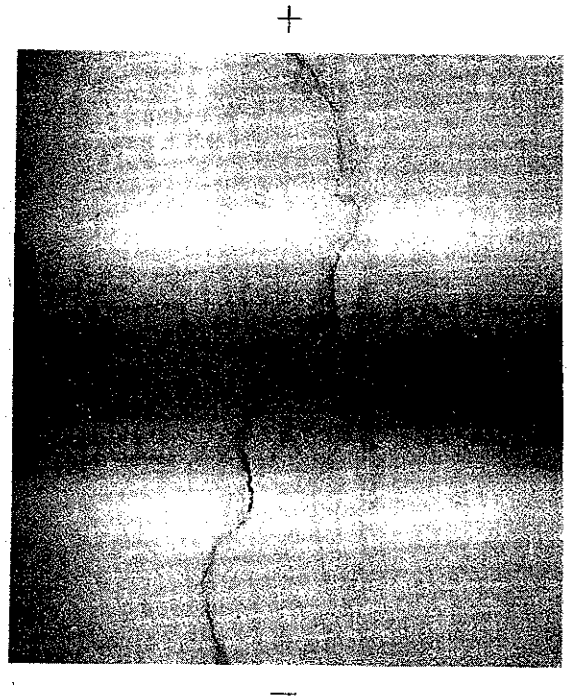

Figure 3-25. Flashover of Polystyrene Recessed Sample (Sample 2)

2-1497

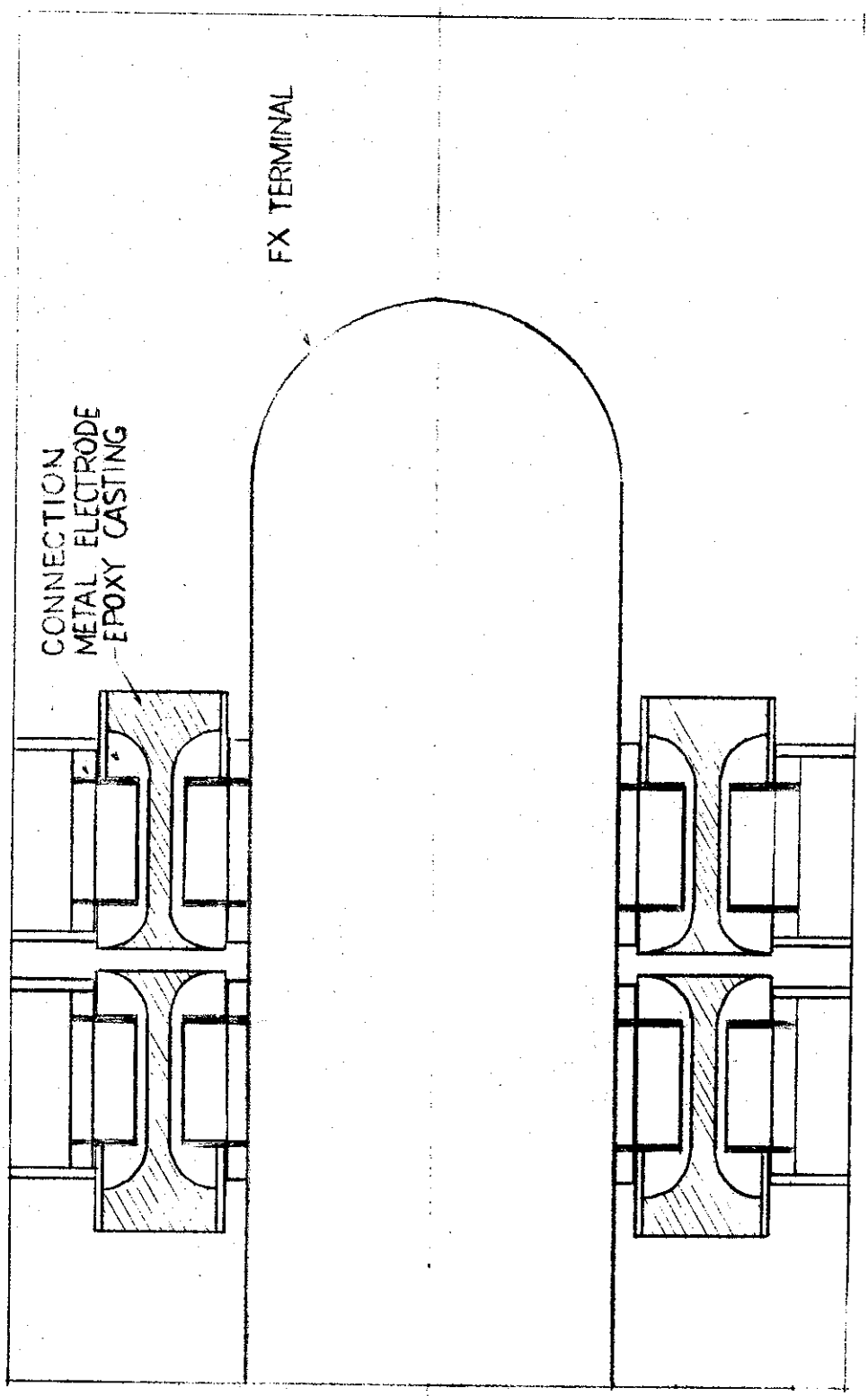

Figure 3-26. Thin Gap Test Setup

1-5062

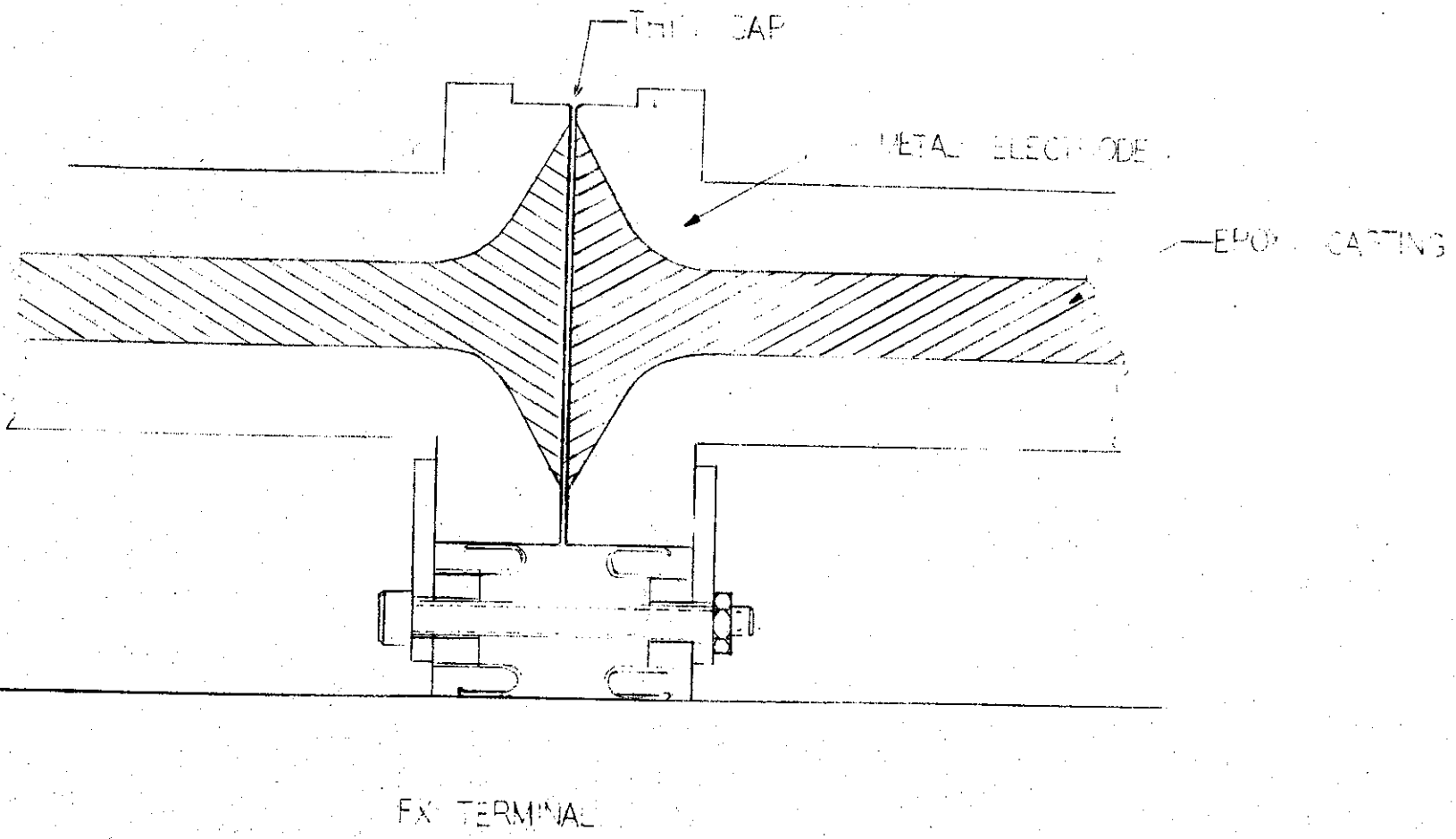

Figure 3-27. Detail of the Thin Gap

for the flashover studies. Allowing for losses in resin transfer, it was calculated that 12 kg of resin would be needed for each test piece. To maximize pot-life, the resin was made up in four batches; each consisting of 3 kg resin plus 135 g of hardener 11. Before adding the hardener, the resin was first agitated on a paint shaker for 20 minutes to improve consistency and then heated to 150 °F. Vacuum degassing after adding hardener was carried out at 2 Torr and took approximately 20 minutes.

(2) Mold and Electrodes (Figure 3-28) - After assembly these were baked for 3 hours at 200 °F and then transferred to a large environmental vacuum chamber where they were kept at 10^{-4} Torr for several hours.

(3) Resin Transfer - This was effected by letting up the degassed resin to atmospheric pressure, the resin then being allowed to transfer to the mold in vacuum. Just before transfer, the mold pressure was raised to 15 Torr (by admitting dry nitrogen) to minimize the chance of bubbles forming in the resin. Filling took place in approximately 5 hours.

(4) Curing - The curing cycle was 24 hours at room temperature, 2 hours at 120 °F and 14 hours at 150 °F.

(5) Preparation for Test - Both test pieces were machined at one end, that is, at the ends which butt on final assembly. During machining, a small crack was evident on the outer edge between the aluminum and the epoxy. This was patched and re-machined. The assembled test piece with contact spring fingers is shown in Figure 3-29 prior to assembly in FX-15. (FX-15 is a 1.5 MV dc machine.)

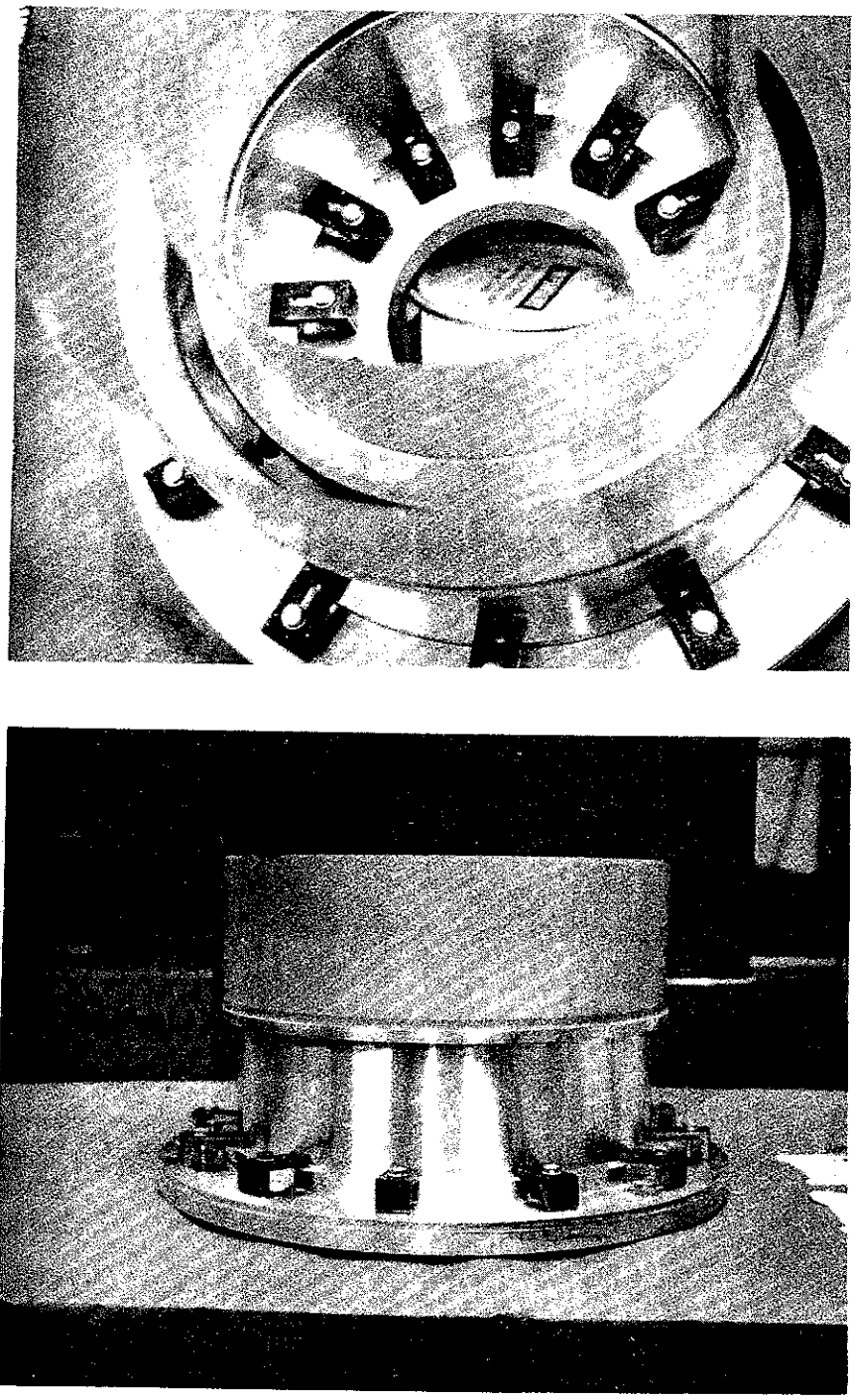

Figure 3-28. Mold and Electrodes for Half of Flashover Test Piece

2-1349

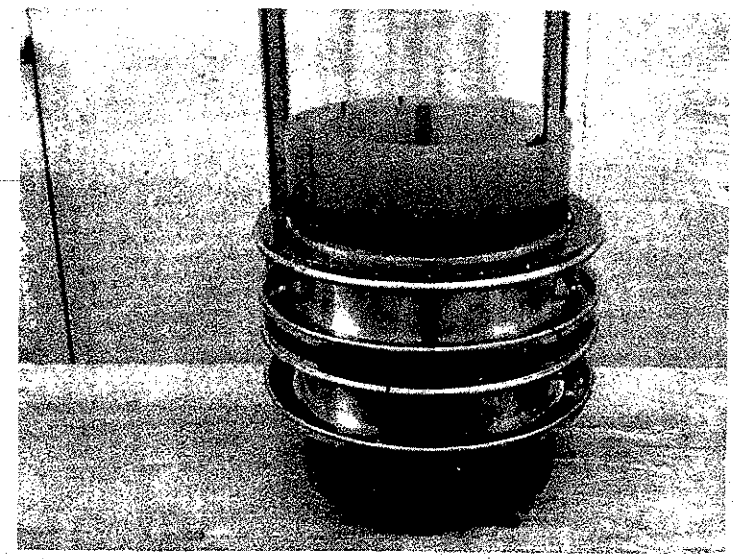

Figure 3-29. Assembled Test Piece

2-1365

3.4.3 Flashover in High Power Gas Tests

The test pieces described were dc tested in a high pressure (285 psig) gas mixture of 10% SF_6 and 90% N_2. The axial gap spacing was .002-inches and the radial flashover distance was two inches. The dc voltage was raised gradually to 400 kV when breakdown occurred. It was then impossible to raise the test voltage beyond a few kilovolts. After dismantling, one sample was observed to have a radial crack at the machined interface. An insulation resistance measurement using a high voltage Megger indicated volume puncture.

The volume punture was found in line with the radial crack but in the uniform field region. Inspection of the aluminum/epoxy interface led to the conclusion that little or no bonding had taken place. Indeed a 0.001-inch gap was evident in places.

Before recasting the test sample, some preliminary tests were carried out to solve the bonding problem. Two questions were posed. First, could the bond be improved by mechanically or chemically treating the surface? Second, could a conducting layer be applied to the aluminum electrode which would adhere strongly to the cast epoxy? The tests and results are summarized below:

Treatment	Result
1. Aluminum-polished down to 600 grit finish; trichlorethylene degrease, acetone rinse.	Poor adhesion.
2. Aluminum-sandblasted followed by degreasing.	Tended to be wetted by the epoxy. Bond reasonable but was probably due to mechanical keying action.
3. Aluminum-Surface polished to 600 grit then etched in an alkaline solution.	Improved bond.

Treatment	Result
4. Aluminum-600 grit finish, degreased, thin coating of silver loaded epoxy (Ecco-coat CC-2) applied.	Over most of the region, when the insulating epoxy was lifted off, it was accompanied by a film of silver epoxy.

Method (4) was adopted as pretreatment of the aluminum electrodes prior to casting.

Several attempts were made to coat electrodes with a flexible epoxy. This would be a transition material between the metal electrode and the filled epoxy. The desired properties of this material would include in addition to flexibility, a high dielectric constant (>20) and a volume resistivity of between 10^6 and 10^{10} ohm cm. No such materials were found. A clear epoxy resin ($\epsilon_r = 4.0$ $\rho = 10^{12}$) was tried and produced a uniform coating. However atmospheric dust proved troublesome and this approach was abandoned.

3.4.4 Preparation and Testing of Second Pair of Test Pieces

A second casting was made to replace the part punctured in the flashover test. An attempt was made to overcome the bonding problem (epoxy to aluminum) by applying a smooth, thin layer of silver loaded epoxy (Ecco coat CC-2) to the electrodes prior to casting. Apart from this change, the casting and preparation procedures were identical to those described previously.

When tested, one piece punctured at 485 kV d.c. Inspection of the puncture revealed that the failure had occurred in the uniform field region. It was noted that the silver epoxy was bonded randomly to the epoxy insulation but this effect may have been caused by the 550 °F bake used to remove the epoxy. The breakdown however occurred at a cathode region (Figure 3-30) where silver epoxy was still in contact.

3.4.5 Conclusions

There are two significant results from these tests on interface flashover:

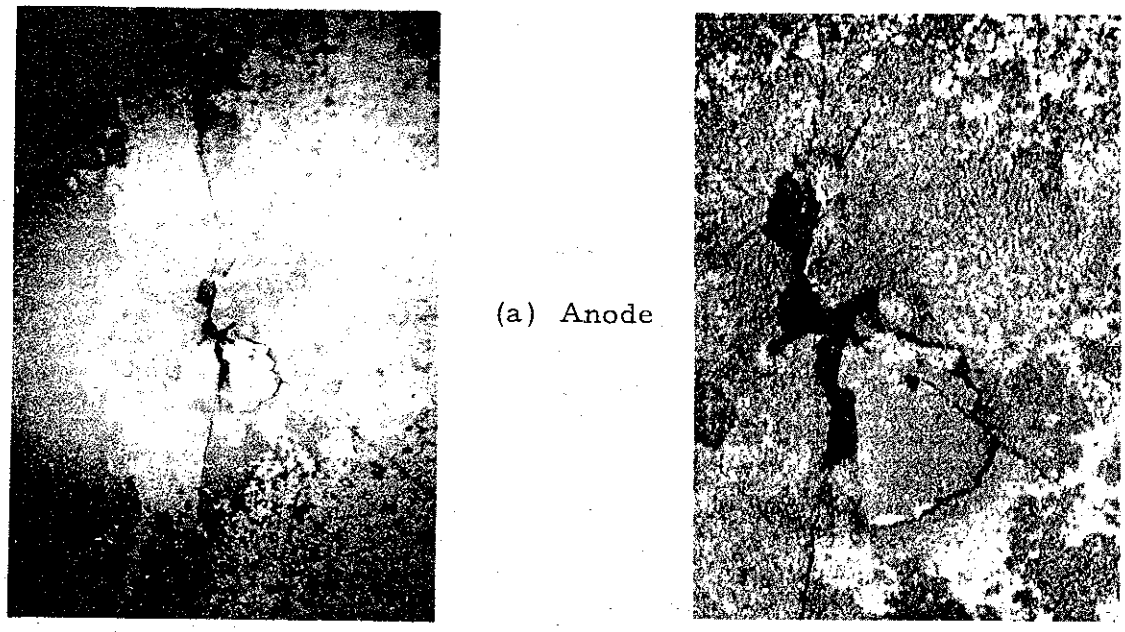

(a) Anode

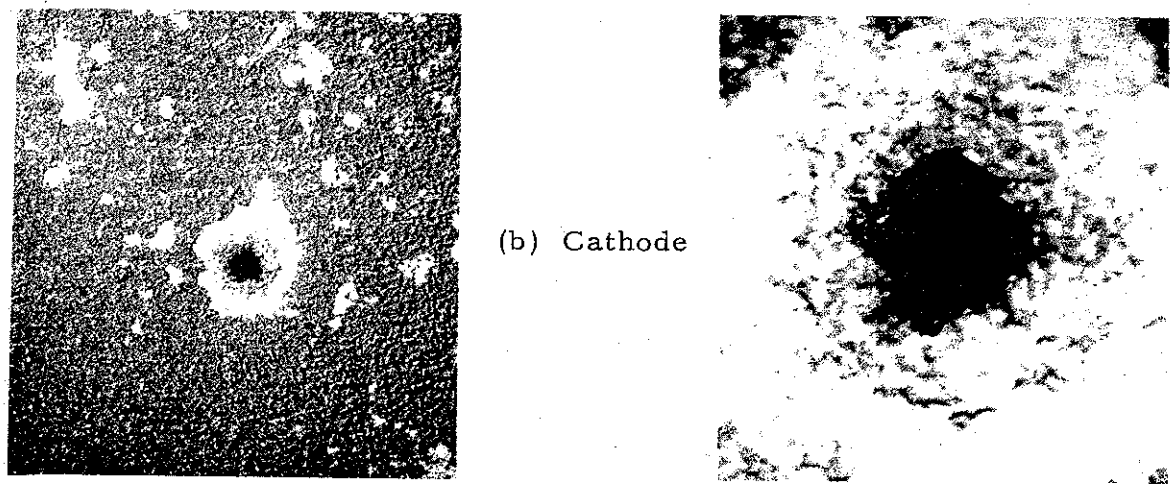

(b) Cathode

Figure 3-30. Photos of Puncture Through 1/2 Inch Radial Wall of Large Flashover Sample (Stycast 2850 Feet) After Baking at 550°F to Remove Aluminum Electrodes (The Aluminum Electrodes Prior To Casting Had Been Etched and Coated with Silver Epoxy (White Areas) Which was Then Smoothed)

2-1468

(1) Flashover strengths in excess of 250 kV/inch can be held (d.c.) in high pressure gas (300 psi A 10% SF_6 90% N_2) over a large surface using this geometry. No flashovers were recorded in the tests. Further work is necessary to determine the limit of this approach.

(2) Volume puncture of the 1/2-inch thick epoxy insulation at 400 kV and 480 kV is 0.8 and 0.96 MV/inch support the idea of a large volume effect in cast insulation. Small test samples (3-4 in^3 of stressed epoxy) had a mean breakdown strength in excess of 2 MV/inch but strengths as low as 1 MV/inch occurred if the epoxy preparation was incorrect. Based on this and the large scatter for cast insulation it would appear that large volumes of highly stressed cast insulation are not practical at this point.

3.5 Surface Flashover in Vacuum

3.5.1 Introduction

The delivery of pulsed energy (a few nanoseconds risetime and several tens nanoseconds pulse width) to a field emission diode operating at tens of ohms, presents no great problem today, even at potentials in excess of ten megavolts. However, when the required diode impedance is about one ohm, residual inductance becomes a limiting factor on risetime. The ideal solution is clearly to transmit the energy via constant low impedance lines from the energy store to the diode. For example, with co-axial geometry a conical line transition and tube could be used.

In practice the limitation is one of dielectric strength at the vacuum/solid interface of the tube. An improvement here, due to improved materials or geometry, results in improved machine performance (risetime and energy transfer). In a practical low impedance tube it is necessary to have a vacuum/solid interface separating the low impedance feed and the diode. The low

impedance feed is best insulated with water or other high dielectric constant material if low impedance and high voltage holdoff is to be achieved. In theory this introduces a further difficulty due to the changing dielectric constants. To maximize energy transmission the conducting wave guiding electrodes should be constructed to direct the energy through the interfaces (water/solid and solid/vacuum) at the Brewster angle. Fortunately, due to the turn-on time of a F.E. diode, a finite risetime is desirable to prevent voltage doubling at the impedance discontinuity produced by the diode being effectively open circuit for a few nanoseconds. This causes unnecessarily high electric stresses on the vacuum/solid interface. For a 10 ns risetime, an impedance discontinuity of less than 2 ns electrical length is permissible without seriously affecting the waveform, providing the excess inductance is within acceptable limits. This approach permits a more practical and reliable design.

The vacuum flashover tests done under this contract were based on this approach.

3.5.2 Surface Flashover in Vacuum

Surface flashover of dielectrics in vacuum under impulse voltage application was not reported in the scientific literature before 1964. Kalyatsky and Kassirov[1, 2] showed that the flashover strength of a 1 mm gap increased as the voltage pulse duration decreased from 3.0 to 0.1 μsec. The shape of the volt-second breakdown characteristic was characteristic of the cathode material and the collapse voltage depended upon the anode material. Smith[3] showed that for much wider gaps the mechanism appeared to be one of secondary multiplication of electrons drawn into the dielectric surface and that conically shaped dielectrics increased the flashover strength. This electron multiplication mechanism was previously suggested by Fryszman[4] et. al., Bugaev and Mesyats[5] showed that the flashover strength increased with shorter pulses but limited at 2 nsecs. At large gap separations the strength was lower.

The first theory of the effect was proposed by Watson[6] who compared his results with those of Smith. Electrons heated by the electric field in

the dielectric are emitted from the surface which charges up enough to draw them back for multiplication. Dielectric samples (glass) with a 45 ° angle and 3/8-inch thick were found to support 670 kV/inch for 90 nsec pulses. The data of Smith showed that for similar 1-inch samples the strength was somewhat smaller, even though 35 nsec pulses were applied.

Additional analysis by Watson and Shannon[7] further supported the theory using additional data from Smith and Martin and Bugaev and Mesyats.

It seems probable therefore that for 30 nsec pulses a flat tube may approach a flashover strength of 1 MV/inch. The effect of insulator depth is believed due to the influence of the surface charge in raising the electron temperature within the dielectric, so increasing the charging rate and lowering the electrical strength.

3.5.3 References

(1) Kalyatsky, I. I. and Kassirov, G. M., Soviet Physics - Tech. Phys. 9, 274 (1964).

(2) Ibid., 9, 1137 (1965).

(3) Smith, I. D., Proc. 1st Symp. on Electrical Insulation in Vacuum (1964).

(4) Fryszman, A., Strzyz, T., and Wasinski, M., Bull. Acad. Polan. Serides Sciences Tech. 8, 7, 379 (1960).

(5) Bugaev, S. P., and Mesyats, G. A., Sov. Phys. - Tech. Phys. 10, 930 (1966).

(6) Watson, A., J. Appl. Phys. 38, 2019 (1967).

(7) Watson, A., and Shannon, J. Proc. 2nd Symp. on Insulation of High Voltages in Vacuum (1966).

3.5.4 Preliminary Work Leading to Vacuum Flashover Tests

Most of the vacuum flashover data reported in the literature has been concerned with samples of material tested under various field configurations.

It is believed however that interaction between the diode and the interface could take place in the form of electron impact and photo effects. In addition since surface flashover is an extremely rapid phenomena it could be affected by the source impedance. The philosophy to test materials under actual diode conditions thus developed.

Field plots were obtained for the output end using a sloping electrolytic tank, assuming a 5 ohm coaxial water line and a tube region catering for diodes 2 - 5 ohms. Electrode shape and interface angles were adjusted to improve the uniformity of the electric field along both interfaces. Figures 3-31, 3-32, and 3-33 show the effect of some geometry variations for the early designs. The proposed test apparatus was however limited to 600 kV at 5 ohms and so the design was modified to shorten the interface length to one inch. Figure 3-34 shows a field plot of the final geometry tested. From the plots, the estimated maximum gradient is $1.3 \times E_{average}$ for the vacuum/solid interface. Thus an improvement in gradient over the co-axial cylinder values has been obtained, with a single transit time from the 5 ohm water line to the diode of less than one nanosecond.

3.5.5 Experimental Apparatus

A low impedance adaptor in the form of an exponential (tapered) transmission line (water insulated) was constructed for FX-25 (an I.P.C. 4 MV 40 ohm 30 ns machine). Figures 3-35 and 3-36 show the general arrangement. Switching out the FX-25 delivers a 30 nS pulse into the 15 ohm water line. At the output end of the line (5 ohms) a correctly shaped solid dielectric cone guides the energy into the F.E. diode region.

Voltage probes were located at two places on the tapered water line and a current shunt mounted in series with the diode. The current shunt had an estimated inductance of 25 nH and thus degraded the current risetime of the output. Figure 3-37 shows voltage traces on the water line for a matching 5 ohm dummy load and Figure 3-38 the corresponding output current trace.

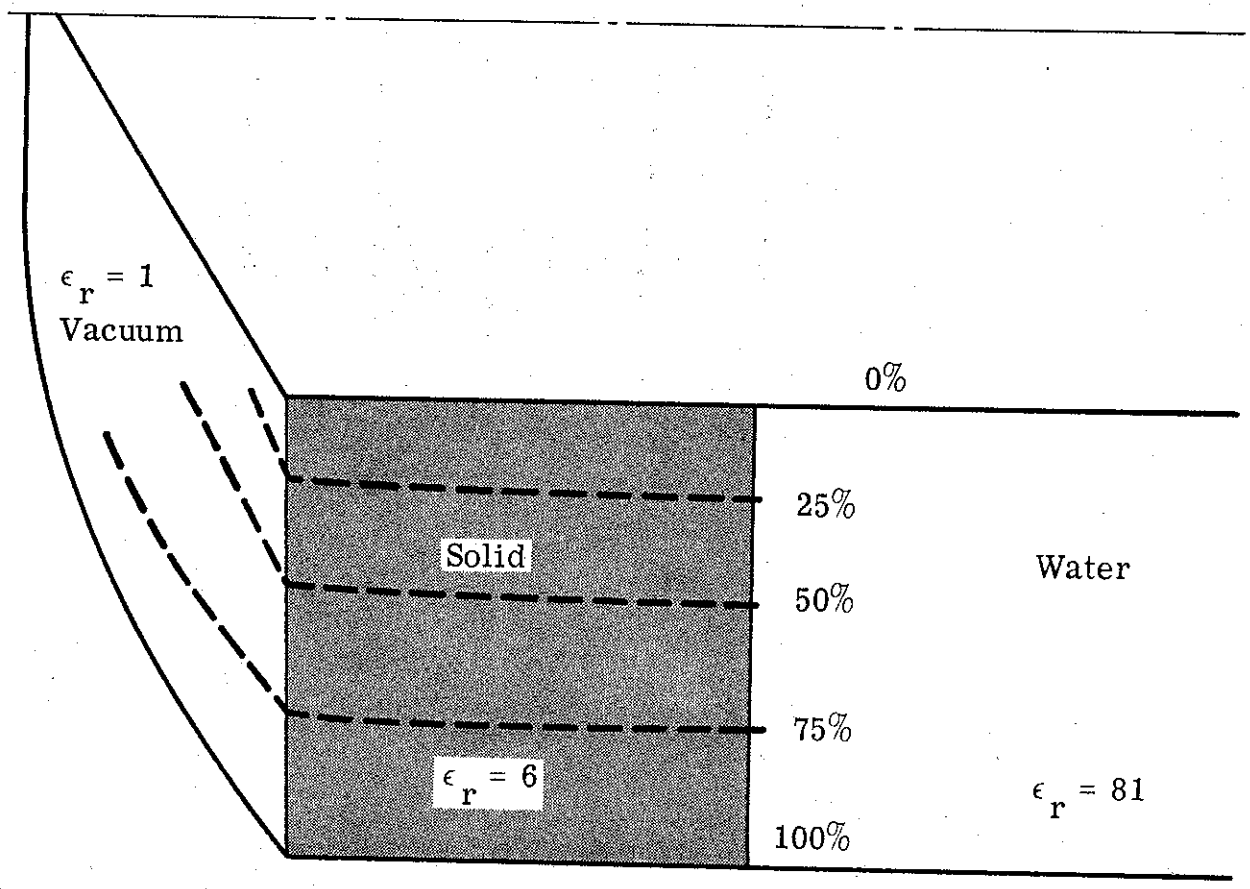

Figure 3-31. Field Plot for Water-Solid-Vacuum Dielectric Interface; Straight Geometry.

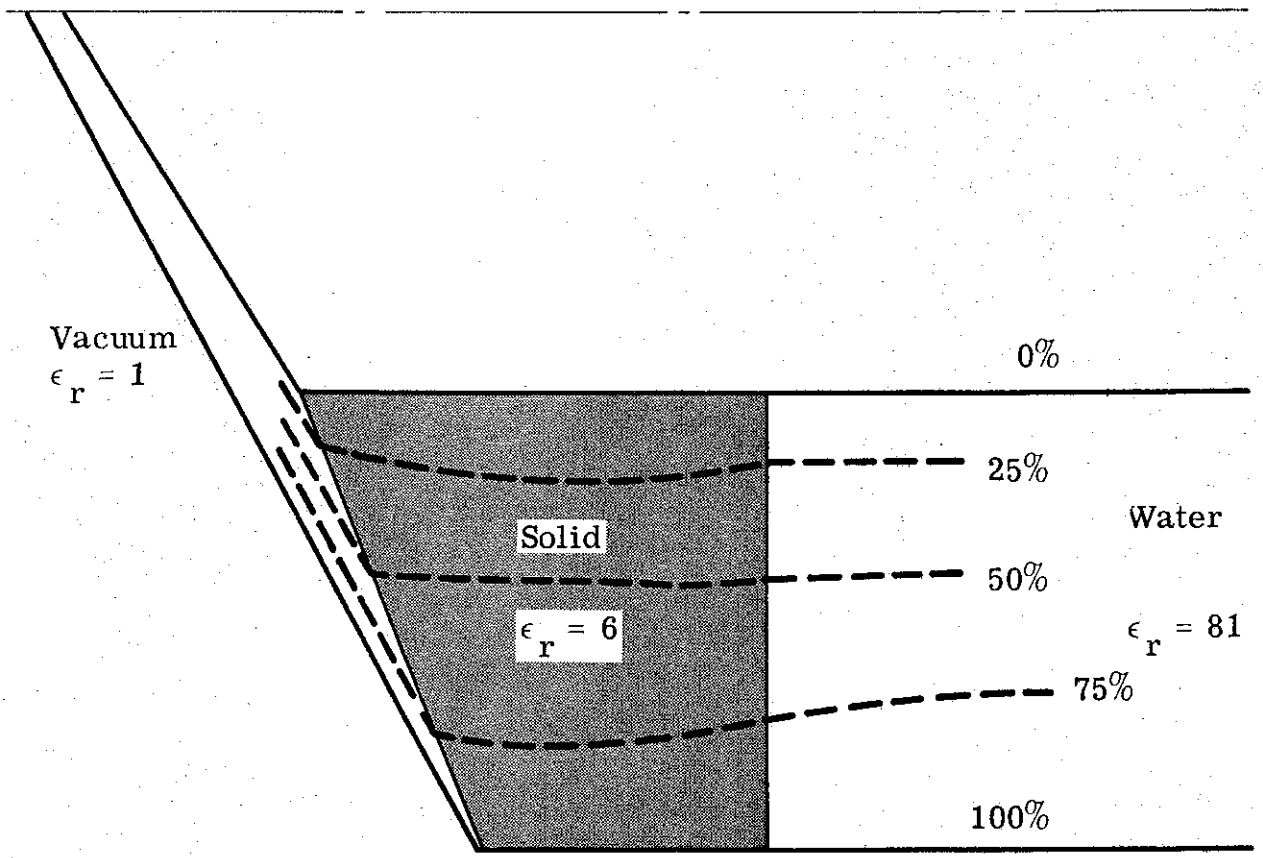

Figure 3-32. Field Plot for Water-Solid-Vacuum Dielectric Interface; Sloped Geometry (A).

1-5048

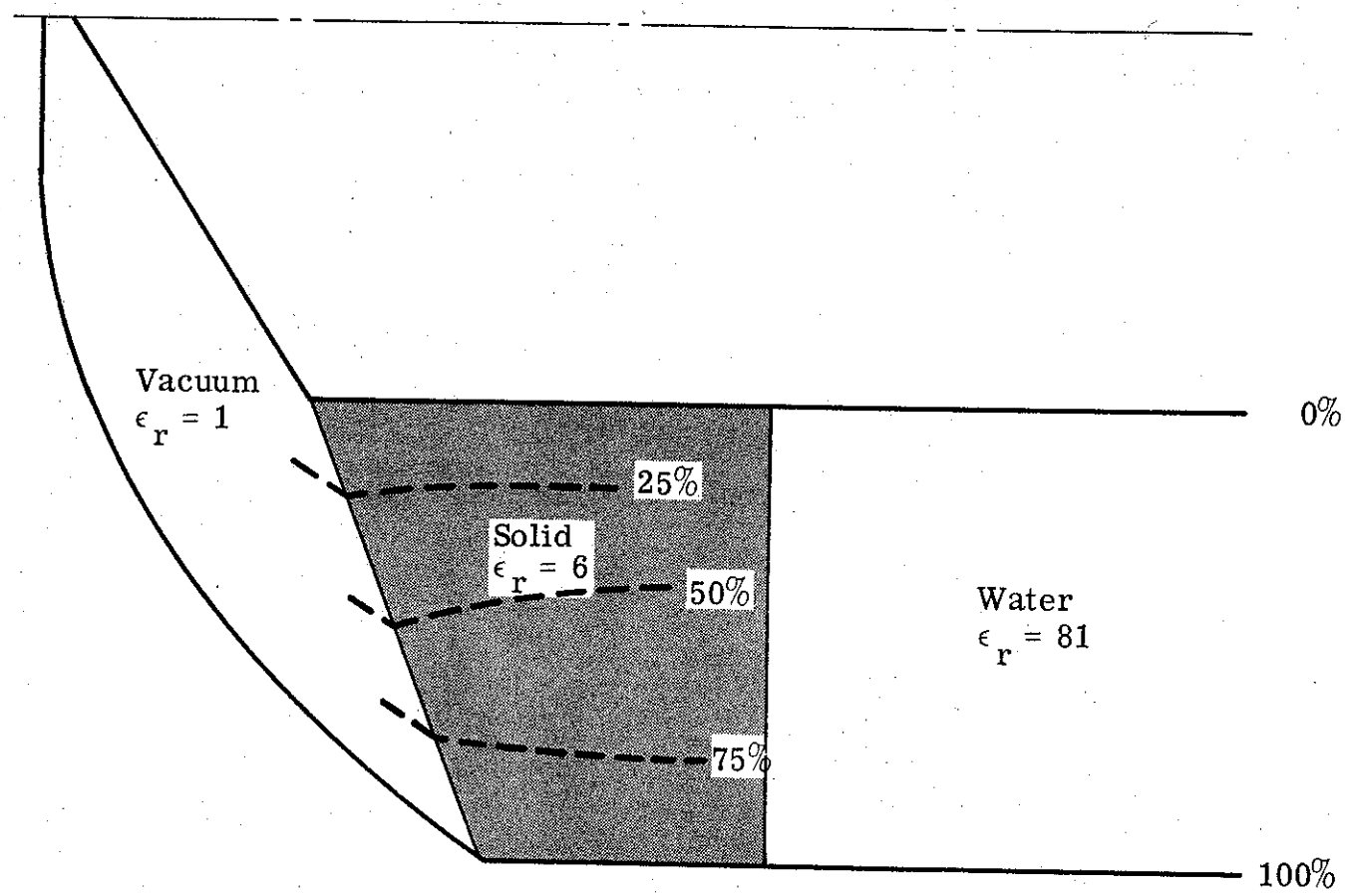

Figure 3-33. Field Plot for Water-Solid-Vacuum Dielectric Interface; Sloped Geometry (B).

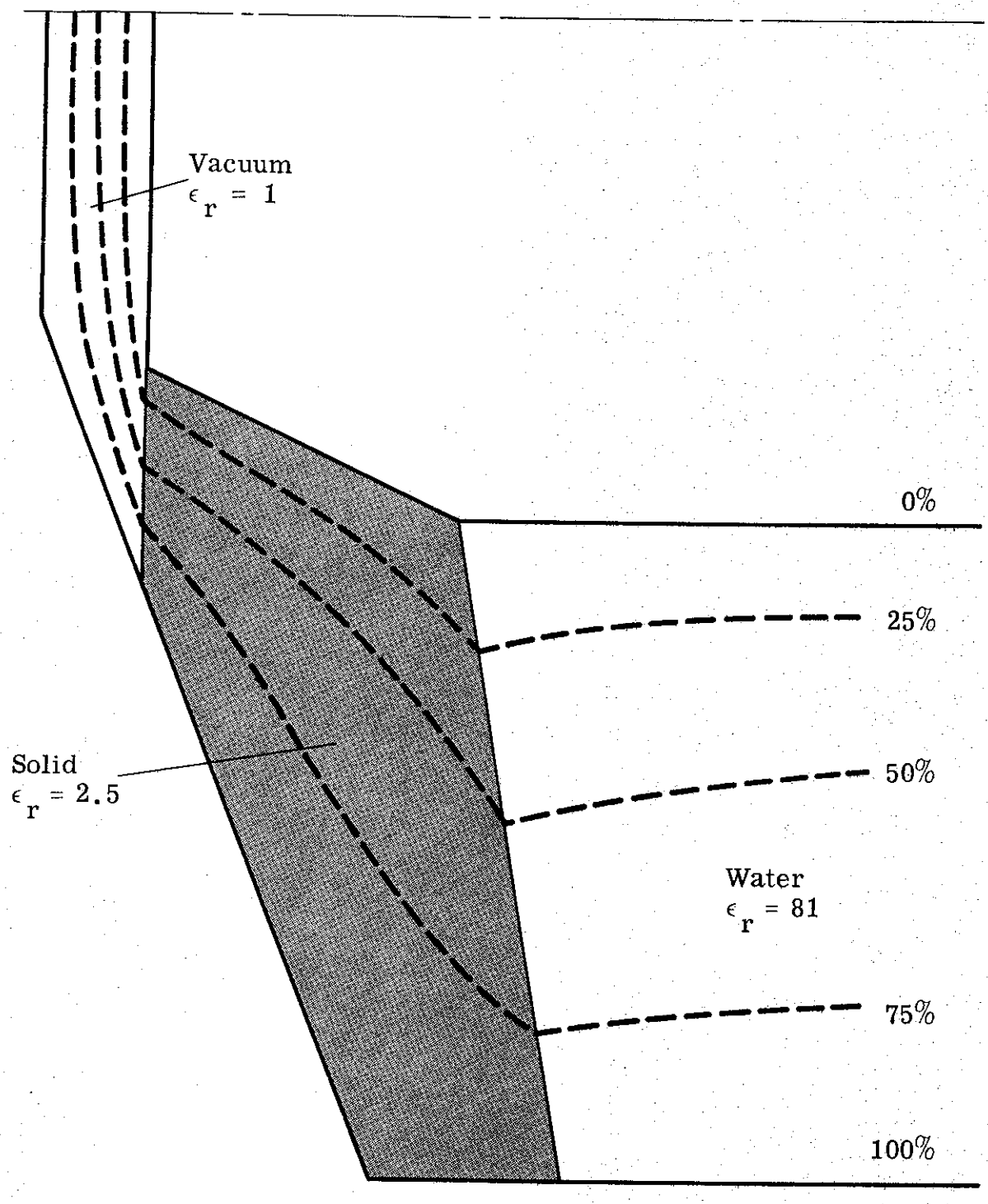

Figure 3-34. Field Plot for Water-Solid-Vacuum Dielectric Interface; Sloped Geometry (C).

1-5050

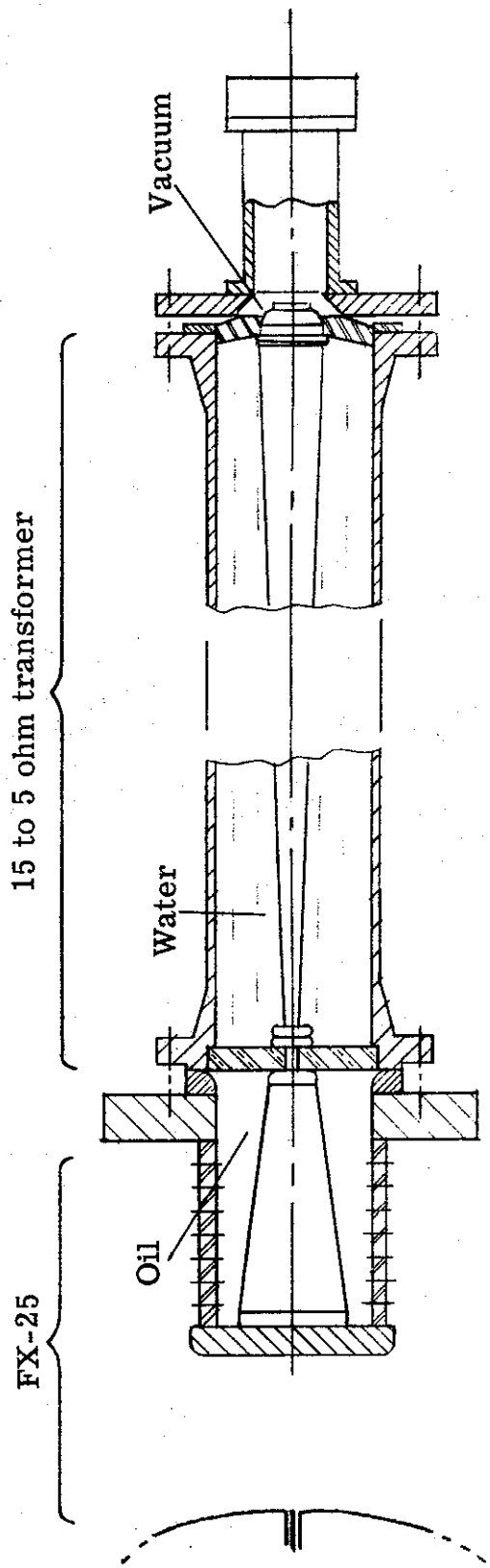

Figure 3-35. Experimental Set-Up for Low Impedance Vacuum Flashover Tests.

1-5046

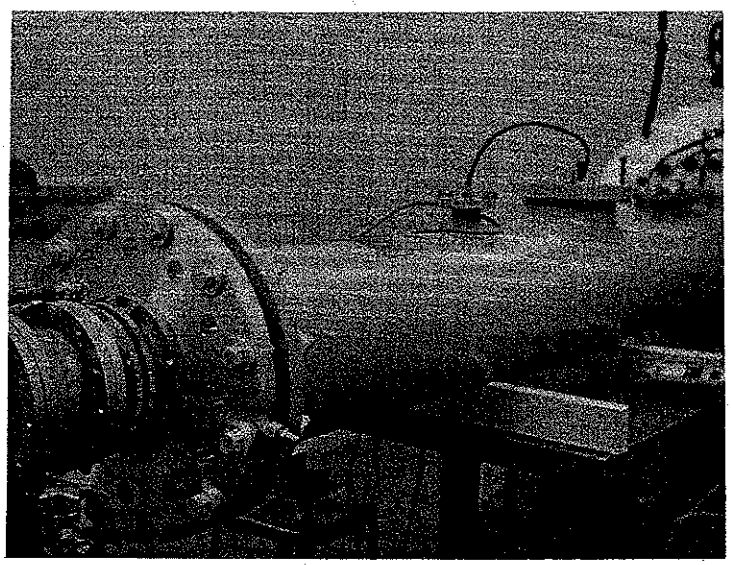

Figure 3-36. Photograph of Adaptor for FX-25 (output end in the foreground).

2-1530

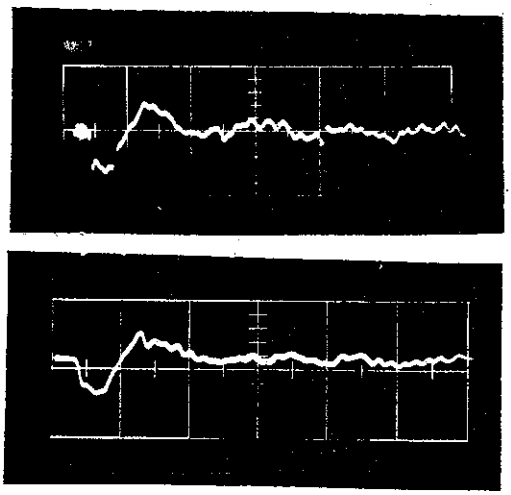

(a)

(b)

Figure 3-37. Voltage traces on tapered water line for matched 5 ohm load.

(a) approx. 1/3 rd down from input.
(b) approx. 2/3 rds down from input
(50 ns/cm)

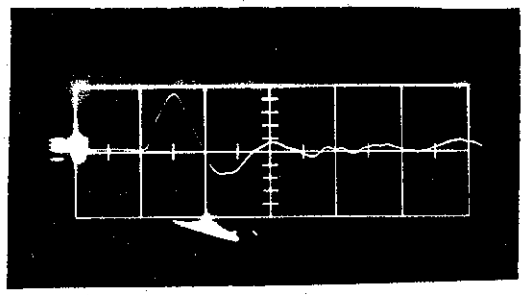

Figure 3-38. Output current trace (26 kA peak) for 5 ohm dummy load (50 ns/cm).

Figure 3-39 shows details of the final geometry in the tube region. It departs slightly from the field plot to accommodate mechanical design requirements. Graphite anode and cathodes were used, each 3-1/4-inch diameter.

3.5.6 Experimental Results

Two materials were tested, cast acrylic and styrene. These materials had performed well in the d.c. puncture tests.

With both test pieces it was possible to operate a 5 ohm diode up to 130 kV providing modifications were made to the anode and cathode triple joints and the diode was in the forward position. The modifications were made after it had been observed that the cathode triple joint was lighting up (Figure 3-40) due to imperfect contact between the metallized plastic and the st.st. cathode holder. Copper wire, 1/8-inch diameter, was placed at both triple joints.

A thin coating of silicone oil on the plastic and the metal surfaces had negligible effect.

Examination of the interfaces after some seventy surface flashovers showed no serious damage. The feathery surface marks on the styrene were a little more obvious than on the acrylic.

3.5.7 Conclusions

Styrene and acrylic interfaces, machined to a suitable configuration can support at least 130 kV for a nominal 30 nS pulse along an interface one inch long. This is the actual length of the interface, however with the copper wire in place, the effective surface length is 3/4-inches. To make realistic comparison with conventional angled interfaces (usually at 45 °) for which the strength is quoted for the metal to metal separation, i.e., surface x 0.707, the breakdown strength of the present interface is 250 kV/inch.

It is believed that significantly better results could be achieved by casting the solid dielectric in intimate contact with the inner and outer metal guiding electrodes and so removing the observed triple joint problems inherent in this design.

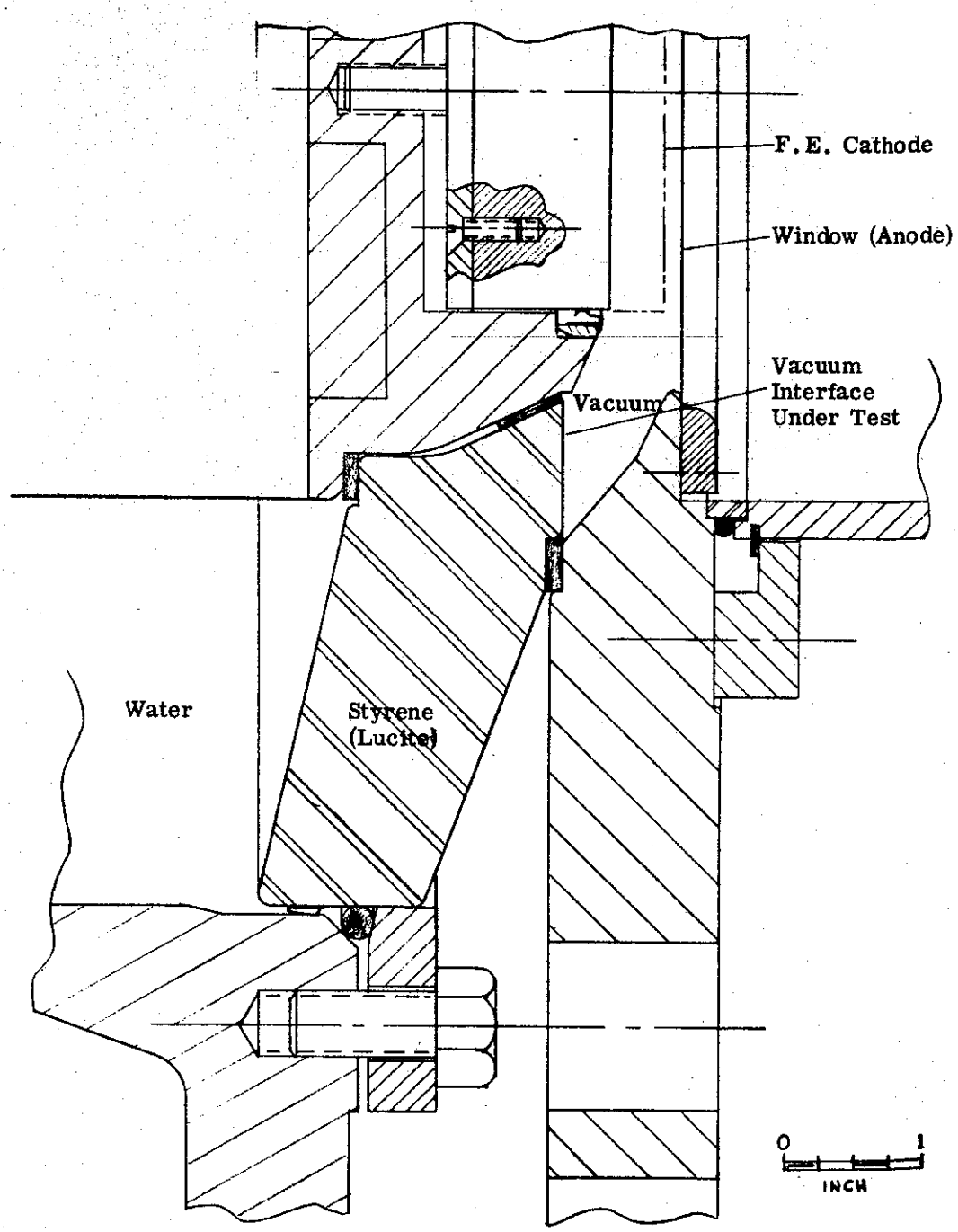

Figure 3-39. Half-section of Output End (Vacuum Flashover Tests).

1-5051

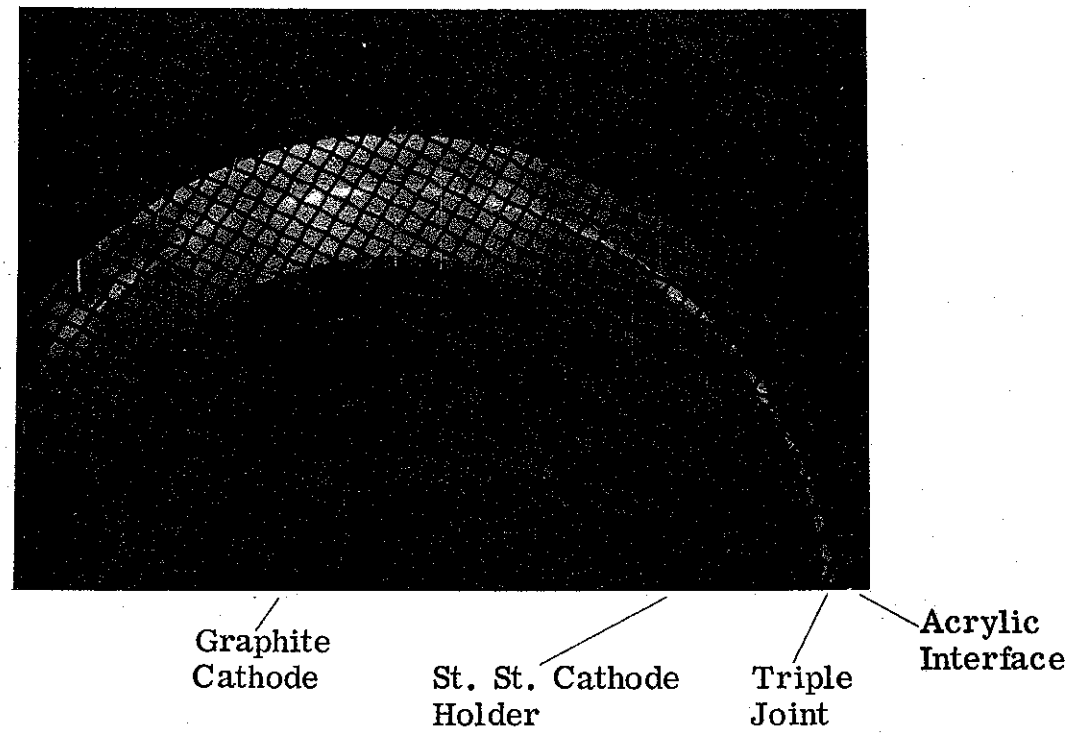

Figure 3-40. View through mesh anode showing cathode triple joint lighting up.

2-1532

SECTION 4.1
NEPTUNE, A HIGH VOLTAGE PULSE GENERATOR

4.0 Introduction and Summary

High voltage, high current electron accelerators are capable of a broad range of applications. Production of x-rays and the creation of shock waves in a target are typical ones. The characteristics of the required electron beam vary according to the application. The hardness of x-rays depends for example on voltage while the intensity depends on the current. The production of shock waves in a target is primarily a function of electron beam pulse energy. However, the depth of deposition is a function of electron energy (i.e., voltage). The pulse width is limited by the physics of the available field emission diode, as an arc develops between anode and cathode after several tens of nanoseconds.

Thus, for the production of high energy pulses two parameters are predetermined. The voltage is determined by the desired characteristics (e.g., penetration depth) and the pulse width is limited by the diode characteristics. This leaves the current as variable, which means that low impedance pulse generators are required for the production of high energy pulses.

To give IPC's staff the ability to stay abreast with this low impedance pulse technology and to produce an additional service facility, the management of High Voltage Engineering and Ion Physics decided then to use inhouse funds to build Neptune A. Neptune A was designed as an 8 ohm water insulated Blumlein system, which was to be charged by a low inductance LC generator. Overvolted water switches were chosen between the LC generator and the Blumlein and between the Blumlein and load. Unfortunately, this choice of switching arrangement was very unsatisfactory and had to be abandoned.

This led to a complete redesign of Neptune A and to the start of the Neptune B program in May of 1969. The target specifications for Neptune B were: 3.4 ohm line impedance, 60 nsec pulse width and a minimum of 1 kJ output in a high fluence electron beam. To save cost and time it was decided to use as much of the Neptune A system as possible. The LC generator was constructed from the same high voltage, low inductance capacitors as the previous LC

generator. The Blumlein was replaced by a single 3.4 ohm line, thus making use of one of the lines in the previous Blumlein generator. The overvolted water switches were, however, replaced by controlled high pressure gas insulated switches. Each switch was to be controlled by a low jitter, fast rising trigger pulse generator.

A further objective of the Neptune B program was to design, build and test a low impedance high voltage pulse generator. Thus the system had to have the capability of command triggering each switch within the system to guarantee efficient energy transfer, a high degree of reproducibility and a low time jitter between a 5 V command signal and electron beam output.

Neptune B consists of an LC generator, a 3.4 ohm coaxial water line and a field emission diode. The LC generator is connected to a coaxial water line at the instant of maximum erected voltage by means of a trigatron controlled high pressure gas insulated switch. The water line voltage rises, and, again at the peak, a specially designed switch connects the field emission diode to the water line. This switch is a low inductance, multichanneled, high pressure gas switch which has an inherent jitter of less than ±1 nanosecond with respect to the trigatron input.

The trigatron control of these transfer switches means that the output pulses are of reproducible amplitude and, more particularly, are of maximum energy. In contrast, an overvolted switch is usually adjusted to fire at 90% of peak voltage which implies, for two such switches in series, a 35% energy loss. Pulse risetimes in the field emission diode are 25 nsecs and design studies on the output show that this may be reduced to 15 nsecs. The time jitter between a 5 V command signal and electron beam output is on the order of ±5 nsec r.m.s. which indicates that the switching arrangements chosen could be used where several modules have to be synchronized with

each other. The fluence reproducibility achieved is better than 5% and the maximum beam energy achieved is 2 kJ under mismatch conditions.

SECTION 4.2
OVERALL DESIGN PHILOSOPHY

The previous section outlined the rationale behind the construction of Neptune B. At the outset, a low impedance pulse generator, in the megavolt range, with a very low time jitter was envisaged. This generator would produce electron beams from a field emission diode, preferably with a fast risetime, uniform energy and good reproducibility. It was necessary to make maximum use of existing hardware.

A block diagram of the generator is shown in Figure 4-1 . A command pulse initiates Switch I which erects an LC generator. The LC generator is then connected, via Switch II, to a fast energy store or water line. When this is fully charged, Switch III connects the field emission diode, which produces the required electron beam. An overall view is shown in Figure 4-2 .

The voltage limitation, pulse length and impedance of the generator are set by the dimensions of the fast energy store. The output pulse risetime is principally limited by the inductance of the last switch, or Switch III and the inductance of the tube. The time and amplitude jitters of the system (i.e., the reproducibility) are set by the switch closure sequence.

The design voltage on the line was set at 1 MV, and, due to field emission diode characteristics at these levels, the pulse length should be approximately 60 nanoseconds. The existing Neptune A hardware could provide a coaxial line whose conductor diameters were 40-inches and 26-inches. When filled with water, these tubes form a line of the correct length and of 3.4 ohms impedance. Calculations show that 1 MV could be supported by a 40-inch coaxial line whose impedance is as low as 1 ohm, thus assuring an ample safety margin for the 3.4 ohm line. The symmetry of the coaxial geometry favors a smooth, low inductance transition between the water line and the field emission diode.

The output risetime is limited by the inductance of Switch III, the transition to the diode, and the inductance of the cathode stalk in the diode. The largest part of this is due to Switch III. This is discussed more fully in

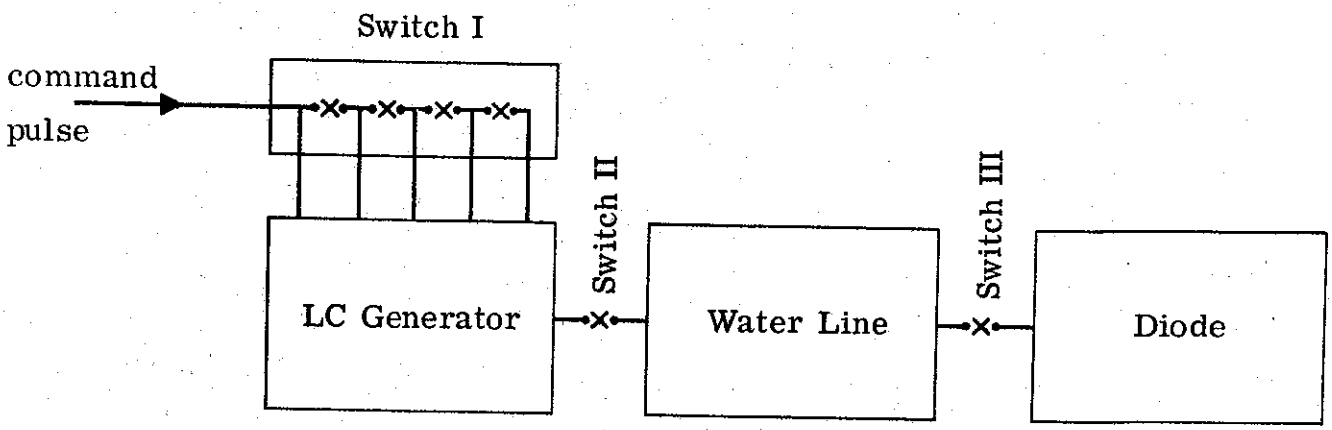

Figure 4-1. Block Diagram of Neptune B System.

1-5064

section 4.8. For minimum inductance it has to be short and it is also shown that a multichannelled design is superior to a single channel design. Each channel is separately triggered to ensure that each gap closes and also to ensure minimum jitter.

Probably the most important aspect of the work is the control of the switch closure sequence. From the outset, it was decided to use trigatrons in all stages. The alternative, overvolted gaps, suffers from large inherent jitter due to the statistical nature of the breakdown process. To justify this assertion, we should examine the system shown in Figure 4-3 . The LC generator erects, its voltage being a cosinusoidal function of time. To ensure that Switch II closes at the first peak, an overvolted gap would be set to close at 90% of maximum voltage (or 81% energy). A time jitter obviously leads to a significant amplitude jitter due to the appreciable value of dV/dt. The time jitter would be appropriate to the erection time of the generator, viz. >100 nanoseconds. In a similar manner, the water line charges as a cosinusoidal function of time and Switch III, if overvolted, would cause further jitter. Thus, the use of overvolted gaps would give rise to large amplitude variations together with a time jitter so large that synchronization with similar systems would be impossible.

The command trigger sequence used is shown in Figure 4-3 . Each switch is initiated by trigatrons controlled from a master pulse generator. The jitter of each stage is thus only the jitter of the associated trigger generators, as the trigatron jitter can be kept very small. Trigger pulses may be generated with very fast risetimes and transmitted with low distortion and hence that jitter may be kept small. This is in contrast to the much slower processes associated with high voltage, high capacity generators and stores. The result is that both Switch II and Switch III are closed at the maximum voltage peaks of the LC generator and the water line respectively. Time jitter in the closure of these switches affects the amplitude of the output very little as $dV/dt \simeq 0$ at these points. The system is thus more efficient. The jitter of the output pulse with respect to a 5 volt command and initiating pulse is simply the sums of the jitter of Switch III and its trigger generator together with that of the field emission cathode. This may be kept under ± 5 nanoseconds.

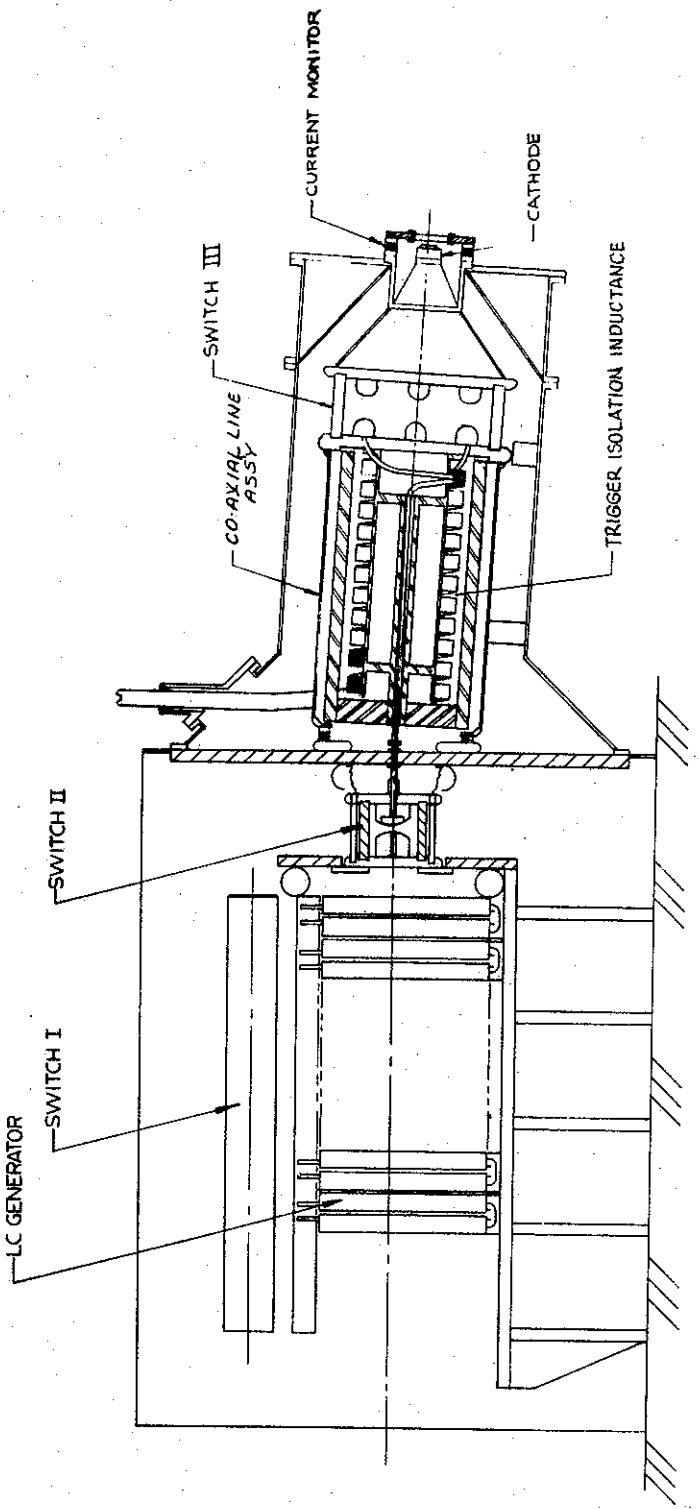

Figure 4-2. Neptune B Assembly

1-4339

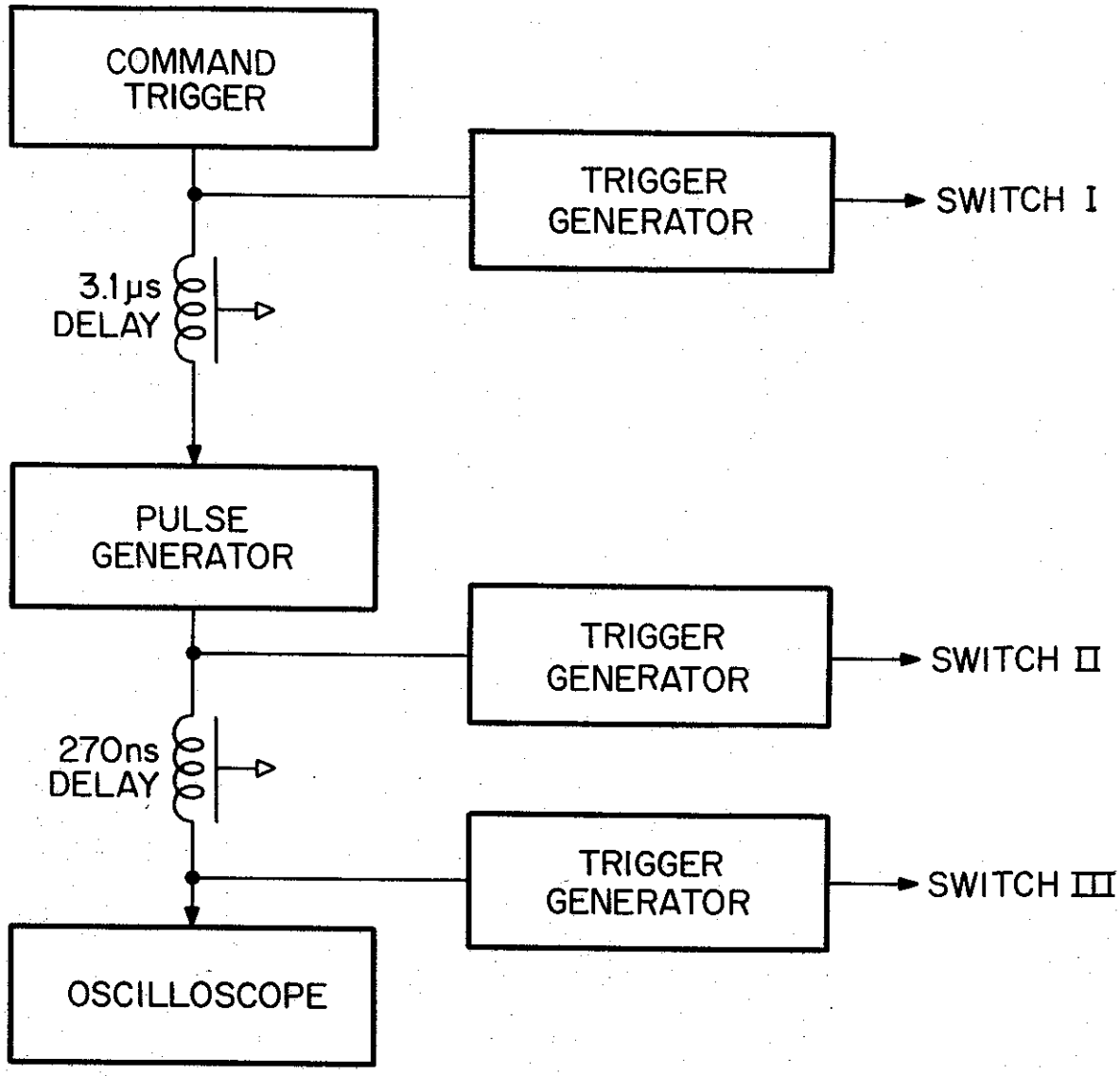

Figure 4-3. Schematic of Triggering Circuit for Neptune B

1-4449

This Page Intentionally Left Blank

An overall view of the system was shown in Figure 4-4 . The LC generator is a stack of 16 0.43 μF capacitors charged in pairs with two DC supplies of opposite polarity. Four coupled triggered gaps (Switch I) reverse the polarities on eight of the capacitors in a conventional way. The components were available from Neptune A. The details including the novel triggering scheme are described in section 4.3. The entire generator including Switch II is immersed in transformer oil. The coaxial water line assembly is shown on the right, a 2-inch thick sheet of lucite separates the generator and the water line. The water line is a coaxial line 40-inches OD and 24-inches ID and 38-inches long. It is made of stainless steel both for corrosion resistance and for maximum voltage strength. The water is continuously purified to keep losses to a minimum.

Switch III is a multichannel high pressure gas switch since switching in this medium is better understood than in solids or liquids. In addition, it is the only medium in which multichannel operation in the megavolt region has been successfully demonstrated.

The isolation of the switches from the trigger generators was accomplished inductively. In order not to degrade the risetime of the trigger pulse, the trigger pulses were sent along coaxial cable which was itself wound into an inductive helix. This helix was wound inside the center conductor of the water line and consisted of five RG17 cables; one for Switch II and four for Switch III.

The field emission diode is constructed so that the anode-cathode gap and the cathode diameter may be varied. This is described in section 4.11. The dimensions of the diode are determined principally by the voltage strength of the bushing. This is 5-3/4-inches long, 16-inch diameter and expected to withstand 500 kV, which is the maximum voltage under matched conditions.

The entire generator, including the control room is 11 yards long. The view, from the diode end, is shown in Figure 4-4 .

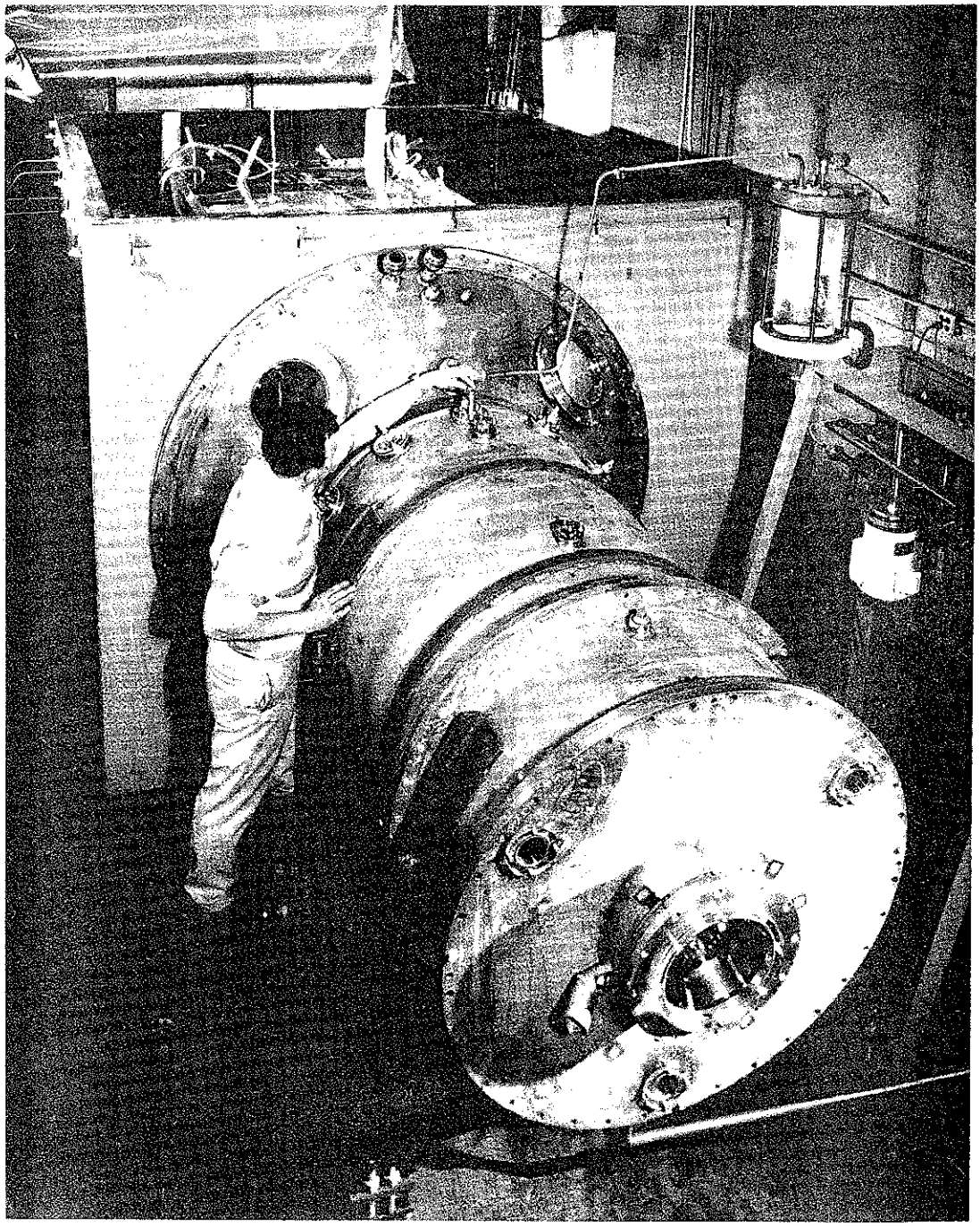

Figure 4-4. View of Neptune from Load End

2-900

SECTION 4.3
LC GENERATOR

4.3.1 Design Considerations

The design of the LC generator was partly determined by the availability of components from Neptune A. These components consisted principally of low inductance, 80 kV 0.43 μF capacitors, a lucite container for these capacitors and a metal enclosure for the generator. One end of this enclosure had a 2-inch thick, 6 foot diameter lucite interface between oil and water to take the output of the generator.

The design objective for the LC generator was the ability to pulse charge a water line 1 meter long, between 3-1/2 and 1 ohm characteristic impedance, to a voltage of 1 MV in the shortest possible time. The requirement for rapid charging is to minimize stress problems in the water line. The generator was to be reliable and protected against fault conditions.

The enclosure was strengthened and filled with transformer oil. The LC generator was rebuilt so that Switch II could also be fitted in the enclosure. Switch II was installed in the oil tank and not in the water tank, since this arrangement made use of the superior holdoff strength of oil and reduced the stress time on the interface from 3 μsec to 300 nsec.

It is essential to guard against various types of failures. Short or open circuited loads will not cause trouble if adequate damping is provided. Both series and parallel damping have been fitted to the generator and are discussed in section 3.6. Another type of failure, to which LC generators are prone, is switch gap failure in the swinging circuit on one pair of capacitors in the main bank. If this occurs, the voltage on that pair of capacitors is nearly doubled, leading to an expensive failure. To guard against this, an elaborately coupled triggering circuit was evolved and is discussed in section 4.3.3.

The LC generator enclosure is outlined in Figure 4-2. A bank of 16 0.43 μF capacitors was mounted on a lucite platform with a conducting strip on the underside. The capacitors were connected in series; with the high voltage end protected by a stress dome and connected to Switch II.

The discharge time was limited by this switch. The bank was charged, via 3 copper sulphate solution resistors mounted alongside the main capacitors, from two 100 kV DC power supplies. The bank was erected by a four gap switch (Switch I), initiated by trigatrons. Switch I was mounted on the top of the main bank of capacitors together with its associated coupling capacitors. The circuit diagram is shown in Figure 4-5. The whole assembly was then immersed in transformer oil.

4.3.2 Switch I

Switch I initiates the swinging circuits in the generator. The various gaps in Switch I must close in a known time sequence, so that the swinging circuits reach the maximum reverse voltage simultaneously.

The requisite control is obtained by mounting 4 pairs of 1-inch diameter electrodes in a common envelope. A trigger pin is mounted in each positive electrode. The range of voltages that are required to be controlled by each gap extends from 50 to 120 kV. Electrode separation and gas pressure determine the maximum hold off voltage and also, together with the trigatron geometry, the minimum triggerable voltage.

Figure 4-6 shows these voltages as a function of gas pressure and composition. The trigger pulse applied to the trigatron was 11 kV. This is less than the output of the trigger generator due to the capacity in shunt with the trigger pin. It should be noted that the gap voltage is twice the charging voltage as the bank is charged from (+) and (-) supplies. Nitrogen and nitrogen/argon mixtures were also tried, but the standard deviations (or variability) were much greater.

The next parameter required is the gap closure time sequence. The gas pressure in Switch I was adjusted so that the self-breakdown voltage was about 56 kV. Two sets of measurements were taken viz: time interval between command trigger and gap one closure and then the time interval between command trigger and gap four closure. The charging voltage was 30 kV. The measurements were then repeated for a charging voltage of 40 kV. It can be seen from Figure 4-7 that both gaps close earlier and with less jitter as the charging voltage

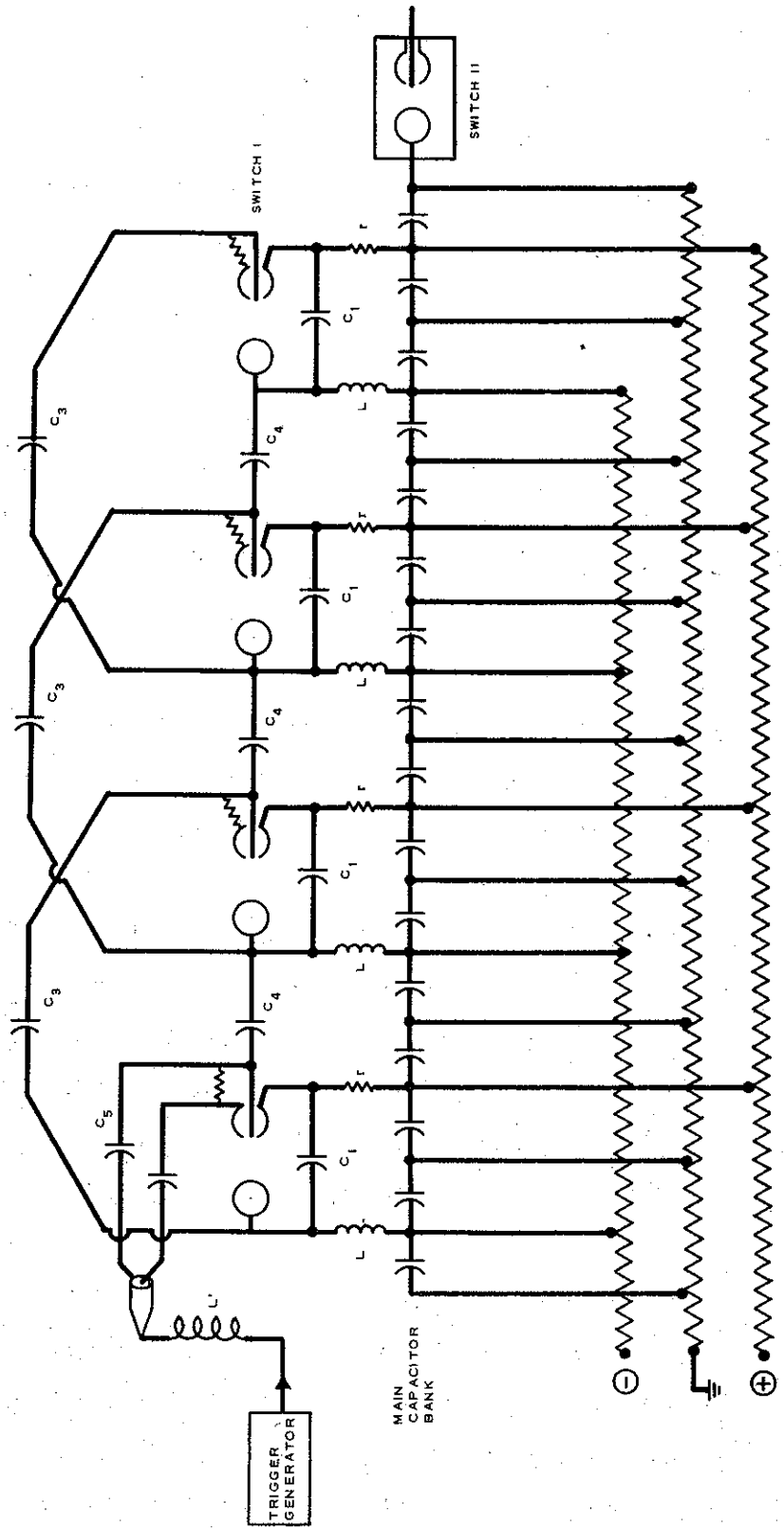

Figure 4-5. LC Generator Circuit Diagram

1-5065

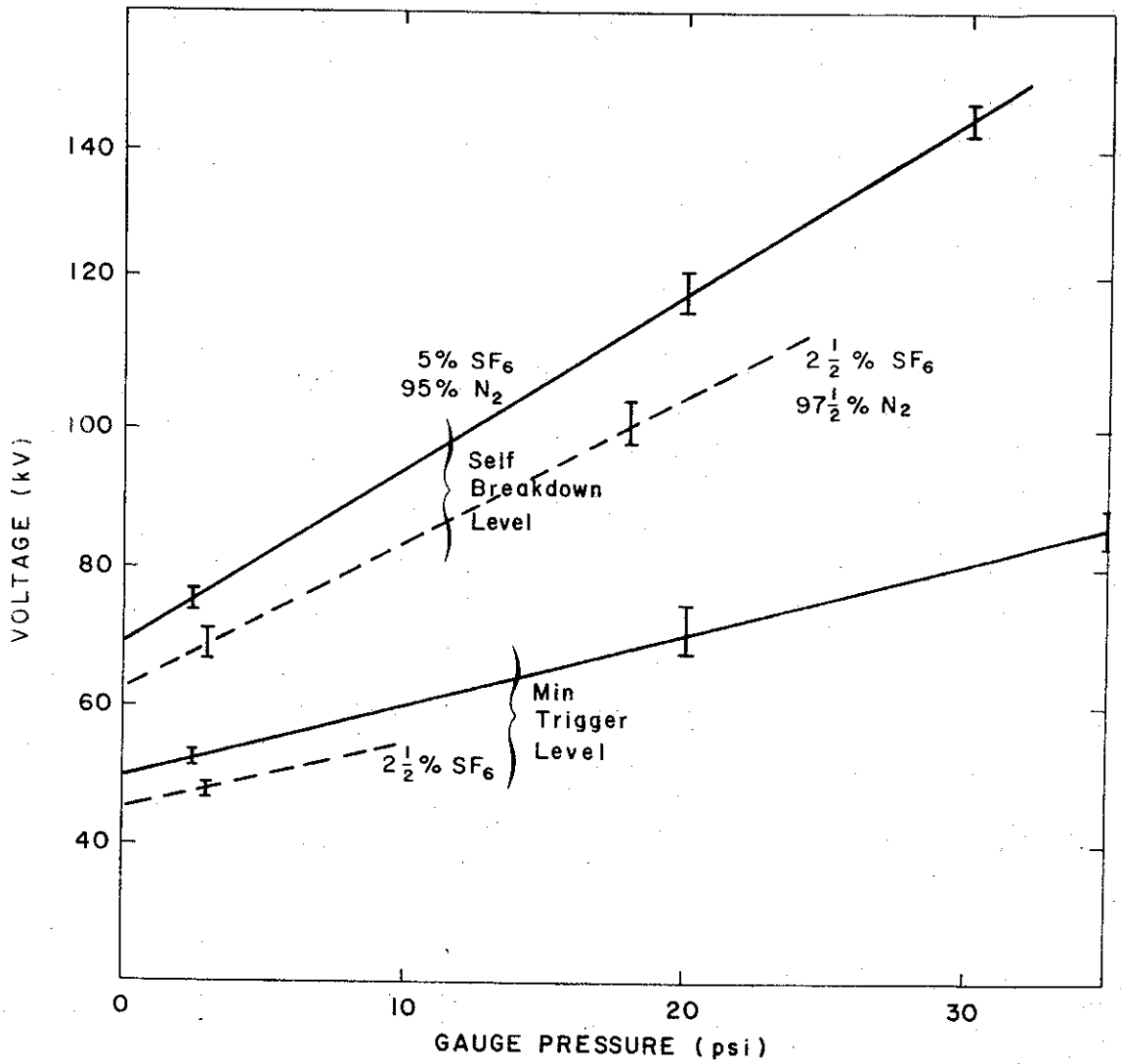

Figure 4-6. Switch I Voltage vs Pressure
(Bars Define Standard Deviations)

1-4338

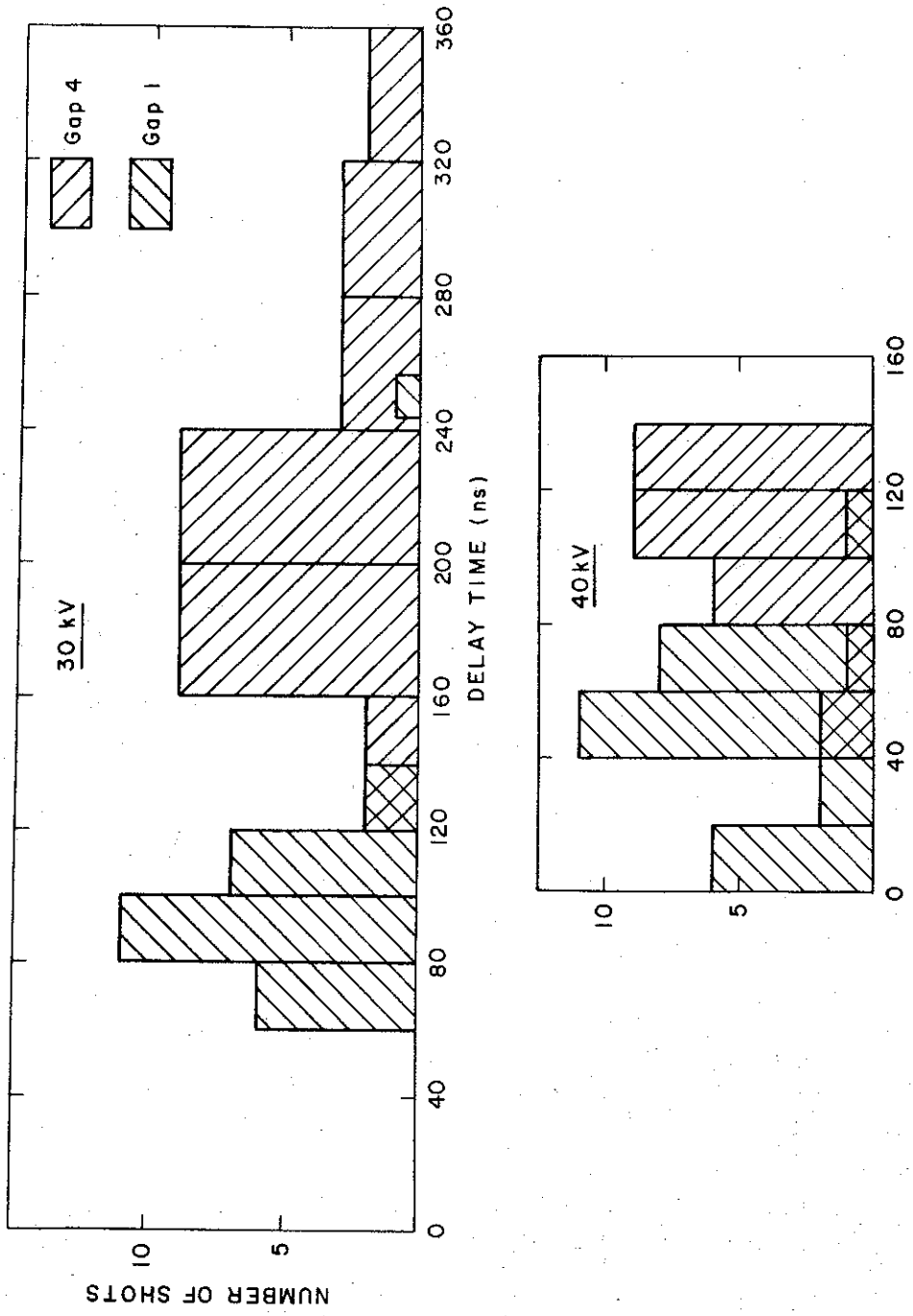

Figure 4-7. Switch I Delay

1-4337

is brought nearer to self-breakdown. The mean delay between closure of gaps one and four is 123 nanoseconds at 30 kV and 58 nanoseconds at 40 kV. The sum of the standard deviations is 87 nanoseconds at 30 kV and 45 nanoseconds at 60 kV; however, it is clearly very pessimistic to sum these as the command trigger (and gap one closure) jitter is thus counted twice instead of being differenced out.

This measurement is a factor in the choice of erection time, as a large jitter/erection time ratio would cause significant voltage output variations. The delay between the firing of gaps 1 and 4 may be compensated by fine tuning of the swinging circuit, as explained in section 4.3.5. To accommodate the larger gaps and high voltages, a delay of 200 nsec was assumed; Figure 4-9 indicates that an error of 100 nsec gives less than 1/2% output voltage reduction.

4.3.3 Trigger Connections

The overall circuit is shown in Figure 4-5, and the trigger circuit is shown in Figure 4-8. An external trigger initiates gap one closure and the heater capacitor C_1 keeps the arc alive until the main bank capacitors are discharging. The impulse caused by the collapse of the gap voltage is transmitted via capacitors C_2 and C_3 to the trigger of the next gap. C_2 is not shown on Figure 4-5 as this is really stray capacity in the main capacitor bank. This stray capacity is approximately 400 pF. The following gaps are triggered in a similar manner.

As was mentioned in section 4.3.1, it is essential that all gaps fire. A failure of one gap to fire results in the voltage increasing by 75% in the affected pair of capacitors. To guard against this, the capacitors C_4 were added. These fulfill the same function as C_3, but the trigger signal is propagated backwards. Thus, if gap 2 should accidently fire during charge, perhaps due to dust, the capacitors C_2 and C_3 will transmit the signal to gaps 3 and 4. Meanwhile gap 1 is triggered by capacitors C_4 and C_2. A similar action would occur if gap 3 or gap 4 should spontaneously close.

The initiating trigger pulse must be transmitted to the first gap, preferably to the positive electrode. This is initially at between 25 and 60 kV,

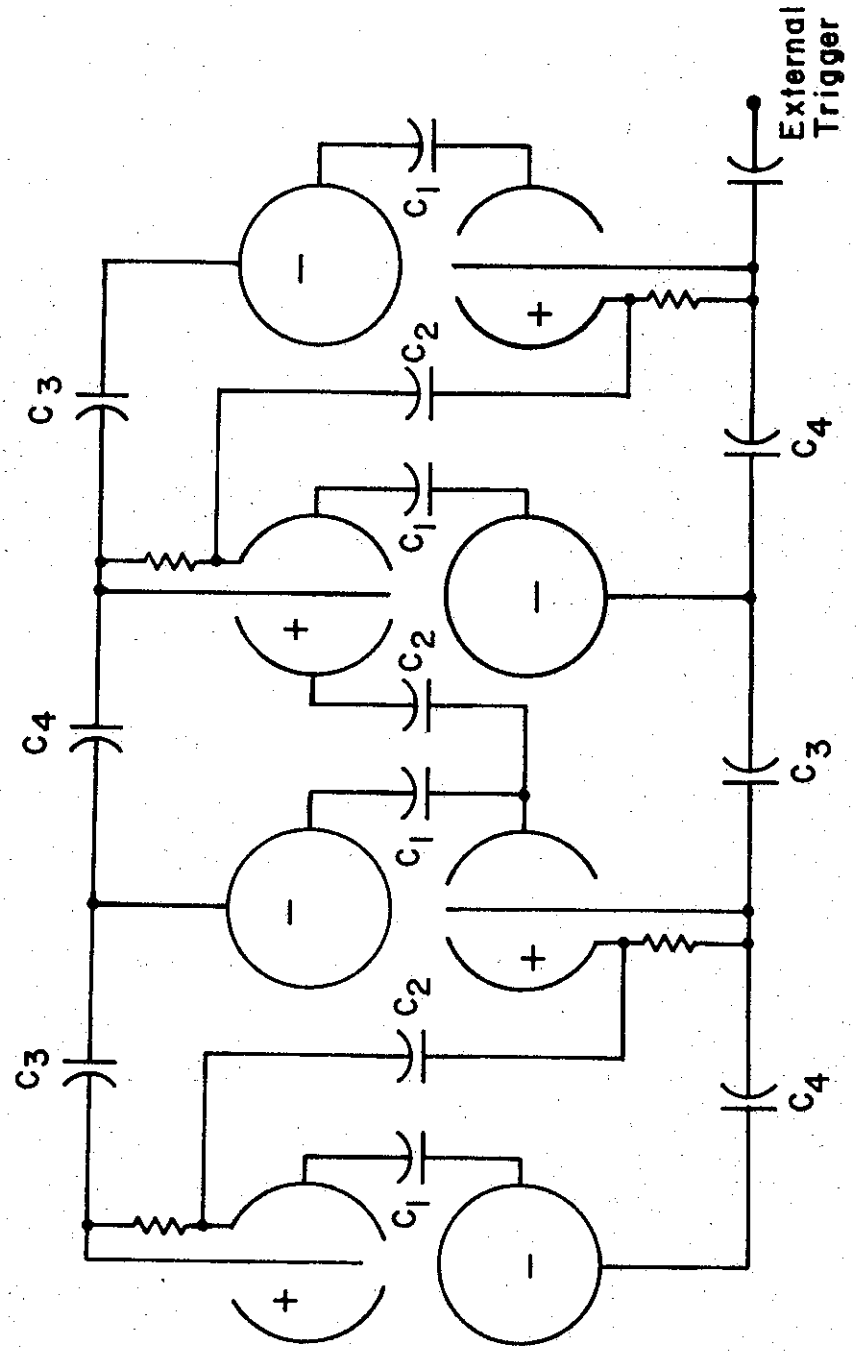

Figure 4-8. Schematic of Coupling Capacitor Arrangement for Switch I

1-4021

but upon generator erection, reverses to three times this value. Isolation is accomplished by means of the capacitors C_5 shown in Figure 4-5. The first tests showed that large transient voltages appeared across these capacitors and to reduce these voltages it was necessary to wind the trigger cable into a coil, shown as L'.

4.3.4 Generator Capacity

The capacitors available for the LC generator are 0.43 μF 80 kV rating with a series inductance of 37 nH. It was decided to connect up 16 of these giving a generator capacity of 27 nF and an inductance of 0.6 μH. This number is a compromise. The required voltage per capacitor for a given water line voltage decreases as the number of capacitors increases. However, the relationship is not linear as the reduction of the generator capacity reduces the capacitative multiplication factor, i.e., the ratio of max. water line voltage to maximum LC generator voltage. In addition, the larger the capacitor bank, the larger the generator inductance and hence the charging time (or stress time) for the water line increases. The inductance of the generator was assumed to be 37 nH/capacitor plus 0.5 μH for Switch II.

Table 4-1 gives the LC generator voltage, the voltage per capacitor and the stress time on the water line in μsecs, required to charge the water line to 1 MV. Water lines of 1-1/2 and 3-1/2 ohms, 52-inches long were considered, as it is perfectly feasible to modify the present line to work below 1-1/2 ohms at 1 MV. It should be noted that no allowance for damping has been made and that the trigger circuits associated with Switch I are simplest if the number of capacitors is divisible by four.

Thus 16 capacitors form a reasonable compromise and lead to a generator capacity of 27 nF. This may be compared with the water line capacity which is approximately 11 nF.

Table 4-1. LC generator characteristics with different numbers of capacitors.

LC Generator Voltage, MV	Capacitor Voltage, kV	Stress Time Nanoseconds	Number of Capacitors
Z = 1.5 Ohms			
.720	90.06	.196	8
.776	77.56	.195	10
.831	69.22	.193	12
.886	63.27	.192	14
.941	58.81	.191	16
.996	55.34	.190	18
1.051	52.56	.190	20
1.106	50.29	.189	22
1.161	48.39	.188	24
Z = 3.5 Ohms			
.594	74.31	.146	8
.618	61.81	.147	10
.642	53.48	.148	12
.665	47.52	.149	14
.689	43.06	.150	16
.713	39.59	.151	18
.736	36.81	.152	20
.760	34.54	.153	22
.783	32.64	.153	24

4.3.5 Erection Time

This is not a critical parameter, provided that the erection time is long compared to the charging time of the water line and to the jitter in Switches I and II.

However there are some other important considerations. The impulsive forces on the windings that make up the induction L and the erosion on Switch I electrodes are increased by a faster erection. On the other hand, a slow erection increases the life of the main bank capacitors but also increases the stress time on the generator insulation. It is also advisable to provide damping in the event of misfire. This may be done by inserting a low resistance r in series with the circuit and by providing larger parallel resistors. Figure 4-5 shows these two, the earth resistor providing the parallel damping. In order to employ both forms of damping, the parameter $2\sqrt{\frac{L}{C}}$ should be approximately twenty times the series resistance r and 1/20 the parallel resistance. The two resistors are most conveniently made from resistive wire and copper sulphate solution and the practical limitations of these define a permissible zone for L and hence the erection time. It is desirable to reduce the effect of mutual and stray inductances in the circuit. This is most easily accomplished by increasing the lumped inductances, which increase the erection time. The erection time of the generator was chosen to be 3.2 μsec. The measurements on Switch I indicated that delay between gaps one and four averaged about 110 nanoseconds and we will assume that this delay was equally apportioned between successive gaps. Consequently we may calculate the various inductances that are required for the four swinging pairs of capacitors so that all four pairs reach maximum reverse voltage simultaneously. Four inductances were computed and wound into formers and fitted in place. The resonant frequencies were checked by a bridge and fine adjustment was achieved by positioning of the inductance. This procedure is not strictly necessary, but the gain in efficiency is well worth the small additional effort.

As was shown in measurements on Switch I, the delay between gaps 1 and 4 varied as the operating voltage and also there was an inherent jitter.

The sum of these was certainly under 150 nanoseconds. When the LC generator had erected, Switch II may be fired and the LC generator connected to its load.

In order to achieve a known voltage output, Switch II is triggered with a low jitter generator. Switch II may thus be fired before or after the LC generator has reached maximum voltage. In practice, it is set to fire at maximum voltage.

Figure 4-9 illustrates the effect of jitter. The vertical axis gives the percent loss of voltage, referred to maximum, and the horizontal axis is the jitter. Pairs of curves are shown, corresponding to different operating points, i.e., the position of the mean of Switch II firings referred to maximum. For example, if Switch II is fired 200 nanoseconds before maximum, on average, and the jitter is ±150 nanosecond, Figure 4-9 shows that the voltage loss ranges from 0.1 to 2.9%, or a range of 2.8%.

If the LC generator is discharged on average at 90% maximum voltage, this corresponds to an operating point of 650 nanoseconds. Figure 4-9 shows that a 250 nanosecond jitter causes the voltage loss to range from 3.8 to 18.3% or a range of 16.1% (referred to the 90% mean). This result is typical of over-volted switch operation.

In practice the delay range in Switch I and the jitter in Switches I and II total less than 200 nanoseconds and the operating point may be set within 100 nanoseconds, leading to a maximum voltage loss of 2%. Measurements of voltage output confirm this calculation.

4.3.6 Damping Requirements

In the event of misfire of Switches I or II,or in the event of a breakdown in the water line, sufficient damping should be provided in the generator to protect the main capacitors. On the other hand, too much damping leads to inefficiency. Two forms of damping, to deal with both open and short circuit cases, have been fitted to the generator and are illustrated in Figure 4-10. Low value resistors were constructed from resistive wire and put in series with the inductances of the swinging circuits. The parallel damping resistor

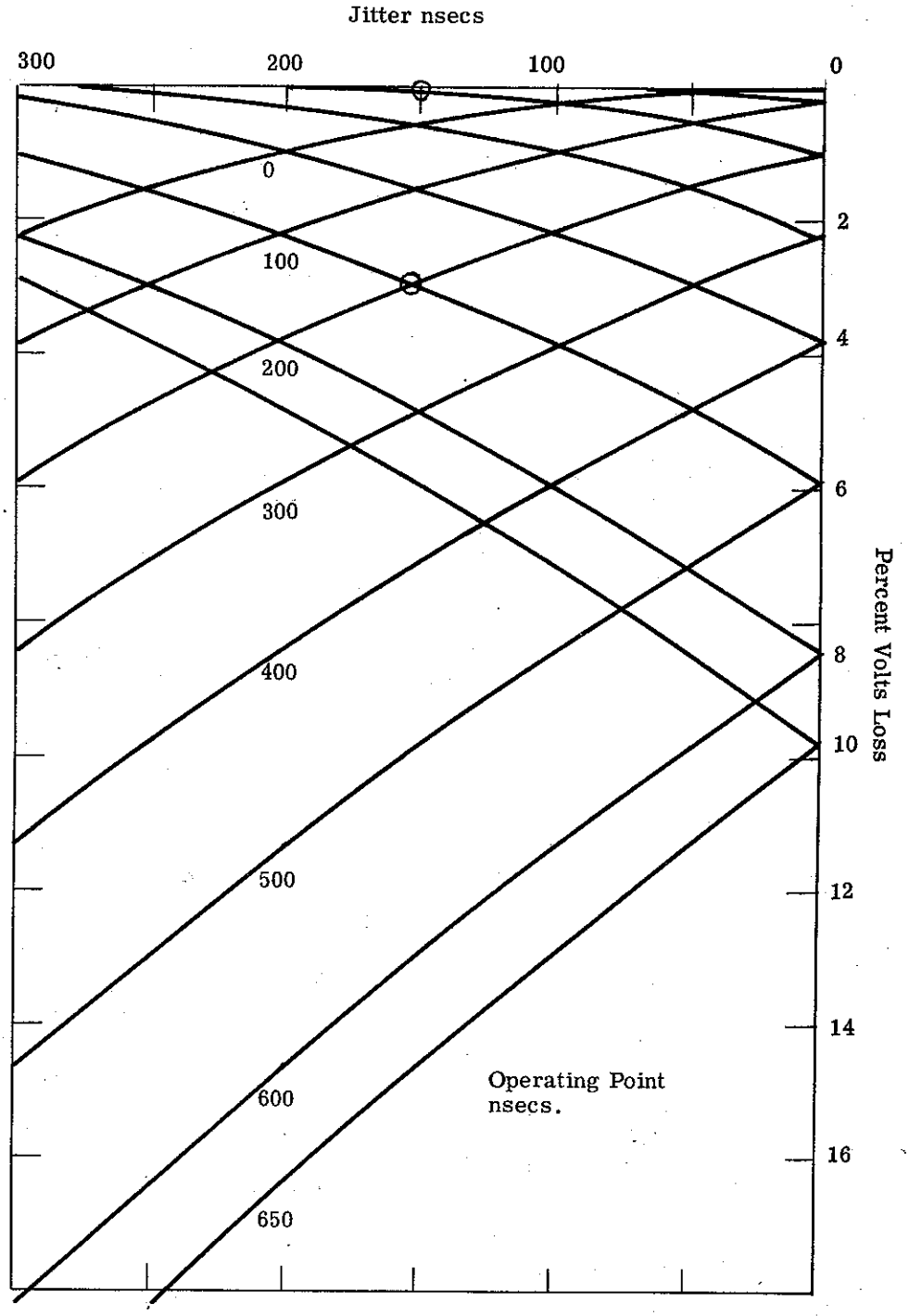

Figure 4-9. LC Generator Voltage Efficiency
Half Period 3.2 μsec.

1-5066

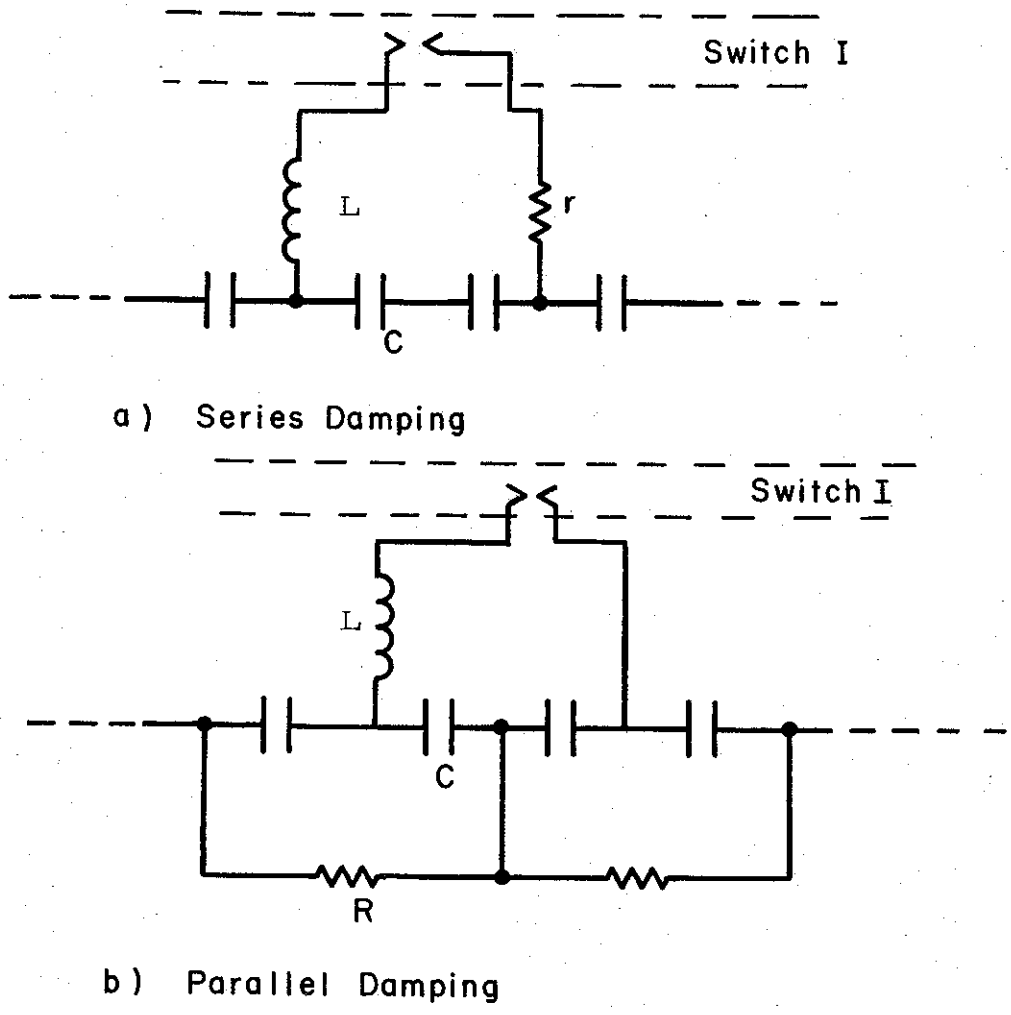

Figure 4-10. LC Generator Damping Circuit Configuration.

1-5053

part of the charging circuit, in particular the earthy line, was the usual copper sulphate solution resistor.

The analysis of series damping is trivial, but in practice the damping resistor is not flexible in that a change in the wire size can give rise to a change in circuit inductance and hence affect the erection. However, series damping is efficient in that only the highly stressed swinging capacitors are damped and thus the erected generator voltage is reduced by only half the damping coefficient of each swinging circuit.

The parallel damping case may be modeled as shown in Figure 4-11. The Laplace transforms of the voltages across the capacitors are given in Figure 4-11. These may be inverted, using a standard computer program.

For low values of R, the capacitors are effectively in parallel and the voltage on the static capacitor oscillates. We are interested in high values of R. Inserting our values, L = 4.8 μH, C = 0.43 μF, the oscillation maximum occurs at 3.2 μs. Table 4-2 shows the values of the voltage across the capacitors near the maximum for various values of R. Initial voltages were taken as 100 volts. It can be seen that for damping values of interest, the static capacitor is damped about twice as fast as the swinging bank. The voltage across the static capacitors was followed over a longer period of time and the results are shown in Table 4-3. It can be seen that in our range of interest, the static capacitors may show a voltage <u>increase</u> at certain parts of the cycle.

For higher values of R, the ratio of static/swinging capacitor voltage damping decreases. It was decided to fit approximately 5% damping via the parallel resistor and 5% via the series resistor. The effect of parallel damping on the erection time is very small at these levels.

The generator has been tested with both open and short circuit loads without failure. The only effects of these were to overload some trigger coupling capacitors. These were replaced with capacitor chains of higher voltage rating and in addition, these were fitted with stress relieving rings. The trouble has not recurred. The effect of altering the load conditions during discharge is more complex and is discussed in section 4.5.

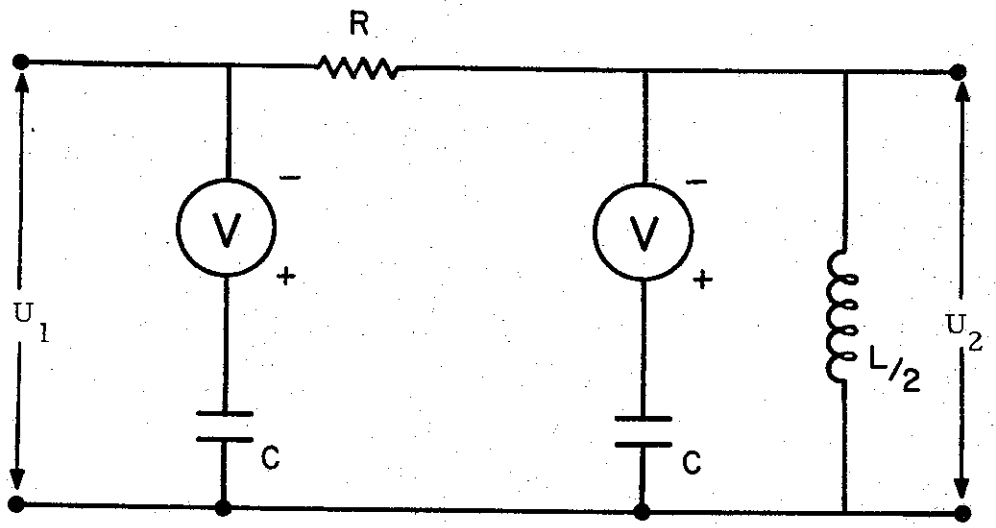

V is step function generator, assumed to be 100 volts

$$U_1(S) = \frac{V}{S} - \frac{2V}{S^4 C^2 RL + S^3 2LC + S^2 2RC + 2S}$$

$$U_2(S) = - \frac{VCL(S^2 RC + 2S)}{S^3 C^2 RL + S^2 2LC + S\,2RC + 2}$$

Figure 4-11. Model of Parallel Damping

1-5052

Table 4-2. Capacitor Voltages for Various Values of Parallel Damping Resistors

Initial Capacitor Voltages 100 Volts

Time (μs)	Voltage on Static Capacitor	Voltage on Swinging Capacitor
R = 30 ohms		
2.9	81.84	-85.49
3.0	80.53	-87.66
3.1	79.23	-88.97
3.2	77.33	-89.42
3.3	76.64	-89.02
3.4	75.36	-87.77
3.5	74.11	-85.70
R = 40 ohms		
2.9	87.57	-87.84
3.0	86.86	-90.02
3.1	86.18	-91.33
3.2	85.55	-91.76
3.3	84.97	-91.30
3.4	84.45	-89.97
3.5	83.99	-87.78
R = 50 ohms		
3.0	87.80	-91.53
3.1	86.96	-92.84
3.2	86.13	-93.25
3.3	85.3	-92.76
R = 60 ohms		
3.0	89.72	-92.61
3.1	89.01	-93.92
3.2	88.3	-94.33
3.3	87.6	-93.83

Table 4-3. Static Capacitor Voltages

Initial Voltage 100 Volts

Time (μs)	Voltage	
	R = 40	R = 60
0.5	99.89	99.92
1.0	99.14	99.52
1.5	97.32	98.16
2.0	94.37	96.04
2.5	90.63	93.13
3.0	86.86	89.72
3.5	83.99	86.21
4.0	82.96	83.02
4.5	84.34	80.51
5.0	88.09	78.85
6.0	99.1	77.91
6.5	103.2	78.08
7.0	104.25	78.16
7.5	101.18	77.78
8.0	94.12	76.69
8.5	84.39	74.83

The measured value of the voltage of the generator was 88% of that calculated for the undamped case. Figure 4-12 shows 3 cycles of the voltage. Note that the voltage does not quite return to zero between peaks. This is due to the fact that the four swinging banks have slightly different oscillating frequencies. They are designed to be in phase at the first crest.

4.3.7 Results and Monitoring

The LC generator voltage was monitored by a known copper sulphate solution resistor fitted along the capacitor bank and graded with it. The voltage across a 0.206Ω resistor, in series with the copper sulphate resistor, gives the LC generator voltage. Figures 4-12 and 4-14 show the traces obtained from this monitor under open circuit and normal load conditions.

A sampling Rogowski was fitted to the output to monitor current, however, the nature of the configuration precluded its use for calibration.

The output from the generator is fixed by the DC charging voltage applied to the capacitor bank and the accuracy of firing Switch II. It is, of course, necessary to adjust the pressure in Switch I for the charging (or output) voltage of interest (see Figure 4-6). As explained in section 4.3.5, jitter should cause the output to vary less than 2%. The other errors come from the DC charging voltage setting and the temperature sensitivity of the monitoring resistor, which is 1.4%/°C.

The output of the generator is 16 times the DC charging voltage multiplied by the efficiency. The efficiencies measured over a period of one month, corresponding to about 150 shots, vary from 85 to 92%, a range of 8% at least half of which may be attributed to the temperature variation of the monitor.

Misfires, due to operation of Switch I with the incorrect pressure, results in either erection without command triggering or extremely late erection, depending on whether the gas pressure in Switch I is too low or too high. In neither case is the LC generator connected to its load by Switch II and the damping mechanisms have bled the energy away without problem. As can be seen from Figure 4-6, an operating range of 25% may be used for a given Switch I

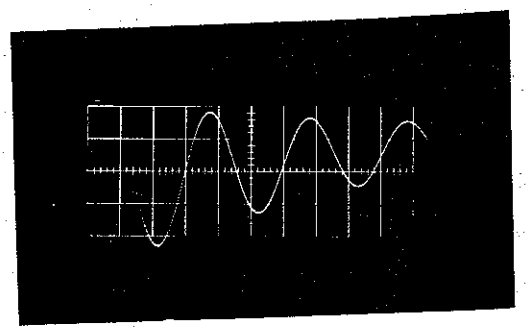

Figure 4-12. LC Generator Voltage.
Trace 2μsec/cm. 130 kV/cm.

2-1533

setting. Thus the generator, over a period of over 2,000 shots, has delivered controlled voltage outputs within ± 2%.

SECTION 4.4
SWITCH II

The function of Switch II is to hold off the LC generator voltage until a command trigger initiates connection of the generator to the water line. The switch is mounted in the center of the lucite interface separating the LC generator oil insulated tank from the water in the water line, as shown in Figure 4-2.

The inductance of Switch II should be small enough to allow the water line to be charged rapidly. This inductance is primarily determined by the placement of the switch and is approximately 1/2 μH. As the inductance of the capacitor bank is approximately 0.6 μH, the water line charging time is thus about 300 nanoseconds.

Figure 4-13 shows a sectional view of the switch. The electrodes are 5-1/2-inches in diameter and set 2-inches apart. It is designed to work up to 300 psig with a gas mixture of 97-1/2% nitrogen and 2-1/2% sulphur hexafluoride.

Figure 4-2 shows the triggering connection to Switch II. The anode is a trigatron with a 1/8-inch diameter trigger pin set in a sharp edged 3/8-inch diameter hole. This increases the field emission of electrons from the main electrode. The range of operation is gratifyingly large, viz for a constant LC generator voltage of 380 kV, Switch II triggered satisfactorily from 55 to over 200 psig.

Figure 4-14 shows the LC generator voltage and Switch II firing for two representative pressures. A very slight (< 50 nsecs) increase in gap closure time may be seen at the higher pressure. The gap closure jitter is about 15 nsecs and is too small to be seen on the LC generator voltage trace. It has a negligible effect on the LC generator output. The effect on the water line voltage is greater but still less than 4%.

The gas mixture deteriorates with use and it has been necessary to change the gas twice during the testing.

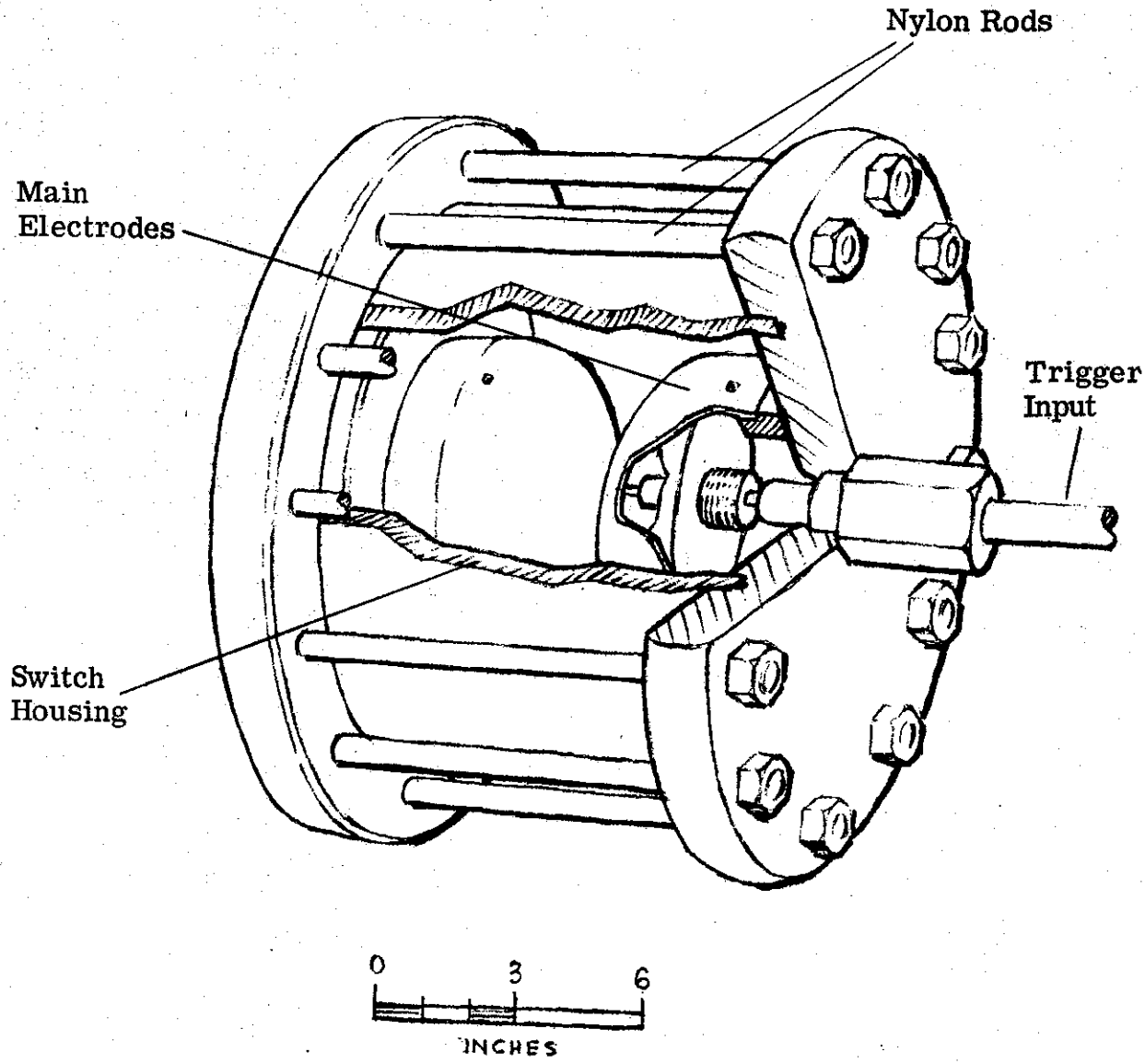

Figure 4-13. Switch II of Neptune B.

1-5067

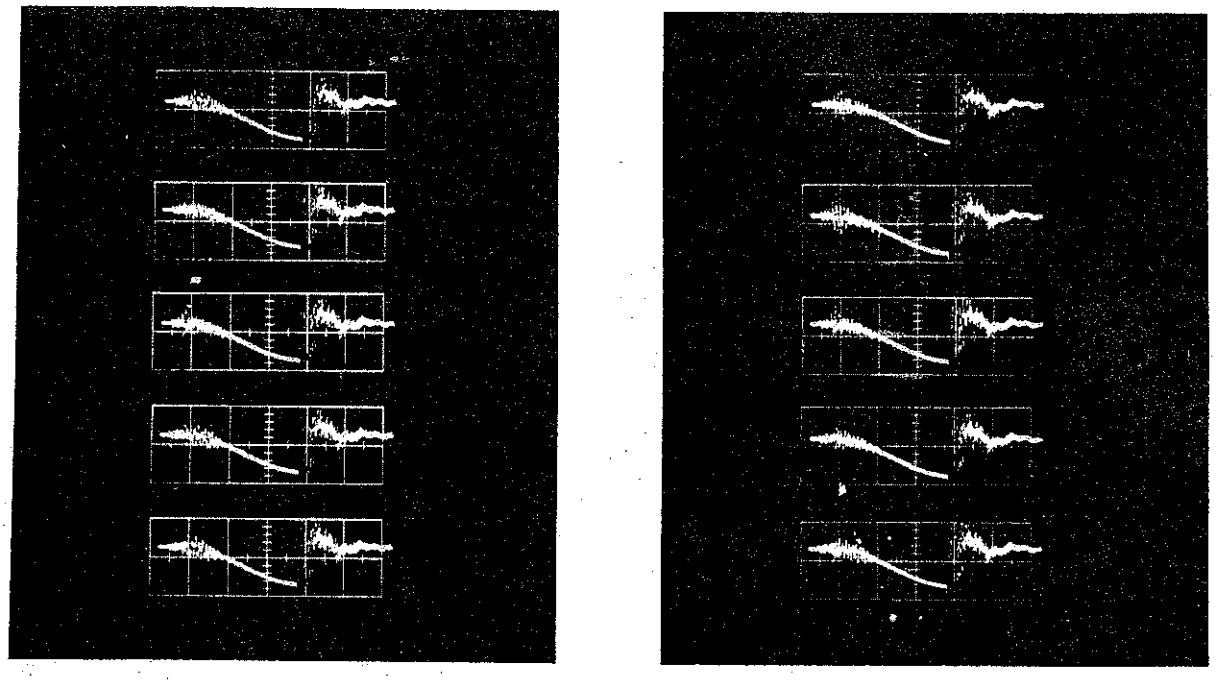

Switch II Gas Pressure

55 psig

180 psig

Figure 4-14. LC Generator Voltage

100 ohm Load Connected by Switch II
at Point of Maximum Voltage

Charging Voltage 27 kV per Capacitor
Scale 1 μs/cm

2-1504

Switch II has been fired about 2,000 times. It has been disassembled once to check electrode erosion and the opportunity was taken to buff the electrodes. The electrode erosion was not severe.

SECTION 4.5
COAXIAL LINE

4.5.1 Choice of Dielectric

The coaxial line acts as a store for energy which is to be dumped into the field emission diode. It is desirable to maximize this energy and the maximum energy storage density of a material is given by ϵE_{BD}^2 where ϵ is the dielectric constant and E_{BD} is the maximum field the material will stand without rupture. This parameter has a very high value for water which was therefore chosen.

However, further considerations modify this. The first consideration is the time factor. The field emission cathode switches on and the diode is active for some tens of nanoseconds, perhaps 50. Then, plasma from the electrodes shorts the diode out and further energy supply is both useless and dangerous. Thus we desire to maximize the energy available from a transmission line during the working period of the diode, i.e. we wish to maximize the power output. This is proportional to energy storage divided by wave velocity i.e., $\sqrt{\epsilon}\ E_{BD}^2$.

The second consideration is size. If we arbitrarily fix line voltage V and line impedance Z then the mean radius R of the line is decided if we are to work the insulation at its maximum field. The electric field E is uniform across the dielectric for a low impedance line (viz. $RE \gg Ve$). The power output of the line is V^2/Z.

Also

$$Z = \frac{60\ V}{R\sqrt{\epsilon}\ E}$$

Hence

$$R > \frac{60\ V}{Z\sqrt{\epsilon}\ E_{BD}} \qquad \text{as} \quad E < E_{BD}$$

We may fix any two of the three variables V, Z and R. It is clearly desirable to maximize the parameter $\sqrt{\epsilon}\ E_{BD}$. For Neptune B, V and Z are given. The material with the largest value of $\sqrt{\epsilon}\ E_{BD}$ will give the smallest line.

The modification due to the area effect (i.e. $E_{BD} \propto \text{area}^{-0.1}$) is to alter the parameter to $\epsilon^{0.55}\ E_{BD}$.

A third consideration, important only in the largest systems requiring a very fast risetime, is electrical size. There is a difficulty in initiating energy flow in the required TEM mode. The parameter of importance is the circumference of the line measured in nanoseconds, viz. $\frac{2\pi R\sqrt{\epsilon}}{c}$. If we keep this constant, the power available from a line is proportional to $V E_{BD}$; or $V E_{BD}\ \epsilon^{0.2}$ if we correct for the area effect. The dielectric loss factor must also be considered for this purpose.

As shown above, different power combinations of the parameters ϵ and E_{BD} must be optimized depending on the objective of the task. The criterion for Neptune B was maximization of power flow within a given impedance and voltage range rather than the achievement of very fast risetimes. Table 4-4 lists the relevant parameters for some liquids; ϵ is the relative dielectric constant and E_{BD} is the breakdown strength. The breakdown strength is a function of time and electrode area and it was convenient to normalize to water.

Thus water, the alcohols and caster oil are the most attractive liquids. Bearing in mind the availability of the Neptune A housing, which is designed for the compact dimensions that water makes possible, water was chosen as the preferred medium.

Table 4-4. Electrical Characteristics of Selected Liquids.

Liquid	Dielectric Constant ϵ	E_{BD} Normalized	$\sqrt{\epsilon}\, E_{BD}^2$	$E_{BD}\sqrt{\epsilon}$
Water	81	1	9	9
Ethyl Alcohol	24	1.53	11.5	7.5
Methyl Alcohol	33	1.44	12	8.3
Glyarine	44	0.48	1.54	3.2
Caster Oil	4.7	2.37	12.1	5.1
Transformer Oil	2.4	1.59	3.98	2.5
Ethylene Glycol	38	1	6.2	6.2

4.5.2 Impedance

The Neptune A housing which was available was 40-inches diameter and 80-inches long. This would accommodate a coaxial line capacitor up to 46-inches long. The breakdown strength of water is not simply described, as it varies with electrode area and polarity, pulse length and field uniformity.(1)

For the positive electrode

$$E_{BD} = \frac{0.275}{A^{0.1}\,\tau^{1/3}} \quad \text{MV/cm}$$

and for the negative electrode

$$E_{BD} = \frac{0.63}{A^{0.07}\,\tau^{1/3}} \quad \alpha \ .$$

(1) J. C. Martin, AWRE Report SSWA/JCM/6511/B.

where the electrode area A is in square cm and the effective pulse length is in μsecs. α is defined as

$$\alpha = 1 + 0.12 \sqrt{\frac{E_{max.}}{E_{mean}} - 1} \quad .$$

The next step is to calculate the capacity of water lines of various impedances. The charging time from the LC generator varies as this capacity. The stress time is defined as the time between $0.63\,V_{max.}$ and $V_{max.}$. The fields on the inner and outer conductors may be claculated and expressed as a percent of the breakdown field. This was done for a line 38-inches long charged to 1 MV from the LC generator described in section 4.3.

Table 4-5. Breakdown Strength of Various Water Lines.

Z ohms	Stress Time μsecs	E_{mean}	α	$\frac{100\,E_{max.}}{E_{BD}}$	
				Inner Conductor	Outer Conductor
1.0	.184	.143	1.03	27.15	75.90
1.2	.175	.121	1.04	22.80	62.20
1.3	.171	.112	1.04	21.15	56.98
1.5	.164	.099	1.04	18.53	48.70
1.7	.157	.088	1.04	16.52	42.35
2.0	.149	.077	1.05	14.34	35.37

It can be seen that the outer conductor is the most dangerous and that a 1-1/2 ohm line may be built with reasonable safety. Due to the availability of a 24-inch diameter cylinder for use in the inner conductor, it was decided to use 3.4 ohm impedance line. The margin of safety is thus ample, referring to

inner/outer breakdown stress. However, as discussed in section 4.7, the constraints on the trigger isolating inductance were tightened by this choice.

4.5.3 Mechanical Description

The water line is shown towards the right of Figure 4-2. A stainless steel cylinder 24-inch diameter and 45-inches long is supported on two Lucite wedges inside an outer stainless steel housing. The coaxial line formed by the 24-inch diameter inner and the 40-inch diameter portion of the outer is the effective part of the coaxial capacitor. It is about 38-inches long.

The inner cylinder contacts the LC generator terminal by means of bellows, as shown in Figures 4-2 and 4-15. The other end of the coaxial line is connected to Switch III. Figure 4-2 also shows trigger cable assembly which is a group of cables wound inductively on a Lucite former and insulated from the 24-inch diameter cylinder by Lucite shields. The water dielectric is continuously purified by means of filters and a demineralizer. The water is deionized to better than 1 MΩ cm, which loads the line by approximately 1,000 ohms. The line is protected from ringing by means of copper sulphate solution damping resistors which connect the inner and outer cylinders by means of spring fingers. The resistance in shunt across the line is about 40Ω. Figure 4-16 shows an overall view of the system, with one of these resistors being adjusted.

4.5.4 Monitoring

The voltage on the water line is monitored by means of copper sulphate solution resistive dividers of conventional design. These dividers are 355Ω and 4kΩ paired with 66.7 and 726 mΩ and they are in the same axial position as the damping resistors together with an identical outline except for the low resistance section, which is composed of carbon resistors. An opening for the insertion of a thermometer is provided, as the water purification cycle causes temperature changes and therefore resistance changes in the monitor resistances.

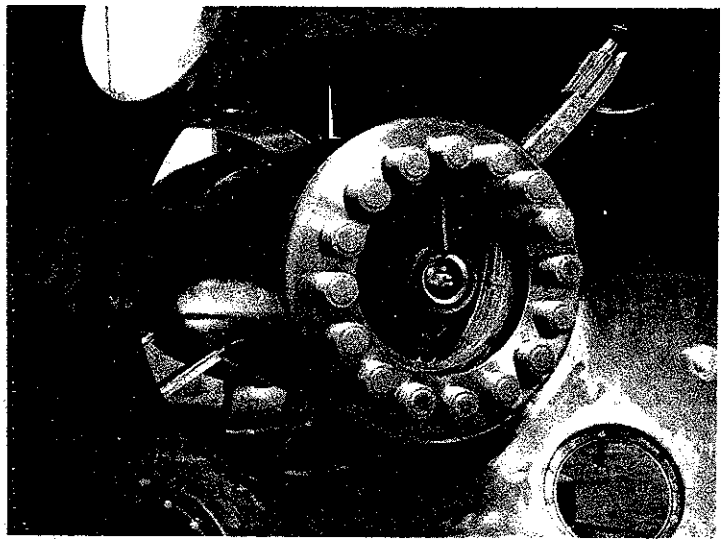

Figure 4-15. Center Conductor and Trigger Isolation Assembly Installed in Water Line.

2-1498

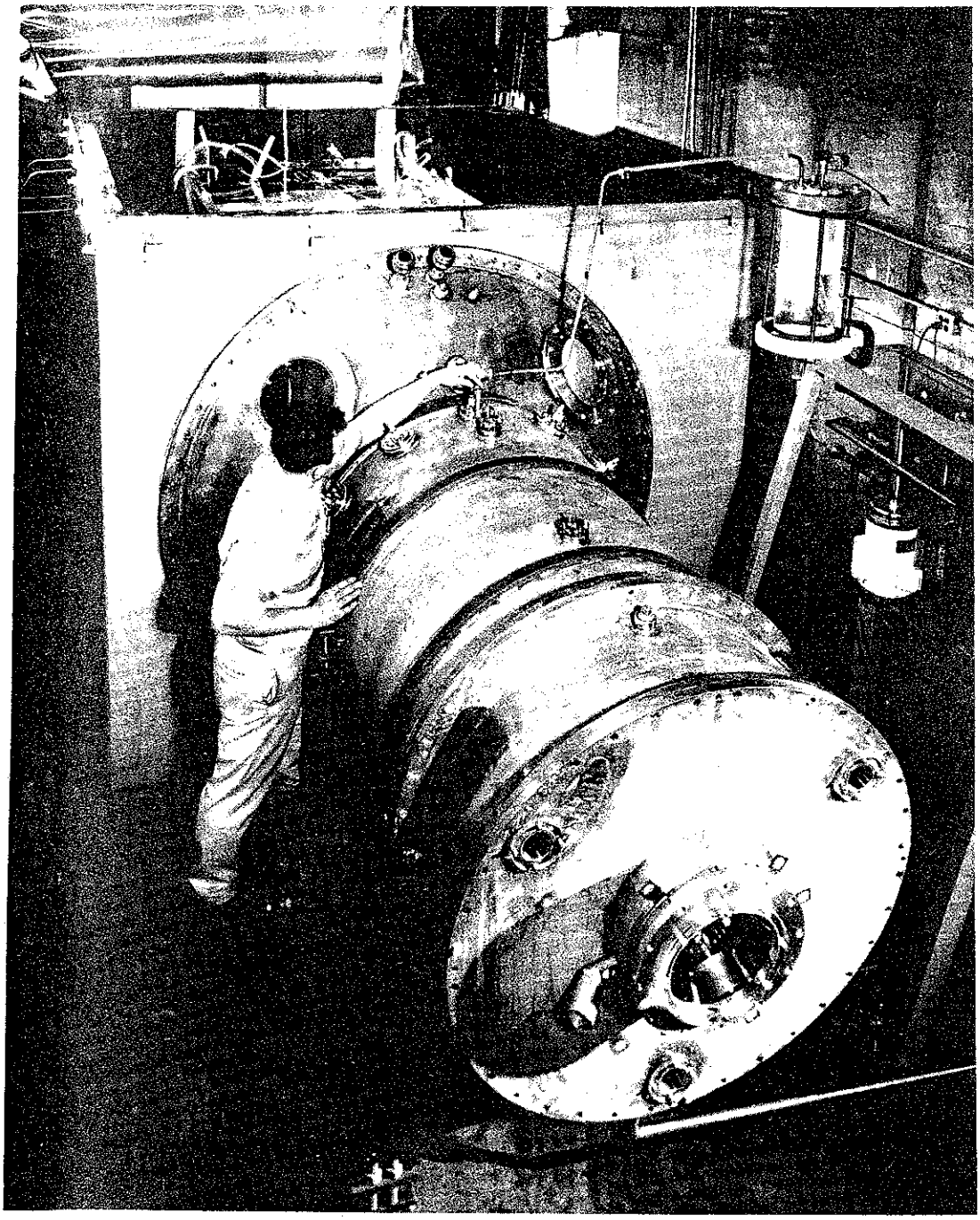

Figure 4-16. View of Neptune. Water Line and Diode in Foreground.

2-900a

4.5.5 Peak Voltage

The water line starts charging when Switch II connects the erected LC generator. The voltage on the water line then rises to a peak, at which point Switch III should be triggered and the energy dumped into the required load. If Switch III is not triggered, the voltage on the line oscillates as shown in Figure 4-17.

The maximum amplitude of the water line voltage is determined by the LC generator, which has already been discussed in section 4.3, and the damping resistances fitted the line to supress ringing (see below). The trigger isolation inductance and its associated capacitance have a smaller but not negligible effect. The amplitude of the water line voltage at the instant of firing Switch III is proportional to the voltage applied to the load. This is a function of the jitter in both Switch II and Switch III. Figure 4-18 shows the percent voltage loss for various operating points (i.e., distance of the mean point of Switch III firing from peak voltage) and for various total jitters of the two switches. It is easy to place the operating point within 20 nanoseconds and the jitter (predominantly Switch II) can be kept to 20 nanoseconds. Figure 4-18 indicates a maximum voltage loss of 5% for this jitter performance.

4.5.6 Voltage Waveforms in the Water Line

The LC generator pulse-charges the water line through the generator inductance and Switch II. Near the peak of the charging cycle, Switch III connects the load to the water line. This process is the sum of three processes with three different time scales. The slowest process is the erection of the LC generator; over 3 μs. For phenomena less than 1 μs duration, the generator may be represented as a capacitor of 27 nF and an inductance of 1 μH. The next fastest processes are the voltage excursions on the line and on the generator when the load R_L is connected by means of Switch III or by a breakdown elsewhere in the line. The fastest process is the transmission of power from the line to the load when SW III operates. The 10 nF capacitor is really a transmission line 30 ns long, and hence may deliver its energy to matched load in a minimum of 60 ns.

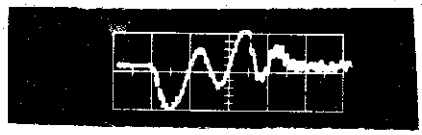

Scale 500 ns/cm
500 kV/cm

Figure 4-17. Water Line Voltage

(Note breakdown of Switch III at peak positive voltage.)

2-1505

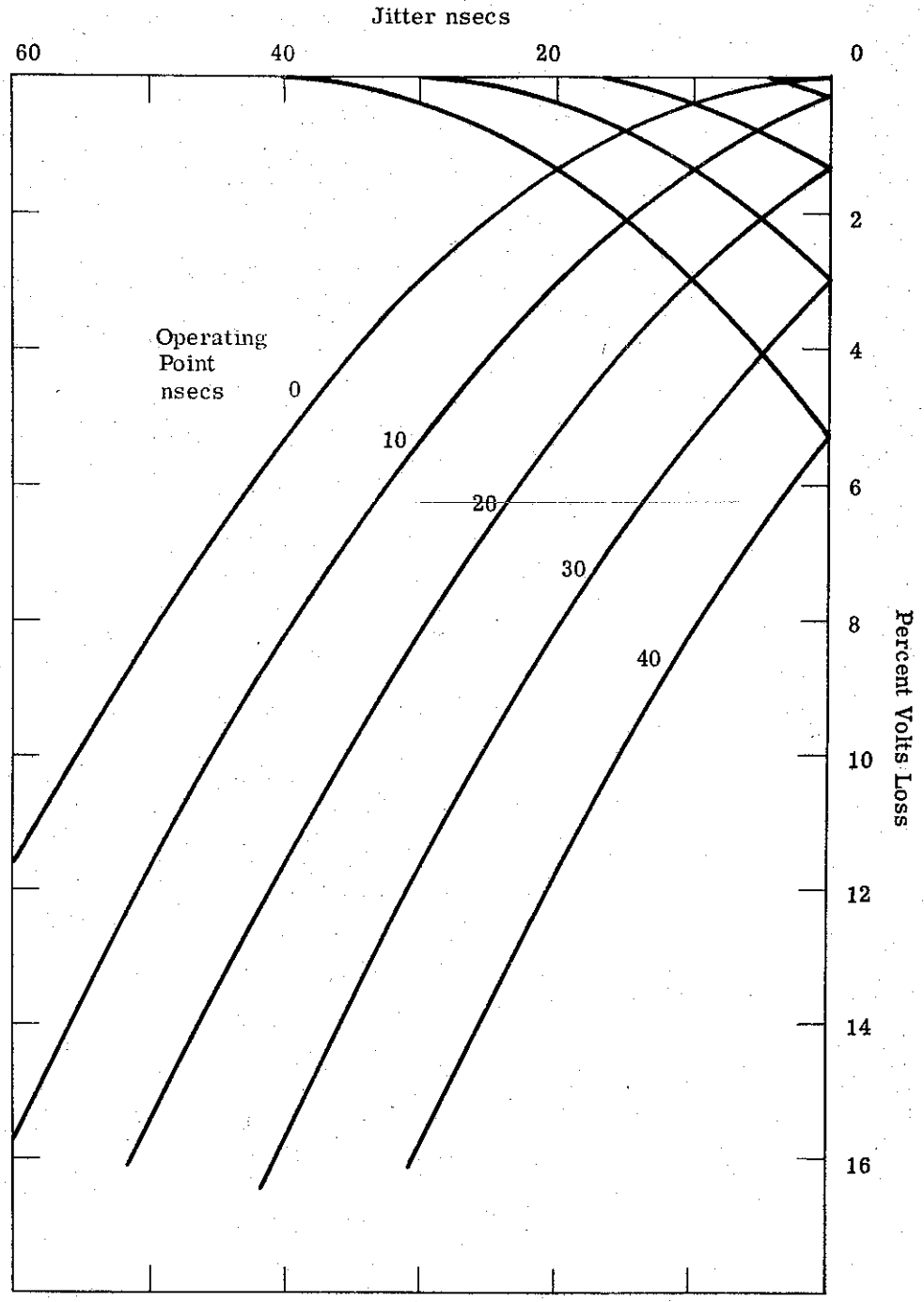

Figure 4-18. Water Line Voltage Efficiency Half Period 270 ns

1-5068

In practice, when the water line voltage is maximum the line is connected to a field emission cathode where impedance varies with both voltage and time. This impedance is very high for some nanoseconds and then falls to a few ohms. The cathode geometry is adjusted until this impedance is 3-1/2 ohms. After 50 nsecs or so, the cathode-anode gap is shorted by a plasma. This acts like a switch and the impedance falls to a few milliohms.

At this point both the LC generator and the water line ring at amplitudes that depend on the time of firing of the 'plasma switch'. The ringing has the time scale 100 ns to 1 μsec. This behavior is so like a fault condition that for convenience, both fault and normal conditions are examined together in the next section.

4.5.7 Damping

To reduce the voltage ringing, both the water line and the LC generator are fitted with damping resistors. The LC generator resistors have been described in section 4.3. A circuit model suitable for examining voltage waveform on the LC generator and the water line, for the time range 100 nsecs to 1 μsec, is shown in Figure 4-19. The generator is represented as a 27 nF capacitor C series with 1 μH. The coaxial line may be represented as a capacitor of 10 nF in parallel with a leakage, or shunt, resistance $R_s \cong 100\Omega$ and the trigger isolation inductance of 7 μH. The load resistor, R_L, may range from 10Ω to 0.01Ω and may be a dummy load, a field emission cathode or an arc. Finally the cathode may be shorted out with a 'plasma switch'. This model is rather cumbersome and may be simplified for various circumstances.

Figure 4-20 shows the equivalent network of the water line and LC generator when Switch III is not triggered. Figure 4-21 shows the response of this circuit which may be compared with Figure 4-17, the observed water line voltage.

Figure 4-22 shows a model for normal operation. The operation of the 'plasma switch' is modelled by simply modelling the circuit for a given time and then resolving for a different R_L, using the conditions obtained from the first part of the solution.

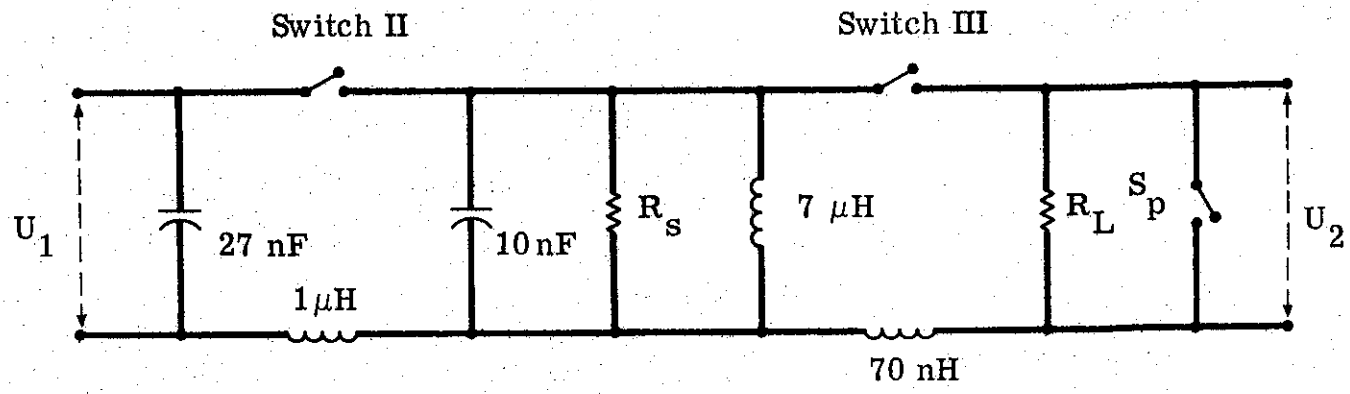

U_1 and U_2 are LC generator and cathode voltages

R_s is the shunt damping resistor on water line

R_L is the impedance of field emission cathode

S_p is the plasma switch, which shorts out the cathode

Figure 4-19. Neptune Circuit Model for Fault Conditions.

1-5069

C_1 & L_1 -- represents the LC generator

C_2 -- represents the water line

R -- represents the damping load on the water line

L_2 -- represents the inductance of the trigger isolation

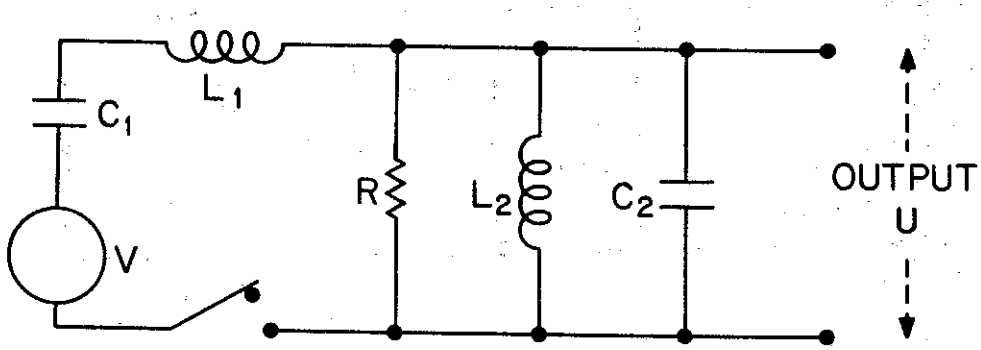

$$U = \frac{sV/L_1C_2}{s^4 + s^3/RC_2 + s^2\left[1/L_1C_2 + 1/L_2C_2 + 1/L_1C_1\right] + s/L_1C_1C_2R + 1/L_1L_2C_1C_2}$$

Figure 4-20. Model of LC Generator and Water Line

1-4450

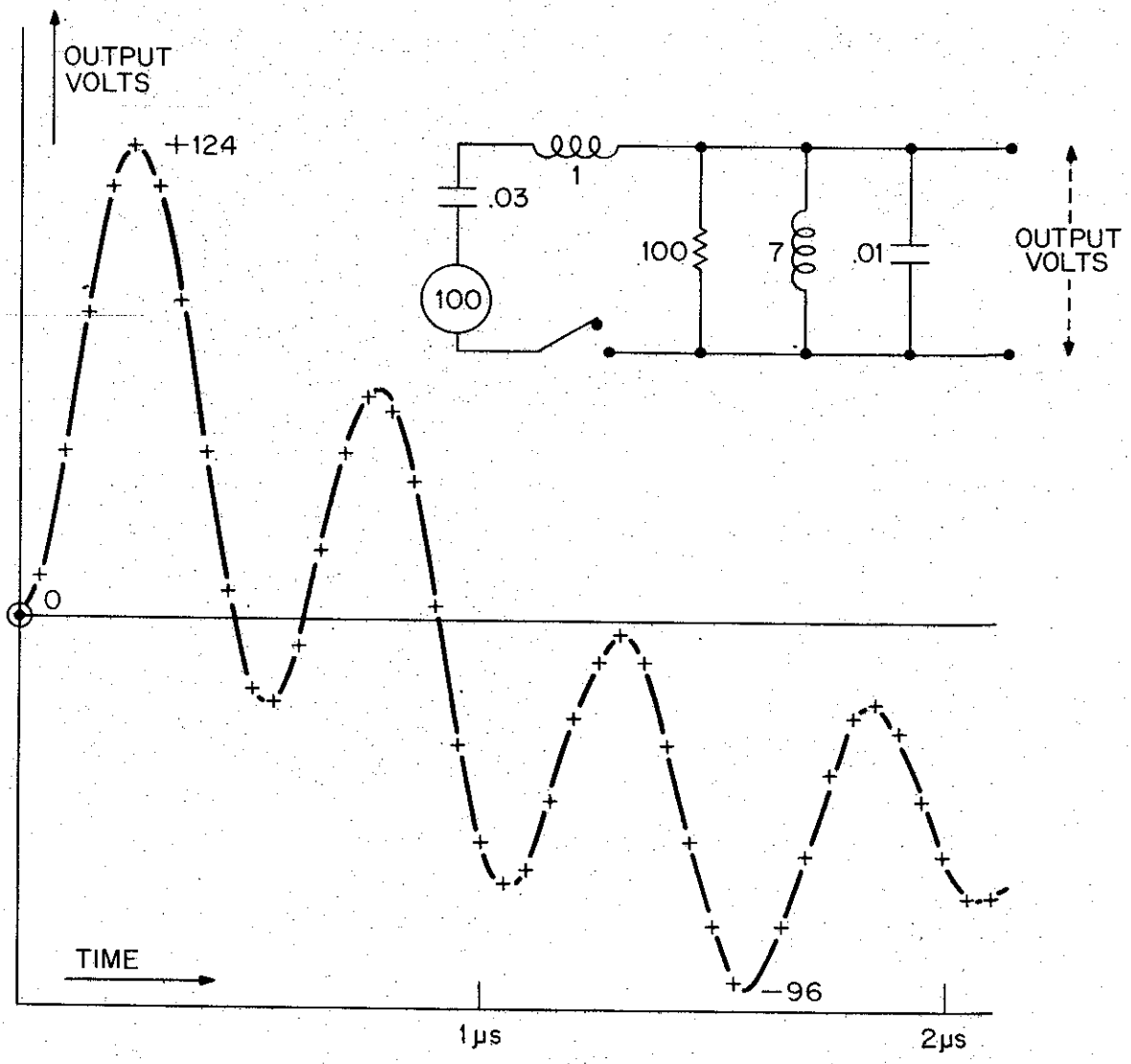

Figure 4-21. Calculated Voltage Response of Water Line - Normalized to 100 Volts Input.

1-4451

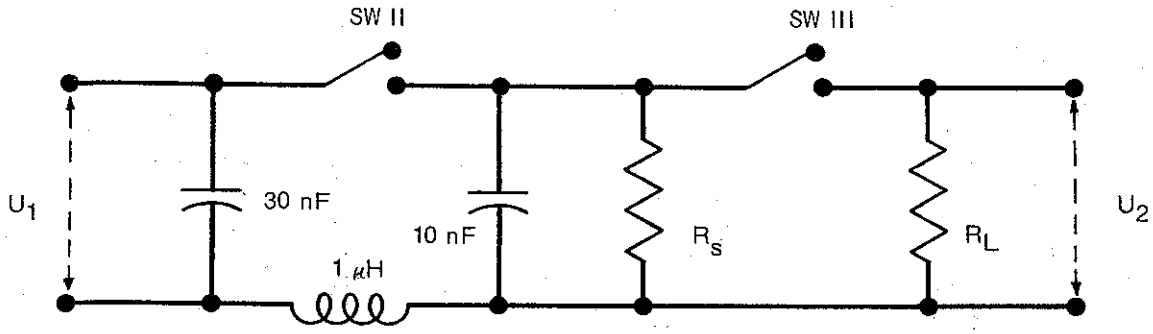

Figure 4-22a. Circuit Model .

U_1 and U_2 are generator and cathode voltages.

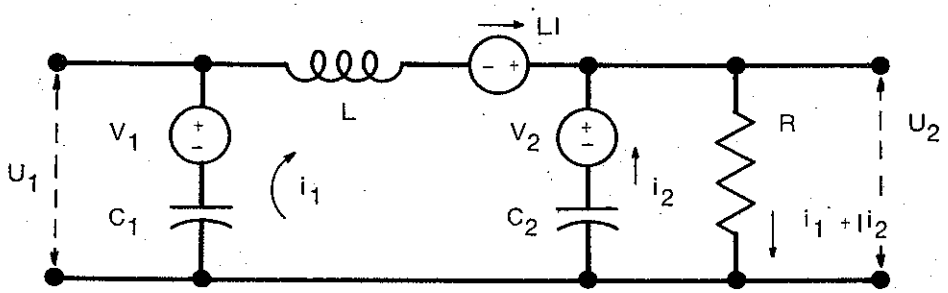

Figure 4-22b. Equivalent Circuit for Figure 4-22a.

$$U_1(s) = \frac{s^2V_1 + s(V_1/RC_2 - I/C_1) + V_1/LC_2 + V_2/LC_1 - I/RC_1C_2}{s^3 + s^2/RC_2 + s(1/C_1 + 1/C_2)/L + 1/LRC_1C_2}$$

$$U_2(s) = \frac{s^2V_2 + sI/C_2 + V_1/LC_2 + V_2/LC_1}{s^3 + s^2/RC_2 + s(1/C_1 + 1/C_2)/L + 1/LRC_1C_2}$$

$$i_1(s) = \frac{s^2 I + s(V_1 - V_2)/L + I/RC_2) + V_1/LRC_2}{s^3 + s^2/RC_2 + s(1/C_1 + 1/C_2)/L + 1/LRC_1C_2}$$

1-4421

Figure 4-23 shows the effect on the LC generator of a short circuit load (R_L = 0.01Ω). The initial voltage in the generator was normalized to 100 volts. The time T is the interval between closure of Switches II and III in μsecs.

It can be seen that the LC generator suffers severe reversal unless Switch III is triggered accurately. For comparison the water line and the LC generator voltages on matched load are shown in Figure 4-24. The figures should be 'blurred' by 60 nanoseconds to allow for transit time effects.

A short circuit between cathode and anode causes the water line to ring at a frequency of 6 MHz. This frequency is determined by the water line capacity and the total inductance of Switch III, the transition between the line and the cathode and the short circuit itself.

Consequently damping is necessary on the water line. It is convenient to place shunt resistors across the line. The lowest value resistors compatible with reasonable voltage efficiency are required.

Figure 4-25 shows one circuit chosen to model the damping. The LC generator is represented by 1 μH inductance and 0.03 μF capacitance and the water line by 0.01 μF capacitor with the damping resistor R in shunt.

Table 4-6 shows the peak water line voltage as a function of the damping resistance together with the secondary peaks on the generator and the water line. The initial LC generator voltage is normalized to 100 volts in all cases.

Table 4-6. Water Line and Generator Voltages

Damping Resistor, Ohms	Peak Water Line Voltage	Maximum Secondary Peak	
		Water Line	LC Generator
333	145	139	96
100	137	117	86
33	119	72	63
10	80	11	none

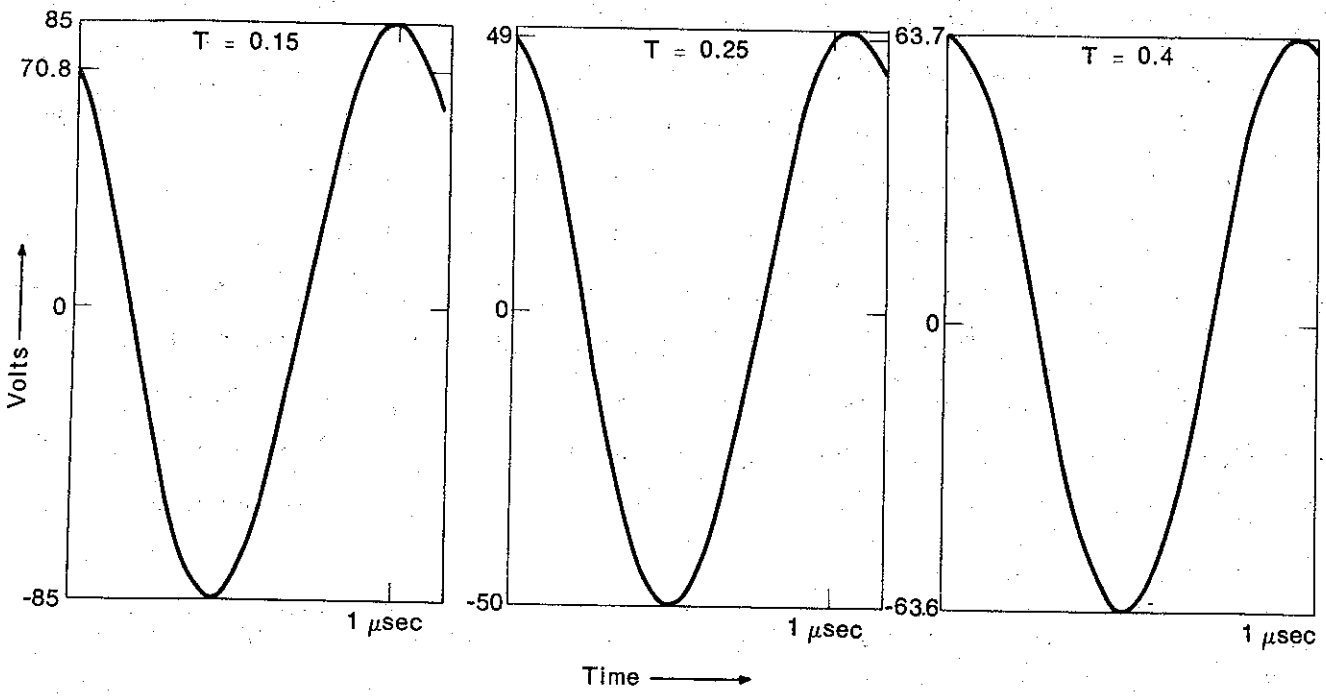

Figure 4-23. LC Generator Voltage Under Fault Conditions.

$R_L = 0.01\Omega$

T is interval between closures of
Switch II and Switch III

1-4425

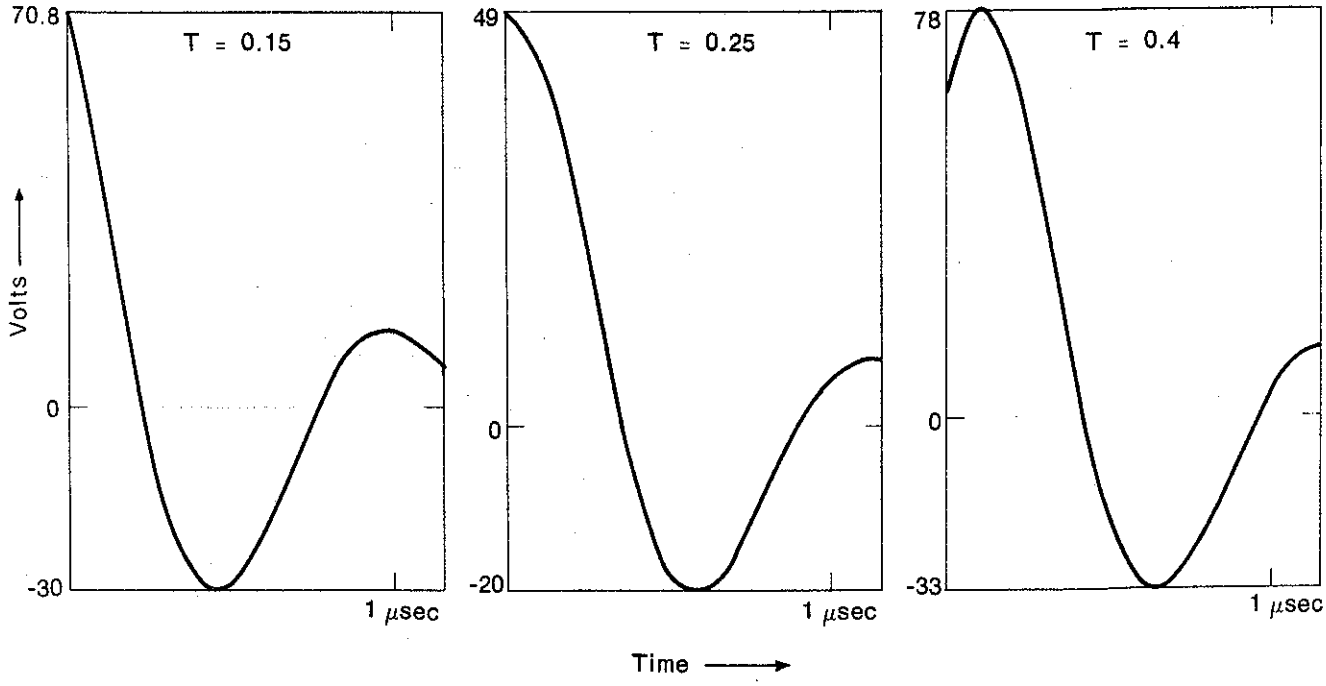

LC Generator Voltage

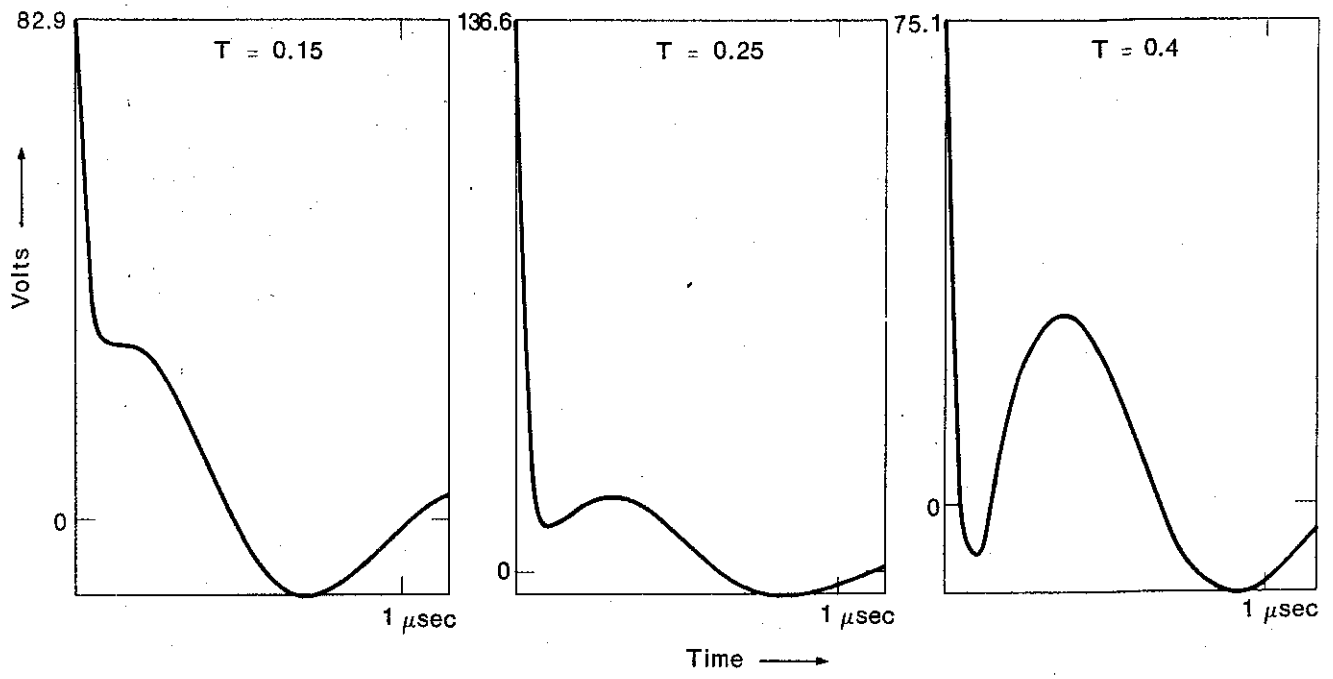

Waterline Voltage

Figure 4-24. Transient Voltages $R_L = 3\Omega$

1-5077

This Page Intentionally Left Blank

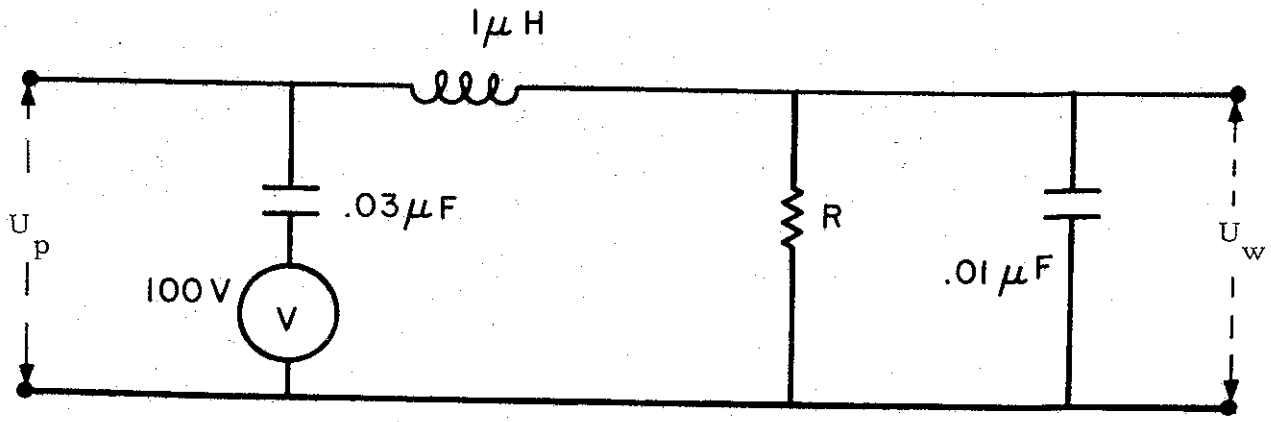

V is step function generator, normalized to 100 volts

$$U_w(S) = \frac{10^4}{S^3 + \frac{100\,S^2}{R} + \frac{400\,S}{3} + \frac{10^4}{3R}}$$

$$U_p(S) = \frac{100\,(S^2 + \frac{100\,S}{R} + 100)}{S^3 + \frac{100\,S^2}{R} + \frac{400\,S}{3} + \frac{10^4}{3R}}$$

Figure 4-25. Model of Water Line Damping

1-5054

The results are slightly modified by including the trigger isolating inductance as shown in Figure 4-20. The peak and maximum reverse voltage on the water line is given in Table 4-7 as a function of the damping resistance. As above, the LC generator voltage is normalized to 100 volts.

Table 4-7. Water Line Voltage Excursions as a Function of Damping Resistance

Damping Resistance Ohms	Peak Water Line Voltage	Maximum Reverse Voltage
100	124	96
80	122	92
60	118	79
40	112	62
30	106	51

Comparison of Tables 4-6 and 4-7 show that the trigger isolation is responsible for the loss of approximately 11% voltage. It can be seen that a damping resistor of the order of 50 to 100 ohms is suitable for the suppression of ringing while maintaining reasonable efficiency.

As discussed in section 4.7, voltage loss due to the trigger cable could be eliminated by triggering Switch III from the positive electrodes. This is illustrated in Figure 4-32.

SECTION 4.6
TRIGGER GENERATORS

4.6.1 Trigger Command System

The main command system is shown in Figure 4-3. The command trigger pulse generator is a commercially available unit viz.: Datapulser 101. This initiates the trigger generator for Switch I which is described in section 4.6.2. In addition LC generator monitor oscilloscope and a second pulse generator are triggered.

The second pulse generator initiates the trigger generator which fires Switch II and is described in section 4.6.3. In addition, the pulse generator triggers the water line monitor oscilloscope and also the low jitter trigger generator, described in section 4.6.4, which fires Switch III. The switching sequence is controlled by delay lines, as shown in Figure 4-3.

The amplitude variation of the LC generator is controlled by the combined jitters of Switch I and II and the jitters of their associated trigger generators. This is shown in Figure 4-9 . Similarly the amplitude variation of the water line voltage is due to the combined jitter of Switches II and III together with their associated trigger generators. This is illustrated in Figure 4-18.

The time jitter between an initial 5 V command signal and the output beam is comprised of the jitter in one Datapulser, the trigger generator of Switch III, Switch III itself and the jitter in the turnon time of the beam. This jitter was kept under ± 12 nsec total. Most of this jitter was in the trigger generator for Switch III and this jitter can be further reduced.

The output pulse is monitored most conveniently by an oscilloscope triggered by a third pulse generator with its internal delay set to about 3/4 μsec.

In order to use Neptune at maximum efficiency the time sequence for triggering the three switches must be carefully adjusted. The most convenient method is to adjust the internal delays of the pulse generators (Datapulsers). The jitter of these units is very small and the output pulse risetime remain small, under 5 nsec. However, the delay setting is easily disturbed and as with

any other electronic equipment, prone to drift. Thus, lumped delay lines have been substituted in places. However, they suffer from the disadvantage that the risetime of the output pulse is degraded by an amount proportional to the delay. This may degrade the jitter performance.

4.6.2 Trigger Generator for Switch I

The trigger generator which initiates the firing of the first gap in Switch I has been designed for low jitter in the output pulse, fast risetime and superior reliability. Approximately 3000 shots have been fired during the course of this program without encountering any difficulties.

The basic components include a fast thyristor pulse circuit, an unregulated 10 kV power supply and a two stage pulse amplification. An incoming trigger signal gates the thyristor circuit to produce a pulse which in turn fires the PFN spark gap. A circuit diagram is shown in Figure 4-26.

First, the thyristor circuit consists of 6 thyristors connected in series and charged to 600 V. A +5 V signal fires the gate of the first thyristor, and coupling circuits cause the other 5 thyristors to switch in rapid succession. When the last one switches, the chain dumps a capacitor into the primary of a toroidal pulse transformer. The transformer secondary voltage is applied to the trigger pin of a trigatron gap. Delay of this circuit is about 20 ns, and jitter is a fraction of a nanosecond. The output risetime is about 30 ns, and the amplitude about 6 kV. The thyristors were chosen over avalanche transistors because of their anticipated reliability in possibly harsh environments, i.e., their junctions are designed to carry heavy currents and do not utilize a breakdown mode. Development of this circuit was carried out under a separate contract.

The second basic component is the high voltage pulse-forming section. It consists of a two-stage Blumlein with trigger gap and charging connections, mounted in a closed can to reduce electrical noise and to make the unit safer to use. The active line consists of two 9 foot lengths of R G8 cable connected in parallel and coiled into a compact cylinder. A spark gap is attached at one end and the output pulse is taken from the ground braid at the other end

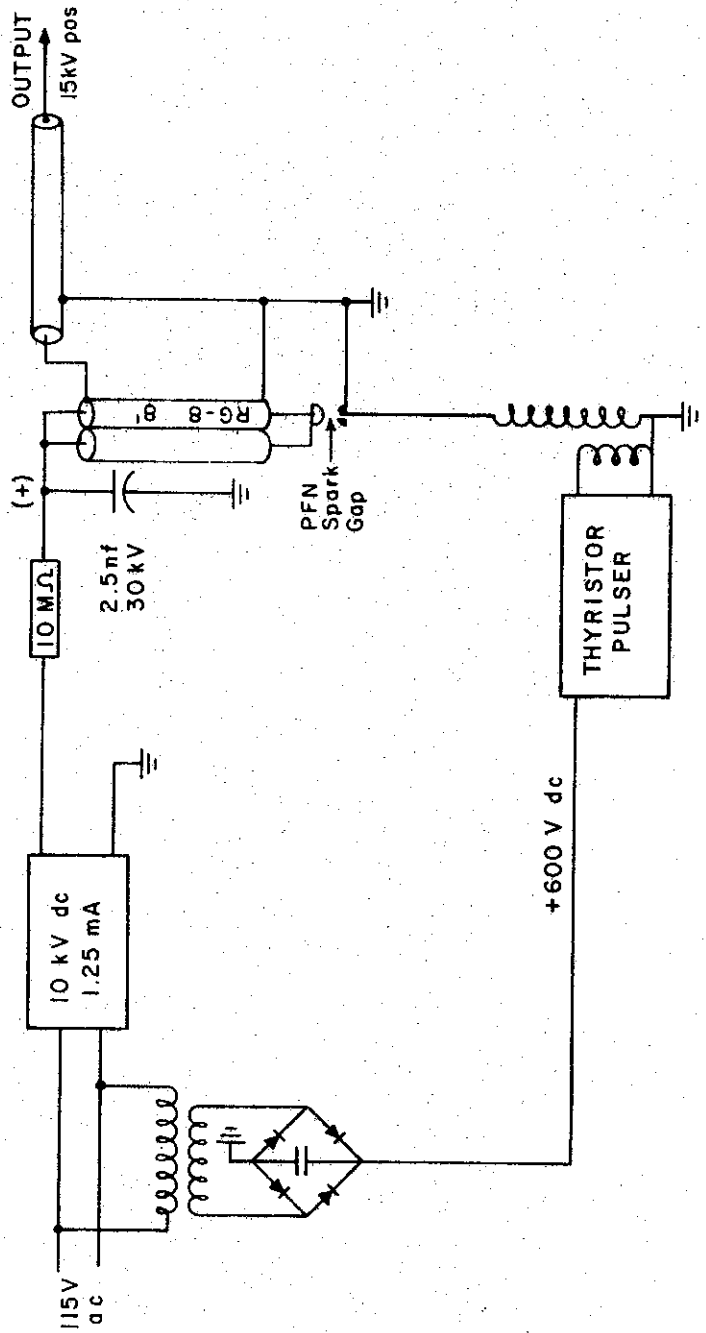

Figure 4-26. 20 kV Trigger Generator for Switch I.

1-4026

of the cylinder. A 2,500 pF capacitor mounted along the axis of the coil serves as the passive, or non-switched line of the PFN. Typical measured performance data are listed below.

INPUTS:	(1) External: +6 V into BNC on panel (2) Manual
OUTPUT:	15 kV (positive) into 100 ohm load 15 ns risetime ~ 30 ns pulse length (to 50% point) <1 ns jitter (single shot)
INPUT TO OUTPUT DELAY:	75 ns (including 12 ns in output cable)

4.6.3 Trigger Generator for Switch II

The first stages of the trigger generator for Switch II are similar in design and function to the trigger generator for Switch I. The first stage is a solid state Marx circuit which can be triggered by a signal of a few volts amplitude and 20 ns or more widths. The output of this Marx circuit is amplified by a pulse transformer and is used to fire a trigatron gap of a 20 kV pulse generator. This signal is then used to trigger the first stage of a three stage Marx generator. The output of this Marx generator is then used to initiate gap closure of Switch II. The capacity per stage of this open air Marx generator is 5 nF with a maximum charging voltage of 30 kV per stage.

A schematic diagram of the trigger generator is shown in Figure 4-27. The 10 - 90% risetime of the output pulse into a 50Ω load is better than 15 nsec. The delay and associated jitter between a 5 V input pulse and output pulse is shown in Figure 4-28 as a function of charging voltage. From this figure it can be seen that the jitter is less than ±15 nsec. total (Figure 4-28 shows maximum jitter, not r.m.s. jitter).

Eventhough this jitter is rather high it has very little effect on the amplitude variation of the LC generator output, as the erection time of the LC generator is over 3 μsec. From Figure 4-9 one can see that the resultant amplitude variation as a result of this jitter is less than 1/4% if the point of Switch II closure is adjusted to the point of maximum voltage on the LC generator.

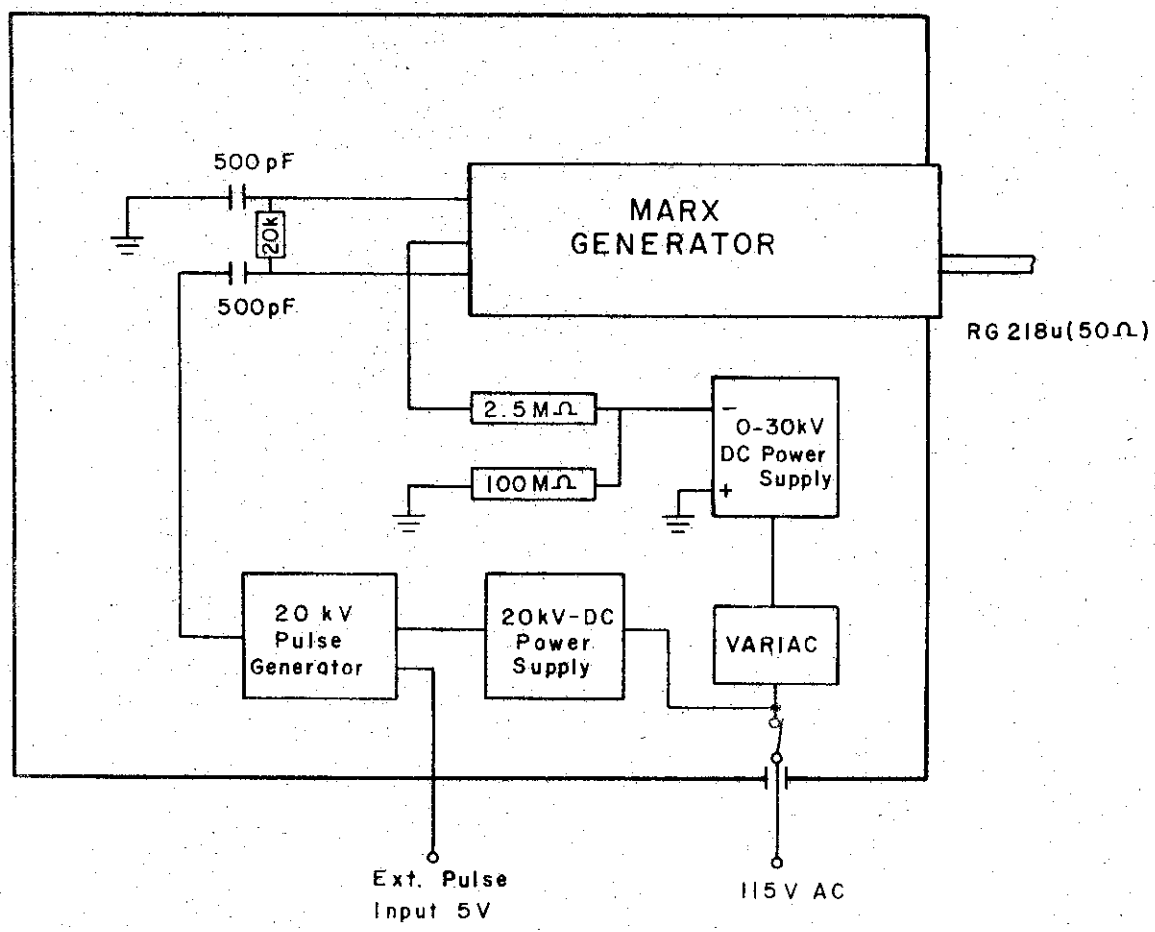

Figure 4-27. Block Diagram of Trigger Generator for Switch II

1-407la

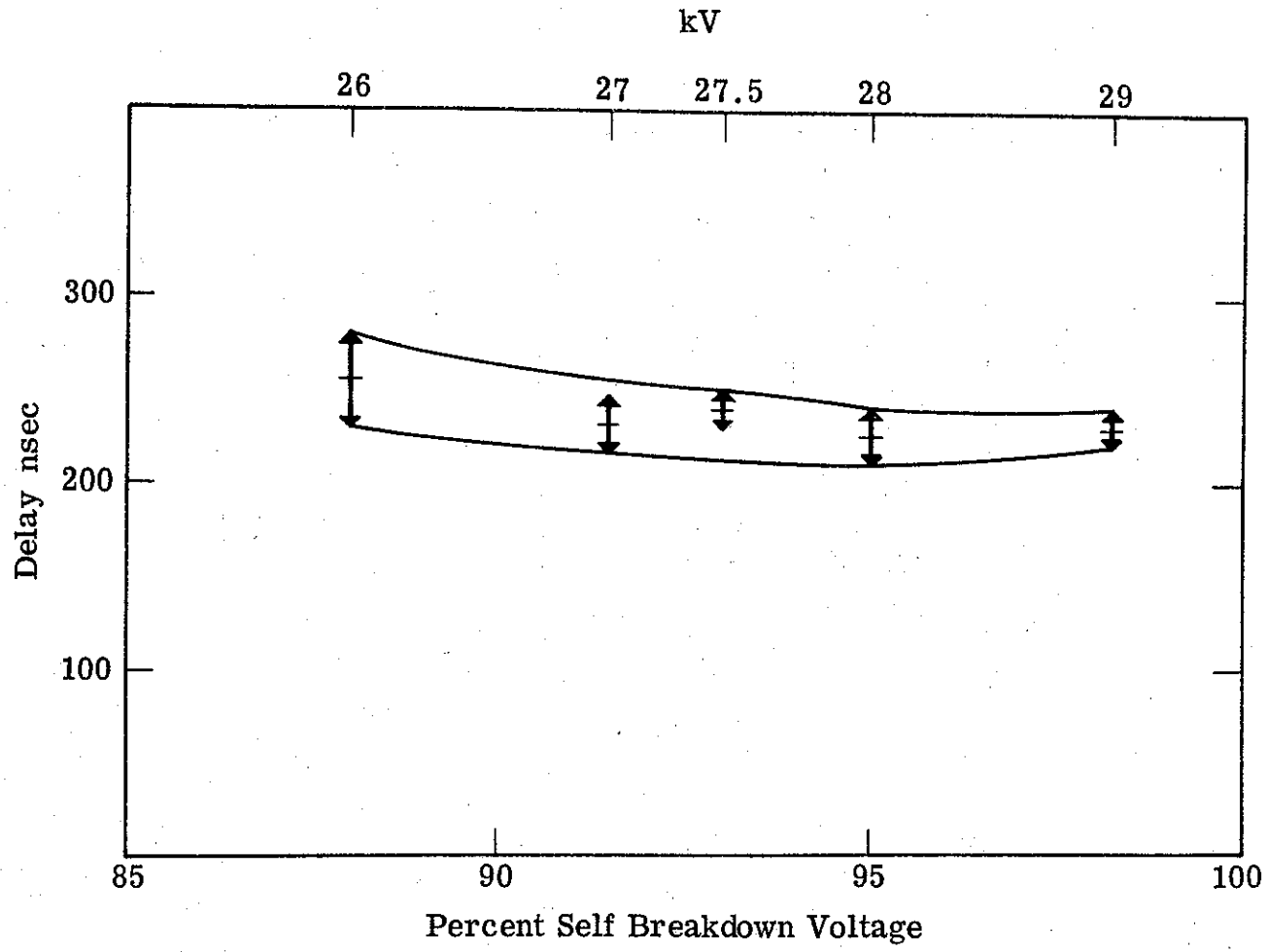

Figure 4-28. Delay and Jitter of Trigger Generator of Switch II.

4.6.4 Trigger Generator for Switch III

The trigger generator for Switch III is identical to the one for Switch II with the exception of the Marx generator, which is operated at an elevated pressure and has five stages with 7.5 nF capacity per stage. The maximum charging voltage per stage is again 30 kV. To minimize the jitter of this Marx generator, both the first and the second stage was triggered by means of a trigatron arrangement.

The performance of this trigger generator is shown in the next three figures. Figure 4-29 shows the effect of the output impedance on output voltage and risetime. This result is especially important in connection with the initiation of multiple discharge channels across a gap. Figure 4-29 shows a twofold increase in risetime and a twofold decrease in amplitude when going from one 50 Ω output cable to eight. Figure 4-30 shows the effect of the gap spacing between the output cable and the last stage of the Marx generator. From the test results shown, one can see the advantage in operating this gap close to self-breakdown voltage. Figure 4-31 shows the delay and jitter of the trigger generator. It can be seen that the delay and jitter is reduced in comparison with the trigger generator for Switch II. This reduction is a result of operating the Marx generator at elevated pressure and triggering the first two stages.

The jitter between a 5 V command signal and output pulse from the Marx generator operated at 90% of selfbreakdown was better than ±3 nsec rms or ±12 nsec max. for a 50 shot sample. The allowable window for a voltage variation of 5% of the output voltage from the Neptune B system is more than 40 nsec, as seen in Figure 4-9 . This window of 40 nsec must be compared with the total jitter in both Switch II and Switch III, which is ±27 nsec max. or ±6 nsec rms, indicating thus a maximum voltage variation of approximately 3%.

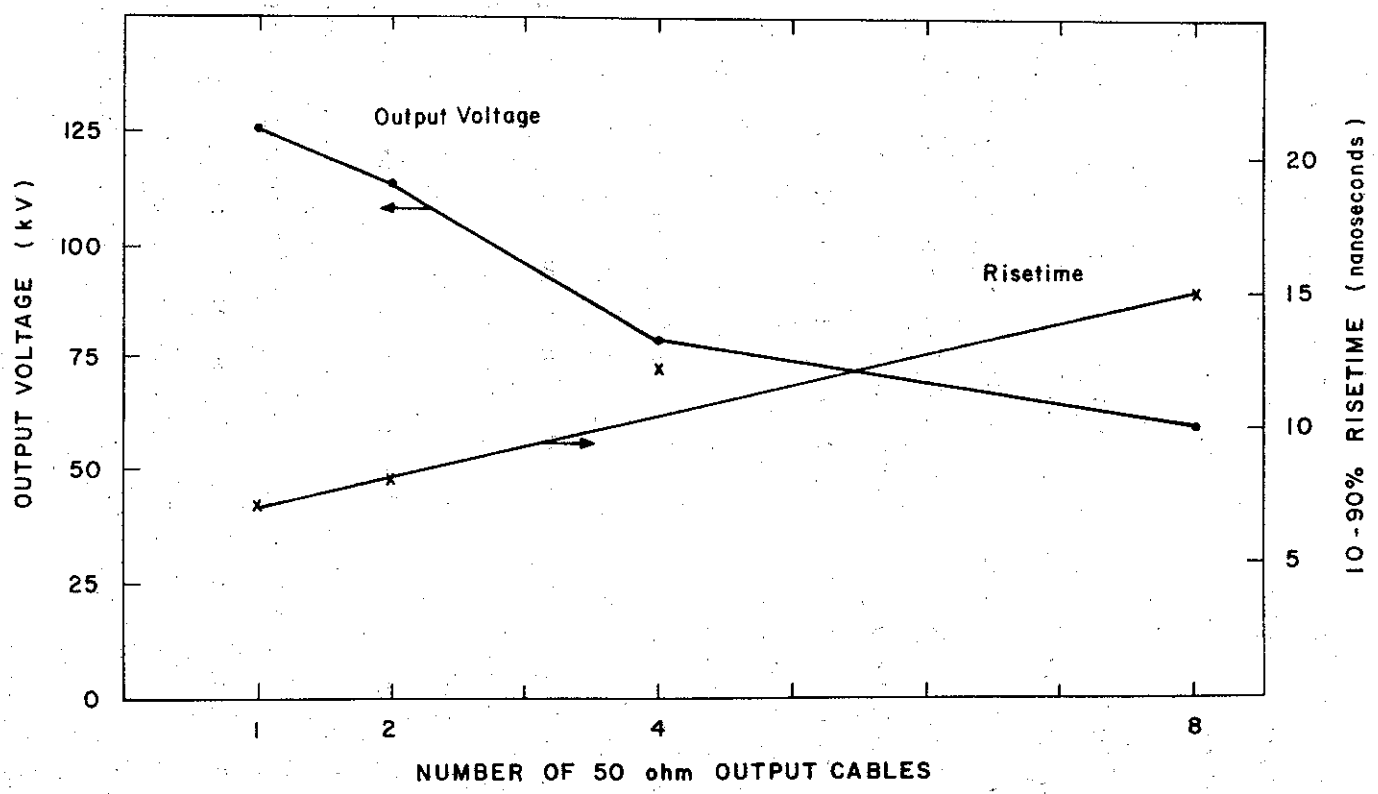

Figure 4-29. Influence of the Number of Output Cables on Risetime and Amplitude of Output Pulse From a 5 Stage Marx Generator (Capacity per Stage: 7.5 nF; Charging Voltage 30 kV; Self-Breakdown Voltage of all Gaps Including the Last One ~ 32 kV)

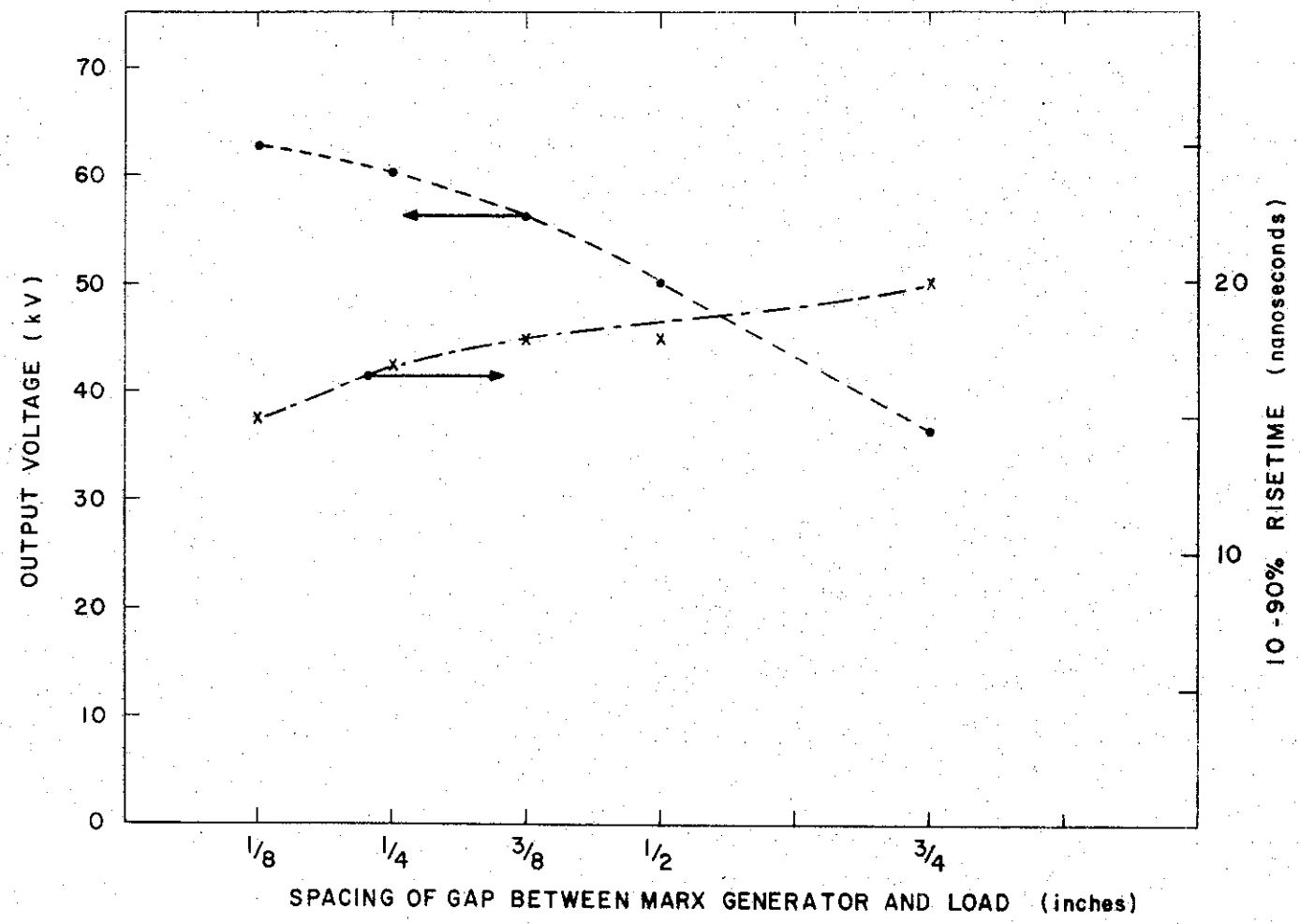

Figure 4-30. Influence of the Spacing of the Output Gap of the Marx Generator on Risetime and Amplitude of the Output Pulse of a 5 Stage Marx Generator (Capacity per Stage: 7.5 nF; Charging Voltage 30 kV; eight Output Cables at 50 Ohms each; Self-Breakdown Voltage of all Gaps Excluding the Output Gap ~ 32 kV)

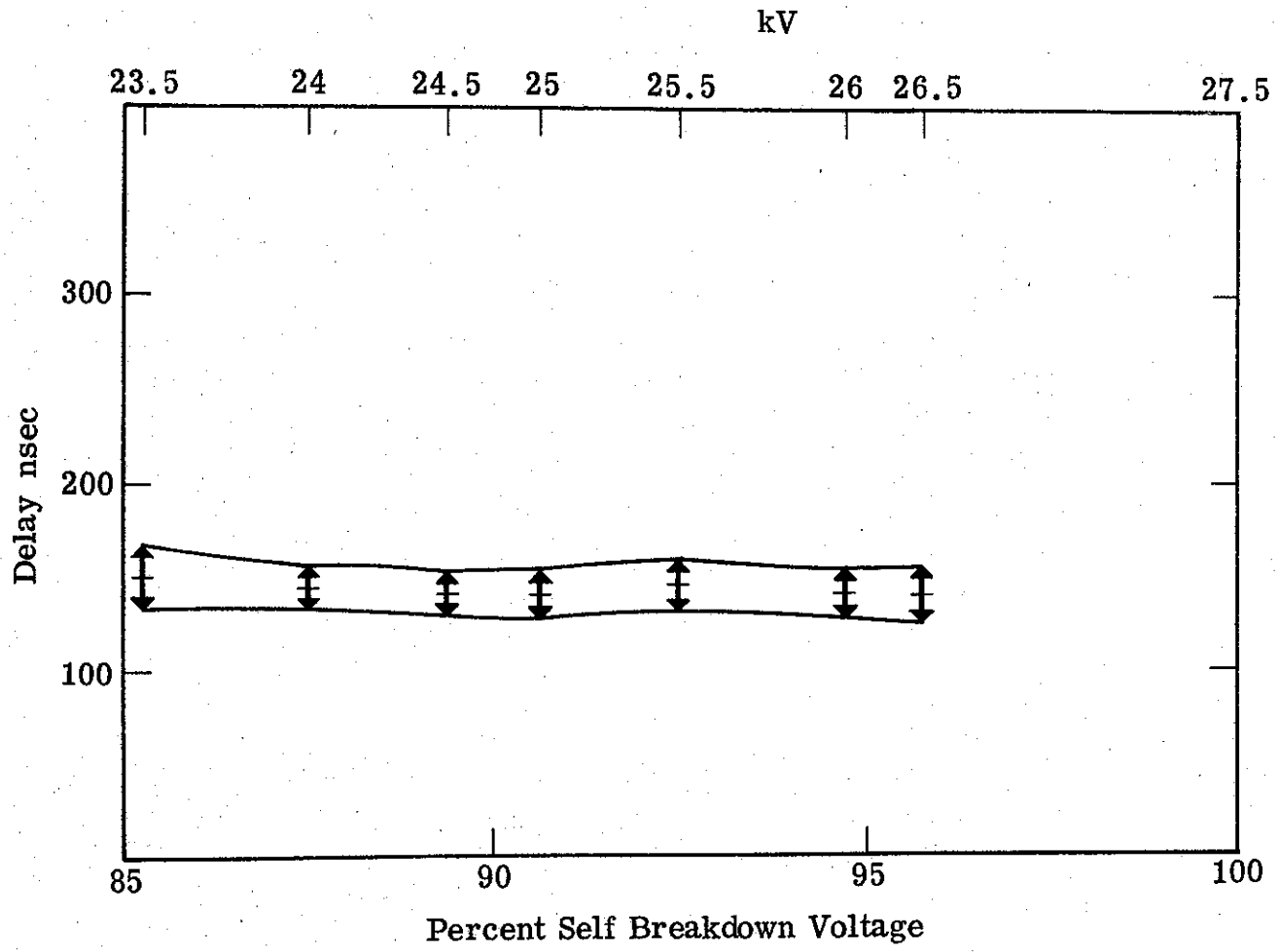

Figure 4.31 Delay and Jitter of Trigger Generator of Switch III.

SECTION 4.7
TRIGGER ISOLATION

4.7.1 Description

Both Switches II and III operate at high voltage from which it is necessary to isolate the trigger generators. Compactness and the problems of entry, dictate that this isolation be situated in the water line. The obvious location is inside the inner conductor of the coaxial water line, between the two switches. The other possible locations are inside the LC generator for Switch II and between the cathode and Switch III for Switch III trigger.

The alternative location for Switch II is less desirable as the stress time is much longer and the working range of the switch would be less. In the case of Switch III, there was physically insufficient room to accommodate the isolation component within the bounds set by the available outer conductor.

For both switches, fast rising, high amplitude pulses are required for minimum jitter. As these are best transmitted through coaxial cable without breaks, the obvious isolation mechanism is the use of coaxial cable wound into an inductive helix.

This is shown in Figure 4-2. Five cables, one of which goes to Switch II, are combined and wound into a helix which is placed inside the inner conductor of the water line. The helix is constrained by a lucite tube which also serves to insulate it from the inner conductor. The cables are connected to the four gaps in Switch III, triggering the required discharges on command. The isolation of the trigger generator from the switch is achieved by using the inductance of the helical assembly. The geometry of the helix was chosen to maximize the inductance. The maximum number of turns is limited by breakdown between turns. The diameter of the helix is not very important, as the increase in inductance caused by an increase in diameter is counterbalanced by the "shorted turn" effect from the water line inner conductor (effectively a shield). The calculated inductance as a function of diameter is given below.

Diameter, Inches	12	14	15	16	17	18	20
Shield Reduction Factor	.79	.76	.66	.60	.55	.49	.33
Inductance, μH	5.89	6.96	7.52	7.78	7.94	7.86	6.4

The water line voltage is dropped along this helix. This means that the end turn is very close to ground voltage and it needs to be isolated both from the endcap of the water line and from the cable which triggers Switch II. Figure 4-2 shows the Lucite insulation for this. Mechanically, the weight of the cables is taken on a Lucite former, which is supported by a flange at one end and by shims underneath the outer shield at the other. Each turn of the helix is strapped to the Lucite former to avoid movement.

The trigger isolation should preferably not load the water line appreciably. In practice this is not possible. As stated above, it is difficult to increase the inductance, in shunt with the water line, to more than about seven times the charging inductance. As discussed in section 4.5.7 and illustrated in Figures 4-17 and 4-21, the shunt inductance modifies the voltage waveform on the water line. From a simple sinusoid, oscillating between zero and full voltage, the waveform changes to a double sinusoid with nearly 80% reversal. However, the loss of voltage on the first peak, i.e., the point at which Switch III fires and dumps the energy, is only about 10%.

Another factor is the distributed capacitance between the helix and the water line inner conductor. Part of the rationale behind the fitting of a Lucite shield between the two is the reduction of this capacitance. A large capacity between the helix, particularly the earthy end and the water line, results in a greater load capacity to be charged by the LC generator. The result would be loss of efficiency. The Lucite shield reduces this capacity to about 5% of the water line capacity, which may be neglected.

It is readily apparent that it is difficult to contrive ample amounts of both inductive isolation and voltage insulation. The inner conductor is not quite big enough. If it were possible to lengthen the transition region between Switch III and the field emission diode, the arrangement shown in Figure 4-32

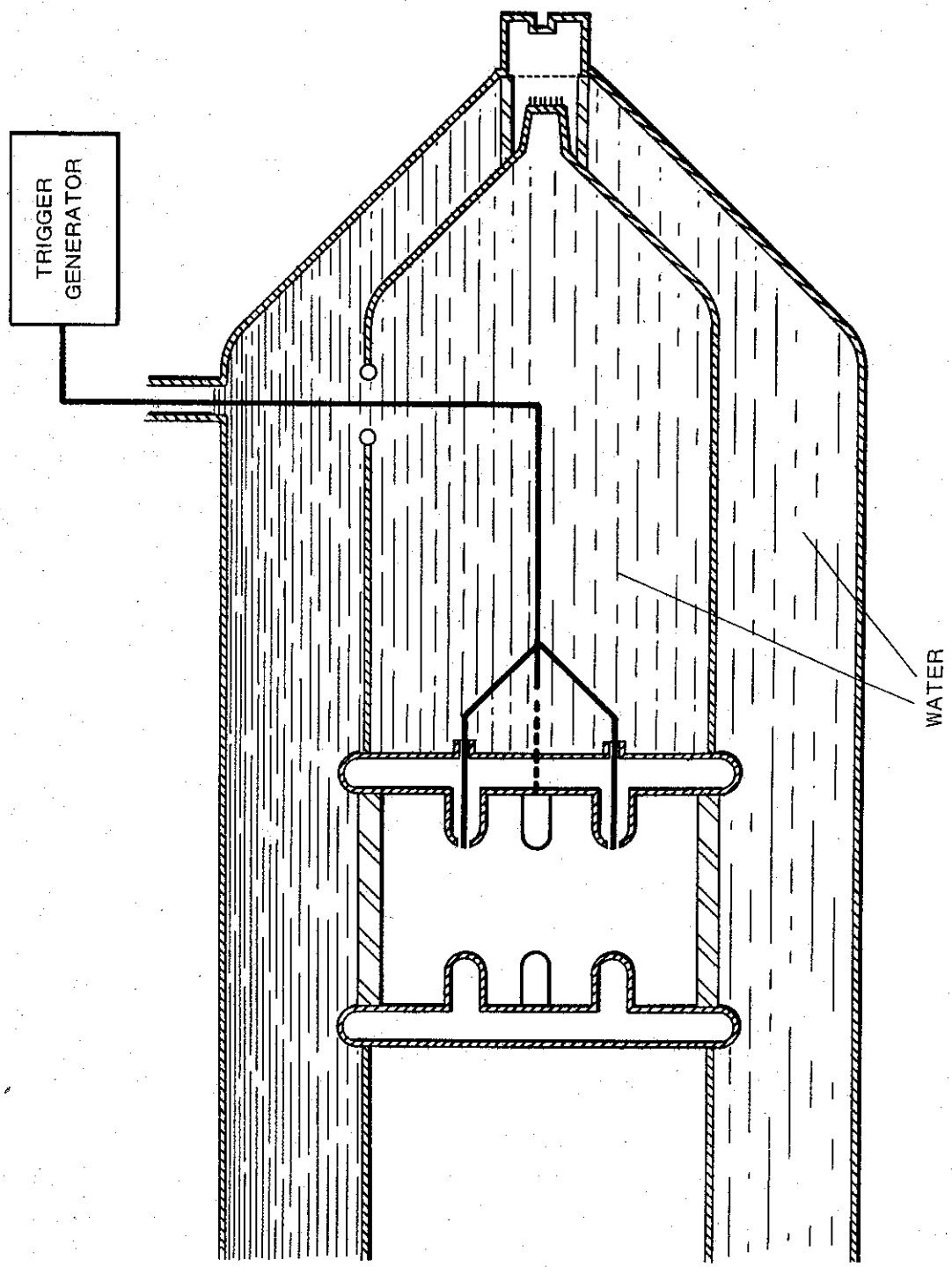

Figure 4-32. Alternative Scheme for Triggering Final Switch

1-5071

would be very attractive. In this case, the isolation is the double transit time of the signal along the trigger cables. The advantage is simplicity in construction in that no lucite shield between cable and cylinder is required. The voltage stresses will be small and short lived. The coaxial water line is not shunt loaded and the trigger cable entrance problem is eased by the reduced stress time. There are two disadvantages; the first is that Switch III would be triggered from the positive electrode, a mode of operation that has not been fully proven in practice. The second is that the transition region is made asymmetric by the trigger cable entrance. This could, as discussed in section 4.8, degrade the risetime slightly.

However, this alternative had to be rejected as both the cost and delivery time of a new outer conductor, to replace that available from Neptune A, were incompatible with the Neptune B program.

4.7.2 Breakdown Problems

The helix must not break down

(1) from turn to turn
(2) to the inner conductor of the water line
(3) at the entrance of the trigger cable assembly to the water line
(4) between Switch II cable and the end turn

The cases (2) and (4) are simple. Sheet, or tube, stock Lucite of the thickness necessary to hold the voltage is simply inserted as required; bearing in mind the necessity for providing only long tracking paths at discontinuities. Field enhancement, due to sharp corners, is almost completely absent as the field gradients are large only in regions of low dielectric constant, i.e., the Lucite insulation.

Turn to turn breakdown is more serious, as it is desirable to wind the helix with maximum inductance. This implies the least distance between turns. A conservative maximum field limit was chosen; 20% of water breakdown

field assuming that the field gradient along the helix is uniform, but including the enhancement factor of the round cables. This may seem unduly conservative, but the effects of distributed capacitative coupling between the helix and the inner conductor, cable braid roughness and also any self resonant effects in the helix, reduce the margin considerably. Allowance also has to be made for the lucite surfaces parallel to the helix, though experiment has shown that 10 - 20% field reduction is sufficient.

The entrance of the trigger cable into the water line is even more critical. The design is complicated by the fact that the breakdown field from a positive electrode (in this case, the trigger cable assembly) is less than the maximum field from a negative surface by a factor between 2 and 3. The relevant maximum field stresses (E_{max}) that may be applied to electrodes in water, have been found, experimentally, by J. C. Martin[2] to be:

$$E_{max} = \frac{0.275}{T^{1/3} A^{0.1}} \qquad \text{for (+) electrodes}$$

and

$$E_{max} = \frac{0.63}{T^{1/3} A^{0.07}} \left(1 + 0.12 \sqrt{\frac{E_{max}}{E_{mean}} - 1}\right) \text{ for (-) electrodes}$$

where T is pulse time in microseconds, and A is electrode area in square cm. The field between a cylinder and a torus cannot be analyzed exactly but a close approximation is to model it as two torii. Several configurations were programmed for a computer and the resulting fields are shown in Figures 4-33 and 4-34. The fields are normalized to maximum breakdown stress. It may be seen from these graphs that an optimum design is very different from the configurations with normal dielectrics. The greater propensity of the positive electrode to initiate breakdown, in this case the center cable, may be compensated by reducing the ring diameter.

[2]J. C. Martin, AWRE Report SSWA/JCM/6511/B.

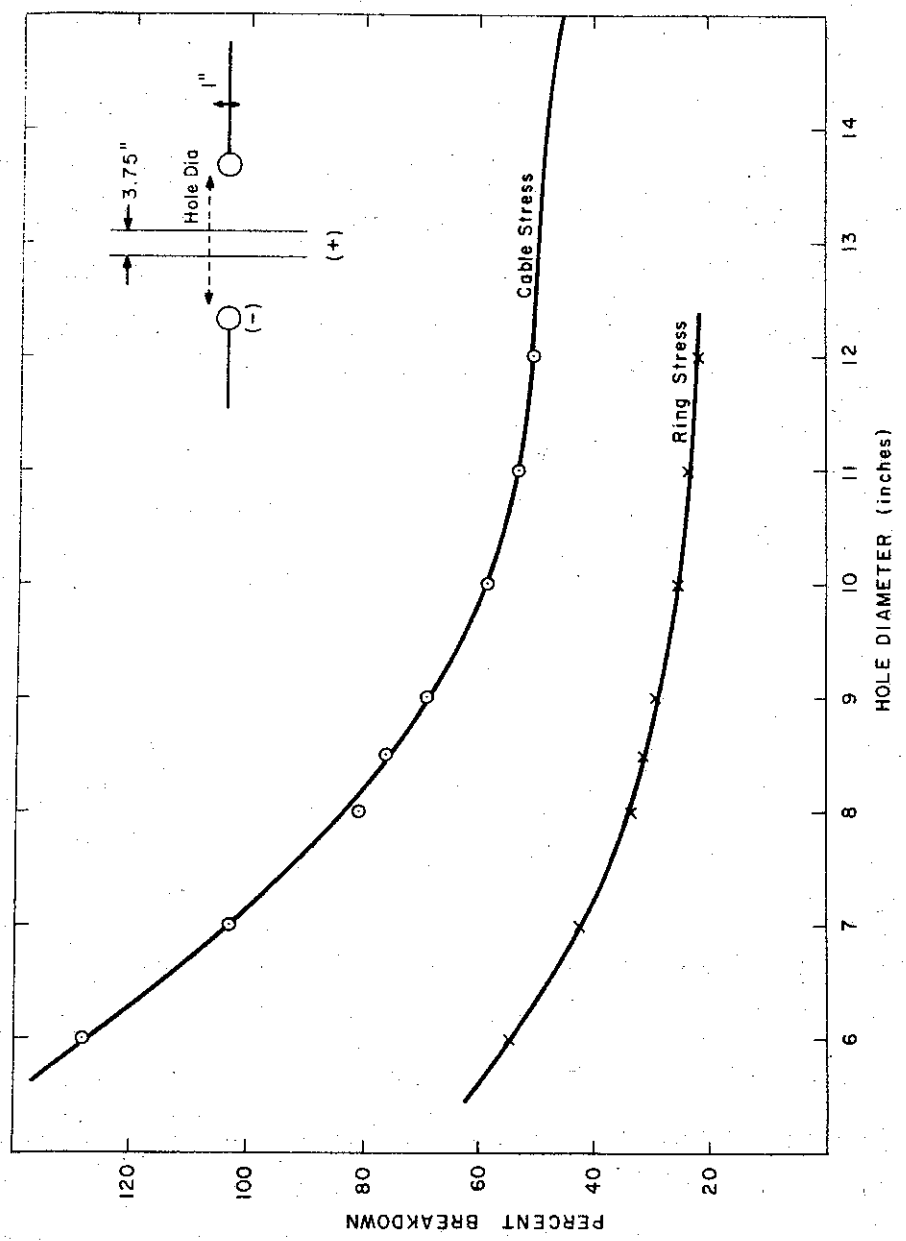

Figure 4-33. Electrical Stress on Feedthrough of Trigger Cable through Water Line

1-4028

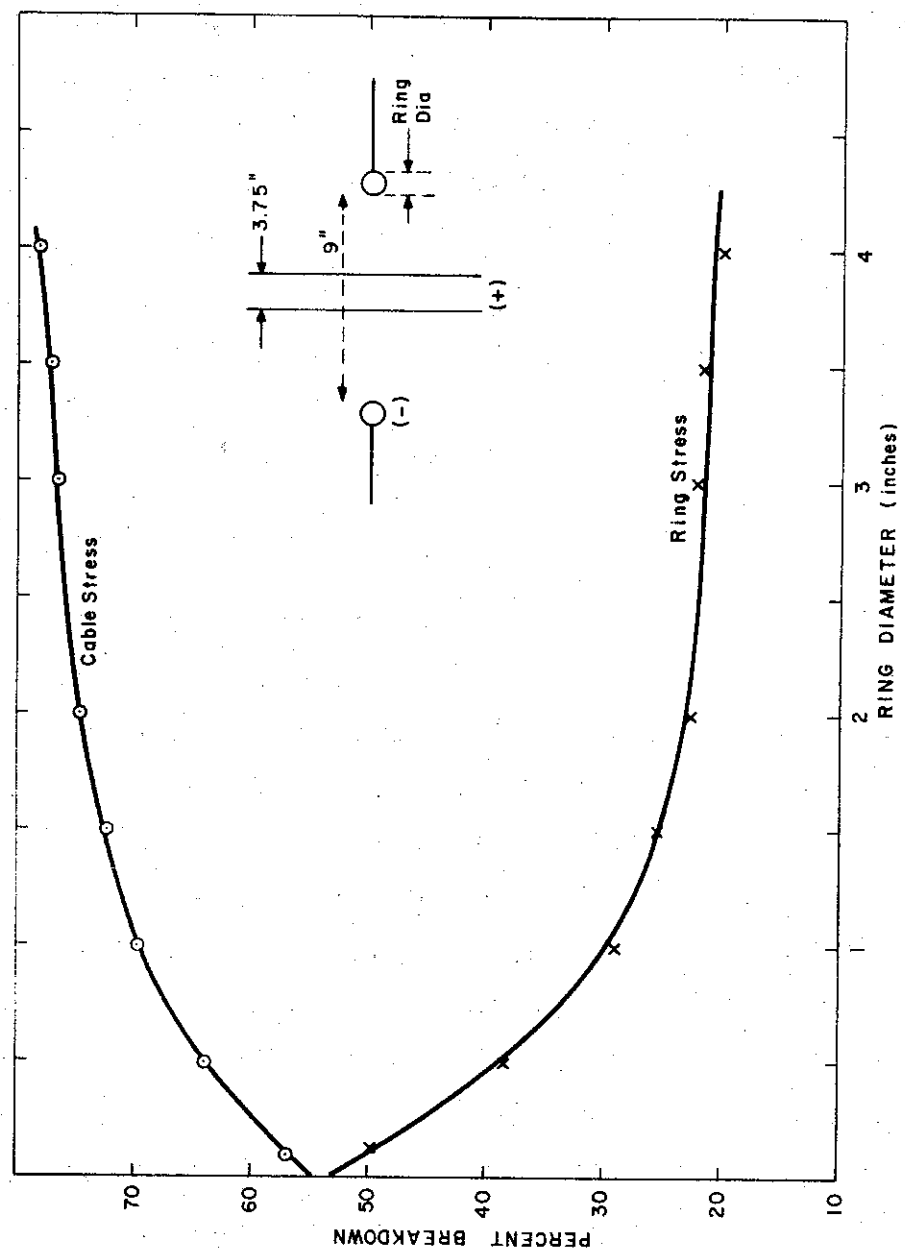

Figure 4-34. Electrical Stress on Feedthrough of Trigger Cable through Water Line

1-4029

SECTION 4.8
SWITCH III

4.8.1 Design Considerations

Switch III between the water line and the field emission tube is one of the most critical components of the whole system, since its performance will greatly influence the voltage risetime at the field emission tube. Ideally, this would require the switch to form a transmission line of impedance identical to that of the water line. As this is clearly impossible, the design has to be most carefully considered.

Any form of switch must constrain the current path(s) into a few narrow channels. Clearly then, the switch must appear as a high impedance transmission line, or could be viewed as a lumped inductance. The 10 - 90% risetime of the output current is $\frac{2.2L}{Z_o + Z_l}$ where L is the switch inductance and $(Z_o + Z_l)$ is the line and load impedance. The switch may also act as a mode converter, which could have the effect of inductance. Minimum inductance clearly requires minimum switch length. However, this is in direct conflict with voltage holdoff. To ensure adequate voltage handling, the switch was designed conservatively, with a view to shortning it later. In the event, however, the electrical stress handled by the switch was much greater than expected, viz. the gaps held off 400 kV/cm rather than the 250 kV/cm expected. There is then considerable potential for improvement by simple shortning of the switch.

If the switch is to be multichanneled then the channels must form simultaneously, or very nearly so. Otherwise, if one gap is closed in advance of the others, then the voltage across the other gaps is rapidly decreased and they are unable to fire. It can be shown that a low inductance switch must be multichanneled. Also, if such a switch is to be consistent, then either it must have enough channels for the shot-to-shot-variation in the number of channels to be unimportant or it must have each gap separately triggered so that every gap closes reliably.

A triggered switch has the advantage that it may be adjusted to fire at the instant of maximum water line voltage and hence discharge the maximum amount of energy into the field emission diode. This is in contrast to an overvolted switch which typically fires at 90% maximum water line voltage (or 80% energy). In addition, both the amplitude and the time jitter may be held to a minimum with the use of a triggered switch.

It is also desirable to make the switching medium separate from the coaxial line insulation. The coaxial dielectric has been chosen for maximum energy storage, a parameter irrelevant to the choice of switching medium. In addition, it could well be desirable to experiment with switching media without gross modifications to the line geometry.

High pressure gas was chosen as the switching medium. The most important reasons are that it is better understood than either solid or liquid and that it is the only medium in which reliable multichannel megavolt switching has been successfully demonstrated. The additional advantages are that the operating voltage may be adjusted by simply varying the gas composition or pressure and also that the low capacity between the switch electrodes ensures a low prepulse on the field emission diode. The gas used was a mixture of nitrogen and sulphur hexafluoride in a ratio of 97/3.

4.8.2 Mechanical Description

Figures 4-35 and 4-36 show the final form of Switch III and Figure 4-2 shows it in situ. The dielectric medium of Switch III is gas at a pressure of 200 psig since high pressure gas is better understood as a switching medium than are liquids or solids. The four sphere gaps are mounted in one envelope to keep gap conditions uniform. The gap distance is adjustable. To keep the inductance to a minimum, the gaps were placed on the largest possible diameter consistent with safe bushing thickness and safe electrode to bushing distance. This diameter is 11-inches, compared with the 24-inch diameter of the water line.

Trigger pins are fitted to the negative electrodes and each trigatron is connected to a separate supply cable for maximum independent trigger power.

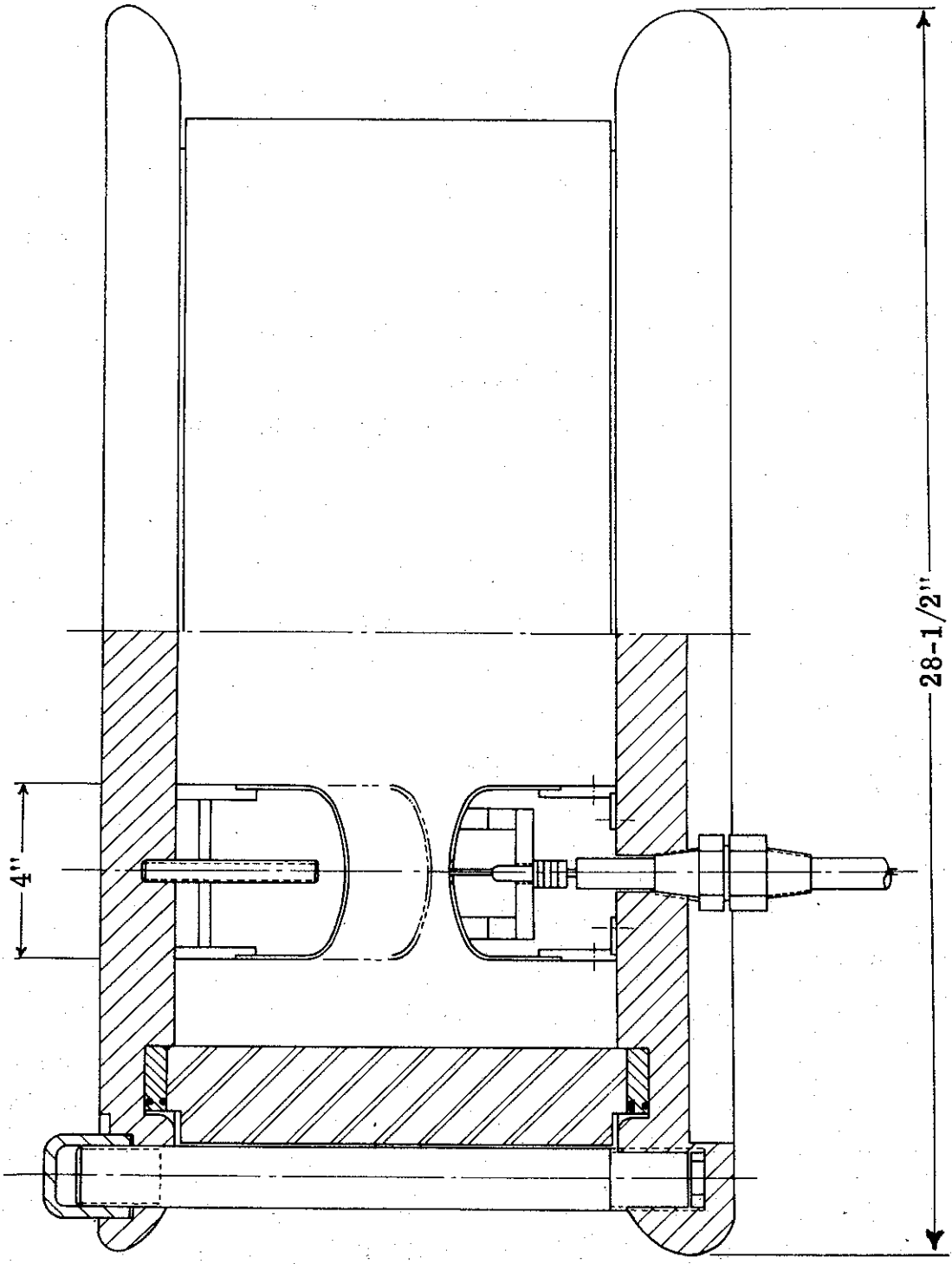

Figure 4-35. Switch III.

1-4027

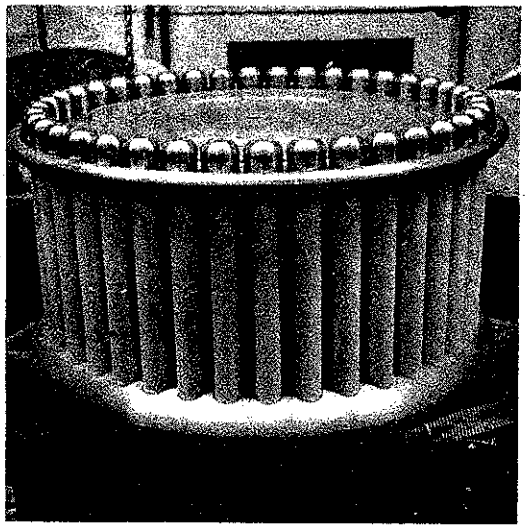

Figure 4-36. Switch III Assembled for Pressure Testing

2-1534

The design of these trigatron differs from that in Switch II as the trigger pin is negative to the electrode in Switch III. The trigger pin is left sharp and the 3/8-inch hole is the electrode rounded so as to increase field emission from the pin. The high gas pressure imposes a considerable strain on the bushing and the tie rods. As may be seen from the figure, two expansion joints are in series with the bushing to allow for creep in the Delrin tie rods.

The bushing is made of crossed-linked styrene (Dielco) which has been tested at IPC. Apart from tracking liability (or flashover), this material seems distinctly superior to Lucite. The flashover weakness can be alleviated by suitable surface treatment.

The pressure plates are made of aluminum to reduce weight and allendyned to reduce corrosion problems. As shown in the figure, the radius of curvature facing across the bushing is twice the radius of curvature facing the outer conductor of the water line. The larger radius of curvature minimizes the field along the bushing near the positive electrode of the switch. When the switch closes, both pressure plates are negative to the outer conductor and can tolerate a smaller radius of curvature as a negative electrode in water may support 2 to 3 times the stress that a positive electrode can support.

4.8.3 Multichannel Operation

It was stated above that multichannel operation was essential for low inductance. To reliably establish several channels, each gap must close before the voltage across it falls due to the other gap closures. If each gap is separately triggered, it is easy to ensure that the trigger pulses are simultaneous and approximately equal in amplitude. It is then necessary to keep the sum of the jitters of trigger gap closure and main gap streamer crossing time less than the gap voltage collapse time and the time taken for this to affect the neighboring gaps.

The trigger gap jitter may be kept small by the use of fast rising 100 kV pulses. By maintaining a sharp edge on the negative electrode, field emission can be enhanced, and a 10 nsec closure in the trigger gap with 1 nsec jitter can be accomplished. The streamer crossing time jitter is reduced by

increasing streamer velocity. This may be done by increasing gas pressure, which in turn leads to shorter gaps and crossing times. The jitter between the current and the trigger pulses was too small to be measured, but it was certainly under ±1 nanosecond. The voltage collapse time is affected by switch inductance. Thus a low inductance switch is more difficult to operate in a consistant multichannel mode.

Switch III operated reliably in a multichannel mode. Figure shows the output from Neptune when fitted with a 3.8Ω dummy load. This clearly shows the risetime degradation brought about by the successive disconnection of trigger cables from Switch III. There is only a small difference in risetime when 3 or 4 channels are initiated. This is probably due to the large inductance of the dummy load which masked the inductance improvement of Switch III. Judging from the erosion marks on the four electrodes of Switch III there is no indication that one of the channels is misbehaving.

It could also be noted that each set of 5 shots is successive and thus the consistency of triggering the gaps is excellent.

Figure 4-37 shows risetimes for various numbers of channels with a 1-inch gap, while Figure 4-38 shows risetimes for 1/2 and 1-inch gaps with 4 channels operational. It is interesting to note that multichannel operation is far more important for achieving low inductance switching than decreasing the gap length.

4.8.4 Inductance of Switch III

As stated above, the risetime of the output pulse is limited by the switch inductance. The inductance of Switch III is clearly lowest if the line current can be shared by many arc gaps working as close to the outer diameter of the coaxial line as possible, and with a short arc length. Figure 4-39 shows the inductance as a function of number of channels for two different mean diameters of channel location.

The next consideration is the media between the arc channels and the outer diameter of the coaxial line. For example, should the bushing be increased in OD, past the pressure plate and near to the outer diameter? The signal

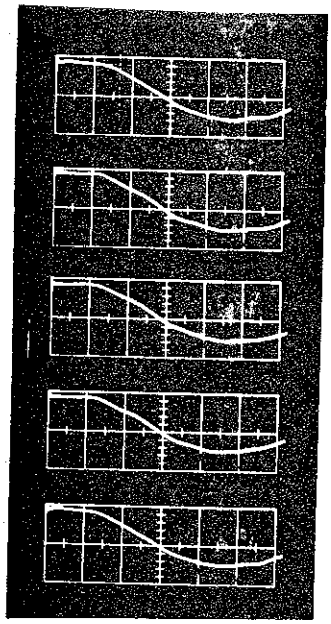

one (1) trigger cable
18.4 kV on Marx

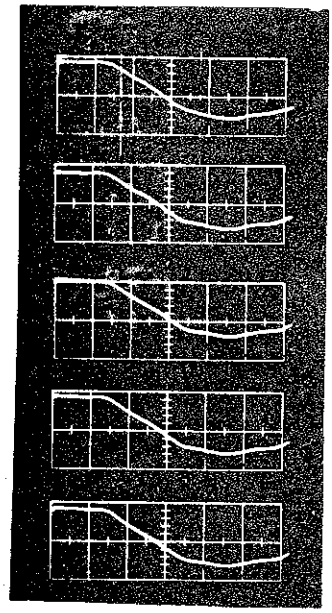

two (2) trigger cables
19.9 kV on Marx

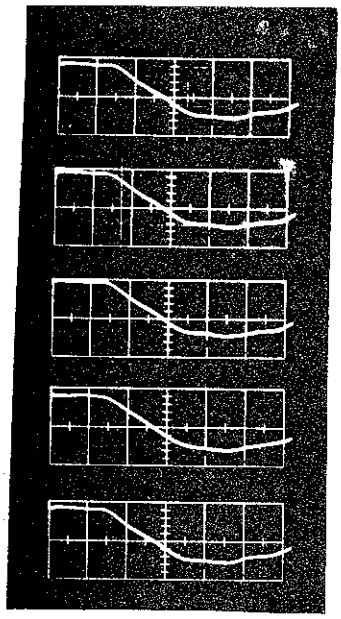

three (3) trigger cables
21.6 kV on Marx

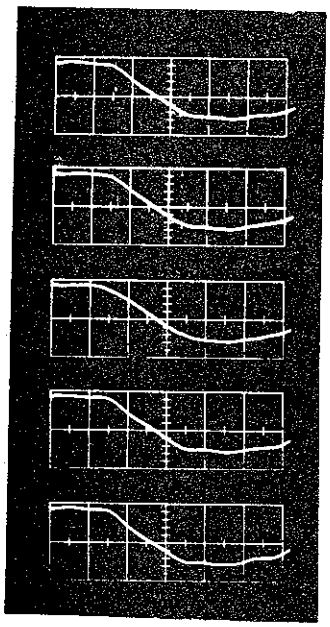

four (4) trigger cables
23 kV on Marx

Figure 4-37. Output pulse of Neptune B into $CuSO_4$ load for different number of discharge channels in Switch III.

Scale: 20 ns/div.
Peak current: 60 kA

2-1502

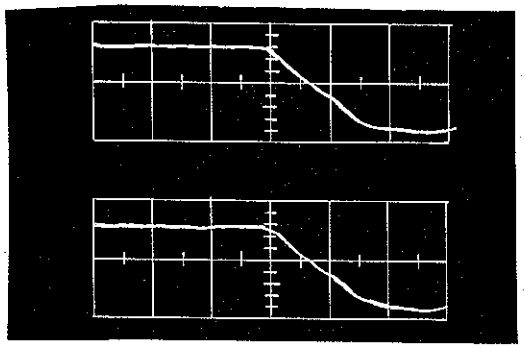

a. 1/2" Gap.

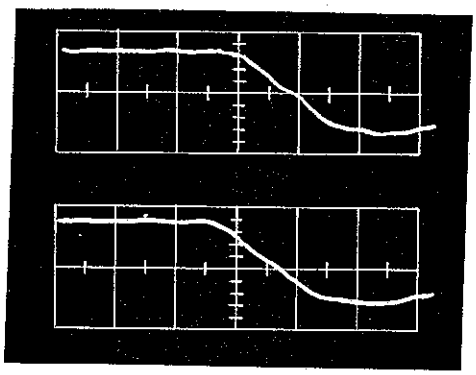

b. 1" Gap.

Figure 4-38. Load current as function of Switch III gap.
Peak amplitude ~ 60 kA
Trace 20 ns/cm

2-1535

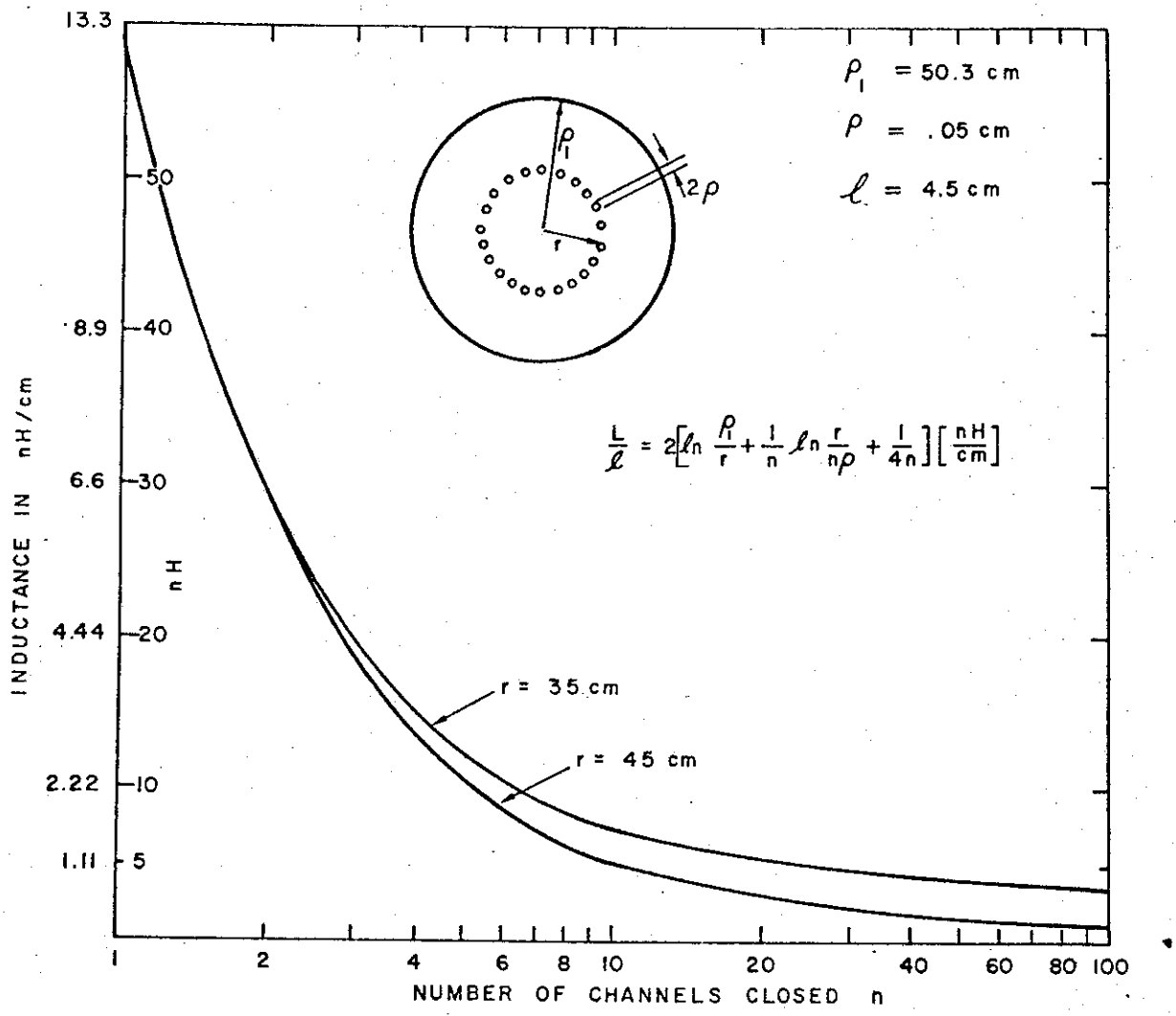

Figure 4-39. Inductance vs Number of Channels

1-5055

transit time of the switch is reduced but the transmission line is of higher impedance. So, the switch was modeled as a transmission line of high impedance and examined theoretically. The risetime was found to be completely fixed by the inductance of the switch, and the capacity of the line was irrelevant. The reason for this is simple. It was shown that the risetime degradation caused by a high impedance section of line is proportional to $Z\tau$, the line impedance multiplied by the time taken for the pulse front to traverse the high impedance section. This equals $\sqrt{L/C} \times \sqrt{LC} = L$, the line inductance.

It was necessary to place the spark gaps on a small BCD. The maximum diameter of the pressure plates was fixed by breakdown considerations. The tie rods had to be inside this diameter and the bushing had to be inside the rods. (Intercharging the two gives even worse results.) The wall thickness of the bushing was determined by the gas pressure and the electrodes again had to be spaced off the bushing so that the field along the bushing was reasonably uniform. The electrode diameters must be greater than the gap to maintain a reasonable gap/self breakdown voltage ratio. Small electrodes would require a longer gap, which increases the switch inductance considerably. Thus, the 4 arc channels were put on an 11-inch BCD, which compares with the water line inner and outer diameters of 24-inches and 40-inches.

The inductance of polycore cable is given by

$$\frac{L}{\ell} = 2\left[\ell n \frac{\rho_1}{r} + \frac{1}{n} \ell n \frac{r}{n\rho} + \frac{1}{4n}\right]\left[\frac{nH}{cm}\right]$$

where

- n is the number of channels
- ρ_1 is the outer radius
- ρ is the core radius
- r is the base circle radius
- ℓ is the channel length (see Figure 4-39)

This formula ignores skin effect, but comparison with a formula for eccentric coaxial line, shows that the inductance is over-estimated by a maximum of 15% for practical cases.

The inductance of the switch may then be calculated as two polycore cables (strictly three) in series. One section is formed by the arc channels and the other is formed by the shanks of the spherical electrodes. Figure 4-40 gives the inductance of a switch, 10-inches long, as a function of arc length (or electrode separation) and number of channels. The electrode diameter is assumed to be 4-inches, and arc diameter 0.01-inch. The outer conductor diameter is 40-inches, the intervening dielectric not being important, as explained above. The discontinuity inductance between sections has been ignored, as experiment shows it to be small. It can be seen that the inductance of the spark channels per unit length is less than 3 times that of the electrode shanks. It is clear that not only should the arc lengths be short, but that the entire switch be of minimum length. The dependence on assumed arc channel diameter is slight, see Table 4-8.

Table 4-8. The Gap Inductance of Switch III in Nanohenries Assuming 1-inch Gap and Various Arc Diameters.

Channel Number				Arc Diameter
1	2	3	4	
55.11	29.08	20.89	16.94	0.001"
43.42	23.23	16.99	14.02	0.01"
31.72	17.38	13.09	11.09	0.1"

4.8.5 Mode Conversion

Any switch between transmission lines involves a change of current path geometry. Maxwells equations must be satisfied at the discontinuity and this is achieved by the superimposition of the various modes of propagation. Those modes of propagation which are cutoff throughout the discontinuity region for the highest frequencies of interest may be regarded as merely adding to the

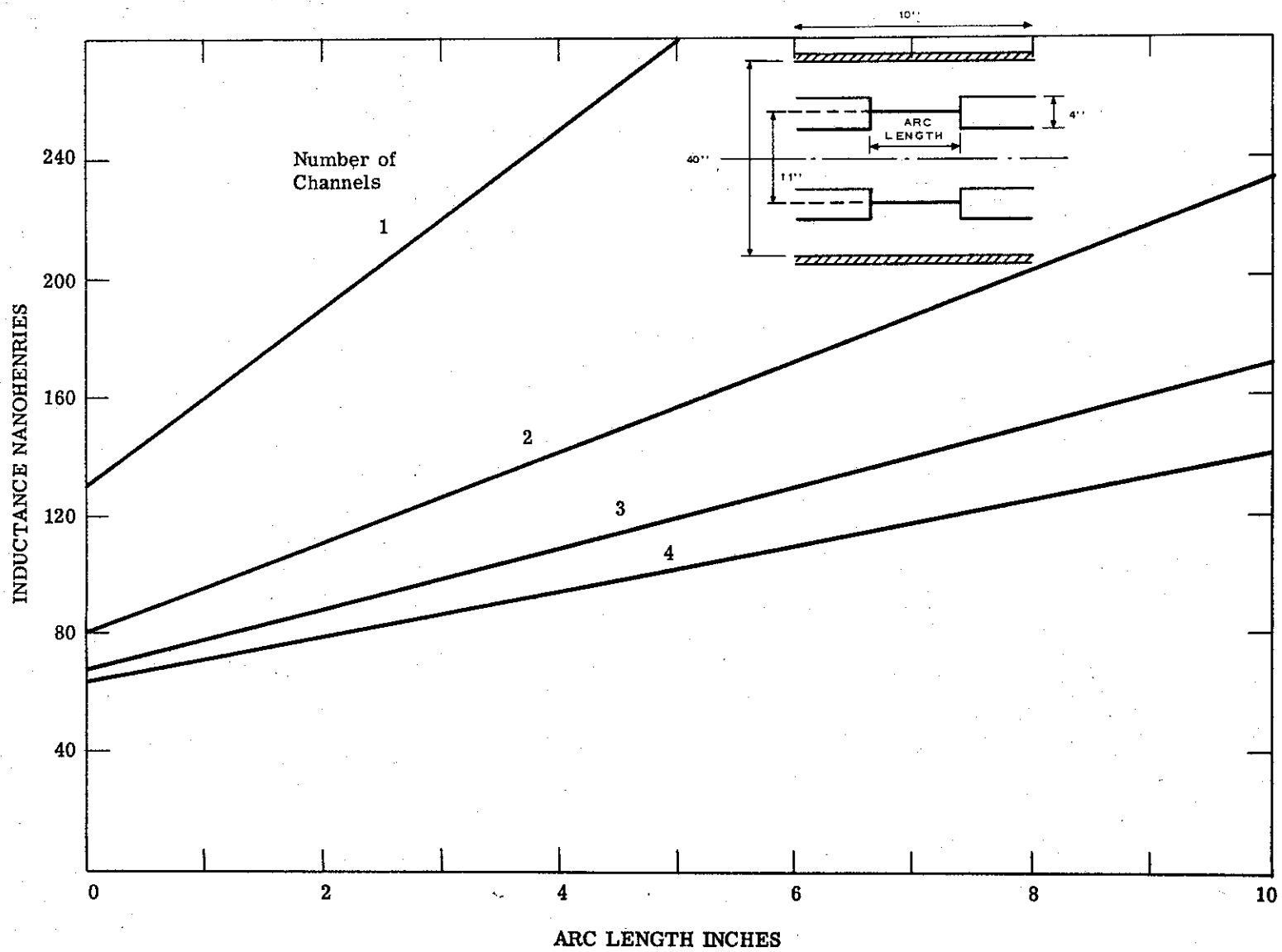

Figure 4-40. Inductance of Switch III as Electrode Separation Increased.

series inductance (or shunt capacity) of the equivalent circuit network. However, some modes may be excited which can propagate out of the discontinuity region in either direction. This is a loss of energy. For example, in Neptune B, Switch III will tend to excite E_{01}, E_{41} and H_{41} modes in addition to the TEM mode of interest. The E_{01} and H_{41} modes are most likely to be propagated back along the water line and also down the conical line towards the cathode. However, they are cutoff before reaching the cathode and must be reflected. This energy can only flow through a cathode or dummy load if it is reconverted into the TEM mode. These effects would be important in Neptune B with pulse risetimes of 10 ns and 15 ns for the E_{01} and H_{41} modes respectively.

Consequently, these effects were ignored in the design of Switch III, but clearly the achievement of faster risetimes requires their consideration.

4.8.6 High Voltage Operation

The voltage holdoff of the switch is shown in Figure 4-41 for a 1/2-inch gap, as a function of gas pressure. The voltage was that required to fire Switch III at peak water line voltage, so that the stress times on the switch were identical. Note the linear increase with pressure. This is in strong contradiction to d.c. operation where the holdoff strength increases very slowly above about 150 psig.

The triggering range of Switch III has not been checked, but it is satisfactory. At a gap setting of 3/4-inches and filled with 175 psig of nitrogen/sulphur hexafluoride mixture, the switch operated from 560 kV to 770 kV. The lower end, for just triggering was not checked, but the upper end was very close to self breakdown. The range of Switch III is, in practice, most easily extended by changing the gas pressure.

The effect on the switch inductance of utlizing various numbers of channels has been discussed already and is shown in Figure 4-40. The effect of changing the gap of Switch III is shown in Figure 4-38 (keeping total switch length constant). It can be seen that the length of the arc channels is not the factor limiting current risetime.

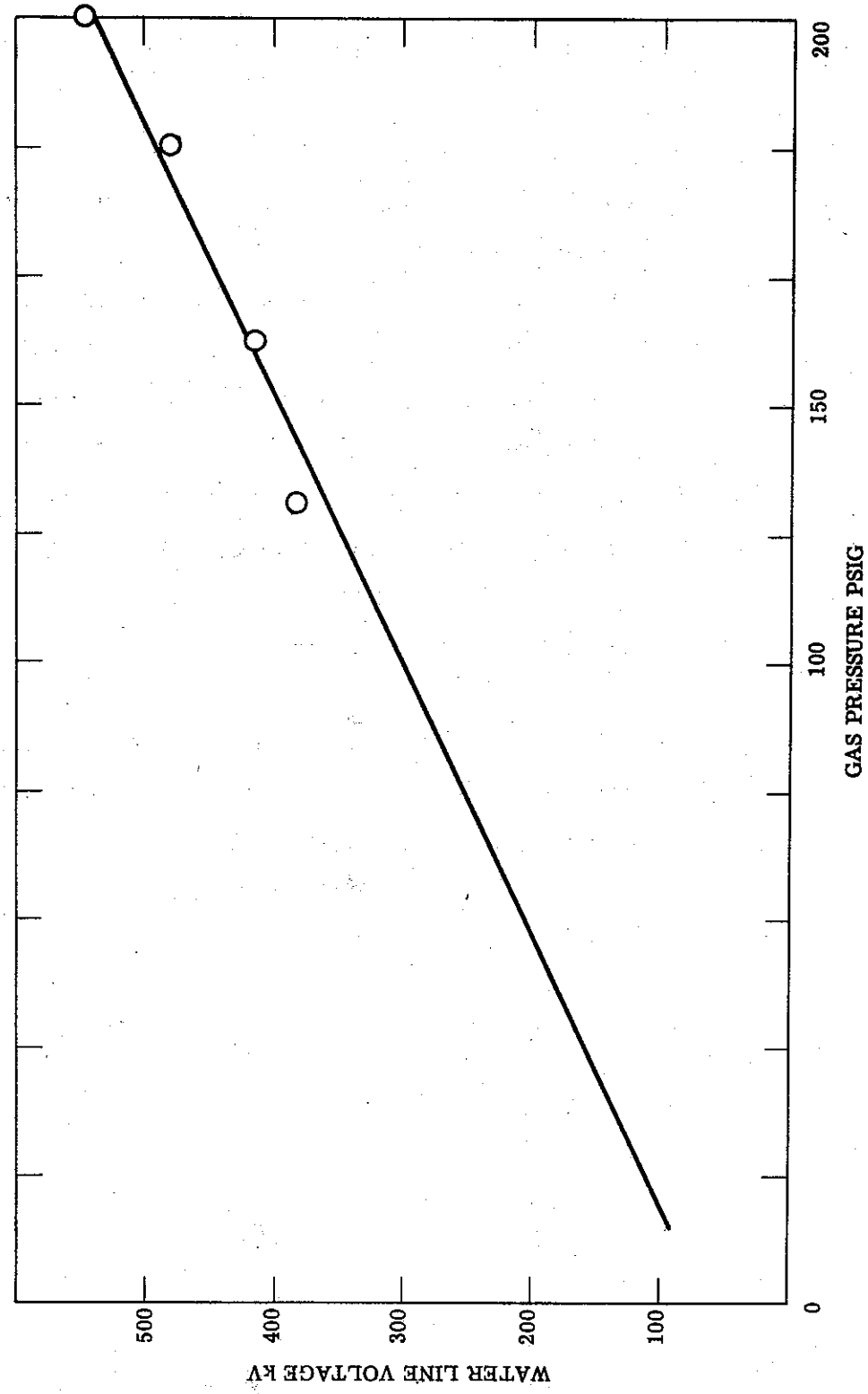

Figure 4-41. Self Breakdown Voltage of Switch III
Electrode Gap 1/2"

1-5073

The jitter between the output current and the trigger pulse was measured by mixing a delayed sample of the trigger pulse with the output current monitor. This jitter was less than ±1 nanosecond maximum range. The switch was at its usual operating point of 1-inch gap, 150 psig pressure. Gap closure time was approximately 20 nanoseconds.

The results show that it is desirable to shorten the switch. The switch is 10-inches long and reference to Figure 4-40 shows that if the switch were shortened to 6-inches, the inductance of the switch would be reduced 30%. The flashover strength of the bushing should allow this. The switch would be improved mechanically as less allowance would be required for creep in the plastics. The bushing length would still be six times the gap setting and the electrodes would still have an appreciable length of cylindrical shank. This operation is comparitively simple, but could not be carried out due to shortage of time.

The risetimes obtained from the machine operating into a matched load agree with those calculated from Figure 4-40. The inductance was also checked by running Neptune into a short circuit and measuring the oscillation frequency.

SECTION 4.9
NEPTUNE B MODELLING STUDIES

4.9.1 Introduction

As soon as the general physical and electrical design of Neptune B had been decided, it became evident that modelling studies would be desirable to assess the effect of the front end region (Switch III, conical taper, tube/diode) on the system risetime. Since only this part of the design was to be investigated, the model could be considerably simplified. A model scale of one-half was chosen since the physical size then turned out to be easy to work with. A fast rise square pulse generator was used to drive the model.

4.9.2 Description of the Model

The model, shown schematically in Figure 4-41 and in the photographs of Figures 4-42, 4-43, and 4-44, is an approximate half-scale model of the Neptune B front end with a simulated switch gap, shortened main energy store and a conically tapered input section connected to a fast Tektronix 109 pulser. It is placed vertically within a plywood box filled with water.

The input section is a straight conical taper of 16-inch length. It is fed by a specially designed connector and transition section inserted through the bottom of the water box. The main energy store is a 16-inch long coaxial structure of wave impedance 3.5Ω when filled with water. The simulated switch gap consists of eight evenly spaced 4.5 mil copper wires inserted through lucite spacers of various thicknesses. The front end is a 10-inch long conical taper with the inner cone consisting of two parts to permit the insertion of a water-proof structure consisting of a circular aluminum plate with a 3-inch long lucite ring of 6-inches diameter bonded to it. The second half of the inner output cone (see Figure 4-43) is terminated resistively by means of four 12 ohm carbon compound resistors in parallel with a resistive voltage divider output probe consisting of a 150Ω resistor feeding into a 50 ohm coaxial cable. The combined resistance of the termination is 2.9 ohms. Two identical capacitive probes

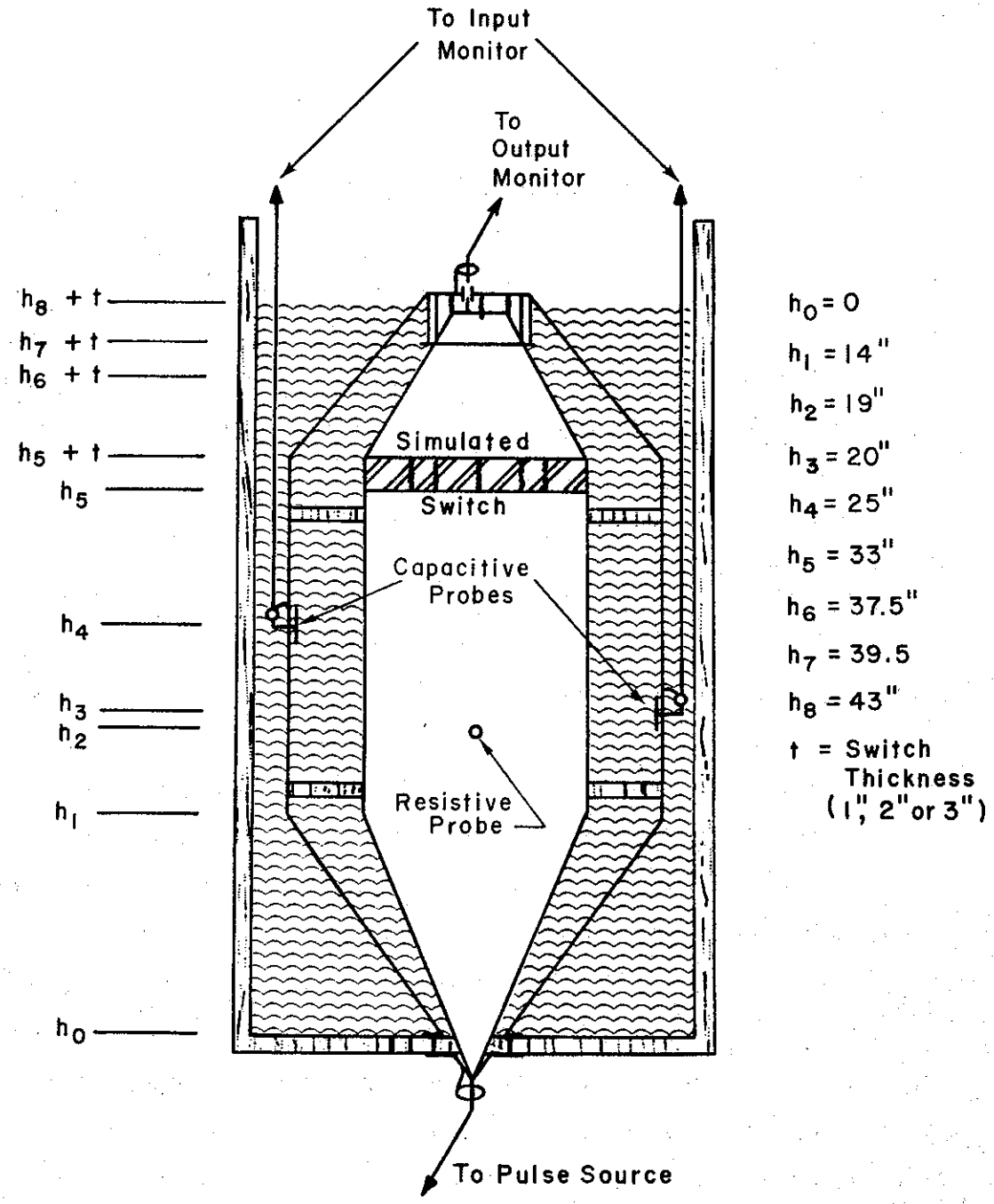

Figure 4-41a. Schematic Representation of the Neptune B Model

1-4075

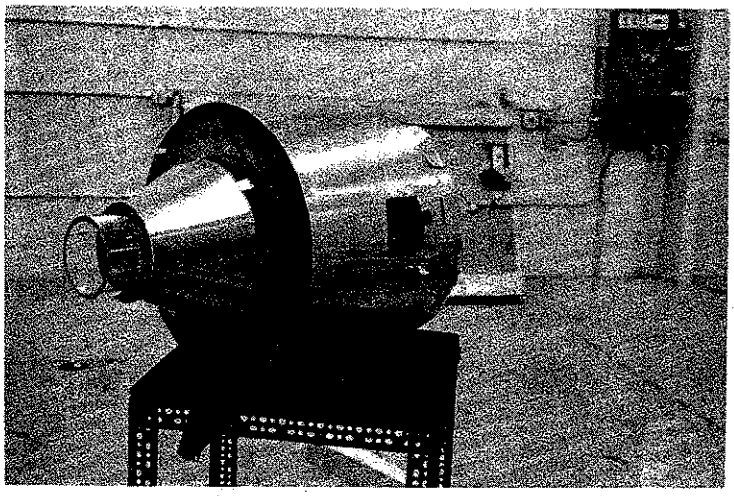

Figure 4-42. Oblique Front View of the Neptune Model with Outer Output Cone and Second Half of Inner Output Cone Removed

2-1343

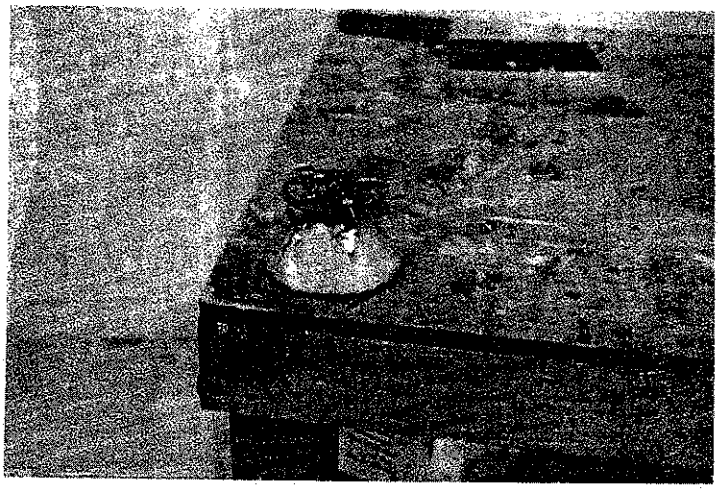

Figure 4-43. Second Half of the Inner Output Cone with Resistive Termination and GR Connector for the Output Pulse

2-1344

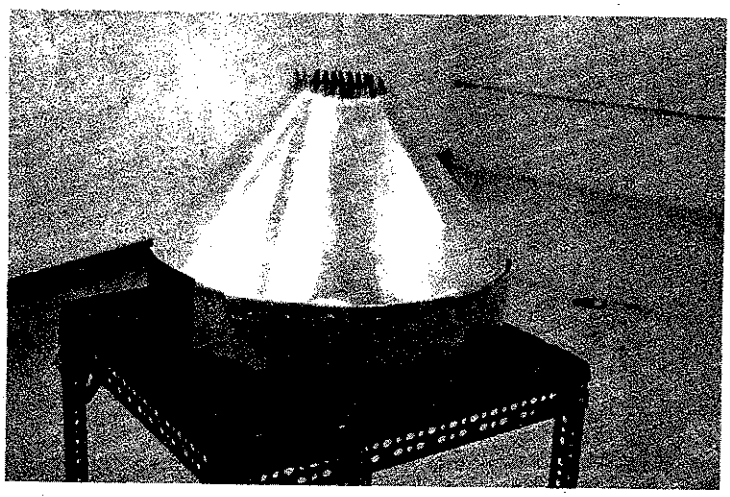

Figure 4-44. Outer Output Cone

2-1345

were introduced at different distances from the simulated switch gap. These probes are three-inch square copper plates, one-quarter inch from the outer cylinder, having 50Ω coaxial cables connected to their centers through 150Ω resistors. Two probes were inserted, rather than one, in order to facilitate identification of the various pulses which are due to reflections from discontinuities within the model, and which are superposed on the driving pulse to be monitored.

The switch configuration shown in Figure 4-41a, and in the photograph. The heights h_1 through h_8 are useful for calculating signal transit times between various points on the model and are also used later on to indicate the position of the water surface. The pulse source referred to in Figure 4-41a is a Tektronix 109 pulser which produces a train of fast-rise square pulses of width 63 ns.

4.9.3 Modelling Procedure

The two capacitive probes showed response times of about 1 ns and a square pulse shape upon correction for exponential decay with an RC-time constant of about 130 ns. Superposed on these square pulses are small-amplitude, fast oscillations with a period of approximately 2.4 ns, close to the calculated pulse transit time across the probe capacitor of 2.25 ns. There are also large-amplitude pulses of relatively short duration superposed on the square pulses; these were expected and can in most cases be identified with certainty as reflections from discontinuities within the system.

Originally, tap water was used in the water line since it was felt that this ought to be sufficient for a low-voltage, low-impedance (3.5Ω) system of such short length (less than 4 feet). It was found, however, that the use of tap water did, in fact, cause significant loss of pulse amplitude, and the tap water was therefore replaced with distilled water. Figure 4-45 shows the pulses obtained at the output of the system, with tap water to the various levels indicated. The particular switch-model configuration employed for a figure is identified by means of a four-number code as follows:

Water level as shown in Figure 4-41a.

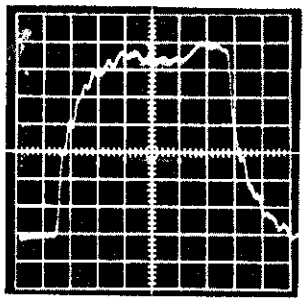

Figure (a)

Water Level: $h_5 + t$

Vertical Sensitivity: 67 mV/div
Horizontal Sensitivity: 10 ns/div

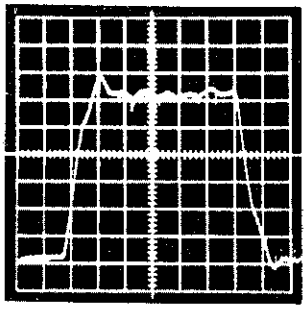

Figure (b)

Water Level: $h_6 + t$

Vertical Sensitivity: 67 mV/div
Horizontal Sensitivity: 10 ns/div

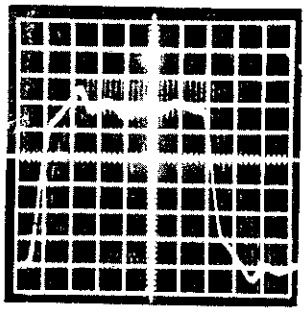

Figure (c)

Water Level: $h_7 + t$

Vertical Sensitivity: 67 mV/div
Horizontal Sensitivity: 10 ns/div

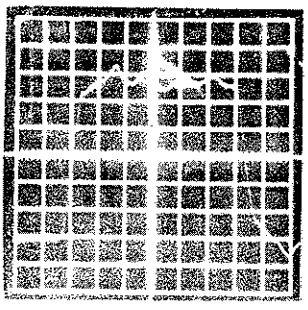

Figure (d)

Water Level: $h_8 + t$

Vertical Sensitivity: 67 mV/div
Horizontal Sensitivity: 10 ns/div

Figure 4-45. Pulses at Output with Tap Water; Switch (22/1 - 8/8)

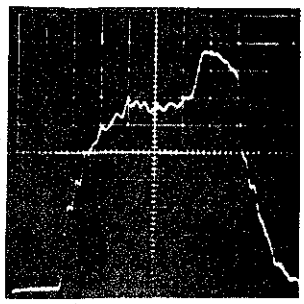

Figure (a)

Vertical Sensitivity: 106 mV/div
Horizontal Sensitivity: 10 ns/div

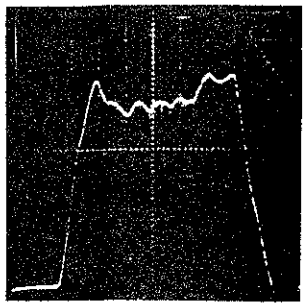

Figure (b)

Vertical Sensitivity: 106 mV/div
Horizontal Sensitivity: 10 ns/div

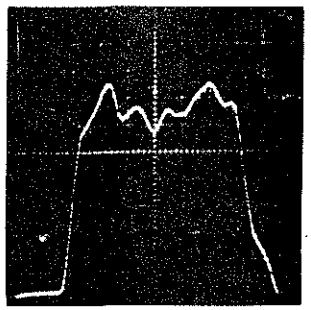

Figure (c)

Vertical SensitivityP 106 mV/div
Horizontal Sensitivity: 10 ns/div

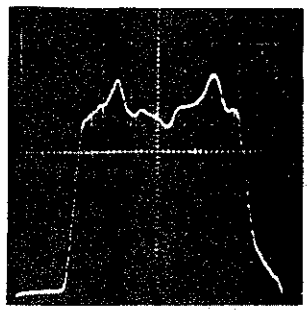

Figure (d)

Vertical Sensitivity: 106 mV/div
Horizontal Sensitivity: 10 ns/div

Figure 4-46. Pulses at Output with Distilled Water; Switch (22/1 - 8/8)

Switch (D/t - N/d)

where

D is the diameter of the lucite disc, in inches; the value of D is either 22 or 13, corresponding, respectively, to the lucite's extending all the way to the outer conductor, and to its being cut to be flush with the inner cylinder.

t is the thickness of the lucite disc, in inches, (where the disc thickness has two discrete values, due to grooves in the lucite disc, the smaller value of t is put in parentheses after the larger value).

N is the number of simulated spark channels through the lucite, spaced uniformly along the circumference of a circle of diameter

d which is measured in inches.

This code is used for Figures 4-45 through 4-57, as well, and for Figure 4-59.

Figure 4-46 should be compared with Figure 4-45, but note that the vertical scales are different in the two sets of pictures. Figure 4-46 corresponds to the same experimental conditions as does Figure 4-45, except for the use of distilled water instead of tap water. The comparison is interesting in several respects. The increased pulse amplitude with distilled water in the system is clearly evident. Identification of the near-square main body of the output pulse is facilitated by observation of Figure 4-45, since the superposed reflection-peaks are strongly attenuated here due to the impure water. Furthermore, the relative prominence of peaks can sometimes provide a clue to their identity. Note, for instance, the fact that the second peak in Figure 4-46d is somewhat larger than the first peak, whereas in Figure 4-45d the relationship is the opposite. The reason is that the second peak has traversed a greater distance through the lossy water than has the first. This is consistent with the identification (from measurements of their time-delays relative to the pulse front) of the first peak as caused by a transient reflection from the tube followed by an in-phase reflection from the relatively high impedance of the simulated switch

(total distance traversed: 20-inches) and of the second pulse as caused by a reflection from the switch gap, followed by an in-phase reflection from the impedance mismatch at the input connection at the bottom of the water box (total distance traversed: 77-inches).

4.9.4 Experimental Results

With the exception of Figures 4-46 and 4-54, all photographs were taken with a 3Ω load. With the exception of Figures 4-45 and 4-46, all photographs were also taken with the water level at $h_8 + t$ as shown in Figure 4-41. All picture sequences beginning with Figure 4-47 show the pulses obtained from the two capacitive probes as well as two pictures of the pulse at the output, the first showing the entire pulse, the second view of the pulse front on an expanded time base.

Figures 4-45 and 4-46 illustrate the effect of using impure water in the system. Figure 4-47 shows the effect of removing the impedance discontinuity at the switch and can be used to determine the response time of the front end of the model, including the tapered section, the water-lucite-air transition and the load. The switch was removed altogether for this experiment and replaced by a 13-inch diameter, 1-inch thick metal disc. Clearly, there is a reflection of a transient, "inductive" type from the supposedly matched output. This is seen very clearly on the capacitor probe. (Figure 4-47a and 4-47b) where the reflected peak is superposed on the main body of the pulse, but it can also be seen in the picture of the pulse at the output (Figure 4-47c) (as well as by the capacity probe) as a small peak on the trailing edge of the pulse, delayed by 70 ns with respect to the pulse front, corresponding to a double traversal of the entire system. The pictures of Figure 4-47 are furthermore notable for the absence of any other reflections, as well as for very good risetimes in Figures 4-47c and 4-47d. The step response of the output section (exclusive of the switch gap) is, in fact, seen to have a risetime of less than 4 ns. It should be pointed out here that all times in this section refer to the model which is roughly a half-scale Neptune B. All time (in particular, risetimes) should therefore be multiplied by a factor of 2 if data pertaining to a full-scale Neptune B are desired.

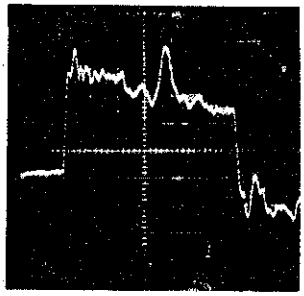

(a) Capacitor Probe at Level h_3

Vertical Sensitivity: 12.5 mV/div
Horizontal Sensitivity: 10 ns/div

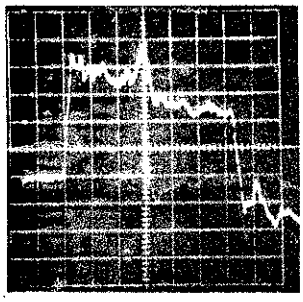

(b) Capacitor Probe at Level h_4

Vertical Sensitivity: 12.5 mV/div
Horizontal Sensitivity: 10 ns/div

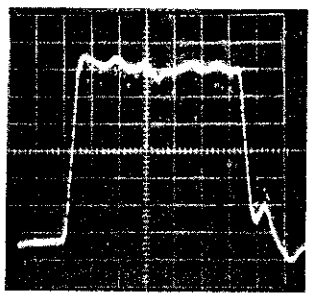

(c) Output

Vertical Sensitivity: 106 mV/div
Horizontal Sensitivity: 10 ns/div

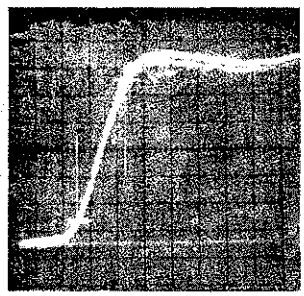

(d) Output

Vertical Sensitivity: 106 mV/div
Horizontal Sensitivity: 2 ns/div

Figure 4-47. Capacitor Probe and Output Response with Switch Shorted Out.

2-1369

Figures 4-48 and 4-49 illustrate the effect of moving the eight switch channels out from a circle of 8-inch diameter to one of 13-inch diameter. Only slight changes in the pulses can be seen for the one-inch-long switch gap employed here. The probe pictures (4-48a and 4-49a) show three distinct reflection peaks superposed on the main pulse. The first peak is due to reflection of the incident pulse front from the switch gap, the second to reflection from the tube, and the third to reflection from the switch gap, followed by in-phase reflection from the input connection at the bottom of the water box. These pulses can also be seen in Figures 4-48b and 4-49b, as well as in most of the probe pictures following. It should be noted that the second peak is less well-defined than it was in Figures 4-47a and b where the reflection from the tube did not have to traverse a high-impedance switch on its way back to the probe.

Figures 4-50 and 4-51 show the effect of removing two of the switch channels, in this case located next to one another. As could be expected, an increase in risetime is associated with a reduction in the number of spark channels. This increase is only slight, however (see Table 4-9 below). It is interesting to observe the increased amplitude of the peaks in Figure 4-51b. The probe at level h_4 is located immediately ahead of the missing channels and thus sees more of a reflection from the switch than does the probe at level h_3 which is on the opposite side of the cylinder.

The question of how to define risetimes is not a straightforward one, because of the reflection peaks superposed on the square output pulses. If one measures the time between the 10% and 90% amplitude points on the pulse front, based on an educated guess of where the top of the underlying forward pulse is located, one gets the risetimes in column 1 of Table 4-9 below. If, instead, one defines the pulse amplitude as that of the first peak of the output pulse, one gets the 10% to 90% risetimes in column 2. These show a trend which is exactly opposite to that of column 1. Column 1, however, makes intuitive sense in most cases, whereas column 2 does not. It appears, therefore, that meaningful results can be obtained only when risetimes are measured after the estimated transient peaks are subtracted from the output pulse. This can be

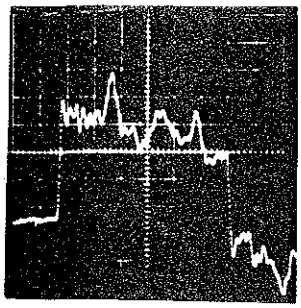

Figure (a)

Vertical Sensitivity: 12. 5 mV/div
Horizontal Sensitivity: 10 ns/div

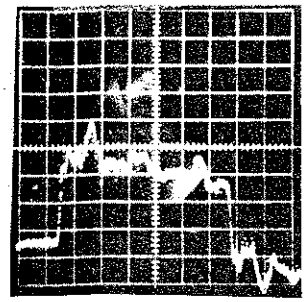

Figure (b)

Vertical Sensitivity: 12. 5 mV/div
Horizontal Sensitivity: 10 ns/div

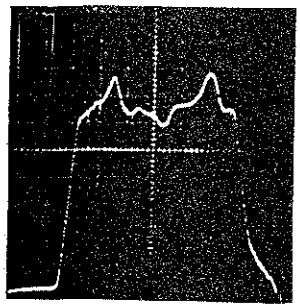

Figure (c)

Vertical Sensitivity: 106 mV/div
Horizontal Sensitivity: 2 ns/div

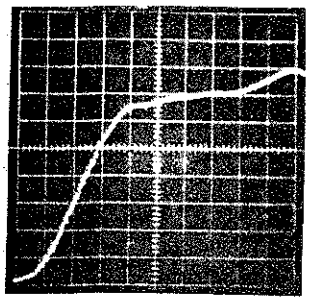

Figure (d)

Vertical Sensitivity: 106 mV/div
Horizontal Sensitivity: 2 ns/div

Figure 4-48. Capacitor Probe and Output Response with 8-Inch Dia. Switch; Switch (22/1 - 8/8).

Capacitor Probe at Level h_3

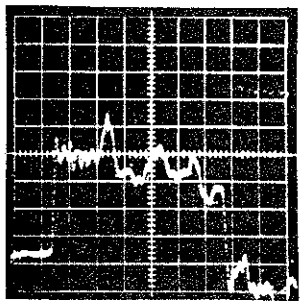

Figure (a)

Vertical Sensitivity: 12. 5 mV/div
Horizontal Sensitivity: 10 ns/div

Capacitor Probe at Level h_4

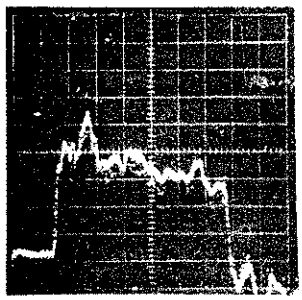

Figure (b)

Vertical Sensitivity: 12. 5 mV/div
Horizontal Sensitivity: 10 ns/div

Output

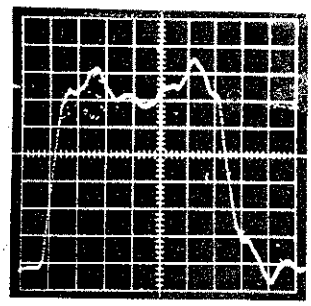

Figure (c)

Vertical Sensitivity: 106 mV/div
Horizontal Sensitivity: 2 ns/div

Output

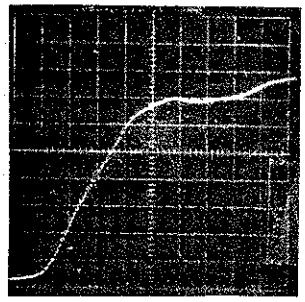

Figure (d)

Vertical Sensitivity: 106 mV/div
Horizontal Sensitivity: 2 ns/div

Figure 4-49. Capacitor Probe and Output Response with 12-Inch Dia. Switch; Switch (22/1 - 8/13).

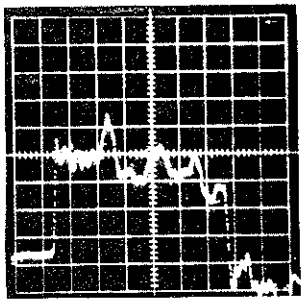

Figure (a)

Capacitor Probe at Level h_3

Vertical Sensitivity: 12.5 mV/div
Horizontal Sensitivity: 10 ns/div

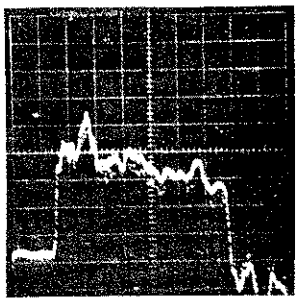

Figure (b)

Capacitor Probe at Level h_4

Vertical Sensitivity: 12.5 mV/div
Horizontal Sensitivity: 10 ns/div

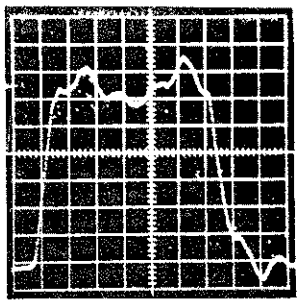

Figure (c)

Output

Vertical Sensitivity: 106 mV/div
Horizontal Sensitivity: 10 ns/div

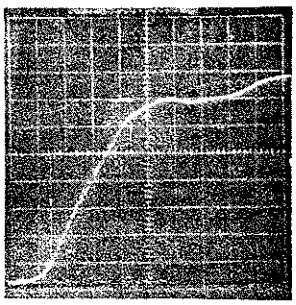

Figure (d)

Output

Vertical Sensitivity: 106 mV/div
Horizontal Sensitivity: 2 ns/div

Figure 4-50. Figure 4-49 Repeated; Switch (22/1 - 8/13).

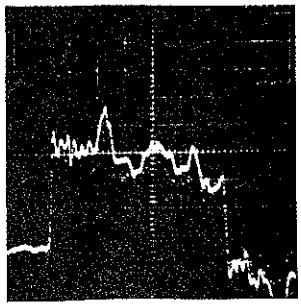

Figure (a)

Vertical Sensitivity: 12.5 mV/div
Horizontal Sensitivity: 10 ns/div

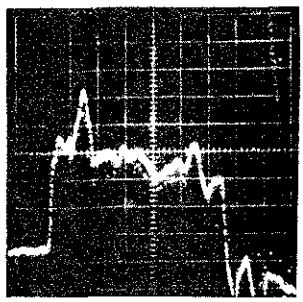

Figure (b)

Vertical Sensitivity: 12.5 mV/div
Horizontal Sensitivity: 10 ns/div

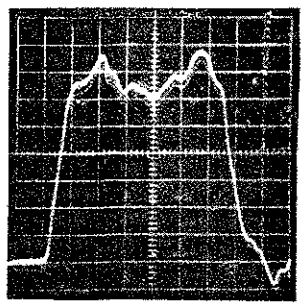

Figure (c)

Vertical Sensitivity: 106 mV/div
Horizontal Sensitivity: 10 ns/div

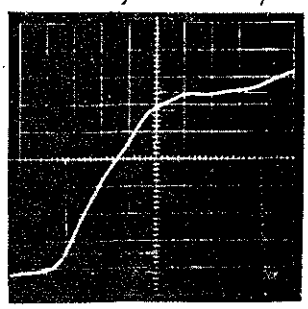

Figure (d)

Vertical Sensitivity: 106 mV/div
Horizontal Sensitivity: 2 ns/div

Figure 4-51. Same as Figure 4-50, Except for 2 Missing "Spark Channels"; Switch (22/1 - 6/13)

Table 4-9. Risetimes

Switch Configuration	Column 1 Risetimes (ns) between 10% and 90% Amplitude Points of the Main Pulse	Column 2 Risetimes (ns) between 10% and 90% Amplitude Points of First Peak
22/1 - 8/13	5.9	15
22/1 - 8/8	5.6	15
22/1 - 6/13	6.4	14
22/2 - 8/8	10.2	14.3
22/2 - 8/6	12.0	13.5
13/2 - 8/6	11.5	12.8
13/3 (1) - 8/6	9.5	9.5

done with the aid of Figure 4-47c which gives an amplitude of the main pulse of 6.7 divisions.

Figures 4-52 and 4-53 show the effect of lengthening the switch gap from 1-inch to 2-inches. The probes show increased reflection peaks from the longer switch gap, and Figures 4-53c and d show a considerably longer rise-time. Associated with the reduced initial transmission through the switch (longer risetime), there is an enhanced second peak.

Figures 4-54 and 4-55 illustrate the effect to be expected when water is permitted to fill the space between the inner and outer conductors of the system in the region of the switch. The reflection peaks are now noticeably broader due to the slower wave propagation through the switch, and a notch has appeared on the rise-portion of the pulse.

A comparison between Figures 4-53 and 4-54 shows the effect of reducing the diameter of the switch circle from 8-inches to 6-inches. An increase in output pulse risetime is noticeable this time as a consequence of the reduction in switch circle diameter. The second peak in Figure 4-54c is also enhanced relative to that of Figure 4-53 (c).

Figures 4-56 and 4-57 show the pulses obtained with under-matched (1.25 Ω) and overmatched (9 Ω) loads, respectively. These should be compared with the matched case of Figure 4-55. The output pulses of Figures 4-55, 4-56 and 4-57 are all plotted on one graph in Figure 4-58, after having been multiplied by scaling factors equal to the inverse of the theoretical voltage-transfer coefficients, which are approximately 1.0, 0.6 and 1.5, respectively. The three curves show obvious discrepancies following the first peak as well as on the trailing edge of the pulse. These were expected, since the unmatched loads will cause reflections of more than a transient nature. The one-ohm load will give rise to a negative reflection, whereas the nine-ohm load will cause a positive reflection. These reflections will return to the output after about 20 ns following reflection from the bottom of the water box. It is interesting to note that very little change in the pulse front (in particular, the pulse rise-time) results from the change in load impedance.

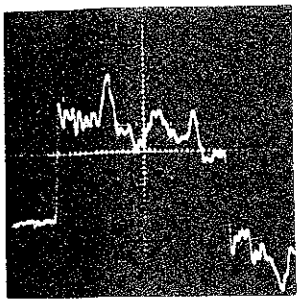

Figure (a)

Vertical Sensitivity: 12.5 mV/div
Horizontal Sensitivity: 10 ns/div

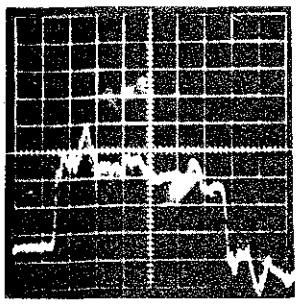

Figure (b)

Vertical Sensitivity: 12.5 mV/div
Horizontal Sensitivity: 10 ns/div

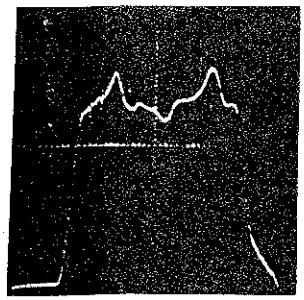

Figure (c)

Vertical Sensitivity: 106 mV/div
Horizontal Sensitivity: 10 ns/div

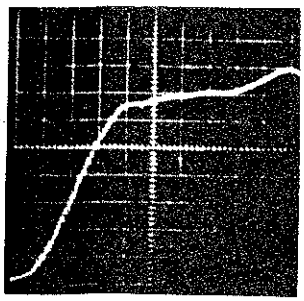

Figure (d)

Vertical Sensitivity: 106 mV/div
Horizontal Sensitivity: 2 ns/div

Figure 4-52. Capacitor Probe and Output Response with Switch (22/1 - 8/8).

Figure (a)

Capacitor Probe at Level h_3

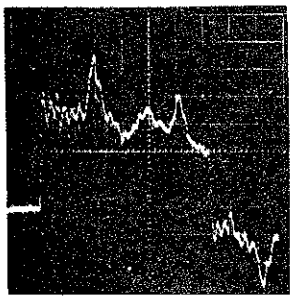

Vertical Sensitivity: 12.5 mV/div
Horizontal Sensitivity: 10 ns/div

Figure (b)

Capacitor Probe at Level h_4

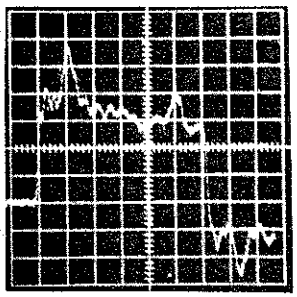

Vertical Sensitivity: 12.5 mV/div
Horizontal Sensitivity: 10 ns/div

Figure (c)

Output

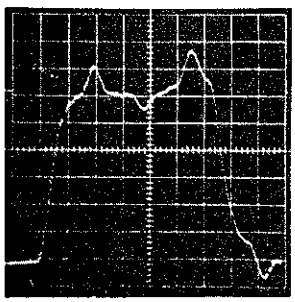

Vertical Sensitivity: 106 mV/div
Horizontal Sensitivity: 10 ns/div

Figure (d)

Output

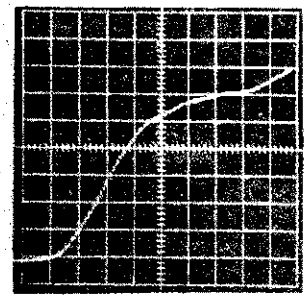

Vertical Sensitivity: 106 mV/div
Horizontal Sensitivity: 2 ns/div

Figure 4-53. Capacitor Probe and Output Response with 2-Inch Long Switch; Switch (22/2 - 8/8).

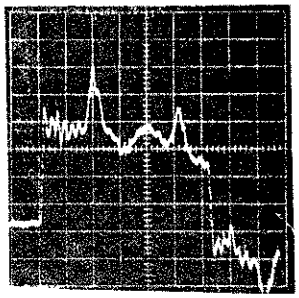

Figure (a)

Vertical Sensitivity: 12.5 mV/div
Horizontal Sensitivity: 10 ns/div

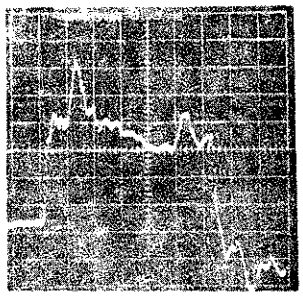

Figure (b)

Vertical Sensitivity: 12.5 mV/div
Horizontal Sensitivity: 10 ns/div

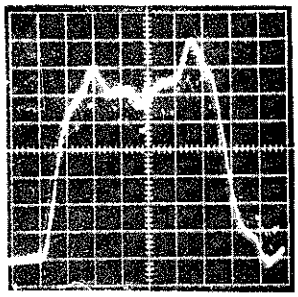

Figure (c)

Vertical Sensitivity: 106 mV/div
Horizontal Sensitivity: 10 ns/div

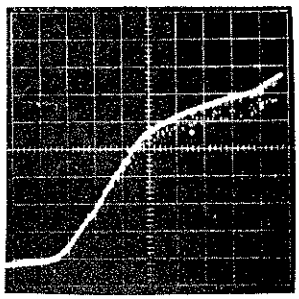

Figure (d)

Vertical Sensitivity: 106 mV/div
Horizontal Sensitivity: 2 ns/div

Figure 4-54. Capacitor Probe and Output Response with no Water Around Switch; Switch (22/2 - 8/6).

Figure (a)

Capacitor Probe at Level h_3

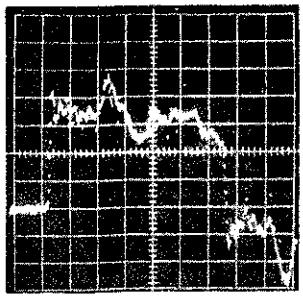

Vertical Sensitivity: 12.4 mV/div
Horizontal Sensitivity: 10 ns/div

Figure (b)

Capacitor Probe at Level h_4

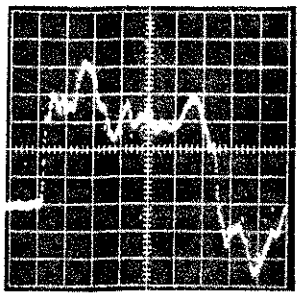

Vertical Sensitivity: 12.5 mV/div
Horizontal Sensitivity: 10 ns/div

Figure (c)

Output

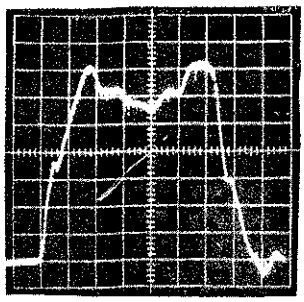

Vertical Sensitivity: 106 mV/div
Horizontal Sensitivity: 10 ns/div

Figure (d)

Output

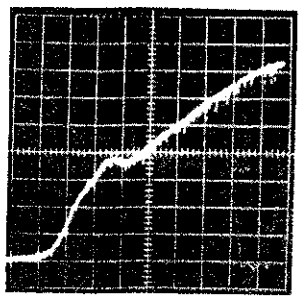

Vertical Sensitivity: 106 mV/div
Horizontal Sensitivity: 2 ns/div

Figure 4-55. Capacitor Probe and Output Response with Water Around Switch; Switch (13/2 - 8/6).

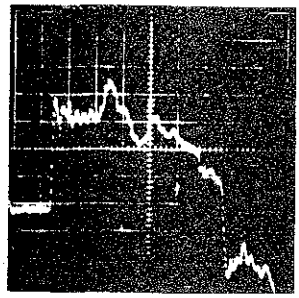

Figure (a)

Vertical Sensitivity: 12.5 mV/div
Horizontal Sensitivity: 10 ns/div

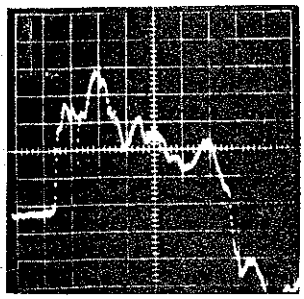

Figure (b)

Vertical Sensitivity: 12.5 mV/div
Horizontal Sensitivity: 10 ns/div

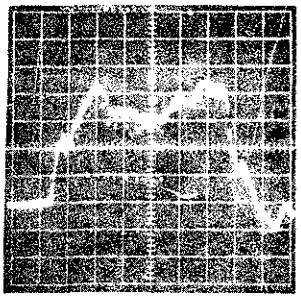

Figure (c)

Vertical Sensitivity: 106 mV/div
Horizontal Sensitivity: 10 ns/div

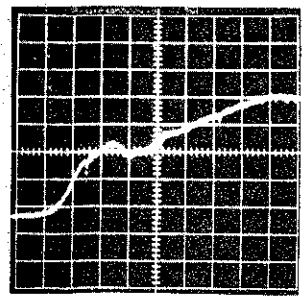

Figure (d)

Vertical Sensitivity: 106 mV/div
Horizontal Sensitivity: 2 ns/div

Figure 4-56. Capacitor Probe and Output Response with 1.25 Ohm Load; Switch (13/2 - 8/6).

Figure (a)

Capacitor Probe at Level h_3

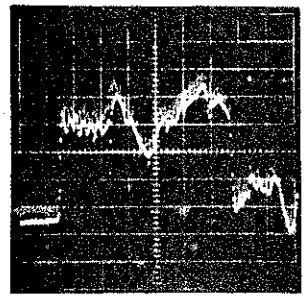

Vertical Sensitivity: 12.5 mV/div
Horizontal Sensitivity: 10 ns/div

Figure (b)

Capacitor Probe at Level h_4

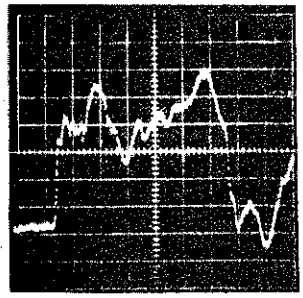

Vertical Sensitivity: 12.5 mV/div
Horizontal Sensitivity: 10 ns/div

Figure (c)

Output

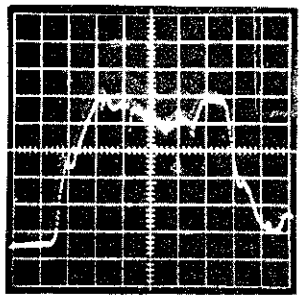

Vertical Sensitivity: 204 mV/div
Horizontal Sensitivity: 10 ns/div

Figure (d)

Output

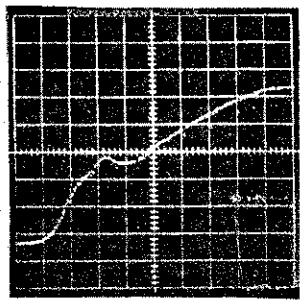

Vertical Sensitivity: 204 mV/div
Horizontal Sensitivity: 2 ns/div

Figure 4-57. Capacitor Probe and Output Response with 9 Ohm Load; Switch (13/2 - 8/6).

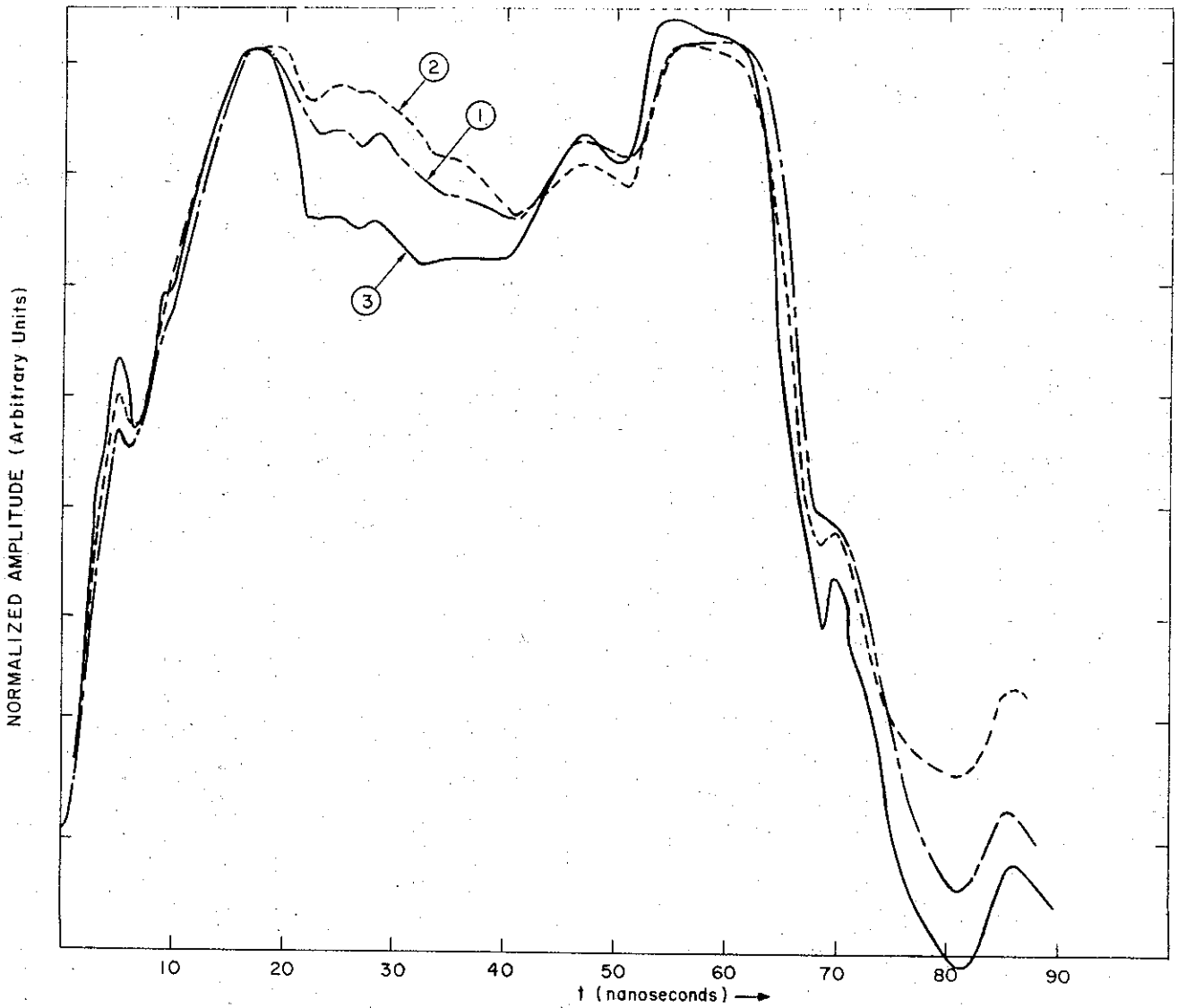

Figure 4-58. Comparison of Amplitude-Scaled Output Pulses for Switch Configuration (13/2 - 8/6)
Curve 1: 3 Ohm Load; Curve 2: 9 Ohm Load; Curve 3: 1.25 Ohm Load

Finally, Figure 4-59 is one of a number of sets of photographs taken to study a switch model which may be more realistic, but which is also more complicated, than those of Figures 4-48 through 4-57. The intention is to model the switch electrode shanks as well as the arc channels. It consists of a lucite disc of 13-inch diameter and 3-inch thickness, with 1-inch deep and 2-inch wide circular grooves cut into both sides of the lucite, the center line of these grooves being along a circle of 6-inch diameter. The eight 4.5 mil copper wires are threaded through small holes in the lucite as before, these holes are uniformly spaced along the circumference of the 6-inch diameter circle which marks the center line of the grooves. Compressible screen rolls are placed in the grooves to provide metallic contact between the two parts of the inner conductor of the system and the switch wires. The reflection peaks from the switch are now both broad and of large amplitude (Figures 4-59a and b), and the output pulse shows a "smeared-out" first peak, a broad and large amplitude second peak (Figure 4-59c), as well as the characteristic notch in the rise portion of the pulse (Figures 4-59c and d). A similar switch is shown in Figure 4-60.

Experiments were also carried out with a simulated switch which is a better approximation to the actual switch which has been designed for the full-scale Neptune B (Switch III). Two aspects of this switch were studied. First, the effect of rings on the edges of the water line center conductor, before and after the switch was investigated. These rings on the edges will produce small lips on the center conductor immediately before and after the switch gap with a brief increase in center-conductor diameter of about 1-1/2-inches in the half-scale model. Next, the effect on the output pulse of failing to trigger one or more of the eight spark channels during a switching operation was investigated. The simulated switch, shown in Figure 4-60, is the same as that used for Figure 4-59, except for the addition here of lips on the center conductor before and/or after the switch. These lips were modelled by means of metallic cylindrical rings which fitted snugly around the center conductor.

Figures 4-61 through 4-68 show three photographs each. The first represents the pulse from the probe located at level h_4 of Figure 4-41, the second shows the pulse across the 3Ω (matched) load at the output; the third is this pulse repeated with an expanded time-base. Figures 4-61 through 4-64

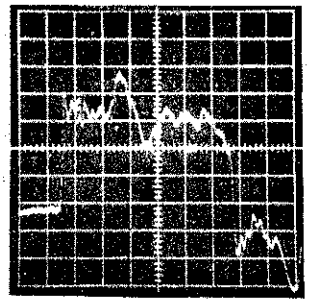

(a) Capacitor Probe at Level h_3

Vertical Sensitivity: 12.5 mV/div
Horizontal Sensitivity: 10 ns/div

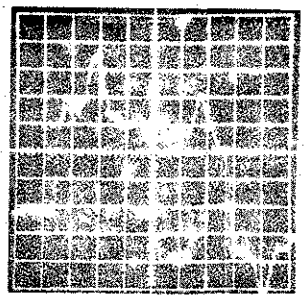

(b) Capacitor Probe at Level h_4

Vertical Sensitivity: 12.5 mV/div
Horizontal Sensitivity: 10 ns/div

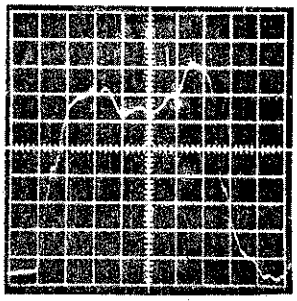

(c) Output

Vertical Sensitivity: 106 mV/div
Horizontal Sensitivity: 10 ns/div

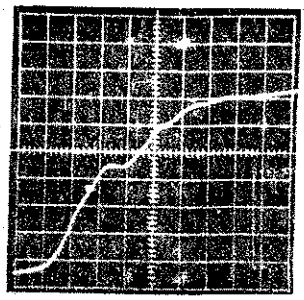

(d) Output

Vertical Sensitivity: 106 mV/div
Horizontal Sensitivity: 2 ns/div

Figure 4-59. Capacitor Probe and Output Response Switch with Electrode Shanks; Switch (13/3(1) - 8/6).

2-1380

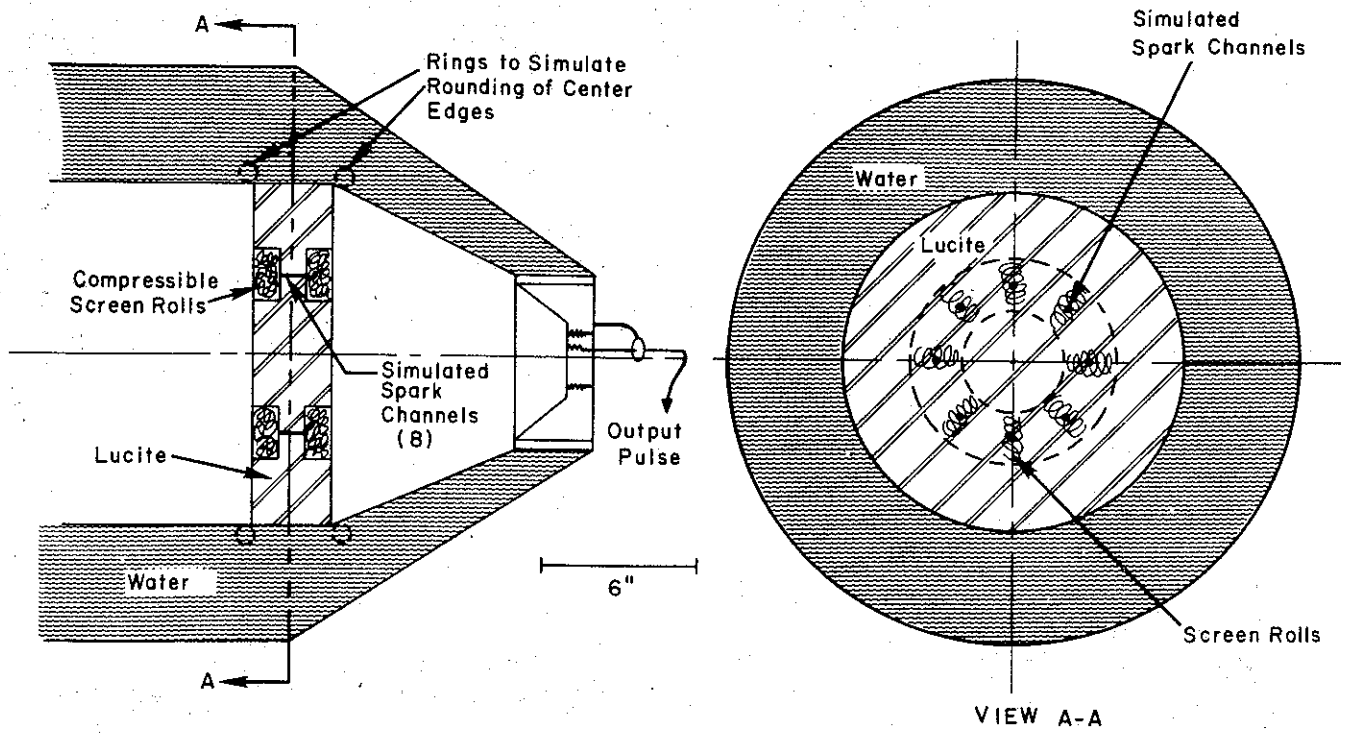

Figure 4-60. Simulated Switch for Half Scale Neptune B Model

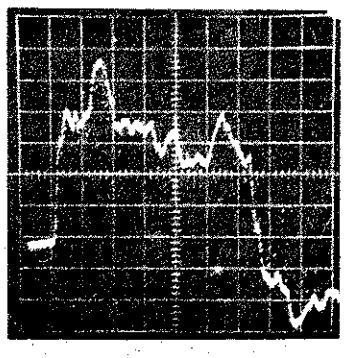

(a) Capacitor Probe
Vertical Sensitivity:
12.5 mV/div
Horizontal Sensitivity:
10 ns/div

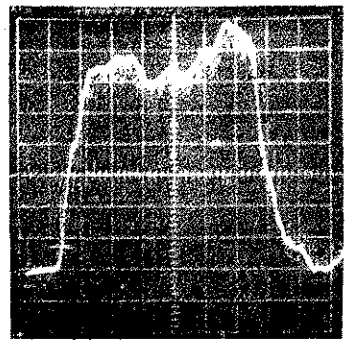

(b) Output Pulse
Vertical Sensitivity:
106 mV/div
Horizontal Sensitivity:
10 ns/div

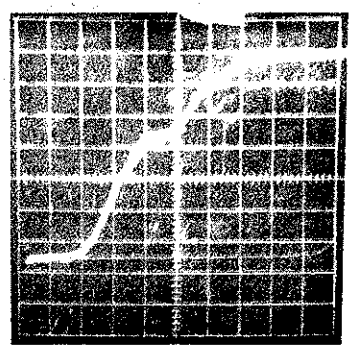

(c) Output Pulse
Vertical Sensitivity:
106 mV/div
Horizontal Sensitivity:
2 ns/div

Figure 4-61. Pulses with all Spark Channels in Place and Rings Removed

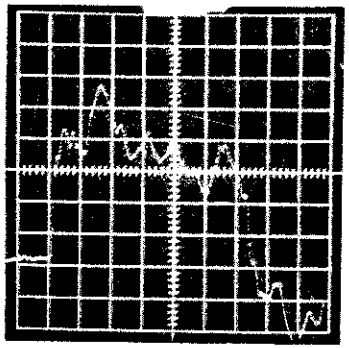

(a) Capacitor Probe
Vertical Sensitivity:
12.5 mV/div
Horizontal Sensitivity:
10 ns/div

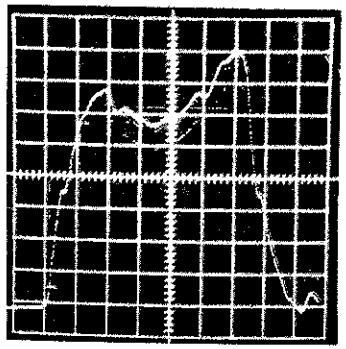

(b) Output Pulse
Vertical Sensitivity:
106 mV/div
Horizontal Sensitivity:
10 ns/div

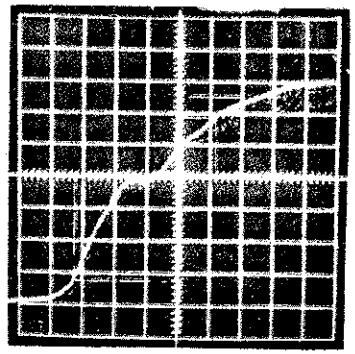

(c) Output Pulse
Vertical Sensitivity:
106 mV/div
Horizontal Sensitivity:
2 ns/div

Figure 4-62. Pulses with all Spark Channels in Place and One Ring Before the Switch

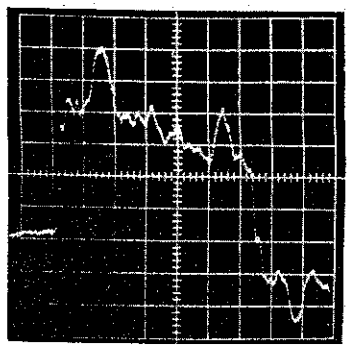

(a) Capacitor Probe
Vertical Sensitivity:
12.5 mV/div
Horizontal Sensitivity:
10 ns/div

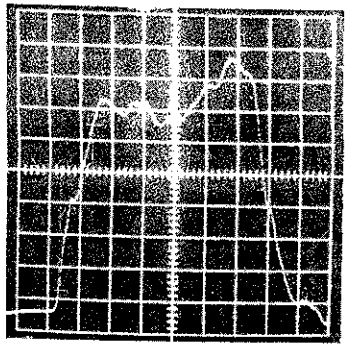

(b) Output Pulse
Vertical Sensitivity:
106 mV/div
Horizontal Sensitivity:
10 ns/div

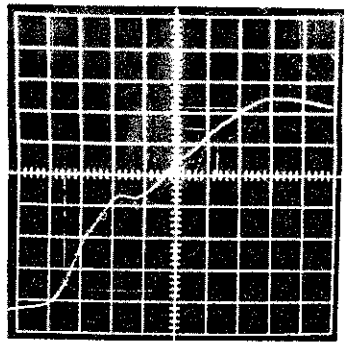

(c) Output Pulse
Vertical Sensitivity:
106 ns/div
Horizontal Sensitivity:
2 ns/div

Figure 4-63. Pulses with all Spark Channels in Place and One Ring After the Switch

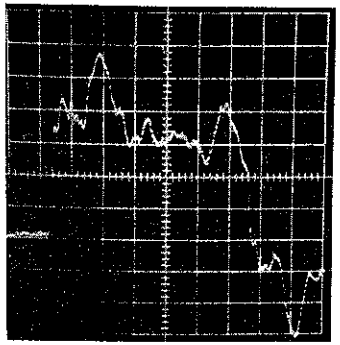

(a) Capacitor Probe
Vertical Sensitivity:
12.5 mV/div
Horizontal Sensitivity:
10 ns/div

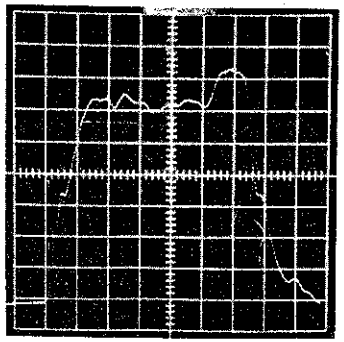

(b) Output Pulse
Vertical Sensitivity
106 mV/div
Horizontal Sensitivity:
10 ns/div

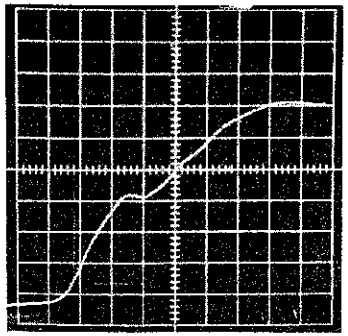

(c) Output Pulse
Vertical Sensitivity:
106 mV/div
Horizontal Sensitivity:
2 ns/div

Figure 4-64. Pulses with all Spark Channels in Place and Rings Before and After the Switch

show the effect of having first no ring, then one, then the other, and finally both rings in place next to the switch. Figures 4-65 through 4-68 show the effect of triggering fewer than the total number of eight spark channels.

The addition of rings before and/or after the switch is seen from Figures 4-61 through 4-64 to degrade the risetime somewhat, although not very much. It appears that when only one ring is used, the ring after, i.e., on the output side of the switch, has somewhat more of a detrimental effect on risetime than the one before the switch. The risetimes range from 8.5 ns with no ring through 9 ns and 9.6 ns with one ring to 10 ns with both rings in place. All risetimes are tabulated in Table 4-10 below: the risetimes are between the 10% and 90% amplitude points, based on an estimate of the true amplitude of the near-square main body of the output pulse, with reflection peaks subtracted. The amplitudes used as the basis for the risetime measurements are listed in Table 4-9 in parentheses following the risetimes.

The most striking effect of the addition of rings is seen in the general output pulse shape. It appears that when both rings are in place the transient, inductive reflection from the dielectric interface at the output is capacitively coupled across the switch gap rather than being reflected from it and returned to the output. The result is that the pulse at the output has a flat-topped appearance for the first 40 ns, without the front peak seen in most of the other output pulses. This flat top is clearly evident in Figures 4-64b and 4-65b, but not in these output pulses shown here where two rings were not used, nor in those shown where rings were not used at all. Transmission of the transient reflection pulse through the switch as described above should be seen by the capacitor probe. Figures 4-64a and 4-65a do indeed have a flat portion, beginning about 20 ns after the first peak of those pulses and testing for about 10 ns, which is not seen in the other probe outputs. Comparison with Figures 4-61a and 4-66a, respectively, which are the corresponding pulses obtained without rings, show a noticeably larger pulse amplitude at this time (40 ns after the pulse front) for the pulses obtained using two rings. This is just the time at which one would expect to see a reflection from the output.

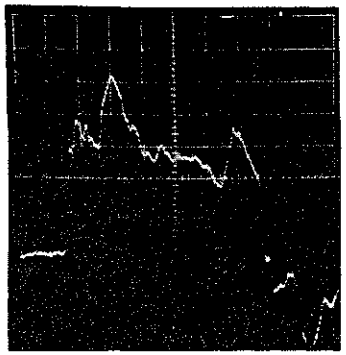

(a) Capacitor Probe
Vertical Sensitivity:
12.5 mV/div
Horizontal Sensitivity:
10 ns/div

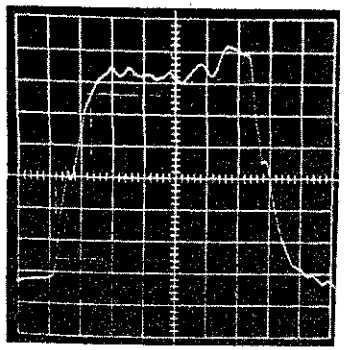

(b) Output Pulse
Vertical Sensitivity:
106 mV/div
Horizontal Sensitivity:
10 ns/div

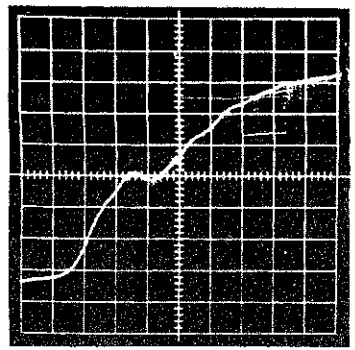

(c) Output Pulse
Vertical Sensitivity:
106 mV/div
Horizontal Sensitivity:
2 ns/div

Figure 4-65. Pulses with One Spark Channel Removed and Rings Before and After the Switch

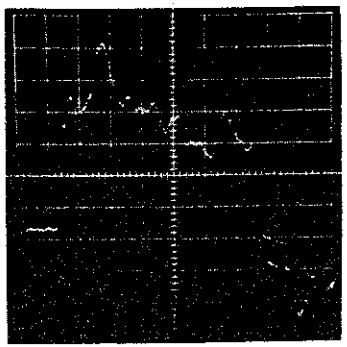

(a) Capacitor Probe
Vertical Sensitivity:
12.5 mV/div
Horizontal Sensitivity:
10 ns/div

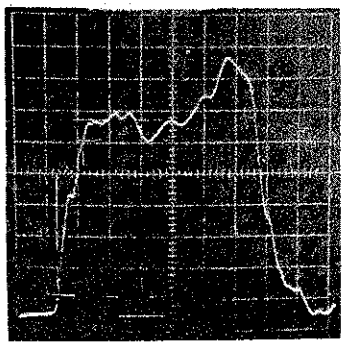

(b) Output Pulse
Vertical Sensitivity:
106 mV/div
Horizontal Sensitivity:
10 ns/div

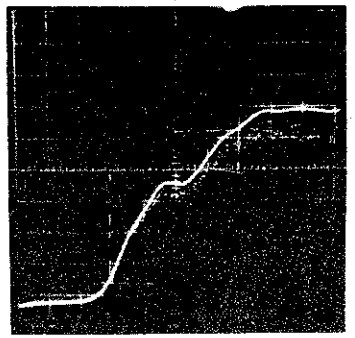

(c) Output Pulse
Vertical Sensitivity:
106 mV/div
Horizontal Sensitivity:
2 ns/div

Figure 4-66. Pulses with One Spark Channel Removed and Rings Removed

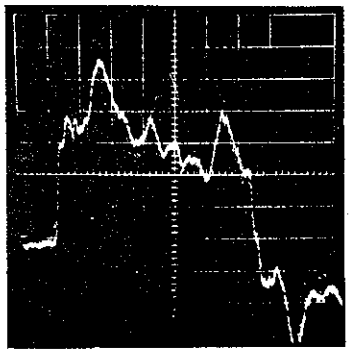

(a) Capacitor Probe
Vertical Sensitivity:
12.5 mV/div
Horizontal Sensitivity:
10 ns/div

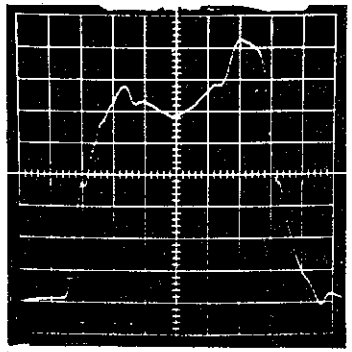

(b) Output Pulse
Vertical Sensitivity:
106 mV/div
Horizontal Sensitivity:
10 ns/div

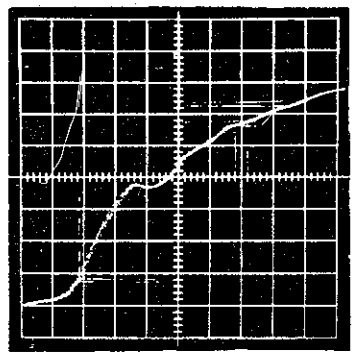

(c) Output Pulse
Vertical Sensitivity:
106 mV/div
Horizontal Sensitivity:
2 ns/div

Figure 4-67. Pulses with Two Spark Channels Removed and Rings Removed

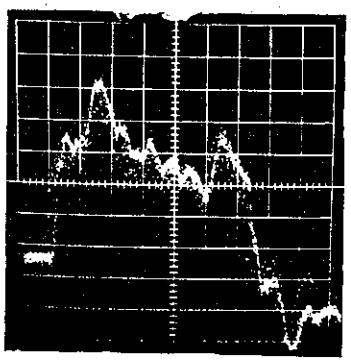

(a) Capacitor Probe
Vertical Sensitivity:
12.5 mV/div
Horizontal Sensitivity:
10 ns/div

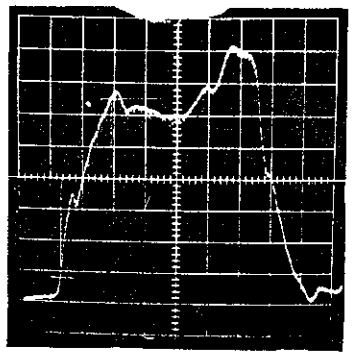

(b) Output Pulse
Vertical Sensitivity:
106 mV/div
Horizontal Sensitivity:
10 ns/div

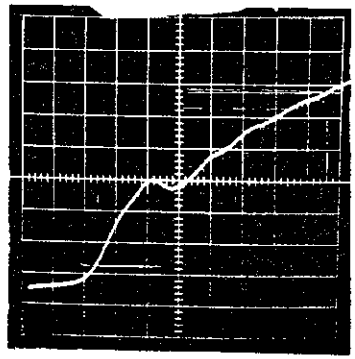

(c) Output Pulse
Vertical Sensitivity:
106 mV/div
Horizontal Sensitivity:
2 ns/div

Figure 4-68. Pulses with Three Spark Channels Removed and Rings Removed

The effect of removing spark channels is seen to be only slight with one channel removed (compare Figures 4-65 and 4-66, corresponding to one channel removed, with Figures 4-64 and 4-61, respectively, corresponding to a full set of eight channels), but quite pronounced with two channels removed (compare Figures 4-64 and 4-61. (When two channels were removed they were taken from diametrically opposite locations on the spark channel circle, when three channels were removed two were diametrically opposite and two were adjacent to one-another.)

The risetimes obtained in this study are tabulated in Table 4-10 below.

4.9.5 Conclusion

It should be stressed that all risetimes mentioned above refer to a half-scale model of Neptune B. They should therefore be multiplied by a factor of 2 in order to be applicable to a full-scale machine. It should also be noted that driving the model with square pulses through a tapered input section is not in every respect equivalent to quasi-statically charging the energy store and then discharging it into a load through a switch gap. In particular, a quasi-statically charged energy store will have charged stray capacitances due to fringing fields around the switch gap. One of these capacitances couples the center conductor to the outer conductor, the other causes coupling across the switch gap from the center conductor to the tapered output cone. In the present modelling experiment these capacitances are initially uncharged.

Measurements were made of the prepulse to be expected in Neptune due to capacitive coupling across the open switch gap during the charging of the water line. These measurements indicate a prepulse of about 3% of the charging voltage, which corresponds to about 6% of the output pulse peak in the case of a matched load, more for an undermatched load and less for an overmatched load. The switch model used for the prepulse measurements was the 13-inch diameter, 3-inch thick lucite disc corresponding to Figure 4-59.

Table 4-10. Risetimes

	No Ring	One Ring Before Switch	One Ring After Switch	Both Rings
Eight spark channels	8.5 ns (6.5 div*)	9 ns (6.5 div*)	9.6 ns (6.5 div*)	10 ns (6.5 div*)
Seven spark channels	8.5 ns (6.2 div*)			11 ns (6.5 div*)
Six spark channels	10.6 ns (6.2 div*)			
Five spark channels	12 ns (6.2 div*)			

*Pulse amplitudes used for risetime determination.

Finally, using the results of this study, it was predicted that a 4 channel output switch on Neptune B would give a risetime of about 28 ns. The actual risetimes which have been measured on the system agree quite well with this number.

SECTION 4.10
MACHINE OPERATION WITH DUMMY LOAD

4.10.1 Experimental Conditions

In order to test the capability of Neptune, a dummy load of 3.8Ω was fitted in place of the field emission diode. This permitted rapid firing of the machine with a consistent load. The stray inductance associated with this load was about 50 nH, which is equivalent to 3.1Ω at 10 MHz. This load is constant with time and is sufficiently massive not to heat up enough to affect its resistance.

In actual operation a field emission diode impedance is large for some nanoseconds before assuming its design value and the impedance suffers a second catastrophic fall when the plasma gap closes. The resistive load used cannot duplicate this behavior but should be satisfactory for about 60 nanoseconds. It will give a value for the current risetime that is pessimistic due to a lower initial impedance and also to a larger inductance.

Neptune B will work satisfactorily from 330 kV to 660 kV without resetting the gaps of any of the three switches. No sign of water line breakdown has been observed.

4.10.2 Monitoring

Two monitors were employed, a current-monitor in series with the dummy load and a voltage monitor in the conical transition.

The current monitor is simply a multitude of carbon resistors spaced uniformly around the cylinder surrounding the dummy load. The resistance is 10.96 mΩ and the pulse voltage is measured in an oscilloscope. The signal is over 500 volts, much greater than any pickup.

The voltage monitor is an NRL type capacity probe, four of which were originally intended to monitor voltage changes around Switch III. The intention was to monitor the number of gaps closing. However, it was soon clear that the four gaps closed reliably, rendering the monitors unnecessary.

Consequently, a resistor was added to lengthen the time response and two probes were fitted near the dummy load. The resistor reduces the probe output and considerable noise pickup resulted. However, the probe proved useful in determining diode impedance, as may be seen from the results.

The voltage monitor was rarely used during the dummy load tests as we may assume that the dummy load is linear and time invariant, at least to the accuracy of the voltage monitor.

4.10.3 Jitter

The time jitter of Neptune is the jitter of Switch III closure. This, in turn, is almost entirely that of the associated trigger generator as the jitter time between trigger pulse and gap closure is too small to be measured and is certainly under 2 nanoseconds. Figure 4-69 gives the output current through the dummy load in 5 successive shots displayed so as to show total system jitter. The time of firing of Switch III is weakly dependent on the water line voltage, viz: approximately 0.2 ns/kV.

The amplitude jitter is primarily a function of Switch II and Switch III time jitter. Figure 4-70 shows 5 successive shots, a range of 3% current jitter is normal. A longer term drift is apparent from day to day. This is primarily due to the water in the water line. This changes resistivity and hence the loading on the coaxial water line. Slow changes in the inherent delay of the trigger generators have also been observed and give rise to amplitude changes. These effects can reduce the output voltage by up to 10% but may, in principle, be corrected for by simply repurifying the water and changing the delays in the trigger command system.

4.10.4 Transient Effects and Load Impedance

Under dummy load conditions, prepulse is absent as may be seen in Figure 4-69. Similar traces, but with the more exacting field emission diode shows the same result. This is mostly due to the fact that, being gas insulated, the capacity across Switch III is small and hence the diode is decoupled from the rest of the system until Switch III fires.

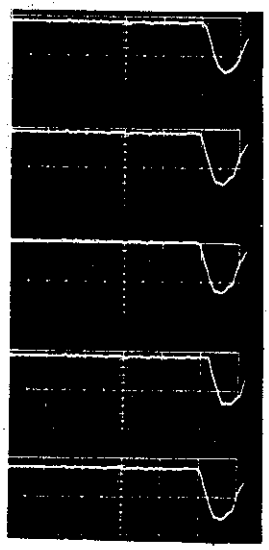

Figure 4-69. Neptune Output Current

Scale 50 kA/cm
100 ns/cm.

Oscilloscope triggered from first command pulser so as to show total system jitter.

1-4443

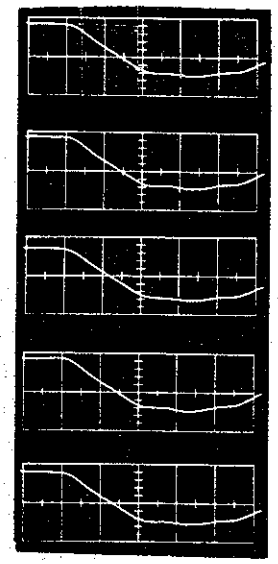

Figure 4-70. Neptune Output Current.

Scale 50 kA/cm
20 ns/cm

Neptune B discharged into 3.8 ohm load.

1-4448

The risetime is limited primarily by the inductance of Switch III and the conical transistion. Figure 4-70 shows the risetime to be about 30 nanoseconds with a matched load (3.8Ω). Figure 4-71 shows the output waveform on other time scales.

The normalized output current is compared for different values of the load in Table 4-11.

Table 4-11. Risetime and Output Current as a Function of Load.

Load, ohms	0	3.65	6.8
Risetime nsec Normalized	40	30	30
Maximum Current	1.8	1	0.67

The average of these indicates a water line impedance of 3-1/2 ohms, as expected.

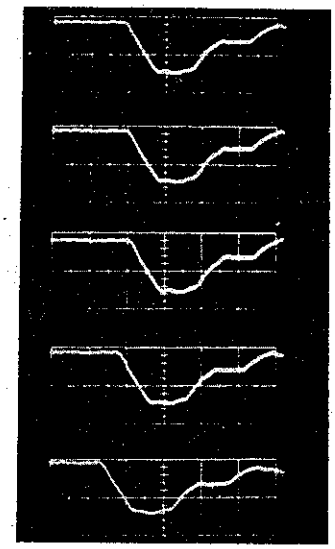

Scale 50 ns/cm

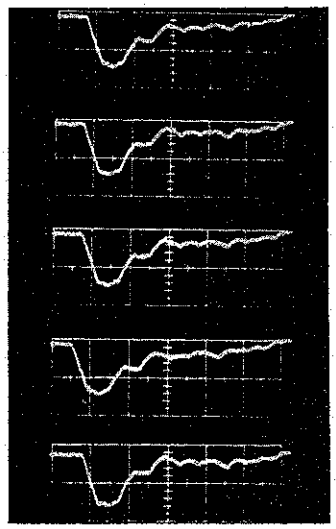

Scale 100 ns/cm

Figure 4-71. Neptune Output Current.

Scale 50 kA/cm

2-1536

SECTION 4.11
ELECTRON BEAM TESTS

4.11.1 Introduction

This section contains the results of the preliminary electron beam studies on Neptune B. As seen in Figure 4-72, the energy stored in the 3.4 ohm coaxial water line is discharged through Switch III into a 3.4 ohm tapered conical water transmission line which delivers the energy to the field emission tube. The tube housing, separating the water from the vacuum, is simply a lucite cylinder 14-inches in diameter and 5-3/4-inches in length. The tube inductance is approximately 30 nanohenries. The purpose of the lucite filler ring will be explained later.

The following diagnostics were used to record the beam parameters; a capacitive voltage probe (ref. 1) in the water line near the base of the tube, an 11 milliohm return current monitor similar to that described in reference 2, a 3-inch diameter total stopping carbon calorimeter for total energy measurements, and a 1/2-inch diameter (1.3 cm^2) and 1-inch diameter (5.1 cm^2) carbon calorimeter for fluence measurements. Depth dose calorimetry was performed at the lower fluences with packages of alternate layers of blue cellophane and aluminum foils to obtain rough estimates of the electron kinetic energy.

4.11.2 Experimental Results

In the first attempt to extract a direct electron beam from Neptune B, both flat and crosshatched 4-inch diameter carbon cathodes were used along with an 0.0005-inch aluminized mylar anode. The charging voltage on the water line was set conservatively low at ~600 kV. For an optimum anode cathode gap spacing of 1 cm, the electron beam current was 60 kA and the electron beam peak kinetic energy was ~200 keV as estimated from depth dose techniques. However, the total measured beam energy of 350 Joules and current duration of 30 nanoseconds were smaller than expected from previous tests with a 3.8 ohm copper sulphate dummy load. Vacuum flashover in the tube was suspected but

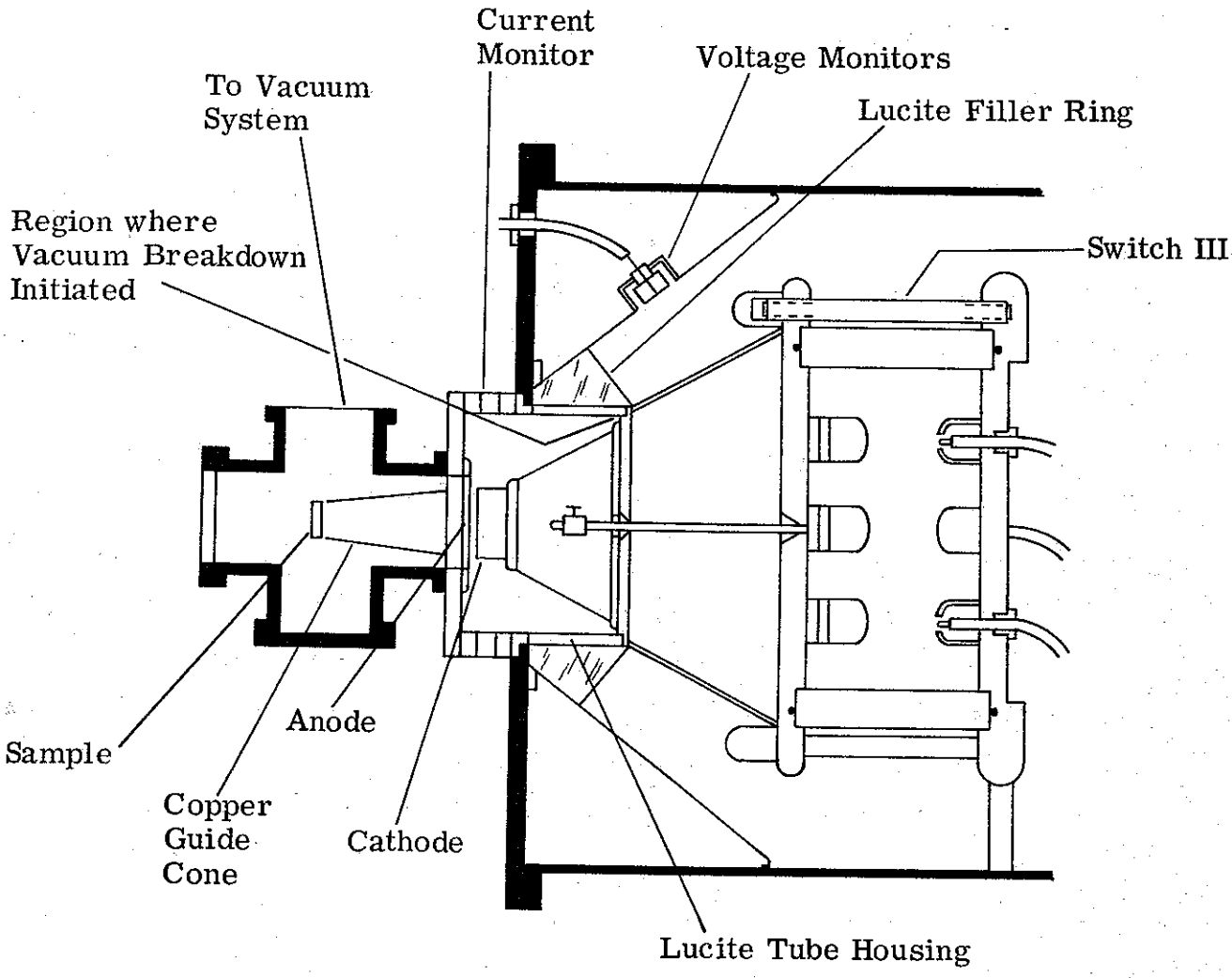

Figure 4-72. Sectional View of Neptune B Front End.

1-5074

final interpretation had to await a diode voltage trace synchronized to the diode current trace as the capacitive voltage probe had not yet been installed.

After a capacitive voltage probe was installed in the tapered water line, vacuum flashover in the tube was immediately indicated. The lucite tube, upon disassembly, showed evidence of vacuum flashover along the 5-3/4-inch length of the inside of the tube. This was believed to have occurred because of the high electric field intensities encountered at the lucite-vacuum interface near the base of the tube. As a result of these observations, the following changes were made.

(1) The 13-inch inside diameter of the lucite tube was bored out by 1/32-inch to remove any flashover damage.

(2) Provisions were made to remove eight delrin tension-rods which had been previously located inside the tube housing along the 5-3/4-inch length.

(3) Most important, a lucite filler ring was constructed and inserted in the tapered water line surrounding the tube. Figure 4-72 shows the final configuration. This final change was made to reduce the electric field intensity at the discontinuity near the base of the tube.

The next phase of electron beam tests showed that the above changes cured the vacuum flashover problem at these voltage levels. The results, using a needle cathode and an optimum cathode-anode spacing of 1 cm are presented below:

(1) The diode current pulse (Figure 4-73) had increased in duration and now more closely resembled the current pulse shape through the dummy load. Its amplitude was 64 kA and duration 70 nanoseconds FWHM.

(2) The diode voltage pulse (Figure 4-73) measured with the capacitive probe in the water line closely resembled the diode current pulse. The voltage probe, which was calibrated against the dummy load voltage and current,

Diode Current

Measured with return current shunt.

Scale 50 ns/cm
80 kA/cm

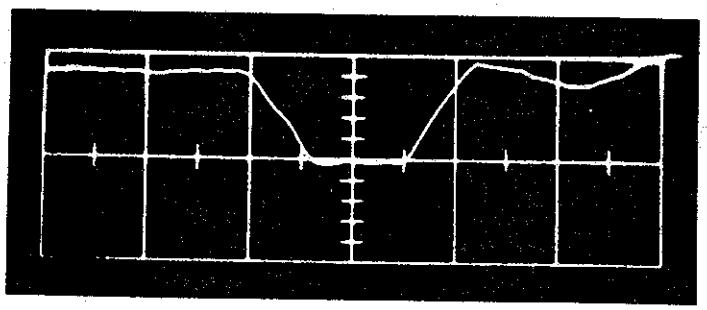

Diode Voltage

Measured with capacitive voltage probe located in tapered water line near tube.

Scale 50 ns/cm
~300 kV/cm

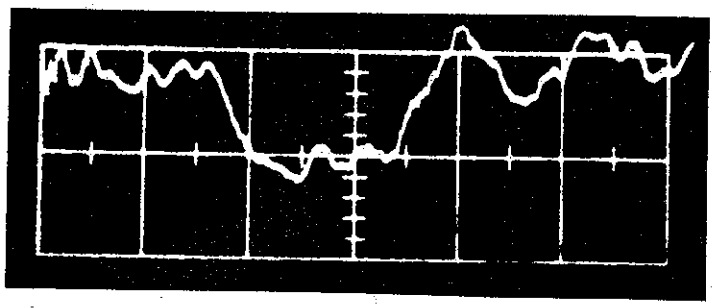

DIODE CHARACTERISTICS

Multipin needle cathode (4-inches diameter)
0.0005-inch aluminized mylar anode
1.0 cm cathode anode spacing

Figure 4-73 Neptune Diode Current and Voltage Traces.

showed a peak electron kinetic energy of approximately 220 keV.

(3) The total electron beam energy as measured with a total-stopping carbon calorimeter placed 1.5 cm behind the anode in the tube vacuum of 5×10^{-4} torr was approximately 1 kilojoule. This figure agrees with rough estimates made from the voltage and current traces and is equal to approximately 2/3 of the total energy stored on the coaxial water line.

(4) A preliminary electron beam focusing attempt resulted in approximately 50 cal/cm^2 over a 1 sq cm carbon calorimeter.

(5) Shot-to-shot reproducibility was ±5% in current and voltage, and ±10% in total energy and fluence.

The cathode used during these latest measurements was a 4-inch diameter multipin needle cathode consisting of 150 commercially available stainless steel pins each 0.021-inches in diameter. The diode impedance as measured with the voltage and current traces is approximately 3.4 ohms. This value is consistent with the Childs Law relation for a planar diode:

$$Z = \frac{k}{V^{1/2}} \left(\frac{d}{r}\right)^2$$

where:

V is in megavolts
d is cathode-anode separation, and
r is cathode radius.

Our measured value for k is $\approx$ 135 which is higher by almost a factor of two than measurements by other groups. This higher value probably results from our low needle density.

Since these measurements, several new cathodes have been built and tested including a 4-inch and 2-inch diameter 250 pin, needle cathode. The most promising cathode was a 2-inch diameter plasma cathode consisting of stycast 2850 epoxy set in concentric grooves on a brass disk (See Figure 4-74). This cathode gave optimum results for a 4 mm gap spacing thus agreeing with Child's Law for a value of $k \approx 60$ which is consistent with measurements from other groups. The main advantages of the plasma cathode over the needle cathode are ability to be easily cleaned between shots and consistently uniform beam profiles. After several high beam current shots, the needle cathode seemed to develop hot spots which caused the beam to wander off center between the cathode and the anode. In contrast, the plasma cathode is easy to clean and after more than 200 shots, it still produced a perfectly concentric beam. A newly developed technique for stretching the thin aluminized mylar anode very taut has also contributed to beam uniformity and reproducibility.

At a water line voltage of 700 kV corresponding to a peak beam kinetic energy of ~250 keV, vacuum flashover recurred. The capacitive voltage monitor showed the flashover initiating after about 70 nanoseconds towards the end of the current pulse. We found that, rather than cleaning the tube after each shot, we could inhibit the flashover by letting the tube stay covered with the carbon dust that originated each shot from the burnt mylar anode. It is believed that the carbon dust prevents the buildup of charge on the plexiglass surface thus inhibiting vacuum flashover. This phenomenum should be studied further.

At present, a copper guide cone 7-inches in length with a 2-inch entrance diameter and a 3/4-inch exit diameter has been used with all the tests conducted with the 2-inch diameter plasma cathode. At a water line voltage of ~700 kV and a drift tube pressure of 0.1 torr, the beam fluence at the end of the guide cone was reproducible to within ±10%. The beam fluence over the center square centimeter of the guide cone exit (2.8 cm^2) is ~60 cal/cm^2 and appears uniform both from observation of front surface craters in aluminum and rear surface spall in 0.032-inch aluminum. Figure 4-75 shows the front and rear surfaces of an 0.032-inch aluminum sample irradiated at the guide cone exit. The fluence falls to approximately 40 cal/cm^2 at the edge of the guide cone exit.

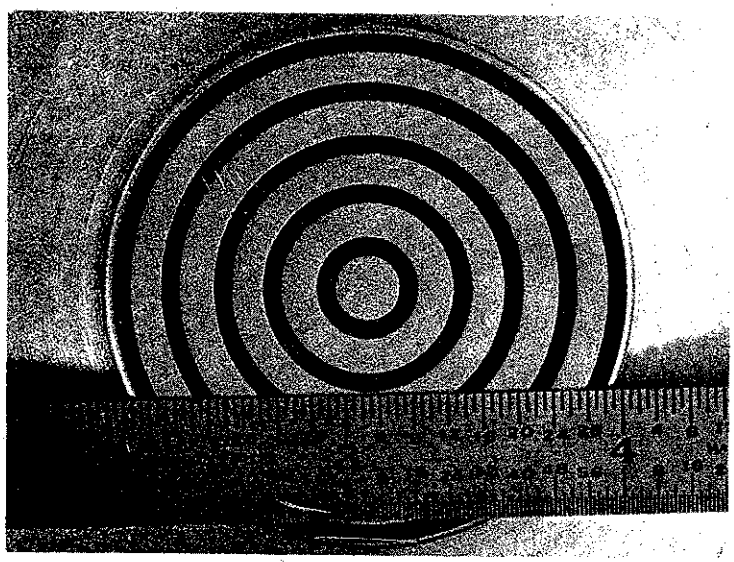

Figure 4-74. Plasma Cathode.

2-1538

Front
Surface
Crater

Rear
Surface
Spall

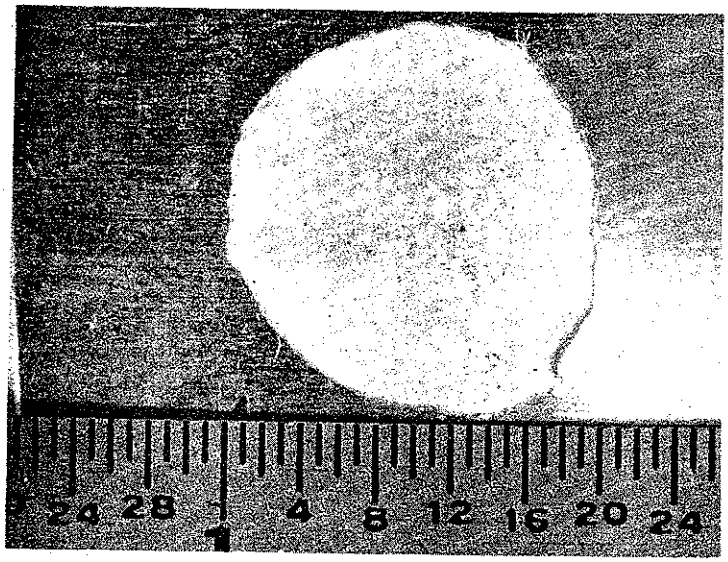

Figure 4-75. Front and rear surface of an irradiated 0.032" aluminum sample.

2-1539

The beam current is 85 kA and the peak kinetic energy is ~250 keV. These parameters give a value of $\frac{\nu}{\gamma} \approx 5$ for the present beam. The total beam energy is ~1300 Joules.

It should be emphasized that the above results are preliminary and should be regarded as qualitative until an extensive beam handling and mapping program is undertaken. It should also be noted that the water line charging voltage of 700 kV is conservatively low and we hope to soon run at 1 MV charging voltage thus doubling the available energy.

REFERENCES

1. Leavitt, Shipman and Vitkovitsky, Rev. Sci. Inst. 36, 1371 (1965).

2. Final Report Contract DA-49-146-XZ553-(III).

SECTION 4.12
CONCLUSIONS AND RECOMMENDATIONS

4.12.1 Conclusions

The work on Neptune B has demonstrated the feasibility of command triggering three series high voltage, high pressure gas insulated switches with nanosecond jitter.

The main implications of this are threefold:

(1) The overall efficiency of the system can be improved by 20% per energy transfer due to the fact that switch closure can be accomplished at the voltage crest and need not be done at the rising portion of voltage wave as in the case of an overvolted switching mode.

(2) The output pulse becomes reproducible within a few percent. This feature is the result of two factors. The first factor is that a small time jitter in the closure of a switch results in a negligible amount of pulse energy variation if the switch may close at the peak of the voltage waveform. The time jitter of a triggered gap is, in any case, much less than that of an overvolted gap. The second factor is that the impedance of the output switch may be kept constant and not be subject to random changes in the number of channels.

(3) The low jitter between command pulse and output pulse allows synchronization of several parallel operating machines.

Since the system has operated up to date for approximately 2,000 shots without any major repairs, it can be concluded that the overall design of this pulser is technically sound and attractive. In particular it has been demonstrated that the low impedance LC generator is a viable alternative to a combination of Marx generator and water transfer capacitor. This is especially important

with regard to the interface between oil and water, which is stressed over a period of several μsec in the case of a slow energy transfer between Marx generator and water capacitor, compared with only a few hundred nsec in the case of a LC generator, assuming that the transfer switch is placed on the oil side. Since the streamer velocity in oil is approximately 10^8 cm/sec* a separation distance of 50 cm would be sufficient to timewise isolate the high voltage structure from the walls. In other words even if the field would be high enough to start a streamer, there would be not enough time for the streamer to actually cross the gap.

4.12.2 Recommendations

As with most prototypes there is also ample room for improvement on the Neptune B systems. Some of the possible improvements are: (1) reduction of switch inductance of Switch III, (2) improved trigger isolation.

4.12.2.1 Reduction of Switch Inductance of Switch III

A reduction of the switch inductance of Switch III will improve the pulse risetime and overall efficiency. This can be accomplished by shortening the length of the switch structure. This shortening is possible, since the breakdown stress across the gap was assumed to be only slightly better than for d.c. conditions. However, experiments have demonstrated that the breakdown strength at 200 psig is at least 50% higher for pulsed conditions, thus allowing a proportional shortening of the switch structure.

Corrugation of the bushing might also be of value to improve the flashover strength of the bushing and thus allow shortening of the overall switch structure.

The switch inductance can also be reduced by placing the spark gaps on a larger diameter. The largest possible diameter is determined by the maximum tolerable stress between the shanks of the gaps and the enclosing wall. This stress can be reduced by filling the remaining volume between the switch and outer conductor with an insulator of a lower dielectric constant than water.

*See: Design Review III, Design Development of the Aurora Facility SR-127-4 July 14 (1969) pg. III-183. (Physics International)

If the spark gaps are placed on a larger diameter it will also be easier to produce a number of channels and the effect of multichanneling will also be greatly enhanced.

Incorporating an impedance transformer between output switch and cathode has also a significant effect on improving the pulse risetime. The pulse risetime is approximately equal to $\frac{2.2\,L}{Z}$, where L is the switch inductance and Z the sum of the impedances on either side of the switch. Since the switch inductance is roughly proportional to the gap separation which is in turn proportional to the voltage across the gap and since the impedance transformation is approximately equal to

$$Z_1 = \frac{V_1^2}{V_0^2} \cdot Z_o$$

one finds that the risetime is shortened approximately proportional to the voltage transformation ratio

$$t_1 = \frac{V_0}{V_1} \quad t_0$$

t_0 - risetime without transformer

t_1 - risetime with transformer

There are however, limits to this improvement, imposed by the breakdown stress in the water line.

In the case that the switch inductance is drastically reduced and the risetime lowered to a few nanoseconds, one is faced with the problem that higher order modes as well as the main TEM wave are excited. For example, the H_{41}, E_{41} and E_{01} will be generated in a four channel switch. Asymmetries will provoke the generation of H_{31}, E_{31}, H_{21}, E_{21}, H_{11} and E_{11}. The amount

of mode conversion depends on the geometry of the switch, together with its environment. Whether the modes are trapped, becoming the socalled 'ghost modes' and contributing to the equivalent switch inductance, or whether the modes propagate out of the switch region depends on both geometry and pulse risetime. In general, a fast rising pulse will generate power flow (in both directions) from the switch region in modes which can never reach the cathode. This can appear both as a contribution to switch inductance and as a loss of energy.

The most dangerous modes are those that propagate at the lower frequencies, viz. the H modes. Fortunately, the simplest method of suppressing propagation increases the voltage holdoff strength of the line. This follows from the fact that the required perturbation of the circular geometry of the inner conductor increases the electric field on the inner conductor and therefore decreases the field on the outer, which is closer to breakdown in the case of a negatively charged low impedance water line.

4.12.2.2 Improvement of the Trigger Isolation

The problem of trigger isolation can be greatly alleviated if the transfer switch between water line and load is switched from the load side. This has the following advantages:

(1) The trigger isolation between ground and high voltage switch can be made by a simple cable connection, as long as the cable is at least half as long as the desired pulse width. This will considerably reduce the complexity and cost.

(2) The voltage between trigger cable and inner conductor that need to be isolated is less and so is the stress duration.

(3) There will be only a negligible loading of the output pulse due to coupling between line and trigger cable.

(4) There will be ample room to install more than four trigger cables. The only disadvantage is the need for a rather long transition section between output switch and cathode. However, in many cases the coaxial transformer can serve as the transition section.